Ammonia - from pollutant to power

Removal and recovery of total ammoniacal nitrogen from residual waters for electricity generation

van Linden, N.

DOI
10.4233/uuid:756b1c69-83a8-4050-ab07-9627a998b6e6

Publication date
2022

Document Version
Final published version

Citation (APA)
van Linden, N. (2022). *Ammonia - from pollutant to power: Removal and recovery of total ammoniacal nitrogen from residual waters for electricity generation*. [Dissertation (TU Delft), Delft University of Technology]. https://doi.org/10.4233/uuid:756b1c69-83a8-4050-ab07-9627a998b6e6

Ammonia – from pollutant to power

Removal and recovery of total ammoniacal nitrogen from residual waters for electricity generation

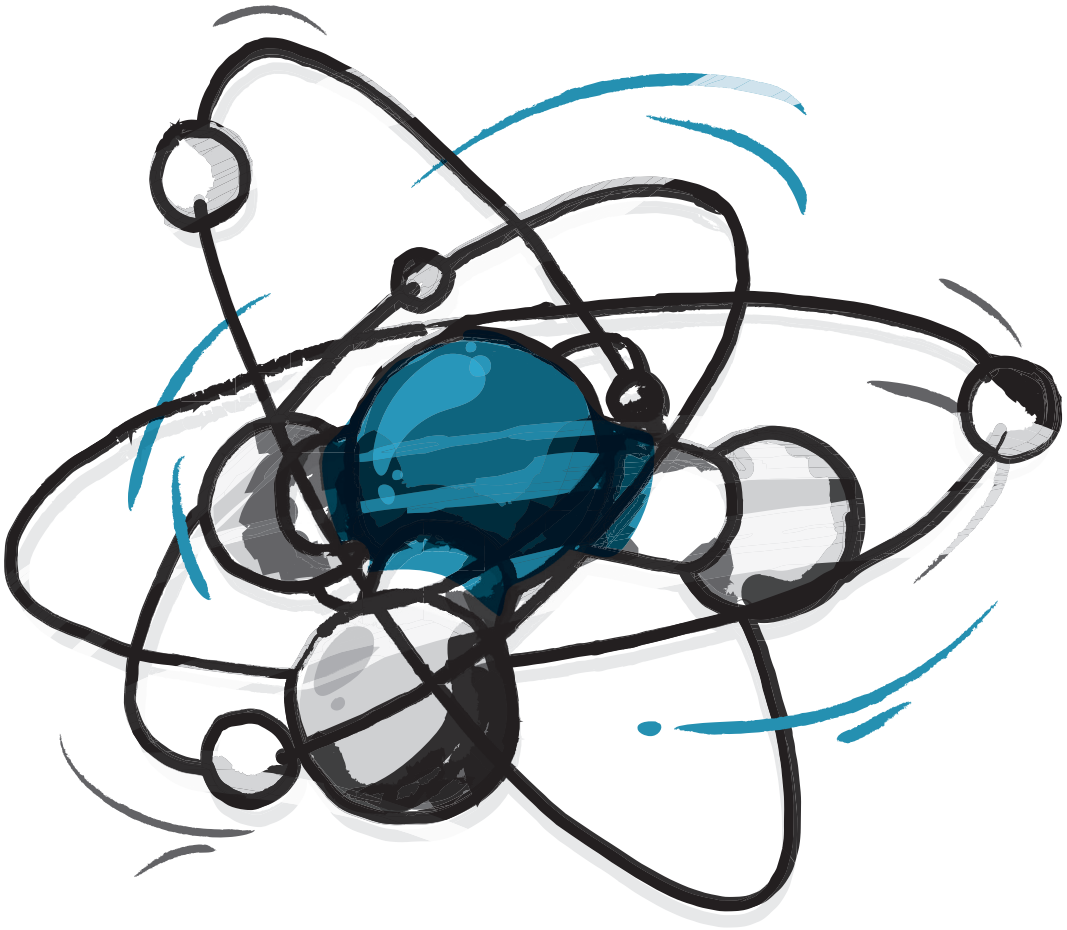

Niels van Linden

Ammonia - from pollutant to power

Removal and recovery of total ammoniacal nitrogen from residual waters for electricity generation

Dissertation

for the purpose of obtaining the degree of doctor
at Delft University of Technology
by the authority of the Rector Magnificus Prof. dr. ir. T.H.J.J. van der Hagen,
chair of the Board for Doctorates
to be defended publicly on
11th of July 2022 at 15:00 o'clock

By

Niels VAN LINDEN

Master of Science in Civil Engineering, Delft University of Technology, the Netherlands
born in Vlaardingen, the Netherlands

This dissertation has been approved by the promotors.

Composition of the doctoral committee:
Rector Magnificus, chairperson
Prof. dr. ir. J.B. van Lier, Delft University of Technology, promotor
Dr. ir. H.L.F.M. Spanjers, Delft University of Technology, promotor

Independent members:
Prof. dr. ir. R. Dewil, Katholieke Universiteit Leuven
Dr. P. Kuntke MSc, Wageningen University & Research / Wetsus
Prof. dr. ir. F.M. Mulder, Delft University of Technology
Prof. dr. A. Purushothaman Vellayan, Rijksuniversiteit Groningen
Dr. ir. D.A. Vermaas, Technische Universiteit Delft

Reserve member:
Prof. dr. ir. L.C. Rietveld, Delft University of Technology

This research was part of the N2kWh – From Pollutant to Power project (14712), funded by Nederlandse Organisatie voor Wetenschappelijk Onderzoek (NWO)) and Agentschap Innoveren & Ondernemen (VLAIO) (former Instituut voor Innovatie door Wetenschap en Technologie (IWT)).

Keywords:
ammonia, electricity generation, electrodialysis, bipolar membrane electrodialysis, vacuum membrane stripping, pervaporation, solid oxide fuel cell

ISBN 978-94-93720-76-3

An electronic version of this dissertation is available at http://repository.tudelft.nl

Abstract

Ammonia (NH_3) is one of world's most-produced chemicals and is mostly used as a raw resource for fertilisers. From the used NH_3-based fertilisers, almost half of the NH_3 ends up in receiving water bodies, leading to eutrophication, eventually resulting in species diversity loss in the aquatic environment. To minimise environmental damage, total ammoniacal nitrogen (TAN) should be removed from residual waters before discharge. Currently, the treatment of residual waters with high TAN concentrations (hereafter nitrogen (N)-loaded residual waters) by biological processes, such as partial nitritation in combined with anammox (reaching TAN removal efficiencies up to 90%), is challenged by the undesired emission of oxidised nitrogen species. In addition, current methods to recover TAN from N-loaded residual waters for reuse purposes require large amounts of energy and chemicals.

Interestingly, NH_3 was recently acknowledged as a carbon-free carrier of energy, having an energy content of 21 MJ·kg-N^{-1}. The fact that NH_3 carries energy, opens possibilities to remove TAN from N-loaded residual waters and subsequently recover NH_3 for the generation of electricity, potentially leading to energy-positive methods to remove TAN from N-loaded residual streams. The objective of this thesis was to assess the feasibility to achieve competitive (approximately 90%) TAN removal from N-loaded residual waters and to use the recovered NH_3 for electricity generation purposes, using a combination of technologies without using chemicals. The used technologies in this thesis are electrodialysis (ED), bipolar membrane electrodialysis (BPMED), vacuum membrane stripping (VMS) and a solid oxide fuel cell (SOFC). To determine the suitability of the combination of technologies, the research conducted in this thesis focused on the mass transfer and achievable concentrations of the various TAN species (ammonium (NH_4^+), dissolved NH_3 and gaseous NH_3), as well as the electrical energy aspects (consumption and generation) for the various technologies.

In this thesis, a literature study in Chapter 2 identifies thirteen potentially suitable N-loaded residual waters from which NH_3 can be recovered for electricity generation purposes. In addition, the literature study provides an overview of potentially suitable technologies to remove TAN from N-loaded residual waters and to recover NH_3 for electricity generation purposes. Each of the selected technologies subsequently served as a research topic in the chapters of this thesis. Research on ED in Chapter 3 shows that applying dynamic current density leads to higher concentration factors to produce concentrated NH_4^+ solutions, at lower electrical energy consumption compared to applying fixed current density. Solutions with NH_4^+ concentrations up to 10 g·L^{-1} were produced by ED at an NH_4^+ removal efficiency of approximately 90%, at an electrical energy consumption of 5 MJ·kg-N^{-1}. Subsequently, research on BPMED in Chapter 4 shows that approximately 90% NH_4^+ removal can be achieved by BPMED, while simultaneously concentrated solutions with NH_3 concentrations of 4.5 g·L^{-1} can be produced without using chemicals, at an electrical energy consumption of 22 MJ·kg-N^{-1}. Furthermore, research on the recovery of NH_3 as a gas by VMS in Chapter 5 and

6 shows that transfer of water (H_2O) is inevitable, leading to the recovery of NH_3-H_2O mixtures when using VMS. Transfer of H_2O is even consistently preferred over the transfer of NH_3, for various feed water compositions, operating conditions and membrane types, when using VMS to recover gaseous NH_3 from water. By providing NH_3 feed water concentrations up to 10 $g \cdot L^{-1}$, NH_3 concentrations of 11 wt% can be obtained in the recovered NH_3-H_2O mixtures. Research on the SOFC in Chapter 6 shows that NH_3-H_2O mixtures with NH_3 concentrations down to 5 wt% can still be used for electricity generation purposes: the SOFC generated of 9 $MJ \cdot kg\text{-}N^{-1}$ of electrical energy. Research on real N-loaded residual streams in Chapter 7 shows the feasibility of ED to achieve competitive (approximately 90%) TAN removal from three real N-loaded residual waters: algae digestion reject water, sludge digestion reject water and fertiliser industry condensate. The treatment of fertiliser industry condensate was not hampered by implications due to the presence of other ions or organics in the feed water. ED, BPMED, VMS and an SOFC were combined to achieve approximately 90% TAN removal from fertiliser industry condensate and to ultimately generate energy from the recovered NH_3-H_2O mixtures. The electrical energy consumption of ED, BPMED and VMS was 38 $MJ \cdot kg\text{-}N^{-1}$, whereas the SOFC generated 11 $MJ \cdot kg\text{-}N^{-1}$. The combination of technologies had a net electrical energy consumption of 27 $MJ \cdot kg\text{-}N^{-1}$, making the proposed system not yet energy-positive in terms of electricity.

For each of the technologies, more research on the mass transfer of the various TAN species, the used (membrane) materials and operating conditions is required to decrease the electrical energy consumption of the ED, BPMED and VMS and to increase the electricity generation of the SOFC, to potentially develop an energy-positive system to remove TAN from N-loaded residual waters.

Samenvatting

Ammoniak (NH_3) is een van 's werelds meest geproduceerde chemicaliën en wordt vooral gebruikt als grondstof voor kunstmest. Van alle gebruikte kunstmest op NH_3 basis, eindigt bijna de helft van de NH_3 in ontvangende waterlichamen, leidend tot eutrofiering, wat uiteindelijk resulteert in het verlies van soorten diversiteit in het waterige milieu. Om schade aan het milieu te minimaliseren, moet ammoniakale stikstof verwijderd worden van restwateren voordat deze geloosd worden. Momenteel wordt de behandeling van restwateren met hoge ammoniakale stikstof concentraties (hierna stikstof-rijke restwateren genoemd) door biologische processen zoals als partiele nitritatie in combinatie met anammox (reikend tot ammoniakale stikstof verwijderingsefficiënties tot 90%) uitgedaagd door de onwenselijke uitstoot van geoxideerde stikstof soorten. Daarnaast hebben huidige methoden om ammoniakale stikstof uit stikstof-rijke restwateren terug te winnen voor hergebruik grote hoeveelheden energie en chemicaliën nodig.

Interessant genoeg werd NH_3 recent erkend as koolstof-vrije energiedrager, met een energie inhoud van 21 $MJ{\cdot}kg\text{-}N^{-1}$. Het feit van NH_3 energie draagt, opent mogelijkheden om ammoniakale stikstof uit stikstof-rijke restwateren te verwijderen en vervolgens de NH_3 terug te winnen voor het opwekken van elektriciteit, wat mogelijk leidt tot energie-positieve methoden voor ammoniakale stikstof verwijdering uit stikstof-rijke restwateren. Het doel van dit proefschrift was het bepalen van de haalbaarheid om concurrerende (ongeveer 90%) ammoniakale stikstof verwijdering uit stikstof-rijke restwateren te behalen en om de teruggewonnen NH_3 te gebruiken voor elektriciteitsopwekking, gebruikmakend van een combinatie van technologieën zonder gebruik van chemicaliën. De gebruikte technologieën in dit proefschrift zijn elektrodialyse (ED), bipolaire membraan elektrodialyse (BPMED), vacuüm membraan strippen (VMS) en een solid oxide fuel cell (SOFC). Om de geschiktheid van de combinatie van technologieën te bepalen, richt het onderzoek in dit proefschrift zich op de massaoverdracht en de haalbare concentraties van de verschillende ammoniakale stikstof soorten (ammonium (NH_4^+), opgeloste NH_3 en gasvormige NH_3), alsmede op de elektrische energie aspecten (verbruik en opwekking) voor de verschillende technologieën.

In dit proefschrift identificeert een literatuurstudie in Hoofdstuk 2 dertien potentieel geschikte stikstof-rijke restwateren waar NH_3 uit teruggewonnen kan worden voor elektriciteitsopwekkingsdoeleinden. Daarnaast verstrekt de literatuurstudie een overzicht van potentieel geschikte technologieën om ammoniakale stikstof uit stikstof-rijke restwateren te verwijderen en om NH_3 terug te winnen voor elektriciteitsopwekkingsdoeleinden. Elk van de geselecteerde technologieën diende vervolgens als onderzoeksonderwerp in de hoofdstukken van dit proefschrift. Onderzoek naar ED in Hoofdstuk 3 toont aan dat het toepassen van een dynamische stroomsterktedichtheid leid tot hogere concentratiefactoren om geconcentreerde NH_4^+ oplossingen te produceren, voor een lager elektriciteitsverbruik dan het toepassen van een vaste stroomsterktedichtheid. Oplossingen met NH_4^+ concentratie tot 10 $g{\cdot}L^{-1}$ werden geproduceerd bij een verwijderingsefficientie van NH_4^+ van ongeveer 90%, voor een elektrisch energieverbruik van 5

MJ·kg-N^{-1}. Vervolgens toont onderzoek naar BPMED in Hoofdstuk 4 aan dat 90% verwijdering van NH_4^+ haalbaar is voor BPMED, terwijl tegelijkertijd geconcentreerde oplossingen met NH_3 concentraties van 4.5 g·L^{-1} werden geproduceerd zonder gebruik van chemicaliën, voor een elektrisch energieverbruik van 22 MJ·kg-N^{-1}. Verder toont onderzoek in Hoofdstuk 5 en 6 naar het terugwinnen van NH_3 als een gas met VMS aan dat overdracht van water (H_2O) onvermijdbaar is, wat er toe leidt dat NH_3 als NH_3-H_2O mengsel teruggewonnen wordt bij het gebruik van VMS. Overdracht van H_2O heeft zelfs consequent de voorkeur boven de overdracht van NH_3, voor verschillende voedingswatersamenstellingen, operationele condities en membraantypes, wanneer VMS wordt toegepast om gasvormig NH_3 uit water terug te winnen. Door NH_3 voedingswaterconcentraties van 10 g·L^{-1} aan te leveren voor VMS, kunnen NH_3 concentraties van 11 gewichtsprocent (m%) bereikt worden in de teruggewonnen NH_3-H_2O mengsels. Onderzoek naar de SOFC in Hoofdstuk 6 toont aan dat NH_3-H_2O mengsels met NH_3 concentraties tot aan 5 m% nog steeds gebruikt kunnen worden voor elektriciteitsopwekkingsdoeleinden: de SOFC wekte 9 MJ·kg-N^{-1} aan elektriciteit op. Onderzoek met echte stikstof-rijke restwateren in Hoofdstuk 7 toont de haalbaarheid van ED aan om concurrerende (ongeveer 90%) ammoniakale stikstof verwijdering te behalen voor drie echte stikstof-rijke restwateren: algenvergistingsrejectiewater, slibvergistingsrejectiewater en condensaat uit de kunstmestindustrie. De behandeling van condensaat uit de kunstmestindustrie werd niet belemmerd door de aanwezigheid van andere ionen of organische stof in het voedingswater. ED, BPMED, VMS en een SOFC werden gecombineerd om een ammoniakale stikstof verwijderingsefficientie van 90% uit condensaat uit de kunstmestindustrie te behalen en uiteindelijk elektriciteit op te wekken uit de teruggewonnen NH_3-H_2O mengsels. Het elektriciteitsverbruik van ED, BPMED en VMS was 38 MJ·kg-N^{-1}, terwijl de SOFC 11 MJ·kg-N^{-1} opwekte. De combinatie van de technologieën had een netto energieverbruik van 27 MJ·kg-N^{-1}, wat het voorgestelde systeem nog niet energie-positief maakte in termen van elektriciteit.

Voor elk van de technologieën is meer onderzoek nodig naar de massa overdracht van de verschillende ammoniakale stikstof soorten, de gebruikte (membraan)materialen en de operationele condities om het elektriciteitsverbruik van ED, BPMED en VMS te verlagen en de elektriciteitsopwekking van de SOFC te verhogen, om zo mogelijk een elektrische energie-positieve methode te ontwikkelen om ammoniakale stikstof uit stikstof-rijke restromen te verwijderen.

Table of Contents

Contents

Table of Contents

Chapter 1.

Introduction

1.1. Production and fate of NH_3

Ammonia (NH_3) is one of the world's most-produced chemicals with more than 178 million tons of NH_3 produced annually (FAO, 2019; The Royal Society, 2020). About 80% of the produced NH_3 is used as fertiliser, while the rest is used as raw material for the fabrication of chemical compounds and explosives (Galloway et al., 2004; Erisman et al., 2008), as depicted in Figure 1-1. Almost 2% of the total world's generated energy is used in the Haber-Bosch process to produce NH_3-based products, contributing to 2% of the global annual CO_2 emission (The Royal Society, 2020). The well-established Haber-Bosch process produces NH_3 from nitrogen (N_2) and hydrogen gas (H_2) at high temperatures (300 – 500 °C) and under high pressure (150 – 300 bar). The production of H_2 accounts for the largest part of the energy consumption (80%) of the Haber-Bosch process (The Royal Society, 2020). When H_2 is generated via methane (CH_4) reforming, the energy consumption of the Haber-Bosch process equals 28 MJ·kg-N^{-1} produced, whereas when H_2 is generated via water electrolysis, the energy consumption of the Haber-Bosch process equals 107 MJ·kg-N^{-1} (Cherkasov et al., 2015). Even though the Haber-Bosch process has been largely improved and is economically attractive, alternative methods for NH_3 production, such as electrochemical routes, are actively studied (Giddey et al., 2013; Garagounis et al., 2019; The Royal Society, 2020).

While NH_3-based fertilisers contribute immensely to feeding the world's human population, the (over)use of NH_3-based fertilisers creates a huge environmental impact (Erisman et al., 2007; Erisman et al., 2008). As depicted in Figure 1-1, 15 – 55% of the total amount of the produced fertilisers ends up in the atmosphere and water bodies (Galloway et al., 2004; Erisman et al., 2007; Matassa et al., 2015). Emission of NH_3 to receiving water bodies via untreated or partially treated residual waters leads to oxygen depletion and eutrophication, resulting in species diversity loss (Erisman et al., 2007). The latter also applies for the emission of other nitrogen species, such as nitrite (NO_2^-) and nitrate (NO_3^-) to receiving water bodies, but this thesis focuses on the possibilities to manage the treatment of NH_3 in residual waters.

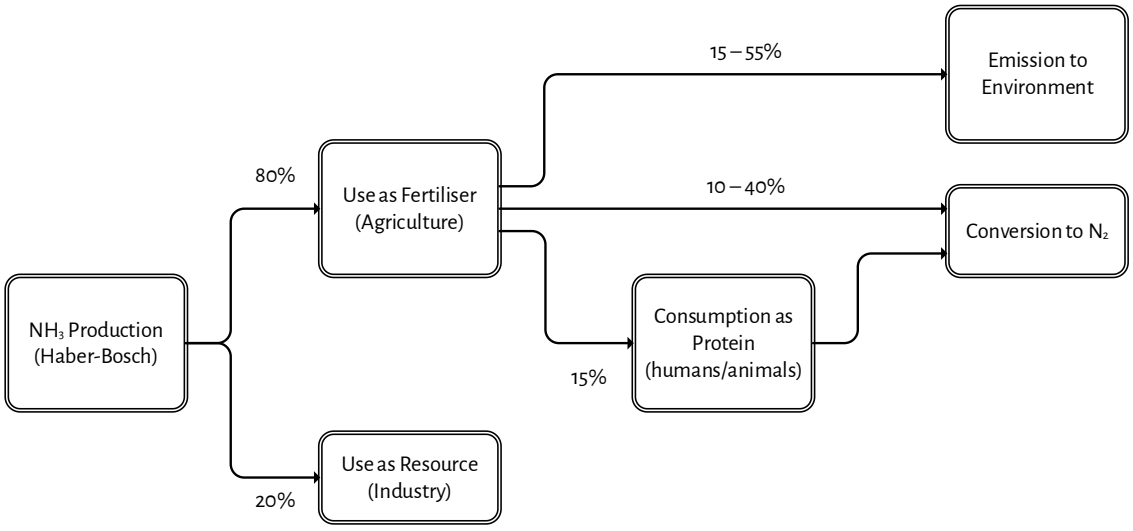

Figure 1-1 - Fate of produced NH_3 by the Haber-Bosch process, based on data provided by Galloway et al. (2004) and Erisman et al. (2008).

1.2. Current treatment of ammonia in residual waters

The presence of NH_3 in water (aqueous solution) can be described as the total ammoniacal nitrogen (TAN) concentration, which is the sum of both dissolved NH_3 gas and ammonium (NH_4^+) ions. TAN can be present in water (aqueous solution) in both mentioned species, of which the distribution mainly depends on the temperature, the pH and the ionic strength of the solution (see Figure 1-3).

1.2.1. Biochemical processes to remove TAN from residual waters

To limit the emission of TAN to receiving water bodies, residual streams that contain TAN should be treated before discharge. Traditionally, TAN is removed by biochemical oxidation to NO_3^- in a process called nitrification, which occurs in biological treatment systems, such as (aerated) lagoons, trickling filters or activated sludge plants. To avoid excessive eutrophication of the receiving water bodies, oxidised N species subsequently needs to be reduced to N_2 in a biochemical process called denitrification. At present, the nitrification-denitrification process (NDN) is commonly applied in sewage treatment and treatment processes for industrial residual waters to remove TAN. To achieve sufficient nitrogen removal, the application of (NDN) requires high hydraulic and solids retention times, which results in large physical installation footprints. However, sewage typically contains relatively low concentrations of TAN: up to 50 $mg \cdot L^{-1}$. This thesis focuses on the treatment of residual streams that are concentrated in TAN: higher than 500 $mg \cdot L^{-1}$.

For the treatment of concentrated (in TAN) residual waters, processes based on partial nitritation in combination with anaerobic ammonium oxidation (PN-anammox) are increasingly applied. An example of a concentrated residual water is the liquid fraction of sludge digestate (reject water) in sewage treatment plants. Through side stream treatment of sludge reject water by PN-anammox, the total TAN load to the NDN processes in the main stream (also called the water line) can be decreased by 15 – 25%, resulting in a decrease in the total energy consumption, compared to returning the sludge reject water back to the water line (Van Hulle et al., 2010; Lackner et al., 2014). In their review, Magri et al. (2013) mentioned that the side stream removal of TAN requires 57 $MJ \cdot kg\text{-}N^{-1}$ removed using NDN via nitrite, and that PN-anammox requires 19 $MJ \cdot kg\text{-}N^{-1}$ removed. Furthermore, Lackner et al. (2014) and Schaubroeck et al. (2015) reported that the energy consumption of side stream TAN removal in full-scale PN-anammox installations ranges between 3 and 15 $MJ \cdot kg\text{-}N^{-1}$ removed. Based on the study of Lackner et al. (2014), the removal efficiency of TAN by PN-anammox reaches up to approximately 90%. As PN-anammox is considered to be the state-of-the-art process for TAN removal from concentrated residual waters, in this thesis, 90% TAN removal is considered to be competitive TAN removal.

Despite the energy advantage of PN-anammox versus NDN, the application of PN-anammox is currently limited to warm side streams with low carbon to nitrogen ratios, as the preferred operating temperature of anammox bacteria is around 35 °C and the growth of these bacteria is outcompeted by other bacteria species in the presence of high concentrations of biodegradable organic carbon in the feed water (Gonzalez-Martinez et al., 2018). Furthermore, there is consensus that the application of both NDN and PN-anammox

processes results in the production and emission of oxidised nitrogen species such as nitrous oxide (N_2O), nitrogen oxide (NO) and nitrogen dioxide (NO_2) (Kampschreur et al., 2009). Especially the emission of N_2O is undesirable, because it is a potent greenhouse gas, having a 296 times higher global warming potential than carbon dioxide (CO_2), according to the IPCC (Prather et al., 2001). The fraction of N_2O emission relative to the total nitrogen load of full-scale biological water treatment plants is reported to be 0 – 15% (Kampschreur et al., 2009; Vasilaki et al., 2019). The wide range in gaseous oxidised nitrogen emission is explained by the diversity in feed water compositions and applied operational conditions, which affect the production of gaseous oxidised nitrogen species by bacteria (Kampschreur et al., 2009; Desloover et al., 2012). According to the review of Desloover et al. (2012), the emission of N_2O during biochemical processes can contribute to 80% of the total greenhouse emissions, expressed in CO_2 equivalents of water treatment plants that process sewage, manure, landfill leachate or industrial effluents. Hence, even though wide ranges are reported for the energy consumption and the emission of gaseous oxidised nitrogen species, currently available literature shows that biochemical removal of TAN consumes energy and results in the emission of strong greenhouse gases. Finally, a recent study by RIVM (2019) showed the presence of legionella in various water treatment plants where PN-anammox is applied, which threatens the applicability of PN-anammox process due to danger to legionella spreading events.

1.2.2. Recovery of TAN from residual waters

In contrast to the application of biochemical technologies to remove TAN from residual waters by destruction, recovery of TAN offers multiple opportunities for reuse. In the last two decades, there has been a growing interest in the recovery of TAN as raw material for fertilisers, using mature technologies such as struvite (magnesium ammonium phosphate) precipitation and ammonia stripping using air or steam (Mehta et al., 2015b). However, recovery of TAN as a resource is not always desirable, because chemicals and energy are typically required to drive the recovery technologies. Moreover, the use of the recovered products can be challenging due to legislation, quality restrictions, storage and transportation costs, and supply and demand mismatches (Mehta et al., 2015b; Zarebska et al., 2015).

Interestingly, NH_3 was recently identified as a suitable energy carrier, as an alternative to carbon-based fuels such as oil and natural gas, because it is carbon-free and the storage and transportation systems are already established (ISPT, 2017; Valera-Medina et al., 2018; The Royal Society, 2020). The chemically bound energy in NH_3 (21 MJ·kg-N^{-1}) can actually be converted into electricity and heat, with N_2 gas and H_2O as final products, while the emission of oxidised nitrogen species is avoided (Staniforth & Ormerod, 2003).

1.3. Research description

1.3.1. General problem description

The generation of electricity from NH_3 recovered from residual waters is a novel concept and opens new opportunities to manage TAN in residual waters. This concept was previously studied in a Dutch research project, in which TAN was removed from sludge reject water by struvite precipitation and NH_3 gas was recovered after thermal struvite decomposition (STOWA, 2013). Subsequently, the recovered NH_3 gas was used as the fuel for a solid oxide fuel cell (SOFC), as described in the papers of Hemmes et al. (2011) and Saadabadi et al. (2020). SOFCs can convert NH_3 to N_2 gas and H_2O while generating both electricity and heat, with the highest reported energy efficiency amongst energy-conversion technologies: up to 60% electrical efficiency, whereas an additional 30% of the chemical energy carried in the fuel can be recovered as heat and the residual part is assigned to the changes in entropy or lost by heat emission to the environment (Stambouli & Traversa, 2002; Lan & Tao, 2014b). However, stoichiometrically, one mole of struvite contains equal moles of nitrogen and phosphorus. Because residual waters that require TAN removal typically contain more nitrogen than phosphorus, struvite precipitation only accounts for limited (15 – 30%) TAN removal (Mehta et al., 2015a; Zarebska et al., 2015). Therefore, the concept as described in the study of STOWA (2013) is in this thesis not considered to be able to achieve competitive (90%) TAN removal. Furthermore, the studies of Xu et al. (2017) and Grasham et al. (2019) addressed the recovery of NH_3 from residual waters for the generation of electricity, but did not elaborate on how to recover NH_3 as a gas from water (aqueous solution), in what concentration NH_3 can be recovered and how much energy can be generated when using gaseous NH_3 recovered from water as a fuel. Hence, it was unclear how NH_3 can be recovered from residual waters and whether the recovered NH_3 can be used for electricity generation.

1.3.2. General considerations

From this point onwards, this thesis will consistently use the following terminology, following the definitions as presented in Chapter 2.2:

- (N-loaded) residual streams: used as a collective term for all N-loaded streams that contain total Kjeldahl nitrogen concentrations higher than 0.5 $g \cdot L^{-1}$ (aqueous, slurries, etc.);
- (N-loaded) residual waters: used when referring to aqueous solutions that contain TAN in concentrations higher than 0.5 $g \cdot L^{-1}$;
- Feed waters: used to refer to aqueous solutions used for experiments;

Furthermore, the following terminology will be used for NH_3 in its various forms and different contexts:

- Ammonia (NH_3): used when referring to the gaseous form), either dissolved in water (aq) or as gas (g);
- Ammonium (NH_4^+): used when referring to the ionised form, dissolved in water (aq);
- Total ammoniacal nitrogen (TAN): used as a collective term for the presence of ammoniacal nitrogen dissolved in water, or as recovered in gaseous mixtures, dissolved or solid form.

To recover NH_3 from N-loaded residual waters for the generation of electricity, many different technologies can be considered. To narrow down the number of technologies and the associating research topics to be studied, this thesis focuses only on technologies that are applicable to the treatment of N-loaded residual waters, containing reduced (or total Kjeldahl) nitrogen in concentrations higher than 0.5 $g \cdot L^{-1}$. The limit 0.5 $g \cdot L^{-1}$ is based on an assessment on the identification and characterisation of concentrated residual streams from which TAN currently is removed and recovered, presented in Chapter 2.2 of this thesis. Furthermore, Chapter 2.3 provides an assessment of various suitable technologies to remove and recover TAN from water. To further narrow down the options for technologies, the following considerations were taken into account:

- To be competitive with currently existing methods for TAN removal from N-loaded residual waters, the TAN removal efficiency of the combination of technologies should be around 90% (Lackner et al., 2014);
- The SOFC is considered to be the most efficient electricity generation technology and can use NH_3 directly as a fuel (Stambouli & Traversa, 2002; Valera-Medina et al., 2018), as also can be concluded from the review on various fuel cell types in Chapter 2.4;
- As electrical energy is released during electricity generation from NH_3, this energy source could be used to drive the technologies for TAN removal and subsequent NH_3 recovery, with the purpose to develop an energy-efficient and chemical-free system. This consideration excludes the potentially suitable application of zeolites and the subsequent regeneration with alkaline solutions to obtain NH_3 as presented by Vecino et al. (2019).

1.3.3. Research objective

The research objective of this thesis is to assess the feasibility of a proposed combination of technologies to allow for competitive TAN removal from N-loaded residual waters and the subsequent generation of electricity from the recovered NH_3. In this thesis, the following aspects were extensively studied:

- Quantification of concentration of various nitrogen species: NH_4^+ (aq), NH_3 (aq) and NH_3 (g) throughout the various studied technologies (in g/L and wt%);
- Electrical energy assessment: determining the required electrical energy consumption of the various technologies and the electrical energy generation of the SOFC, normalised per unit of mass of processed (unless stated differently) nitrogen ($MJ \cdot kg\text{-}N^{-1}$).

By acquiring information on the TAN concentrations and energy, the feasibility of the proposed system is assessed. Furthermore, by optimising the operation of the proposed technologies to remove TAN and recover NH_3 for electricity generation in an SOFC, potentially an electrical energy-positive system may be developed: net generation of electricity during the removal of TAN from N-loaded residual waters, whereas to date, conventional TAN removal process still consumes electrical energy (as depicted in Figure 1-2). To achieve the main objective, this thesis considers various specific topics, focusing on the various proposed technologies.

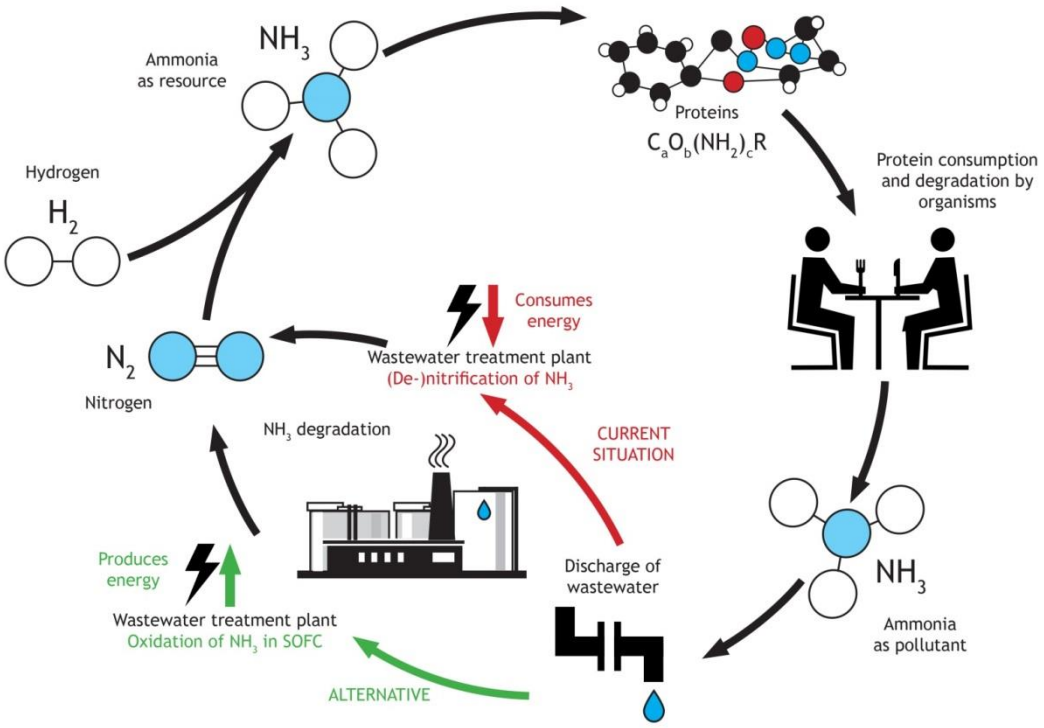

Figure 1-2 - The cycle of nitrogen via TAN, which currently requires energy to manage TAN in N-loaded residual waters (red route), while there are opportunities to generate energy from recovered NH_3 (green route).

1.3.4. Specific technology-based research topics

1.3.4.1. SOFC to generate energy from recovered NH_3

According to Stambouli and Traversa (2002), SOFCs operate at a temperature ranging between 600 to 1,000 ºC and typically use high purity gases as a fuel, such as methane (CH_4) and H_2. As extensively described in Chapter 2.4, SOFCs can also be used to generate energy using NH_3 as a fuel and are considered to be the most efficient energy-conversion technology to generate energy from NH_3. However, there are certain quality restrictions for SOFC fuels. The presence of metal-based salts in the fuel is expected to cause scaling on the anode, whereas the presence of gaseous oxidants in the fuel, such as O_2 and hydrogen sulphide (H_2S) may deactivate the present anode catalyst by oxidation (Papadias et al., 2012). Since SOFCs use gaseous fuels, this thesis focuses on the recovery of NH_3 as a gas from N-loaded residual waters. The recovery of gaseous NH_3 from N-loaded residual waters simultaneously allows for the separation of NH_3 from contaminating metal-based salts and sulphur-based solutes, which are typically present in N-loaded residual waters.

To recover gaseous NH_3 from N-loaded residual waters, various gas stripping technologies can be used, as described in Chapter 2.3.2. Amongst the various gas stripping configurations to recover NH_3 as fuel for an SOFC, vacuum stripping is expected to be most suitable, as no O_2 (expected to act as an oxidant) is supplied, which is the case for conventional gas stripping using air. By using hydrophobic membranes (impermeable for liquids, but permeable for vapours) as physical barriers to separate the liquid (the feed water) and the by

vacuum extracted gas, high contact areas in small volumes can be achieved, leading to a flexible and modular system design. Therefore, in this thesis, vacuum membrane stripping (VMS) is selected for the recovery of gaseous NH_3. However, as described in Chapter 2.3.2, when gaseous NH_3 is recovered from feed water in vacuum stripping applications, evaporation of water (H_2O) takes place, leading to the recovery of NH_3-H_2O mixtures. Because H_2O cannot be used for electricity generation purposes in an SOFC, the presence of H_2O in the fuel should be minimised and thus the NH_3 concentration in the NH_3-H_2O mixtures should be maximised. In this thesis, the fuel for the SOFC is expected to contain H_2O, but it is unknown how much NH_3 should at least be present in the fuel to generate energy. Moreover, it is unknown how much energy can be generated from NH_3-H_2O mixtures. Therefore, the considerations for the use of NH_3-H_2O mixtures as fuels by SOFCs lead to the following specific research topic:

A. NH_3 concentration in NH_3-H_2O mixtures for electricity generation by an SOFC and corresponding energy generation.

1.3.4.2. VMS to recover concentrated gaseous NH_3

Stripping of NH_3 is typically performed at a feed water pH of 9.5, because at this pH, TAN is predominantly present as volatile dissolved NH_3 gas instead of non-volatile NH_4^+ (see Figure 1-3). For stripping NH_3 under vacuum, the driving force of the NH_3 transfer is the NH_3 vapour pressure difference between the liquid feed water and the gaseous permeate. Based on Henry's Law, the higher the dissolved NH_3 concentration in the feed water, the higher the NH_3 vapour pressure in the feed water. Higher NH_3 vapour pressure differences, in their turn, lead to a higher NH_3 transfer rate. By adjusting the feed water composition (TAN concentration, pH, temperature and ionic strength), the transfer of NH_3 can be increased. On the contrary, H_2O transport is predominantly affected by the feed water temperature. Hence, increasing the NH_3 concentration in the feed water may allow for the maximisation of the NH_3 concentration in the recovered NH_3-H_2O mixtures by VMS. Furthermore, the transfer of NH_3 may be improved by adjusting the operating conditions and the membrane type. However, it is unknown how the feed water composition, operational conditions and membrane type affect the NH_3 and H_2O transfer. Moreover, it is unknown how much energy is needed to recover NH_3 as NH_3-H_2O mixtures by VMS. To this end, the considerations for the recovery of NH_3 by VMS lead to the following specific research topic:

B. NH_3 and H_2O transfer and corresponding energy consumption during NH_3 recovery by VMS, as a function of the feed water composition, operational conditions and membrane type.

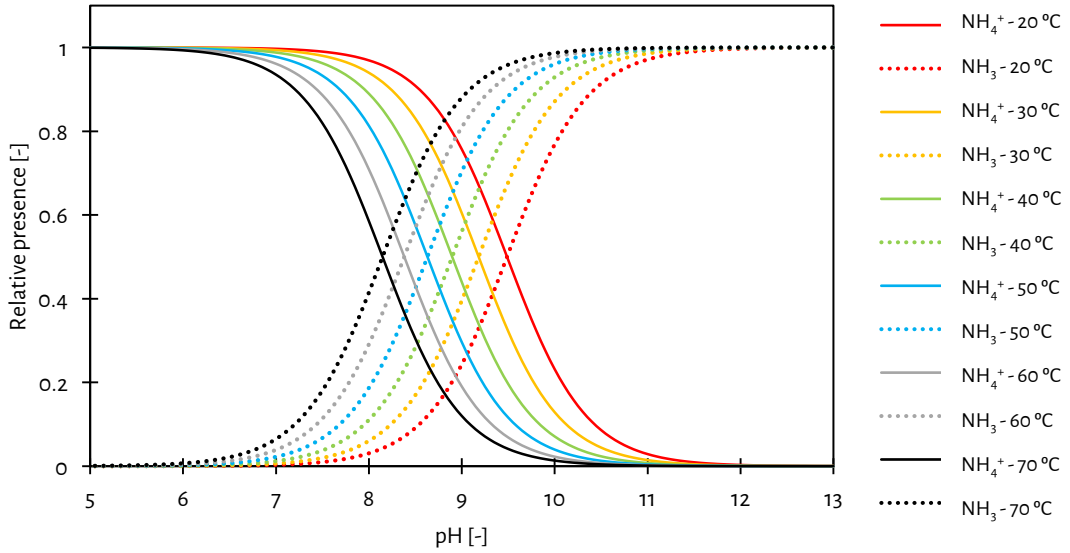

Figure 1-3 - The relative presence (or speciation) of NH_4^+ and NH_3 as a function of the solution pH and temperature. The effect of the ionic strength of the solution on the TAN speciation was not used as a variable in PHREEQC simulations, which provided the data for the graph.

1.3.4.3. ED and BPMED to produce concentrated TAN solutions

To maximise the NH_3 concentration in the recovered NH_3-H_2O mixtures, maximisation of the NH_3 concentration in the feed water is required. Obtaining high NH_3 concentrations in feed waters can be achieved by the addition of chemicals to feed waters with high NH_4^+ concentrations to increase the pH. According to Chapter 2.3.1, electrodialysis (ED) allows for competitive TAN removal from N-loaded residual waters, while simultaneously producing a concentrated NH_4^+ solution. However, there is limited information available on how much energy is required to produce concentrated NH_4^+ solution by ED and how the NH_4^+ concentration can be maximised. To this end, the use of ED leads to the following specific research topic:

C. Competitive NH_4^+ removal and production of concentrated NH_4^+ solutions by ED and corresponding electrical energy consumption;

Finally, according to Chapter 2.3.1, bipolar membrane electrodialysis (BPMED) can be used to produce concentrated NH_3 solutions as a feed for VMS, without using an external supply of chemicals. However, it is unknown whether BPMED can produce concentrated NH_3 solutions, while achieving competitive TAN removal from N-loaded residual waters. Moreover, the is no information on the energy consumption for BPMED to produce concentrated NH_3 solutions. To this end, the use of BPMED leads to the following specific research topic:

D. Competitive NH_4^+ removal and production of concentrated NH_3 solution and corresponding electrical energy consumption by BPMED;

1.3.5. Thesis structure

This thesis covers separate chapters on each specific research topic. All specific research topics are more elaborately introduced in the respective chapters. This thesis contains the following chapters:

1. Chapter 1: background information on the topic, problem description and research topics;
2. Chapter 2: literature review on potentially suitable N-loaded residual streams and technologies for TAN removal and the subsequent electricity generation from recovered NH_3;
3. Chapter 3: ED for simultaneous NH_4^+ removal and the production of concentrated NH_4^+ solutions (specific research topic D);
4. Chapter 4: BPMED for simultaneous NH_4^+ removal and production of concentrated NH_3 solutions (specific research topic C);
5. Chapter 5: selectivity of NH_3 over H_2O transfer during the recovery of NH_3 by VMS, for various membranes and operational conditions (specific research topic B);
6. Chapter 6: achievable NH_3 concentrations in NH_3-H_2O mixtures recovered during NH_3 recovery by VMS and the use of the recovered NH_3-H_2O mixtures as a fuel for an SOFC (specific research topic A and B);
7. Chapter 7: removal and recovery of TAN from real residual streams using a combination of technologies;
8. Chapter 8: conclusions and recommendations.

Figure 1-4 shows a schematic representation of this thesis outline and how the chapters are linked by technologies to remove TAN from N-loaded residual waters and the subsequent generation of electricity from the recovered NH_3. Chapter 1 introduces this thesis and Chapter 2 provides an extensive literature review on potentially suitable N-loaded residual streams and suitable technologies that can be used for TAN removal and recovery. The selection of the selected technologies in this thesis (ED, BPMED, VMS and SOFC) is predominantly based on Chapter 2. The separate technologies were the main subject of research in Chapter 3 (ED), 4 (BPMED), 5 (VMS) and 6 (VMS and SOFC). In the Chapters 3, 4, 5 and 6, synthetic feed waters are used for the conducted experiments. To demonstrate the feasibility of the proposed concept of TAN removal and recovery of NH_3 for electricity generation purposes, Chapter 7 focuses on the treatment of real N-loaded residual streams. Finally, Chapter 8 provides an overview of the conclusions and recommendations from this thesis.

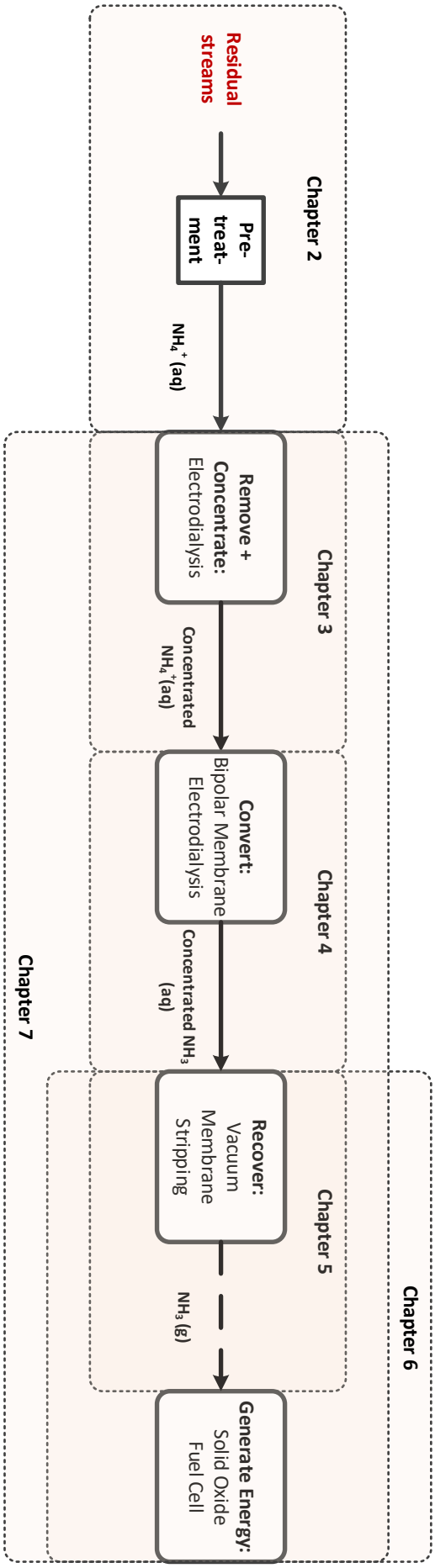

Figure 1-4 - A schematic representation of the structure of this thesis.

1.4. References

Cherkasov, N., Ibhadon, A. O., & Fitzpatrick, P. (2015). A review of the existing and alternative methods for greener nitrogen fixation. *Chemical Engineering and Processing: Process Intensification, 90*, 24-33. doi:https://doi.org/10.1016/j.cep.2015.02.004

Desloover, J., Vlaeminck, S. E., Clauwaert, P., Verstraete, W., & Boon, N. (2012). Strategies to mitigate N2O emissions from biological nitrogen removal systems. *Current Opinion in Biotechnology, 23*(3), 474-482. doi:https://doi.org/10.1016/j.copbio.2011.12.030

Erisman, J. W., Bleeker, A., Galloway, J., & Sutton, M. S. (2007). Reduced nitrogen in ecology and the environment. *Environmental Pollution, 150*, 140-149. doi:https://doi.org/10.1016/j.envpol.2007.06.033

Erisman, J. W., Sutton, M. A., Galloway, J., Klimont, Z., & Winiwarter, W. (2008). How a century of ammonia synthesis changed the world. *Nature Geoscience, 1*, 636. doi:10.1038/ngeo325

FAO. (2019). *World fertilizer trends and outlook to 2022*. Rome, Italy

Galloway, J. N., Dentener, F. J., Capone, D. G., Boyer, E. W., Howarth, R. W., Seitzinger, S. P., Asner, G. P., Cleveland, C. C., Green, P. A., Holland, E. A., Karl, D. M., Michaels, A. F., Porter, J. H., Townsend, A. R., & Vo, C. J. (2004). Nitrogen cycles : past , present , and future. *Biogeochemistry, 70*, 153-226.

Garagounis, I., Vourros, A., Stoukides, D., Dasopoulos, D., & Stoukides, M. (2019). Electrochemical synthesis of ammonia: Recent efforts and future outlook. *Membranes, 9*(9). doi:10.3390/membranes9090112

Giddey, S., Badwal, S. P. S., & Kulkarni, A. (2013). Review of electrochemical ammonia production technologies and materials. *International Journal of Hydrogen Energy, 38*(34), 14576-14594. doi:https://doi.org/10.1016/j.ijhydene.2013.09.054

Gonzalez-Martinez, A., Muñoz-Palazon, B., Rodriguez-Sanchez, A., & Gonzalez-Lopez, J. (2018). New concepts in anammox processes for wastewater nitrogen removal: recent advances and future prospects. *FEMS Microbiology Letters, 365*(6). doi:10.1093/femsle/fny031

Grasham, O., Dupont, V., Camargo-Valero, M. A., García-Gutiérrez, P., & Cockerill, T. (2019). Combined ammonia recovery and solid oxide fuel cell use at wastewater treatment plants for energy and greenhouse gas emission improvements. *Applied Energy, 240*, 698-708. doi:https://doi.org/10.1016/j.apenergy.2019.02.029

ISPT. (2017). Power to Ammonia: From renewable energy to CO2-free ammonia as chemical feedstock and fuel [Press release]. Retrieved from http://www.ispt.eu/media/P2A-press-release-March-2017.pdf

Kampschreur, M. J., Temmink, H., Kleerebezem, R., Jetten, M. S. M., & van Loosdrecht, M. C. M. (2009). Nitrous oxide emission during wastewater treatment. *Water Research, 43*(17), 4093-4103. doi:https://doi.org/10.1016/j.watres.2009.03.001

Lackner, S., Gilbert, E. M., Vlaeminck, S. E., Joss, A., Horn, H., & van Loosdrecht, M. C. M. (2014). Full-scale partial nitritation/anammox experiences - An application survey. *Water Research, 55*, 292-303. doi:10.1016/j.watres.2014.02.032

Lan, R., & Tao, S. (2014). Ammonia as a Suitable Fuel for Fuel Cells. *Frontiers in Energy Research, 2*(35). doi:10.3389/fenrg.2014.00035

Magri, A., Beline, F., & Dabert, P. (2013). Feasibility and interest of the anammox process as treatment alternative for anaerobic digester supernatants in manure processing--an overview. *J Environ Manage, 131*, 170-184. doi:10.1016/j.jenvman.2013.09.021

Matassa, S., Batstone, D. J., Hulsen, T., Schnoor, J., & Verstraete, W. (2015). Can direct conversion of used nitrogen to new feed and protein help feed the world? *Environmental Science and Technology, 49*(9), 5247-5254. doi:https://doi.org/10.1021/es505432w

Mehta, C. M., Khunjar, W. O., Nguyen, V., Tait, S., & Batstone, D. J. (2015a). Technologies to Recover Nutrients from Waste Streams: A Critical Review. *Critical Reviews in Environmental Science and Technology, 45*(4), 385-427. doi:10.1080/10643389.2013.866621

Mehta, C. M., Khunjar, W. O., Nguyen, V., Tait, S., & Batstone, D. J. (2015b). Technologies to Recover Nutrients From Waste Streams: A Critical Review. *Critical Reviews in Environmental Science and Technology, 45*, 385-427. doi:https://doi.org/10.1080/10643389.2013.866621

Papadias, D. D., Ahmed, S., & Kumar, R. (2012). Fuel quality issues with biogas energy – An economic analysis for a stationary fuel cell system. *Energy, 44*(1), 257-277. doi:https://doi.org/10.1016/j.energy.2012.06.031

Prather, M., Ehhalt, D., Dentener, F., Derwent, R., & Grubler, A. (2001). Atmospheric chemistry and greenhouse gases. In *Climate Change 2001: The Scientific Basis, Third Assessment Report*. IPCC: Working Group I of the Intergovernmental Panel on Climate Change.

Schaubroeck, T., De Clippeleir, H., Weissenbacher, N., Dewulf, J., Boeckx, P., Vlaeminck, S. E., & Wett, B. (2015). Environmental sustainability of an energy self-sufficient sewage treatment plant: Improvements through DEMON and co-digestion. *Water Research, 74*, 166-179. doi:https://doi.org/10.1016/j.watres.2015.02.013

Stambouli, A. B., & Traversa, E. (2002). Solid oxide fuel cells (SOFCs): a review of an environmentally clean and efficient source of energy. *Renewable and Sustainable Energy Reviews, 6*(5), 433-455. doi:https://doi.org/10.1016/S1364-0321(02)00014-X

Staniforth, J., & Ormerod, R. M. (2003). Clean destruction of waste ammonia with consummate production of electrical power within a solid oxide fuel cell system. *Green Chemistry, 5*(5), 606-609. doi:10.1039/B307396N

STOWA. (2013). *Struvietprecipitatie in combinatie met stikstofwinning en omzetting in een brandstofcel : evaluatie en verificatie technische en economische haalbaarheid* (9789057736353). Retrieved from Amersfoort: https://www.stowa.nl/publicaties/struvietprecipitatie-combinatie-met-stikstofwinning-en-omzetting-een-brandstofcel

The Royal Society. (2020). *Ammonia: zero-carbon fertiliser, fuel and energy store*. Retrieved from royalsociety.org/green-ammonia

Valera-Medina, A., Xiao, H., Owen-Jones, M., David, W. I. F., & Bowen, P. J. (2018). Ammonia for power. *Progress in Energy and Combustion Science, 69*, 63-102. doi:https://doi.org/10.1016/j.pecs.2018.07.001

Van Hulle, S. W. H., Vandeweyer, H. J. P., Meesschaert, B. D., Vanrolleghem, P. A., Dejans, P., & Dumoulin, A. (2010). Engineering aspects and practical application of autotrophic nitrogen removal from nitrogen rich streams. *Chemical Engineering Journal, 162*(1), 1-20. doi:10.1016/j.cej.2010.05.037

Vasilaki, V., Massara, T. M., Stanchev, P., Fatone, F., & Katsou, E. (2019). A decade of nitrous oxide (N2O) monitoring in full-scale wastewater treatment processes: A critical review. *Water Research, 161*, 392-412. doi:https://doi.org/10.1016/j.watres.2019.04.022

Vecino, X., Reig, M., Bhushan, B., Gibert, O., Valderrama, C., & Cortina, J. L. (2019). Liquid fertilizer production by ammonia recovery from treated ammonia-rich regenerated streams using liquid-liquid membrane contactors. *Chemical Engineering Journal, 360*, 890-899. doi:https://doi.org/10.1016/j.cej.2018.12.004

Xu, L., Dong, F., Zhuang, H., He, W., Ni, M., Feng, S., & Lee, P. (2017). Energy upcycle in anaerobic treatment: ammonium, methane, and carbon dioxide reformation through a hybrid electrodeionization-solid oxide fuel cell system. *Energy Conversion and Management, 140*, 157-166.

Zarebska, A., Romero Nieto, D., Christensen, K. V., Fjerbæk Søtoft, L., & Norddahl, B. (2015). Ammonium fertilizers production from manure: A critical review. *Critical Reviews in Environmental Science and Technology, 45*(14), 1469-1521. doi:10.1080/10643389.2014.955630

Chapter 2.

Residual streams and technologies for ammoniacal nitrogen recovery and energy generation

Based on:

Recovery and applications of ammoniacal nitrogen from nitrogen-loaded residual streams: A review

Zhe Deng, Niels van Linden, Elena Guillen, Henri Spanjers, Jules B. van Lier (2021)

https://doi.org/10.1016/j.jenvman.2021.113096

Abstract

In available literature, no studies assess potentially suitable residual streams for total ammoniacal nitrogen (TAN) removal, technologies for TAN recovery and the generation of electricity from ammonia (NH_3). This chapter presents the results of a literature study on the assessment of the feasibility of residual streams used for TAN removal and technologies allowing for TAN removal and recovery and electricity generation from recovered NH_3.

The first part describes the identification of thirteen (13) so-called nitrogen-loaded (N-loaded) residual streams, which contain at least 0.5 $g \cdot L^{-1}$ of total Kjeldahl nitrogen (TKN), which were subsequently characterised and divided into three categories. Category 1 represents streams with a low TAN/TKN ratio (< 0.5), requiring conversion of organic-N to TAN before TAN recovery. Category 2 represents streams with a high TAN/TKN ratio (≥ 0.5) and high solids content (> 1 $g \cdot L^{-1}$), requiring solids removal before TAN recovery. Category 3 represents streams with a high TAN/TKN ratio (≥ 0.5) and low solids content (≤ 1 $g \cdot L^{-1}$), which are suitable for TAN recovery.

The second part describes the required inputs and obtained outputs of TAN of various TAN recovery technologies. Reverse and forward osmosis and electrodialysis produce concentrated ammonium (NH_4^+) solutions, whereas (bio-)electrochemical cells and bipolar membrane electrodialysis produce concentrated NH_3 solutions. Struvite precipitation, air stripping followed by acid scrubbing and vacuum (membrane) stripping allow for the recovery of TAN as salt, NH_4^+-salt solution or gaseous NH_3, respectively. The respective technologies cover a wide range of feasible TAN concentrations, while the energy consumption is not consistently reported.

The third part discusses combustion-based and fuel cell technologies for the generation of electricity from NH_3. Solid oxide fuel cells allow for the generation of electricity with negligible emission of oxidised N-species, which is still a challenge for combustion-based technologies. Finally, currently available literature lacks information on the generation of electricity using NH_3 recovered from N-loaded residual streams or aqueous solutions as a fuel.

The provided overview may be used to define strategies for TAN recovery from N-loaded streams, based on the composition of the respective stream, suitable recovery technologies and the desired use of the recovered TAN.

Keywords

ammoniacal nitrogen; nitrogen-loaded; residual streams; resource recovery; anaerobic digestion;

2.1. Introduction

2.1.1. Ammoniacal nitrogen recovery

In the last decades, recovery of total ammoniacal nitrogen (TAN) from residual streams by both mature technologies such as chemical precipitation and stripping gained traction, as well as studies to novel technologies such as reverse osmosis (RO) and electrodialysis (ED) (Mehta et al., 2015a; Xie et al., 2016). However, currently available studies discuss the state-of-the-art of different available technologies from the perspective of one specific TAN application: the use of recovered TAN as a resource for fertilisers (Mehta et al., 2015a; Zarebska et al., 2015). Moreover, published review studies overlook or do not explore an important aspect of the TAN recovery potential, which is the existing available residual streams and their composition.

2.1.2. Research objective

This chapter assesses the feasibility of residual streams and technologies that are potentially suitable for TAN removal, TAN recovery in different forms and generation of electricity from recovered NH_3. This chapter is based on an extensive literature study. This chapter aims to provide a wider view on technologies that allow for the recovery of TAN from residual streams, especially residual waters, other than only for energy generation. More detailed information on the application of TAN as a fertiliser or as a resource for chemical and biochemical processes can be found in the review of Deng et al. (2021), which also assesses the application of anaerobic digestion (AD) to convert organically bound nitrogen (N), or total Kjeldahl nitrogen (TKN) to TAN. This chapter contains:

- The identification, characterisation and categorisation of residual streams that are potentially suitable for TAN recovery;
- An overview of various technologies that can be used for NH_3 recovery, based on their principle (concentrate TAN as NH_4^+, NH_3 or recover TAN as NH_3 from the liquid), the main energy input, the end product and challenges;
- An overview of various technologies that can be used for electricity generation using NH_3 as a fuel.

During the identification of suitable residual streams, a wide range of descriptions of the term "nitrogen-loaded": "nitrogen rich", "high nitrogen content" and "high strength nitrogen" was encountered. In this chapter, the term "nitrogen-loaded" (hereafter N-loaded) refers to residual streams containing TKN concentrations of at least 0.5 $g \cdot L^{-1}$ or $g \cdot kg^{-1}$. Furthermore, in this chapter, the term "N-loaded residual streams" refers to all N-loaded streams (aqueous, slurries, etc.), whereas the term "N-loaded residual waters" refers to aqueous solutions.

2.2. N-loaded residual streams

2.2.1. Parameters for characterisation of N-loaded residual streams

To characterise the N-loaded residual streams, this chapter assesses only collected data on various key parameters that should be considered for their treatment to allow for TAN recovery. These parameters concern concentrations of: total suspended solids (TSS), chemical oxygen demand (COD), TKN and TAN. To report consistently, the TSS, COD, TKN and TAN concentrations were normalised to parts per thousand, which corresponds to $g \cdot kg^{-1}$ and $g \cdot L^{-1}$ for solid and liquid streams (assuming a liquid density of 1,000 $g \cdot L^{-1}$), respectively. The TSS indicates the feasibility to use directly physicochemical technologies for the recovery of TAN or the need for pre-treatment by for example filtration. The COD is an indication of the presence of organic matter, which must be decreased before discharge to receiving water bodies. Also, a high COD is likely to induce fouling in the physicochemical technologies for TAN recovery, indicating the need for pre-treatment.

The absolute TKN content is an indication of the amount of nitrogen that is present as both organic nitrogen and TAN. The TAN/TKN ratio indicates the dominant present form of N. Data collected for this chapter suggests that physicochemical technologies, such as stripping and precipitation, can be used for direct TAN recovery, for example, pre-treatment steps such as the conversion of organic nitrogen to TAN or solids removal is not needed, at a TAN/TKN ratio higher than 0.5; TAN/TKN ratios lower than 0.5 suggest that the organic nitrogen must be first converted to TAN to allow for recovery of TAN.

When it is necessary to convert organic nitrogen to TAN, the COD/N ratio must also be considered. Typically, when the COD/N ratio of residual streams falls within a certain range (for example, 20 - 30), biochemical technologies such as AD are suitable to decrease the organic matter content, without potential problems of nitrogen shortage or inhibition (Rajagopal et al., 2013). Regarding the nitrogen in the COD/N ratio, this could refer to either the TN (including organic and inorganic N) or the TKN. It must be noted that under anaerobic conditions TKN is assumed to be equal to TN so the COD/N ratio can be calculated with TKN or TN.

2.2.2. Identification and characterisation of N-loaded residual streams

For this chapter, data on N-loaded residual streams from approximately 150 studies was obtained, all using real residual streams either for analytical or experimental research purposes. For each identified N-loaded residual stream, at least three independent references were used and the average, minimum and maximum values of the characteristic parameters are reported. The N-loaded residual streams are divided into four different groups, based on their origins: solid residual streams, manure, liquid residual streams (all domestic) and residual streams reported to originate from industrial processes. The obtained average, minimum and maximum values are presented in Figure 2-1. In the text, only average values are referred to. More details on the consulted references, such as the TSS, COD, TKN and TAN content, the respective units, used treatment technologies and reference details can be found in the supplementary material of the review of Deng et al. (2021).

2.2.2.1. Solid residual streams

The first group includes: bio- and food waste, the organic fraction of municipal solid waste (OFMSW) and spent biomass, such as the waste activated sludge from wastewater treatment plants (WWTPs) and algal sludge (Mata-Alvarez et al., 2000). Typical TSS values for bio- and food waste and OFMSW are 269 and 333 $g \cdot kg^{-1}$ (ranges can be consulted in Figure 2-1), respectively, while the COD content is 428 and 644 $g \cdot kg^{-1}$, respectively. For the spent biomass streams, the TSS and COD are considerably lower than for bio- and food waste and OFMSW: 49 and 50 $g \cdot kg^{-1}$, respectively. The typical TAN content of the solid residual streams is 1 $g \cdot kg^{-1}$. Furthermore, the TKN ranges between 3 – 12 $g \cdot kg^{-1}$ and is mainly represented by the presence of proteins (Braguglia et al., 2018; Ganesh Saratale et al., 2018). The relatively low TAN/TKN ratios (ranging from 0 to 0.3) indicate that direct TAN recovery will be challenging. To allow for effective TAN recovery, the TAN/TKN ratio must be increased by converting organic nitrogen to TAN. For bio- and food waste and OFMSW, the COD/N ratio is 47 and 60, respectively, whereas for spent biomass the COD/N ratio is 14, because of the lower COD content. Anaerobic (co-)digestion is a widely applied technology to treat these solid residual streams, due to the relatively high COD (> 10 $g \cdot kg^{-1}$) and nitrogen contents (> 0.5 $g \cdot kg^{-1}$) (Hartmann & Ahring, 2005; Keucken et al., 2018). Anaerobic (co-)digestion allows for the simultaneous decrease of the solids and COD content of the residual streams, while the organic nitrogen is converted to TAN, increasing the TAN/TKN ratio.

2.2.2.2. Manure

The second group concerns manure, which is frequently reported to contain high levels of TAN and TSS, and is often considered to be problematic for its treatment via AD (Massé et al., 2014; Rodriguez-Verde et al., 2018). Manure is divided into poultry, cattle and swine manure. Poultry manure has the highest TSS, COD and TKN: 521, 661 and 35 $g \cdot kg^{-1}$, respectively. Despite the low TAN/TKN ratio (TAN/TKN close to 0) of poultry manure, its absolute TAN content is high, for example, 2 $g \cdot kg^{-1}$, practically 92% nitrogen is present as organic nitrogen in poultry manure. Cattle and swine manure have a much lower content of TSS, for example, 81 and 24 $g \cdot kg^{-1}$, respectively, COD, for example, 58 and 36 $g \cdot kg^{-1}$, respectively, and TKN, for example, 4 $g \cdot kg^{-1}$. The TAN of cattle manure is 1 $g \cdot kg^{-1}$, whereas swine manure has a TAN of 4 $g \cdot kg^{-1}$. The nitrogen in cattle manure is predominantly present as organic nitrogen (TAN/TKN ratio is 0.4), whereas in swine manure nitrogen is already present predominantly as TAN (TAN/TKN ratio is 0.7). The COD/N ratio of the various types of manure ranges between 8 and 32. According to the consulted studies, manure is mainly treated by AD but, due to the high level of TAN, is often co-digested with other organic residues to suppress the negative effects of the presence of TAN during the AD processes (Hartmann & Ahring, 2005; Mata-Alvarez et al., 2014).

2.2.2.3. Liquid residual streams (residual waters)

The third group includes leachate, the liquid fraction of raw swine manure (swine liquid) and human (source-separated) urine. The TSS of swine liquid and urine streams is below 1 $g \cdot L^{-1}$, whereas conversely, leachates can contain high amounts of suspended solids (19 $g \cdot L^{-1}$). Regarding COD, leachates and swine

liquid contain 26 and 31 g·L^{-1}, respectively, whereas human urine ranges between 5 and 10 g·L^{-1}. The TKN content for all the liquid N-loaded residual streams (N-loaded residual waters) ranges between 3 and 7 g·L^{-1}. For leachate, swine liquid and stored human urine, the TAN/TKN is at least 0.8. Fresh human urine, however, has a TAN/TKN ratio of 0.0, because nitrogen is still present as urea. When urine is stored, urea is hydrolysed to TAN, increasing the TAN/TKN ratio. When leachates contain high TSS and COD and have a high COD/N ratio, anaerobic (co-)digestion can be applied for the treatment of the organic fraction (Lei et al., 2018; Montusiewicz et al., 2018).

2.2.2.4. Industrial residual streams

The fourth group concerns those N-loaded residual streams that have an industrial origin, such as mining and fertiliser industry and fish/fishmeal processing. Amongst these industrial N-loaded residual streams, fishery residual water has the highest COD content (110 g·L^{-1}) and TKN content (3 g·L^{-1}), and the TKN is mostly present as organic nitrogen (TAN/TKN ratio of 0.3). Residual streams originating from mining and fertiliser industries have a much lower COD content (1 and 0 g·L^{-1}, respectively), while all nitrogen is present as TAN (TAN/TKN is 1.0). The TAN content of mining and fertiliser industry residual streams is 5 and 2 g·L^{-1}, respectively. For the treatment of fishery residual streams, AD has been used (Guerrero et al., 1999), whereas physicochemical TAN recovery technologies and biological oxidation processes were used to treat mining and fertiliser residual water (Noworyta et al., 2003; Huang et al., 2011). Finally, there are also specific (industrial) N-loaded residual streams that are not represented in Figure 2-1, but are considered to be N-loaded and therefore potentially interesting for recovery. For example, TAN content of glutamate wastewater ranges between 16 - 19 g·L^{-1} (Yang et al., 2005; Wang et al., 2011); pectin wastewater can contain around 1.4 g·L^{-1} (Degn Pedersen et al., 2003); slaughterhouse wastewater ~ 0.7 g·L^{-1} (Kundu et al., 2013); nuclear wastewater ~ 35 g·L^{-1} (Gain et al., 2002); coking wastewater can contain between 0.2 - 0.6 g·L^{-1} (Jin et al., 2013; Lin et al., 2018) and ion exchange brine up to 3.9 g·L^{-1} (Vecino et al., 2019). These residual streams also have a high potential for TAN recovery, but insufficient information on their composition and current treatment is available for further assessment.

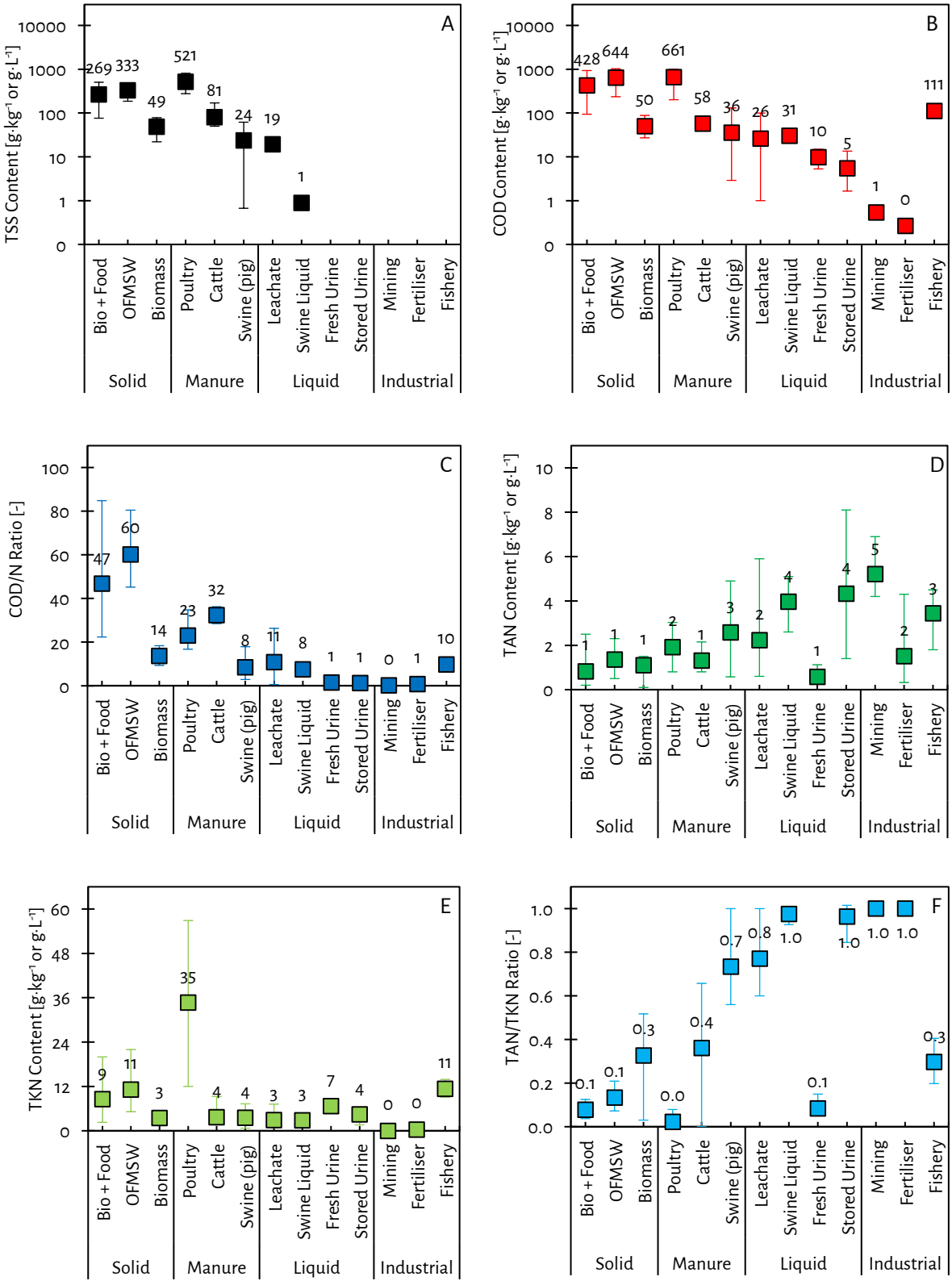

Figure 2-1 - An overview of the identified N-loaded residual streams and their characteristics in terms of TSS (A), COD (B), TKN (D) and TAN (E) content and the respective calculated COD/N (C) and TAN/TKN (F) ratios. The presented values and error bars represent the averages and minimum and maximum values of at least three independently consulted references. The consulted references are extensively presented and referred to in the Supporting Information of the review of Deng et al. (2021).

2.2.3. Categorisation of N-loaded residual streams

2.2.3.1. Category 1: TAN/TKN < 0.5

Category 1 contains N-loaded residual streams with a TAN/TKN ratio < 0.5 and a TSS and COD content both higher than 24 and 36 $g \cdot kg^{-1}$, respectively. For these streams, the TAN/TKN must be increased to at least 0.5 to allow for subsequent effective TAN recovery. The N-loaded residual streams that require this organic nitrogen to TAN conversion step are bio- and food waste, OFMSW, spent biomass, poultry and cattle manure. Various biochemical and physicochemical processes, such as AD, can be used to increase the TAN/TKN ratio by conversion of organic nitrogen to TAN, while simultaneously the TSS and COD content is decreased. The conversion of organic nitrogen to TAN by AD is discussed in the review of Deng et al. (2021).

2.2.3.2. Category 2: TAN/TKN ≥ 0.5, TSS > 1 $g \cdot L^{-1}$

Category 2 contains N-loaded residual streams with a TAN/TKN ratio greater than 0.5 and TSS concentrations higher than 1 $g \cdot L^{-1}$. The application of AD to treat various organic N-loaded residual streams from category 1 leads to the generation of digestate (which falls into this category), having a TAN/TKN ratio greater than 0.5. Direct TAN recovery is possible by solids-tolerant recovery technologies, such as struvite precipitation and air stripping (see 2.3) for digestate with TSS up to 1 $g \cdot L^{-1}$. However, for recovery technologies that are prone to fouling (mostly membrane-based technologies), the feed stream must be made free from solids by using solid-liquid separation (centrifugation or belt-press filtration), sedimentation, sand filtration, micro- or ultrafiltration.

2.2.3.3. Category 3: TAN/TKN ≥ 0.5, TSS ≤ 1 $g \cdot L^{-1}$

Category 3 contains N-loaded residual streams with a TAN concentration higher than 0.5 $g \cdot L^{-1}$, a TAN/TKN ratio greater than 0.5 and TSS ≤ 1 $g \cdot L^{-1}$. Within category 3, the liquid residual streams (residual waters), such as solids-free leachate, filtered swine liquid and urine and various industrial N-loaded residual streams coming from mining and fertiliser industry are placed. According to the obtained data with respect to applied treatment technologies, these residual streams are considered suitable for direct TAN recovery by technologies discussed in 2.3.

2.2.4. Interpretation of categories of N-loaded residual streams

The proposed categories indicate the suitability and the path for TAN recovery. For category 1 streams, the organic nitrogen needs to be converted to TAN to increase the TAN/TKN ratio, which is usually achieved by AD. Then the TAN must be separated from the solids to make the liquid stream or N-loaded residual water suitable for TAN recovery. Hence, category 1 streams require the most (pre-)treatment steps, whereas category 3 streams, require the least. The N-loaded residual waters in category 3 can be found in specific industries, such as mining and chemical industries, and have a high potential for TAN recovery because of their high TAN concentrations and low TSS content. However, access to this information is usually limited.

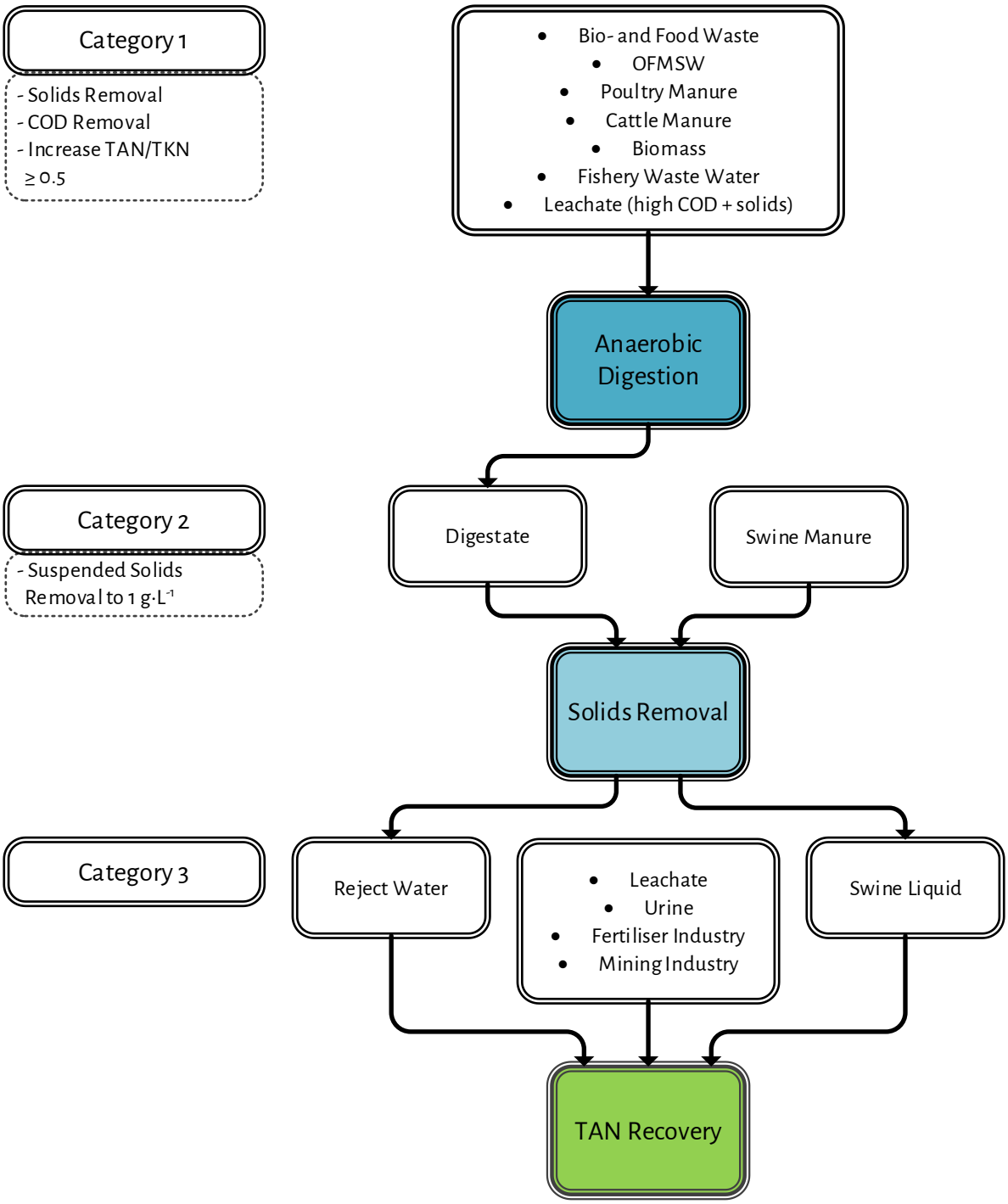

Figure 2-2 - A strategic categorisation of the various N-loaded residual streams, based on their characteristics and required (pre-)treatment before TAN recovery.

2.3. Technologies to recover TAN from N-loaded residual waters

2.3.1. Technologies to concentrate TAN

Solid-liquid separation or complete solids removal is preferred before TAN recovery. To this end, mature technologies such as centrifugation, filter presses, media (sand) filtration or microfiltration and ultrafiltration, can be applied to reduce the TSS concentration to below 1 $g \cdot L^{-1}$ (2%) (Masse et al., 2007; Zarebska et al., 2015). The technologies discussed below are considered to be used at a TSS concentration lower than 1 $g \cdot L^{-1}$ or else after full solids removal.

2.3.1.1. Reverse and forward osmosis

In reverse osmosis (RO), the N-loaded residual water is pressurised to allow for water permeation through a membrane that rejects practically all dissolved substances. To effectively use RO as concentration technology by rejecting TAN and decreasing the volume of the N-loaded residual water, TAN must be present as NH_4^+, because uncharged NH_3 can easily permeate through the membrane (Masse et al., 2008). For example, Mondor et al. (2008a) and Gong (2013) reported final TAN concentrations of 12.8 and 12 $g \cdot L^{-1}$ in the concentrate after using RO to treat filtered swine manure reject water, respectively. The concentration factor (CF), relating the final achieved concentration to the ingoing concentration of the respective N-loaded residual water, was 1.5 and 3.6, respectively. Ledda et al. (2013) achieved TAN concentrations of 5.7 and 7.3 $g \cdot L^{-1}$, with a CF of 4, after treating cow and swine reject water pre-treated by ultrafiltration, respectively. In addition, Schoeman and Strachan (2009a) obtained 1.8 $g \cdot L^{-1}$, CF of 2, after concentrating solid waste leachate by RO. Finally, Fu et al. (2011) used RO to concentrate TAN in simulated acid scrubber effluent and reported a final TAN concentration of 12.6 $g \cdot L^{-1}$ (CF of 3, based on the reported volume reduction and NH_4^+ rejection) and Noworyta et al. (2003) produced an RO concentrate with a TAN concentration of 11 $g \cdot L^{-1}$ (CF of 8) after treating NH_4NO_3 condensate from fertiliser industry.

Forward osmosis (FO) uses a saline draw solution to force water permeation from the feed water by osmosis, while most (except volatile) dissolved substances are rejected by a membrane. Holloway et al. (2007) reported a water recovery of 70% and an NH_4^+ rejection of 92% for the use of FO to concentrate nutrients in filtered sludge reject water, resulting in a final TAN concentration of 4 $g \cdot L^{-1}$ (CF of 3). Interestingly, even though the same water recovery was achieved on manure digestate by Li et al. (2020), the authors did not succeed to concentrate TAN by FO as the rejection of NH_4^+ was less than 40%.

According to the consulted studies, the maximum CF that can be achieved by RO and FO for TAN in N-loaded residual waters is about 6 and 3, respectively. The CF for RO and FO is mainly limited by the water recovery. Furthermore, as a result of the effective rejection (and thus concentration) of substances such as humic acids and multivalent ions by RO and FO, membrane fouling was observed in many studies (Holloway et al., 2007; Masse et al., 2007; Xie et al., 2016; Li et al., 2020), even when pre-treatment by (membrane) filtration was applied. Hence, extensive membrane cleaning is required, to allow for the stable operation to concentrate TAN by RO and FO when substances in the feed stream are present that induce particulate fouling, scaling

or organic fouling. Finally, because the membranes reject practically everything, also other concentrated compounds (organics and salts) are present in the concentrated NH_4^+ solution.

2.3.1.2. (Bio-)electrochemical cells

In (bio-)electrochemical cells ((B)ECs), TAN is transported as NH_4^+ from the anode compartment, through a cation exchange membrane, to the cathode compartment when an electric current is applied. In the last decade, these technologies have been widely applied to recover TAN from N-loaded residual waters as urine and reject water, containing NH_4^+ feed concentrations up to 4 g·L^{-1} (Rodríguez Arredondo et al., 2015; Kuntke et al., 2018). The various types of (B)ECs comprise microbial fuel cells (MFCs), microbial electrolysis cells (MECs) and electrochemical cells (ECs). While MFCs are actually able to recover TAN and simultaneously produce energy, the highest reported NH_4^+ fluxes (0.08 kg-N·m^{-2}·d^{-1}) are 6.5 times lower than for MECs (0.52 kg-N·m^{-2}·d^{-1}) and 4.8 times lower than for ECs (0.38 kg-N·m^{-2}·d^{-1}) (Kuntke et al., 2018). The higher NH_4^+ fluxes in MECs and ECs are attained at the expense of external electricity supply, which results in a higher electrical energy consumption for MECs (4 – 22 MJ·kg-N^{-1}) and ECs (18 – 94 MJ·kg-N^{-1}) compared to the energy-producing MFCs (- 10 MJ·kg-N^{-1}) (Kuntke et al., 2018). The wide range of reported electrical energy consumptions by the (B)ECs can be explained by the very wide range of achieved TAN removal efficiencies (1 – 100%). Based on the reported (B)ECs data, the efforts to decrease the electrode and membrane areas, for which increased NH_4^+ fluxes are required, led to higher electrical energy consumptions.

(B)ECs are actually used to concentrate TAN, and are mostly combined with stripping and scrubbing of NH_3, allowing for actual TAN recovery (Kuntke et al., 2018). Hence, very little attention is paid to the concentrations of TAN obtained in the cathode compartment. The study of Ledezma et al. (2017) reported a final concentration of 26.2 g-N·L^{-1} (CF of 4.5) in the cathode during the recovery of TAN from synthetic urine by a novel MEC, while Kuntke et al. (2014) achieved a concentration of 7 g-N·L^{-1} when concentrating TAN in an MEC (CF of 10). A convenient aspect of (B)ECs is the reduction of water at the cathode side, resulting in the generation of OH^-, allowing for an in-situ pH increase while no chemicals are needed. Hence, the concentrated TAN solution produced by (B)ECs contains dissolved NH_3. Interestingly, no limitations by fouling were reported in the reviews of Kuntke et al. (2018) and Rodríguez Arredondo et al. (2015) while urine, (pig) digestate, reject water leachate were used as feed streams. The apparent tolerance of (B)ECs to blockage by solids and fouling is possibly explained by the relatively wide anode compartments and the fact that the feed water is not pressurised and forced through the membrane.

2.3.1.3. (Bipolar membrane) electrodialysis

Similar to (B)ECs, TAN is transported as NH_4^+ from the N-loaded residual water when an electric current is applied in electrodialysis processes. Because ED contains alternating cation and anion exchange membranes, alternating feed water and concentrate channels are formed. Eventually, the transported TAN ends up as concentrated NH_4^+ in the so-called ED concentrate. Pronk et al. (2006b) applied ED to concentrate 93% of the TAN from source-separated urine and achieved a final concentration of 14.2 g·L^{-1} (CF of 2.9).

Studies performed by Mondor et al. (2008a) and Ippersiel et al. (2012) showed that ED can be used to remove TAN by 75 – 85% from filtered manure reject water and that final TAN concentrations between 14 – 21 g·L^{-1} can be achieved (CF up to 5.6) for an electrical energy consumption ranging between 66 and 71 MJ·kg-N^{-1}. Furthermore, Ward et al. (2018) achieved a CF of 8.5 in the ED concentrate of 120 L by removing 23% of the TAN from 5,400 L sludge reject water at an electrical energy consumption of 18 MJ·kg-N^{-1}, leading to a final TAN concentration of 7 g·L^{-1}. Furthermore, by optimising the applied current density (which will minimise osmotic water transport and ion back-diffusion), the TAN concentration can be increased from 1.5 to 10 g·L^{-1} (CF of 6.7) for 90% TAN removal at an electrical energy consumption of 5 MJ·kg-N^{-1} (van Linden et al., 2019b). By using bipolar membrane electrodialysis (BPMED), TAN can be transported from the N-loaded residual water as NH_4^+ and simultaneously be concentrated as dissolved NH_3 due to the production of OH^- by bipolar membranes, which only requires electricity (van Linden et al., 2020). According to the study of van Linden et al. (2020), at least 85% TAN removal can be achieved by BPMED for the production of 5 g·L^{-1} of NH_3 at the expense of 19 MJ·kg-N^{-1}. Dissolved NH_3 concentrations of 46 and 54 g-NH_3·L^{-1} starting from synthetic NH_4Cl and NH_4NO_3 solutions containing 37 and 45 g-NH_4^+·L^{-1}, respectively, were achieved by Li et al. (2016) and Gain et al. (2002), respectively. A study performed by Pronk et al. (2006c) resulted in the production of a solution containing 2.5 g-NH_3·L^{-1} after treating diluted urine with an initial TAN concentration of 4.9 g·L^{-1} by BPMED, while Shi et al. (2018) used BPMED to completely remove TAN from synthetic pig manure reject water at the expense of 58 MJ·kg-N^{-1}, reaching a final concentration of 13.8 g-NH_3·L^{-1}.

Similar to FO and RO, feed waters with low solids concentrations are desired for ED and BPMED, to avoid particulate fouling between the spacers and membranes. Besides, in available studies on ED to concentrate TAN, organic fouling and scaling on the membranes was reported (Mondor et al., 2009; Shi et al., 2019). Fouling in ED can be reversed and limited by chemical cleaning, reversing the electrode polarity (Shi et al., 2019) or by avoiding the transport of scaling substances (multivalent ions) and humic acids by using selective membranes (Kim et al., 2002). In the few published studies on BPMED to recover TAN from N-loaded residual waters, no information on fouling was reported.

2.3.2. Technologies to recover TAN

2.3.2.1. Struvite precipitation

The addition of magnesium to N-loaded residual waters containing both TAN and phosphate within the optimum pH range (pH = 8 – 9) leads to the precipitation of struvite crystals ($MgNH_4PO_4·6H_2O$, having an NH_4^+ content of 7 wt%), which can be used as fertiliser (Mehta et al., 2015a; Zarebska et al., 2015). Struvite precipitation is widely applied to avoid undesired scaling in pipelines during the transport of digestate and for the recovery of phosphorus. Moreover, struvite formation can directly be achieved in manure reject water, suggesting that struvite precipitation has a high tolerance to the presence of solids in the N-loaded residual water (Mehta et al., 2015a; Zarebska et al., 2015). However, in N-loaded residual waters, TAN is present in excess molar concentrations with respect to phosphate (equal molar concentrations required to form struvite) resulting in a TAN removal efficiency of struvite precipitation limited to 15 - 30% (Mehta et al.,

2015a; Zarebska et al., 2015). The energy consumption of chemical precipitation for the removal and recovery of TAN was reported by Magrí et al. (2013) to be 59 MJ·kg-N^{-1}, taking the use of chemicals into account.

2.3.2.2. (Air) stripping and acid scrubbing

TAN can also be recovered as NH_3 by air stripping (AS), for example from manure and sludge reject water (Magrí et al., 2013; Zarebska et al., 2015) and recovery of TAN from cathode solutions produced by (B)ECs (Kuntke et al., 2018). Because the vapour pressure of NH_3 in fresh air is negligibly low, NH_3 transport from the N-loaded residual water to the air takes place. TAN recovery by AS in stripping towers has a high tolerance of solids as studies reported that no pre-treatment of digestate was required (Mehta et al., 2015a; Zarebska et al., 2015), while it should be noted that scaling of minerals requires cleaning. However, before NH_3 effectively can be stripped, the pH of the N-loaded residual water must be increased to convert NH_4^+ to NH_3, by means of chemical addition, CO_2 stripping or electrochemical reactions (water reduction or water dissociation).

The actual concentrations of NH_3 in the air after NH_3 stripping according to the study of Wang et al. (2010) are below 9,000 ppm (corresponding to 0.9 wt%). Besides, based on the reported NH_3 mass flows and the used air flow rates, the concentration of NH_3 in the air is well below 1 wt% according to the studies of Bonmati and Flotats (2003) and Lei et al. (2007). Hence, by using AS, only diluted gaseous NH_3 is obtained. By subsequent scrubbing of the NH_3 gas-containing air with acid, dissolved NH_4^+ solutions or even solid NH_4^+ salts such as ammonium sulphate ($(NH_4)_2SO_4$), ammonium bicarbonate (NH_4HCO_3) or ammonium nitrate (NH_4NO_3) can be obtained (Bonmati & Flotats, 2003; Ukwuani & Tao, 2016; Kuntke et al., 2018). The energy consumption of AS and subsequent scrubbing in acid ranges from 14 to 50 MJ·kg-N^{-1} and depends strongly on the TAN concentration and temperature of the N-loaded residual water (Mehta et al., 2015a; Zarebska et al., 2015). However, not all reported values consistently consider the energy for the addition of heat and the addition of chemicals.

By using hydrophobic membranes, which are impermeable for liquids, but permeable for vapours and gases, to separate the liquid and gas phase, small installation footprints can be realised by providing a large contact area per unit of volume between the feed water and the permeate. Moreover, the pressure of the liquid can be controlled independently of the pressure of the gas. When an acidic solution is recirculated in the permeate side and the feed water contains dissolved NH_3, stripping and direct scrubbing takes place, resulting in the direct production of a solution containing NH_4^+. This configuration of NH_3 stripping and scrubbing is called direct membrane contactors (DMCS) or transmembrane chemisorption (TMCS).

According to the review studies of Zarebska et al. (2015), Mehta et al. (2015a) and Kuntke et al. (2018), the DMCS or TMCS was widely applied to directly scrub the stripped NH_3 from digestates, reject waters, stored urine and from the cathode compartment solutions from (B)ECs, even though TSS concentrations of up to 20 g·L^{-1} were present. The review of Beckinghausen et al. (2020) reported that the energy consumption was about 4 MJ·kg-N^{-1}, but it remains unclear whether this includes the use of heat and chemicals such as H_2SO_4.

2.3.2.3. Vacuum (membrane) stripping

Finally, stripping of NH_3 also can be achieved by applying a vacuum, which avoids the presence of air in the vapour that contains the stripped NH_3. Ukwuani and Tao (2016) successfully used vacuum stripping (VS) in combination with acid scrubbing to recover NH_3 from water (aqueous solution) at various feed water temperatures and vacuum pressures from manure, food waste, sludge digestate and landfill leachate (containing 1.0 – 6.4 $g \cdot L^{-1}$ of NH_3). According to the review of Beckinghausen et al. (2020), the required energy for TAN recovery by VS was 215 $MJ \cdot kg\text{-}N^{-1}$, which is mainly required for increasing the feed water temperature. However, besides the stripping of NH_3, also water is evaporated during VS and vacuum membrane stripping (VMS) resulting in a gaseous NH_3 and water vapour mixture (He et al., 2018). In fact, the ratio of the NH_3 flux to the total flux (water and NH_3) during VMS to recover at NH_3 at TAN feed concentrations ranging 1 – 4 $g \cdot L^{-1}$ was only 1% (NH_3 concentration of 1 wt%) in unfiltered digestate in the studies of He et al. (2017) and He et al. (2018). However, according to the study of El-Bourawi et al. (2007), the NH_3 in the recovered gas increases from 1.2 to 6.8 wt% when the concentration of NH_3 in the liquid feed is increased from 5 to 20 $g\text{-}NH_3 \cdot L^{-1}$, respectively.

2.3.3. Discussion on TAN concentration and recovery technologies

Table 2-1 provides an extensive overview of the key information of the various technologies to concentrate and recover TAN. For almost all technologies (except for struvite precipitation), the actual energy consumption depends heavily on the feed water characteristics, the operational conditions and the actual performance. In currently available literature, the energy consumption for RO and FO is not directly reported. Hence, to concentrate TAN by RO and FO, high TAN rejections and water recoveries must be achieved, leading to an increase in osmotic pressure throughout the operation, which will ultimately translate to a higher energy consumption. Also, the required information to determine the energy consumption to concentrate TAN is lacking. Therefore, there is a need to assess and normalise the energy consumption to concentrate TAN by RO and FO, which will be a function of the TAN feed concentration and rejection, the water recovery and flow rate, transmembrane membrane pressure and pump efficiency. The same holds for (B)ECs and (BPM)ED, for which the energy consumption to concentrate TAN strongly depends on the feed concentration, the amount of TAN transported, the efficiency of using electric charge and the resistance of the cell and membrane stacks. When sufficient data is available, there is potential to normalise the data and derive technology-specific energy values to concentrate TAN.

Finally, to actually recover TAN as gaseous NH_3, NH_4^+ solution or solid NH_4^+ crystals, the energy consumption must be expressed including the required amount of heat and energy to produce chemicals and to increase the pH and scrub the NH_3. Only when normalised information is available on the various strategies and technologies to recover TAN, fair comparisons between technologies can be made. Eventually, the choice to use a certain technology or combination of technologies will depend on the availability of local resources, the potential to use the recovered products and the financial implications.

Table 2-1 - An overview of the various technologies that can be used to concentrate or recover TAN from N-loaded residual waters.

	Technology	TAN Feed Conc.	Required Input	Solids Tolerance	End products	Product Conc.	Energy Consumption	References
		$g \cdot L^{-1}$	-	-	-	m% TAN	$MJ \cdot kg\text{-}N^{-1}$	
Concentrating TAN	RO	0.9 – 8.5	Electricity	Low	NH_4^+ (aq)	1.3	n.r.	(Mondor et al., 2008a; Schoeman & Strachan, 2009b)
	FO	1.3	Electricity. + salt solution	Low	NH_4^+ (aq)	0.4	n.r.	(Holloway et al., 2007)
	(B)ES	0.7 – 5.8	Electricity	Low	NH_3 (aq)	0.7 - 2.6	-10 - 94*	(Kuntke et al., 2018)
	ED	0.8 – 4.9	Electricity	Low	NH_4^+ (aq)	0.7 - 2.1	18 - 71	(Mondor et al., 2008a; Ippersiel et al., 2012; Ward et al., 2018)
	BPMED	4.9 - 45	Electricity	Low	NH_3 (aq)	0.5 - 1.4	58	(Shi et al., 2018)
Recovery of TAN	Precipitation	n.r.	Base and salt	High	$MgNH_4PO_4 \cdot (6\ H_2O)$ (s)	7	59	(Magrí et al., 2013)
	AS (+ Scrub)	0.5 – 6.7	Electricity, heat and base (acid)	High	NH_3-air (g) (NH_4^+ (aq))	0.9 (7 - 14)	14 - 50	(Mehta et al., 2015b; Zarebska et al., 2015)
	V(M)S	1 - 12	Electricity, heat and base	High	NH_3-water (g)	1.0 - 6.8	215	(Beckinghausen et al., 2020)

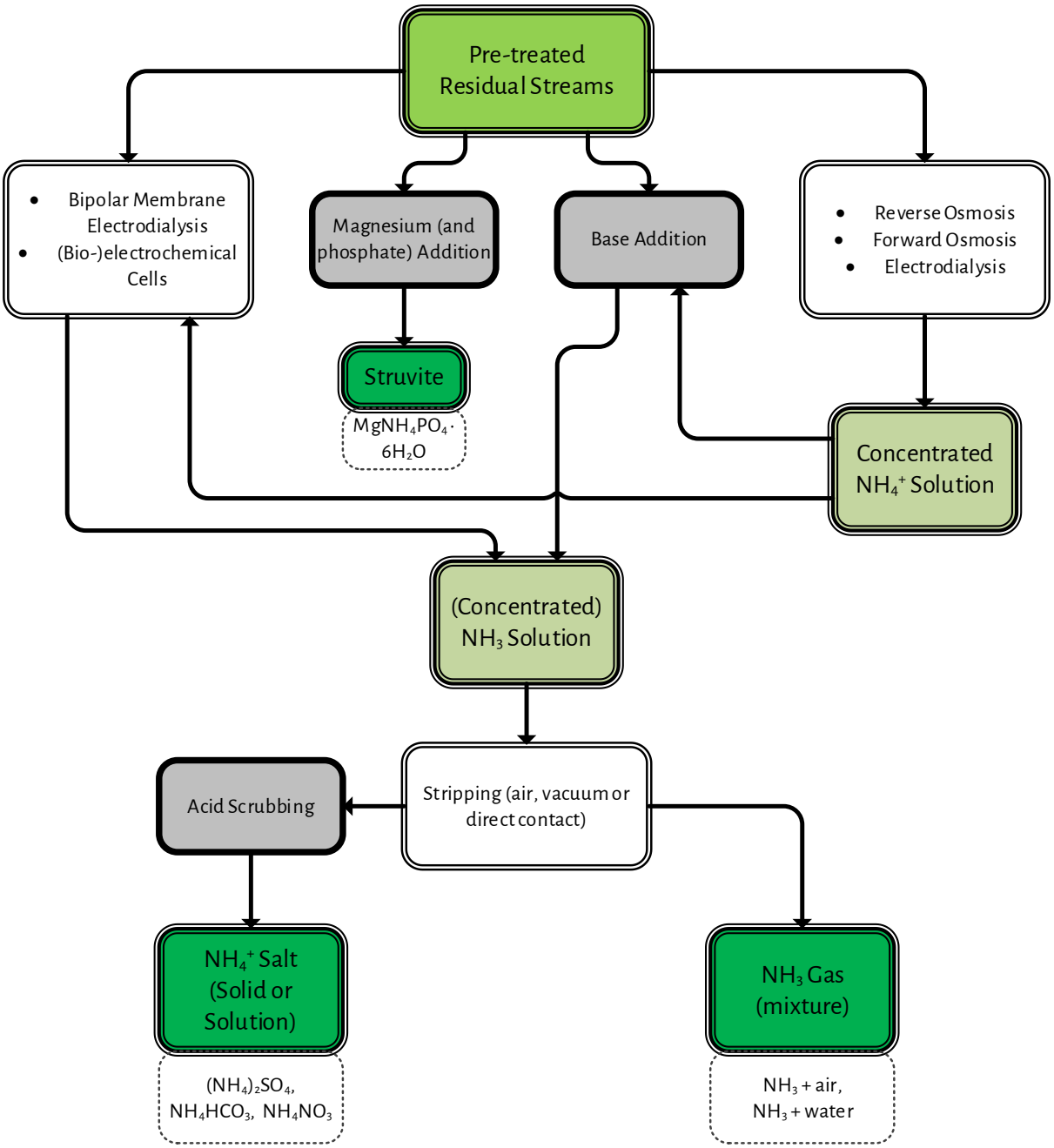

Figure 2-3 - A schematic overview of the various TAN recovery technologies to obtain various TAN products (concerning concentrated NH_4^+ solutions, NH_3 solutions, struvite, solid or dissolved NH_4^+ salts and gaseous NH_3).

2.4. Technologies to generate energy from NH_3

As extensively mentioned, NH_3 can be used as a fuel for the generation of electricity. This chapter focuses on two energy-generation technologies: combustion-based and fuel cell technologies. According to the available information, more research focused on the application of fuel cells, especially due to their scalability advantage, compared to combustion-based technologies. Based on collected data, a general overview of direct NH_3 fuel cells and their operational characteristics and peak power densities is provided in

Table 2-2 (Ni et al., 2009; Lan & Tao, 2014a; Afif et al., 2016).

2.4.1. Combustion technologies

NH_3 can be used as fuel in thermal combustion and propulsion technologies. This is normally done in combination with other fuels, such as H_2, CH_4 or other carbon-based fuels (Valera-Medina et al., 2018). Recent developments in the maritime shipping industry are focusing on using NH_3 in internal combustion engines (Lesmana et al., 2019). In fact, NH_3 is regarded as a key carbon-neutral energy carrier, particularly in the retrofitting of the existing fleet. However, according to the review studies of Kobayashi et al. (2019) and Dimitriou and Javaid (2020), there are challenges when using NH_3 regarding low flammability, emission of unprocessed NH_3 and oxidised nitrogen species (NO_x, N_2O, etc.). Unfortunately, studies with respect to the use of recovered NH_3 and electricity generation with combustion-based technologies are not currently available.

2.4.2. Alkaline (membrane) fuel cells

Alkaline fuel cells (AFCs) use dissolved or molten hydroxide for the transport of hydroxide (OH^-) from the cathode to the anode, whereas alkaline membrane fuel cells (AMFCs) use an anion exchange membrane. In both AFCs and AMFCs, NH_3 is directly electrochemically oxidised by OH^- at the anode, while at the cathode O_2 and water react together with the supplied electrons to OH^- (Lan & Tao, 2014a). However, Lan and Tao (2010) mentioned that the low operational temperature of 25 ºC resulted in a long stabilisation time of the established electric potential difference between the anode and cathode of their AMFC, indicating slow kinetics of the processes. Furthermore, research conducted by Suzuki et al. (2012) showed that the performance of AMFCs is limited by fuel cross-over, caused by the diffusion of NH_3 from the anode to the cathode. Moreover, Suzuki et al. (2012) also showed that poisoning of the metal catalysts with adsorbed nitrogen species takes place at the anode. Finally, the reported maximum power densities for AFCs and AMFCs are only 40 and 16 $mW \cdot cm^{-2}$, respectively, (Ganley, 2008; Lan & Tao, 2010), which is an order of magnitude lower than high-temperature fuel cells.

2.4.3. Solid oxide fuel cells

SOFCs can be divided, based on their ability, to either conduct protons (SOFC-H) or oxygen ions (SOFC-O) through the solid ceramic electrolyte. Because in both SOFC types the operational temperature is well above 500 °C, NH_3 is spontaneously cracked at the anode in the presence of a nickel catalyst, resulting in the production of H_2 and N_2. Initially, nickel was used as a catalyst for H_2-fueled SOFCs (Mahato et al., 2015) and later also appeared to be a good catalyst to crack NH_3 (Fournier et al., 2006). In SOFC-Hs, the electrolyte is proton-conducting, while in SOFC-Os, the electrolyte is oxygen-conducting, implying different reactions to take place. According to the study of Ni et al. (2008), the application of SOFC-Hs could lead to higher electrical efficiencies than SOFC-Os when using NH_3 as fuel due to the place where the oxidation reaction takes place, which affects the activity of the reactants. However, available literature reports higher power densities for SOFC-Os than for SOFC-Hs (Ni et al., 2009; Afif et al., 2016), which is mainly attributed to the low resistance of the oxygen-conducting electrolytes. A maximum power density of 1,190 $mW \cdot cm^{-2}$ for SOFC-Os was reported by Meng et al. (2007), compared to 580 $mW \cdot cm^{-2}$ for SOFC-Hs (Aoki et al., 2018), both using NH_3 directly (without external cracking) as fuel. The higher power density reported for SOFC-O is probably a result of more intensive research activities. Based on review papers of (Ni et al., 2009) and (Afif et al., 2016), it can be concluded that also the design of the cell is important, as the use of anode-supported planar cells results in superior power densities, compared to the use of tubular-supported or tubular cells. Unfortunately, most research on NH_3-fueled SOFCs only reports the achieved power density. In addition to the maximum power density, it is also important how efficient the fuel is used, to determine the actual electrical efficiency. Only a limited number of studies reported the actual electrical efficiency (for example, conversion of chemical energy to electrical energy), which can go up to 70% (Dekker & Rietveld, 2006). A more general review paper on SOFCs by Stambouli and Traversa (2002) also reported that electrical efficiencies of 60% are feasible, while an additional 30% of the chemical energy from the fuels can be used as a high-grade heat. Therefore, SOFCs can potentially effectively use 90% of the total energy content of NH_3, making the SOFC the most efficient technology to reclaim energy from NH_3.

Another advantage of SOFCs over combustion-based technologies and A(M)FCs is the negligible production of oxidised N-species. Staniforth and Ormerod (2003), Ma et al. (2006) and Okanishi et al. (2017) analysed the anode off-gas, and concluded that the concentration of oxidised N-species is below the detection limit, and 0.5 ppm by Dekker and Rietveld (2006). Moreover, the application of SOFC-Hs using NH_3 as fuel will even less likely produce oxidised N-species, because N_2 and O_2 will not be in direct contact, as only H^+ is transported through the proton-conducting electrolyte (Ni et al., 2009). However, a potential challenge for the use of SOFCs is nickel nitridation, which is the formation of nickel-nitrogen (Ni_3N) species at the anode. Nitridation of nickel at the nickel/yttria-stabilised zirconia anode was observed by Yang et al. (2015), who linked this to a decrease in electric potential over the operational run time at an operational temperature ranging 600 – 700 °C. These findings were confirmed by Stoeckl et al. (2019b), who also observed a decrease in electric potential at 700 °C, while using a nickel/yttria-stabilised zirconia anode. However, interestingly,

Stoeckl et al. (2019b) also observed a stable electric potential at an operational temperature of 800 ºC. In a subsequent study by Stoeckl et al. (2020), the electric potential decreased only by 1% over an operational run time of 1,000 hours, when an temperature ranging 815 – 845 ºC was maintained. The authors reported that no structural damage was observed at the anode. However, in this study, a nickel/gadolinium-doped ceria anode was used. Therefore, it remains unclear under what operational conditions and for what anode materials nickel nitridation affects the stable operation of NH_3 in SOFC-Os. For SOFC-Hs, no studies were found that reported on nitridation or production of oxidised N-species.

There are no studies that use NH_3 actually recovered from N-loaded residual streams or waters as a fuel in a fuel cell. In case of recovery from water (aqueous solution), NH_3 will be accompanied by water vapour and potentially by contaminants. Interestingly, the main components of biogas (CH_4 and CO_2), can also be fed to the SOFC-Os, because after CH_4 reforming with steam or CO_2, the produced H_2 and CO also serve as fuel (Gür, 2016; Saadabadi et al., 2019). However, research conducted by Papadias et al. (2012) showed that SOFCs are especially sensitive to contaminants such as H_2S (typically present in biogas), HCl and siloxanes, which deactivate the nickel catalyst and decrease the effective surface of the anode, suggesting that gas cleaning is required before using recovered gases as fuels. Finally, studies on SOFC-Os conducted by Wojcik et al. (2003), Cinti et al. (2016), Stoeckl et al. (2019a) and Stoeckl et al. (2020) showed that it is actually feasible to use mixtures of NH_3 and water vapour as fuel for SOFC-Os. However, the minimum concentration of NH_3 in the fuel was 17% (Wojcik et al., 2003) and it remains unclear whether NH_3 in this concentration can (directly) be recovered from water (aqueous solution). Therefore, more research is required to determine what concentrations of NH_3 can be realised when NH_3 is recovered as a gas from N-loaded residual waters or aqueous solutions and whether SOFCs can work with these concentrations.

Table 2-2 - Various direct NH_3 fuel cells and their operational characteristics and peak power densities according to the review studies of (Ni et al., 2009); Lan and Tao (2014a); (Afif et al., 2016)

Type	Operating Temperature	Electrolyte	Mobile ion	Peak Power Density
AMFC	25 °C	Anion Exchange Membrane	OH^-	16 $mW \cdot cm^{-2}$
AFC	50 – 450 °C	Dissolved/molten OH^-	OH^-	40 $mW \cdot cm^{-2}$
SOFC-H	450 – 750 °C	Ceramic Membrane	H^+	580 $mW \cdot cm^{-2}$
SOFC-O	500 – 1,000 °C	Ceramic Membrane	O^{2-}	1,190 $mW \cdot cm^{-2}$

2.4.4. Discussion on technologies to generate from NH_3

If used as a fuel, the obtained NH_3 concentration is the key. The presence of water vapour or any other additional inert gas stream may reduce the performance of the technology. Additionally, for the fuel cells and in particular, for SOFCs, the presence of certain chemical compounds such as H_2S might deactivate the

catalysts (catalyst poisoning) and potentially need gas cleaning before entering the cell. In the case of the NH_3-fueled combustion engines, NO_x formation and low performance related to the low NH_3 combustion rate are the main challenges. The use of combustion promoters (a second fuel) or partial NH_3 cracking before the combustion are approaches being explored for this challenge.

2.5. Conclusions

Based on the literature study on the identification of N-loaded residual waters and suitable technologies for TAN recovery and technologies for generating energy from NH_3, the following can be derived:

- There is a large potential for TAN recovery from N-loaded residual streams, as thirteen (13) domestic and industrial N-loaded residual streams with a minimum TKN concentration of 0.5 g-N·L^{-1} are identified;
- Categorisation of various N-loaded residual streams can be divided into three categories, based on the required treatment strategy to allow TAN recovery, using the respective TAN/TKN ratio and TSS content:
    - Category 1, representing residual streams with a TAN/TKN ratio < 0.5: require the conversion of organic nitrogen to TAN before TAN recovery;
    - Category 2, representing residual streams with a TAN/TKN ratio ≥ 0.5 and TSS concentration > 1 g·L^{-1}; the removal of solids to enhance the TAN recovery;
    - Category 3, representing residual streams with a TAN/TKN ratio ≥ 0.5 and a TSS concentration ≤ 1 g·L^{-1} (residual waters): suitable for direct TAN recovery.
- Various water treatment technologies are suitable to contribute to the recovery of TAN from N-loaded residual waters:
    - Production of concentrated NH_4^+ solutions by reverse and forward osmosis and electrodialysis (13, 4 and 14 g·L^{-1}, respectively);
    - (Bio-)electrochemical cells and bipolar membrane electrodialysis for the production of concentrated NH_3 solutions (26 and 54 g·L^{-1}, respectively);
    - Struvite precipitation and (air) stripping and subsequent acid scrubbing for the production of NH_4^+ salt (struvite) and NH_4^+-salt solutions, respectively;
    - Vacuum (membrane) stripping for the recovery of NH_3 gas (up to 7 wt%);
- The (normalised) energy consumption for the technologies suitable for TAN recovery is not consistently reported in currently available literature;
- Both combustion-based and fuel cell technologies can be used to generate energy using NH_3 as a fuel:
    - Fuel cell technologies can emit negligible amounts of oxidised N-species, whether NO_x emission is still a challenge for combustion-based technologies;
    - SOFCs outcompete A(M)FCs in terms of power density for generation of electricity using NH_3 as a fuel;
- No information is available on the use of NH_3 recovered from N-loaded residual waters or aqueous solutions as a fuel for combustion-based and fuel cell technologies;

2.6. References

Afif, A., Radenahmad, N., Cheok, Q., Shams, S., Kim, J. H., & Azad, A. K. (2016). Ammonia-fed fuel cells: a comprehensive review. *Renewable and Sustainable Energy Reviews, 60*, 822-835. doi:http://dx.doi.org/10.1016/j.rser.2016.01.120

Aoki, Y., Yamaguchi, T., Kobayashi, S., Kowalski, D., Zhu, C., & Habazaki, H. (2018). High-Efficiency Direct Ammonia Fuel Cells Based on BaZr0.1Ce0.7Y0.2O3–δ/Pd Oxide-Metal Junctions. *Global Challenges, 2*(1), 1700088. doi:10.1002/gch2.201700088

Beckinghausen, A., Odlare, M., Thorin, E., & Schwede, S. (2020). From removal to recovery: An evaluation of nitrogen recovery techniques from wastewater. *Applied Energy, 263*, 114616. doi:https://doi.org/10.1016/j.apenergy.2020.114616

Bonmati, A., & Flotats, X. (2003). Air stripping of ammonia from pig slurry: characterisation and feasibility as a pre- or post-treatment to mesophilic anaerobic digestion. *Waste Management, 23*(3), 261-272. doi:http://dx.doi.org/10.1016/S0956-053X(02)00144-7

Braguglia, C. M., Gallipoli, A., Gianico, A., & Pagliaccia, P. (2018). Anaerobic bioconversion of food waste into energy: A critical review. *Bioresource Technology, 248*, 37-56. doi:10.1016/j.biortech.2017.06.145

Cinti, G., Discepoli, G., Sisani, E., & Desideri, U. (2016). SOFC operating with ammonia: Stack test and system analysis. *International Journal of Hydrogen Energy, 41*(31), 13583-13590. doi:http://dx.doi.org/10.1016/j.ijhydene.2016.06.070

Degn Pedersen, P., Jensen, K., Lyngsie, P., & Henrik Johansen, N. (2003). Nitrogen removal in industrial wastewater by nitration and denitration - 3 years of experience. *Water Science and Technology, 47*(11), 181-188. doi:10.2166/wst.2003.0603

Dekker, N. J. J., & Rietveld, G. (2006). Highly efficient conversion of ammonia in electricity by solid oxide fuel cells. *Journal of Fuel Cell Science and Technology, 3*(4), 499-502. doi:10.1115/1.2349536

Deng, Z., van Linden, N., Guillen, E., Spanjers, H., & van Lier, J. B. (2021). Recovery and applications of ammoniacal nitrogen from nitrogen-loaded residual streams: A review. *Journal of Environmental Management, 295*, 113096. doi:https://doi.org/10.1016/j.jenvman.2021.113096

Dimitriou, P., & Javaid, R. (2020). A review of ammonia as a compression ignition engine fuel. *International Journal of Hydrogen Energy, 45*(11), 7098-7118. doi:https://doi.org/10.1016/j.ijhydene.2019.12.209

El-Bourawi, M. S., Khayet, M., Ma, R., Ding, Z., Li, Z., & Zhang, X. (2007). Application of vacuum membrane distillation for ammonia removal. *Journal of Membrane Science, 301*(1-2), 200-209. doi:10.1016/j.memsci.2007.06.021

Fournier, G. G. M., Cumming, I. W., & Hellgardt, K. (2006). High performance direct ammonia solid oxide fuel cell. *Journal of Power Sources, 162*(1), 198-206. doi:http://dx.doi.org/10.1016/j.jpowsour.2006.06.047

Fu, G., Cai, T., & Li, Y. (2011). Concentration of ammoniacal nitrogen in effluent from wet scrubbers using reverse osmosis membrane. *Biosystems Engineering, 109*(3), 235-240. doi:http://dx.doi.org/10.1016/j.biosystemseng.2011.04.005

Gain, E., Laborie, S., Viers, P., Rakib, M., Hartmann, D., & Durand, G. (2002). Ammonium nitrate wastewaters treatment by an electromembrane process. *Desalination, 149*(1-3), 337-342. doi:10.1016/S0011-9164(02)00806-8

Ganesh Saratale, R., Kumar, G., Banu, R., Xia, A., Periyasamy, S., & Dattatraya Saratale, G. (2018). A critical review on anaerobic digestion of microalgae and macroalgae and co-digestion of biomass for enhanced methane generation. *Bioresource Technology, 262*, 319-332. doi:https://doi.org/10.1016/j.biortech.2018.03.030

Ganley, J. C. (2008). An intermediate-temperature direct ammonia fuel cell with a molten alkaline hydroxide electrolyte. *Journal of Power Sources, 178*(1), 44-47. doi:https://doi.org/10.1016/j.jpowsour.2007.11.093

Gong, H. Y., Z.: Liang, K. Q.: Jin, Z. Y.: Wang, K. J. (2013). Concentrating process of liquid digestate by disk tube-reverse osmosis system. *Desalination, 326*, 30-36. doi:http://dx.doi.org/10.1016/j.desal.2013.07.010

Guerrero, L., Omil, F., Mendez, R., & Lema, J. M. (1999). Anaerobic Hydrolysis and Acidogenesis of Wastewaters From Food Industries With High Content of Organic Solids and Protein. *Water Research, 33*(15), 3281-3290.

Gür, T. M. (2016). Comprehensive review of methane conversion in solid oxide fuel cells: Prospects for efficient electricity generation from natural gas. *Progress in Energy and Combustion Science, 54*, 1-64. doi:https://doi.org/10.1016/j.pecs.2015.10.004

Hartmann, H., & Ahring, B. K. (2005). Anaerobic digestion of the organic fraction of municipal solid waste: Influence of co-digestion with manure. *Water Research, 39*(8), 1543-1552. doi:https://doi.org/10.1016/j.watres.2005.02.001

He, Q., Tu, T., Yan, S., Yang, X., Duke, M., Zhang, Y., & Zhao, S. (2018). Relating water vapor transfer to ammonia recovery from biogas slurry by vacuum membrane distillation. *Separation and Purification Technology, 191*(Supplement C), 182-191. doi:https://doi.org/10.1016/j.seppur.2017.09.030

He, Q., Yu, G., Tu, T., Yan, S., Zhang, Y., & Zhao, S. (2017). Closing CO2 Loop in Biogas Production: Recycling Ammonia As Fertilizer. *Environmental Science & Technology, 51*(15), 8841-8850. doi:10.1021/acs.est.7b00751

Holloway, R. W., Childress, A. E., Dennett, K. E., & Cath, T. Y. (2007). Forward osmosis for concentration of anaerobic digester centrate. *Water Research, 41*(17), 4005-4014. doi:http://dx.doi.org/10.1016/j.watres.2007.05.054

Huang, H. M., Xiao, X. M., Yang, L. P., & Yan, B. (2011). Removal of ammonium from rare-earth wastewater using natural brucite as a magnesium source of struvite precipitation. *Water Science and Technology, 63*(3), 468-474. doi:10.2166/wst.2011.245

Ippersiel, D., Mondor, M., Lamarche, F., Tremblay, F., Dubreuil, J., & Masse, L. (2012). Nitrogen potential recovery and concentration of ammonia from swine manure using electrodialysis coupled with air stripping. *Journal of Environmental Management, 95*, S165-S169. doi:http://dx.doi.org/10.1016/j.jenvman.2011.05.026

Jin, X., Li, E., Lu, S., Qiu, Z., & Sui, Q. (2013). Coking wastewater treatment for industrial reuse purpose: Combining biological processes with ultrafiltration, nanofiltration and reverse osmosis. *Journal of Environmental Sciences, 25*(8), 1565-1574. doi:https://doi.org/10.1016/S1001-0742(12)60212-5

Keucken, A., Habagil, M., Batstone, D., Jeppsson, U., & Arnell, M. (2018). Anaerobic Co-Digestion of Sludge and Organic Food Waste—Performance, Inhibition, and Impact on the Microbial Community. *Energies, 11*(9), 2325. Retrieved from https://www.mdpi.com/1996-1073/11/9/2325

Kim, D. H., Moon, S.-H., & Cho, J. (2002). Investigation of the adsorption and transport of natural organic matter (NOM) in ion-exchange membranes. *Desalination, 151*(1), 11-20. doi:https://doi.org/10.1016/S0011-9164(02)00968-2

Kobayashi, H., Hayakawa, A., Somarathne, K. D. Kunkuma A., & Okafor, Ekenechukwu C. (2019). Science and technology of ammonia combustion. *Proceedings of the Combustion Institute, 37*(1), 109-133. doi:https://doi.org/10.1016/j.proci.2018.09.029

Kundu, P., Debsarkar, A., & Mukherjee, S. (2013). Treatment of slaughterhouse wastewater in a sequencing batch reactor: Performance evaluation and biodegradation kinetics. *BioMed Research International, 2013*. doi:10.1155/2013/134872

Kuntke, P., Sleutels, T. H. J. A., Rodríguez Arredondo, M., Georg, S., Barbosa, S. G., ter Heijne, A., Hamelers, H. V. M., & Buisman, C. J. N. (2018). (Bio)electrochemical ammonia recovery: progress and perspectives. *Applied Microbiology and Biotechnology, 102*(9), 3865-3878. doi:10.1007/s00253-018-8888-6

Kuntke, P., Sleutels, T. H. J. A., Saakes, M., & Buisman, C. J. N. (2014). Hydrogen production and ammonium recovery from urine by a Microbial Electrolysis Cell. *International Journal of Hydrogen Energy, 39*(10), 4771-4778. Retrieved from https://edepot.wur.nl/352760

Lan, R., & Tao, S. (2010). Direct Ammonia Alkaline Anion-Exchange Membrane Fuel Cells. *Electrochemical and Solid-State Letters, 13*(8), B83-B86. doi:https://doi.org/10.1149/1.3428469

Lan, R., & Tao, S. (2014a). Ammonia as a Suitable Fuel for Fuel Cells. *Frontiers in Energy Research, 2*, 35. doi:https://doi.org/10.3389/fenrg.2014.00035

Ledda, C., Schievano, A., Salati, S., & Adani, F. (2013). Nitrogen and water recovery from animal slurries by a new integrated ultrafiltration, reverse osmosis and cold stripping process: A case study. *Water Research, 47*(16), 6157-6166. doi:http://dx.doi.org/10.1016/j.watres.2013.07.037

Ledezma, P., Jermakka, J., Keller, J., & Freguia, S. (2017). Recovering Nitrogen as a Solid without Chemical Dosing: Bio-Electroconcentration for Recovery of Nutrients from Urine. *Environmental Science and Technology Letters, 4*(3), 119-124. doi:https://doi.org/10.1021/acs.estlett.7b00024

Lei, X., Sugiura, N., Feng, C., & Maekawa, T. (2007). Pretreatment of anaerobic digestion effluent with ammonia stripping and biogas purification. *Journal of Hazardous Materials, 145*(3), 391-397. doi:https://doi.org/10.1016/j.jhazmat.2006.11.027

Lei, Y., Wei, L., Liu, T., Xiao, Y., Dang, Y., Sun, D., & Holmes, D. E. (2018). Magnetite enhances anaerobic digestion and methanogenesis of fresh leachate from a municipal solid waste incineration plant. *Chemical Engineering Journal, 348*(March), 992-999. doi:10.1016/j.cej.2018.05.060

Lesmana, H., Zhang, Z., Li, X., Zhu, M., Xu, W., & Zhang, D. (2019). NH3 as a Transport Fuel in Internal Combustion Engines: A Technical Review. *J. Energy Resour. Technol., 141*(7), 070703. doi:https://doi.org/10.1115/1.4042915

Li, Y., Shi, S., Cao, H., Wu, X., Zhao, Z., & Wang, L. (2016). Bipolar membrane electrodialysis for generation of hydrochloric acid and ammonia from simulated ammonium chloride wastewater. *Water Research, 89*(Supplement C), 201-209. doi:https://doi.org/10.1016/j.watres.2015.11.038

Li, Y., Xu, Z., Xie, M., Zhang, B., Li, G., & Luo, W. (2020). Resource recovery from digested manure centrate: Comparison between conventional and aquaporin thin-film composite forward osmosis membranes. *Journal of Membrane Science, 593*, 117436. doi:https://doi.org/10.1016/j.memsci.2019.117436

Lin, P. H., Horng, R. Y., Hsu, S. F., Chen, S. S., & Ho, C. H. (2018). A Feasibility Study of Ammonia Recovery from Coking Wastewater by Coupled Operation of a Membrane Contactor and Membrane Distillation. *International journal of environmental research and public health, 15*(3), 441. doi:https://doi.org/10.3390/ijerph15030441

Ma, Q., Peng, R., Tian, L., & Meng, G. (2006). Direct utilization of ammonia in intermediate-temperature solid oxide fuel cells. *Electrochemistry Communications, 8*(11), 1791-1795. doi:http://dx.doi.org/10.1016/j.elecom.2006.08.012

Magrí, A., Béline, F., & Dabert, P. (2013). Feasibility and interest of the anammox process as treatment alternative for anaerobic digester supernatants in manure processing - An overview. *Journal of Environmental Management, 131*, 170-184. doi:10.1016/j.jenvman.2013.09.021

Mahato, N., Banerjee, A., Gupta, A., Omar, S., & Balani, K. (2015). Progress in material selection for solid oxide fuel cell technology: A review. *Progress in Materials Science, 72*, 141-337. doi:https://doi.org/10.1016/j.pmatsci.2015.01.001

Massé, D. I., Rajagopal, R., & Singh, G. (2014). Technical and operational feasibility of psychrophilic anaerobic digestion biotechnology for processing ammonia-rich waste. *Applied Energy, 120*, 49-55. doi:10.1016/j.apenergy.2014.01.034

Masse, L., Massé, D. I., & Pellerin, Y. (2007). The use of membranes for the treatment of manure: a critical literature review. *Biosystems Engineering, 98*(4), 371-380. doi:https://doi.org/10.1016/j.biosystemseng.2007.09.003

Masse, L., Massé, D. I., & Pellerin, Y. (2008). The effect of pH on the separation of manure nutrients with reverse osmosis membranes. *Journal of Membrane Science, 325*(2), 914-919. doi:http://dx.doi.org/10.1016/j.memsci.2008.09.017

Mata-Alvarez, J., Dosta, J., Romero-Güiza, M. S., Fonoll, X., Peces, M., & Astals, S. (2014). A critical review on anaerobic co-digestion achievements between 2010 and 2013. *Renewable and Sustainable Energy Reviews, 36*, 412-427. doi:10.1016/j.rser.2014.04.039

Mata-Alvarez, J., Macé, S., & Llabrés, P. (2000). Anaerobic digestion of organic solid wastes. An overview of research achievements and perspectives. *Bioresource Technology, 74*(1), 3-16. doi:10.1016/S0960-8524(00)00023-7

Mehta, C. M., Khunjar, W. O., Nguyen, V., Tait, S., & Batstone, D. J. (2015a). Technologies to Recover Nutrients From Waste Streams: A Critical Review. *Critical Reviews in Environmental Science and Technology, 45*, 385-427. doi:https://doi.org/10.1080/10643389.2013.866621

Mehta, C. M., Khunjar, W. O., Nguyen, V., Tait, S., & Batstone, D. J. (2015b). Technologies to Recover Nutrients from Waste Streams: A Critical Review. *Critical Reviews in Environmental Science and Technology, 45*(4), 385-427. doi:10.1080/10643389.2013.866621

Meng, G., Jiang, C., Ma, J., Ma, Q., & Liu, X. (2007). Comparative study on the performance of a SDC-based SOFC fueled by ammonia and hydrogen. *Journal of Power Sources, 173*(1), 189-193. doi:http://dx.doi.org/10.1016/j.jpowsour.2007.05.002

Mondor, M., Ippersiel, D., Lamarche, F., & Masse, L. (2009). Fouling characterization of electrodialysis membranes used for the recovery and concentration of ammonia from swine manure. *Bioresource Technology, 100*(2), 566-571. doi:https://doi.org/10.1016/j.biortech.2008.06.072

Mondor, M., Masse, L., Ippersiel, D., Lamarche, F., & Massé, D. I. (2008a). Use of electrodialysis and reverse osmosis for the recovery and concentration of ammonia from swine manure. *Bioresource Technology, 99*, 7363-7368. doi:https://doi.org/10.1016/j.biortech.2006.12.039

Montusiewicz, A., Bis, M., Pasieczna-Patkowska, S., & Majerek, D. (2018). Mature landfill leachate utilization using a cost-effective hybrid method. *Waste Management, 76*, 652-662. doi:10.1016/j.wasman.2018.03.012

Ni, M., Leung, D. Y. C., & Leung, M. K. H. (2008). Thermodynamic analysis of ammonia fed solid oxide fuel cells: Comparison between proton-conducting electrolyte and oxygen ion-conducting electrolyte. *Journal of Power Sources, 183*(2), 682-686. doi:https://doi.org/10.1016/j.jpowsour.2008.05.022

Ni, M., Leung, M. K. H., & Leung, D. Y. C. (2009). Ammonia-fed solid oxide fuel cells for power generation—A review. *International Journal of Energy Research, 33*(11), 943-959. doi:10.1002/er.1588

Noworyta, A., Koziol, T., & Trusek-Holownia, A. (2003). A system for cleaning condensates containing ammonium nitrate by the reverse osmosis method. *Desalination, 156*(1), 397-402. doi:https://doi.org/10.1016/S0011-9164(03)00373-4

Okanishi, T., Okura, K., Srifa, A., Muroyama, H., Matsui, T., Kishimoto, M., Saito, M., Iwai, H., Yoshida, H., Saito, M., Koide, T., Iwai, H., Suzuki, S., Takahashi, Y., Horiuchi, T., Yamasaki, H., Matsumoto, S., Yumoto, S., Kubo, H., Kawahara, J., Okabe, A., Kikkawa, Y., Isomura, T., & Eguchi, K. (2017). Comparative Study of Ammonia-fueled Solid Oxide Fuel Cell Systems. *Fuel Cells, 17*(3), 383-390. doi:10.1002/fuce.201600165

Papadias, D. D., Ahmed, S., & Kumar, R. (2012). Fuel quality issues with biogas energy – An economic analysis for a stationary fuel cell system. *Energy, 44*(1), 257-277. doi:https://doi.org/10.1016/j.energy.2012.06.031

Pronk, W., Biebow, M., & Boller, M. (2006b). Electrodialysis for Recovering Salts from a Urine Solution Containing Micropollutants. *Environmental Science and Technology, 40*(7), 2414-2420. doi:https://doi.org/10.1021/es051921i

Pronk, W., Biebow, M., & Boller, M. (2006c). Treatment of source-separated urine by a combination of bipolar electrodialysis and a gas transfer membrane. *Water Science and Technology, 53*(3), 139-146. doi:10.2166/wst.2006.086

Rajagopal, R., Massé, D. I., & Singh, G. (2013). A critical review on inhibition of anaerobic digestion process by excess ammonia. *Bioresource Technology, 143*, 632-641. doi:10.1016/j.biortech.2013.06.030

Rodriguez-Verde, I., Regueiro, L., Lema, J. M., & Carballa, M. (2018). Blending based optimisation and pretreatment strategies to enhance anaerobic digestion of poultry manure. *Waste Management, 71*, 521-531. doi:10.1016/j.wasman.2017.11.002

Rodríguez Arredondo, M., Kuntke, P., Jeremiasse, A. W., Sleutels, T. H. J. A., Buisman, C. J. N., & ter Heijne, A. (2015). Bioelectrochemical systems for nitrogen removal and recovery from wastewater. *Environmental Science: Water Research and Technology, 1*(1), 22-33. doi:https://doi.org/10.1039/C4EW00066H

Saadabadi, S. A., Thallam Thattai, A., Fan, L., Lindeboom, R. E. F., Spanjers, H., & Aravind, P. V. (2019). Solid Oxide Fuel Cells fuelled with biogas: Potential and constraints. *Renewable Energy, 134*, 194-214. doi:https://doi.org/10.1016/j.renene.2018.11.028

Schoeman, J. J., & Strachan, L. (2009a). Performance of tubular reverse osmosis for the desalination/ concentration of a municipal solid waste leachate. *Water SA, 35*(3), 323-328. doi:10.4314/wsa.v35i3.76776

Schoeman, J. J., & Strachan, L. (2009b). Performance of tubular reverse osmosis for the desalination/ concentration of a municipal solid waste leachate. *Water SA, 35*, 323-328. doi:10.4314/wsa.v35i3.76776

Shi, L., Hu, Y., Xie, S., Wu, G., Hu, Z., & Zhan, X. (2018). Recovery of nutrients and volatile fatty acids from pig manure hydrolysate using two-stage bipolar membrane electrodialysis. *Chemical Engineering Journal, 334*, 134-142. doi:https://doi.org/10.1016/j.cej.2017.10.010

Shi, L., Xie, S., Hu, Z., Wu, G., Morrison, L., Croot, P., Hu, H., & Zhan, X. (2019). Nutrient recovery from pig manure digestate using electrodialysis reversal: Membrane fouling and feasibility of long-term operation. *Journal of Membrane Science, 573*, 560-569. doi:https://doi.org/10.1016/j.memsci.2018.12.037

Stambouli, A. B., & Traversa, E. (2002). Solid oxide fuel cells (SOFCs): a review of an environmentally clean and efficient source of energy. *Renewable and Sustainable Energy Reviews, 6*(5), 433-455. doi:https://doi.org/10.1016/S1364-0321(02)00014-X

Staniforth, J., & Ormerod, R. M. (2003). Clean destruction of waste ammonia with consummate production of electrical power within a solid oxide fuel cell system. *Green Chemistry, 5*(5), 606-609. doi:10.1039/B307396N

Stoeckl, B., Preininger, M., Subotić, V., Gaber, C., Seidl, M., Sommersacher, P., Schroettner, H., & Hochenauer, C. (2019a). High Utilization of Humidified Ammonia and Methane in Solid Oxide Fuel Cells: An Experimental Study of Performance and Stability. *Journal of The Electrochemical Society, 166*(12), F774-F783. doi:10.1149/2.0781912jes

Stoeckl, B., Preininger, M., Subotić, V., Megel, S., Folgner, C., & Hochenauer, C. (2020). Towards a wastewater energy recovery system: The utilization of humidified ammonia by a solid oxide fuel cell stack. *Journal of Power Sources, 450*, 227608. doi:https://doi.org/10.1016/j.jpowsour.2019.227608

Stoeckl, B., Subotić, V., Preininger, M., Schwaiger, M., Evic, N., Schroettner, H., & Hochenauer, C. (2019b). Characterization and performance evaluation of ammonia as fuel for solid oxide fuel cells with Ni/YSZ anodes. *Electrochimica Acta, 298*, 874-883. doi:https://doi.org/10.1016/j.electacta.2018.12.065

Suzuki, S., Muroyama, H., Matsui, T., & Eguchi, K. (2012). Fundamental studies on direct ammonia fuel cell employing anion exchange membrane. *Journal of Power Sources, 208*(Supplement C), 257-262. doi:https://doi.org/10.1016/j.jpowsour.2012.02.043

Ukwuani, A. T., & Tao, W. (2016). Developing a vacuum thermal stripping - acid absorption process for ammonia recovery from anaerobic digester effluent. *Water Research, 106*108-115. doi:https://doi.org/10.1016/j.watres.2016.09.054

Valera-Medina, A., Xiao, H., Owen-Jones, M., David, W. I. F., & Bowen, P. J. (2018). Ammonia for power. *Progress in Energy and Combustion Science, 69*, 63-102. doi:https://doi.org/10.1016/j.pecs.2018.07.001

van Linden, N., Bandinu, G. L., Vermaas, D. A., Spanjers, H., & van Lier, J. B. (2020). Bipolar membrane electrodialysis for energetically competitive ammonium removal and dissolved ammonia

production. *Journal of Cleaner Production*, 120788. doi:https://doi.org/10.1016/j.jclepro.2020.120788

van Linden, N., Spanjers, H., & van Lier, J. B. (2019b). Application of dynamic current density for increased concentration factors and reduced energy consumption for concentrating ammonium by electrodialysis. *Water Research, 163*, 114856. doi:https://doi.org/10.1016/j.watres.2019.114856

Vecino, X., Reig, M., Bhushan, B., Gibert, O., Valderrama, C., & Cortina, J. L. (2019). Liquid fertilizer production by ammonia recovery from treated ammonia-rich regenerated streams using liquid-liquid membrane contactors. *Chemical Engineering Journal, 360*, 890-899. doi:https://doi.org/10.1016/j.cej.2018.12.004

Wang, Q., Yang, P., & Cong, W. (2011). Cation-exchange membrane fouling and cleaning in bipolar membrane electrodialysis of industrial glutamate production wastewater. *Separation and Purification Technology, 79*(1), 103-113. doi:https://doi.org/10.1016/j.seppur.2011.03.024

Wang, Y., Pelkonen, M., & Kotro, M. (2010). Treatment of High Ammonium–Nitrogen Wastewater from Composting Facilities by Air Stripping and Catalytic Oxidation. *Water, Air, and Soil Pollution, 208*(1), 259-273. doi:10.1007/s11270-009-0164-z

Ward, A. J., Arola, K., Thompson Brewster, E., Mehta, C. M., & Batstone, D. J. (2018). Nutrient recovery from wastewater through pilot scale electrodialysis. *Water Research, 135*, 57-65. doi:https://doi.org/10.1016/j.watres.2018.02.021

Wojcik, A., Middleton, H., Damopoulos, I., & Van herle, J. (2003). Ammonia as a fuel in solid oxide fuel cells. *Journal of Power Sources, 118*(1–2), 342-348. doi:http://dx.doi.org/10.1016/S0378-7753(03)00083-1

Xie, M., Shon, H. K., Gray, S. R., & Elimelech, M. (2016). Membrane-based processes for wastewater nutrient recovery: Technology, challenges, and future direction. *Water Research, 89*, 210-221. doi:http://dx.doi.org/10.1016/j.watres.2015.11.045

Yang, J., Molouk, A. F. S., Okanishi, T., Muroyama, H., Matsui, T., & Eguchi, K. (2015). A Stability Study of Ni/Yttria-Stabilized Zirconia Anode for Direct Ammonia Solid Oxide Fuel Cells. *ACS Applied Materials and Interfaces, 7*(51), 28701-28707. doi:https://doi.org/10.1021/acsami.5b11122

Yang, Q., Yang, M., Zhang, S., & Lv, W. (2005). Treatment of wastewater from a monosodium glutamate manufacturing plant using successive yeast and activated sludge systems. *Process Biochemistry, 40*, 2483-2488. doi:10.1016/j.procbio.2004.09.009

Zarebska, A., Romero Nieto, D., Christensen, K. V., Fjerbæk Søtoft, L., & Norddahl, B. (2015). Ammonium fertilizers production from manure: A critical review. *Critical Reviews in Environmental Science and Technology, 45*(14), 1469-1521. doi:10.1080/10643389.2014.955630

Chapter 3.

Electrodialysis for ammonium removal and producing concentrated ammonium solutions

Based on:

Application of dynamic current density for increased concentration factors and reduced energy consumption for concentrating ammonium by electrodialysis

Niels van Linden, Henri Spanjers, Jules B. van Lier

https://doi.org/10.1016/j.watres.2019.114856

Abstract

Electrodialysis (ED) can be used for total ammoniacal nitrogen (TAN) removal efficiencies by transporting ammonium (NH_4^+) from treating nitrogen-loaded (N-loaded) residual streams, while simultaneously producing concentrated NH_4^+ solutions. However, the effect of osmosis and back-diffusion increases when the NH_4^+ concentration gradient between the diluate and the concentrate increases, resulting in a limitation of the concentration factor and an increase in electrical energy consumption. This chapter shows that operation at dynamic current density (DCD) decreased the effect of osmosis and back-diffusion, due to a 75% decrease of the operational run time, compared to operation at a fixed current density (FCD). The concentration factor increased from 4.5 for an FCD to 6.7 for DCD, while the electrical energy consumption of 90% NH_4^+ removal from synthetic sludge reject water at DCD remained stable at 5.4 MJ·kg-N^{-1}.

Keywords

electrodialysis; current density; ammonium; concentration factor; energy consumption; current efficiency;

3.1. Introduction

Chapter 2 identifies electrodialysis (ED) as a potentially suitable technology to achieve 90% removal of total ammoniacal nitrogen (TAN), while simultaneously producing concentrated ammonium (NH_4^+) solutions. Subsequently, the literature review presented in Chapter 2 of this thesis confirms that ED is a suitable technology for TAN removal from nitrogen-loaded (N-loaded) residual waters, but that the achievable removal efficiency, concentration factor and energy consumption deviate in currently reported literature. Because this chapter focuses on the transport of ions, the main addressed form of TAN is NH_4^+.

3.1.1. Concentrating NH_4^+ by ED

Pronk et al. (2006a) removed NH_4^+ for 85% from source-separated urine for nutrient recovery purposes and concentrated NH_4^+ by a factor of 3.2 with an energy consumption of 96 MJ·kg-N^{-1}. In addition, Mondor et al. (2008b) and Ippersiel et al. (2012) used ED for NH_4^+ recovery from digested swine manure and removed 75% and 87%, respectively, while achieving a concentration factor for NH_4^+ of 2.8 and 5.6, respectively. The energy consumption for removing and concentrating NH_4^+ in these two studies ranged between 18 and 71 MJ·kg-N^{-1}. Furthermore, Wang et al. (2015) achieved full removal of NH_4^+ from sludge reject water by ED for nutrient recovery purposes and obtained a concentration factor of 18. However, the energy consumption was an order of magnitude higher than the other reported studies: 202 – 258 MJ·kg-N^{-1}. Finally, Ward et al. (2018) used ED to recover NH_4^+ from sludge reject water on pilot scale, achieving a concentration factor of 8.5 for NH_4^+. However, the removal of NH_4^+ from the sludge reject water was limited to 23%, while the energy consumption was competitive to partial nitritation in combination with anammox: 18 MJ·kg-N^{-1}.

3.1.2. Problems with concentrating NH_4^+ with ED

The concentration factor for concentrating ions by ED is limited by water (H_2O) transfer (Pronk et al., 2006a; Mondor et al., 2008b; Rottiers et al., 2014; Ward et al., 2018). The ion concentration gradient that establishes across the membranes between the diluate and concentrate causes osmosis (Strathmann, 2004a), resulting in dilution of the concentrate. In addition, the ion concentration gradient causes the concentrated ions to diffuse from the concentrate back to the diluate (back-diffusion) (Strathmann, 2004b). The diffused ions need to be transported back and forth, requiring an additional supply of electrical charge (and thus consumed energy). Back-diffusion, therefore, results in a decrease in current efficiency (Strathmann, 2004b) and an increase in energy consumption. The reported studies on concentrating NH_4^+ by ED either applied a fixed voltage or a fixed current density (FCD). When a fixed voltage is applied, the limiting current density (LCD) may be exceeded at low ion concentrations in the diluate. H_2O dissociates into H^+ and OH^- when the LCD is exceeded, resulting in a decreased current efficiency and an increase in energy consumption (Strathmann, 2010). When an FCD is applied, a current density equal to or lower than the LCD of the aimed diluate ion concentration is applied. However, the application of low current densities leads to low ion transport fluxes, indicating inefficient use of membranes and high operational run times. By decreasing the

operational run time, the effect of osmosis and back-diffusion can be decreased, because an ion concentration gradient will inevitably establish when concentrating ions such as NH_4^+.

3.1.3. Research objective

Previous research showed that ED can effectively be applied to remove NH_4^+ from side streams. This chapter assesses the operation of ED at dynamic current density (DCD) and FCD, aiming to maximise the concentration factor and minimise energy consumption. For DCD operation, the current density is dynamically adjusted in agreement with the decreasing ion concentration of the diluate, without exceeding the LCD. The effect of the current density on the concentrating factor and energy consumption was studied by assessing the H_2O transfer and the NH_4^+ current efficiency during sequencing batch experiments at both the application of an FCD and DCD.

3.2. Materials and methods

3.2.1. Materials

Figure 3-1 presents a schematic representation of the used experimental set-up. A bench-scale PC-Cell 64002 ED cell was used, consisting of a Pt/Ir coated titanium anode and a V4A steel cathode, with an electrode area of 8 x 8 cm^2. In between the electrodes, a ten cell pair membrane stack was placed, consisting of two PCA SC cation exchange end (CEEM), ten PCA SA standard anion exchange (AEM) and nine PCA SK standard cation exchange membranes (CEM) (PCA, 2016b). The membrane stack contained polyethylene/silicone spacers to separate the electrodes and membranes, creating electrode rinse, diluate and concentrate channels. The spacers had a thickness of 0.5 mm and a void fraction of 59%. The lay-out of the electrodes, flow channels and membranes is schematically represented in Figure 3-2.

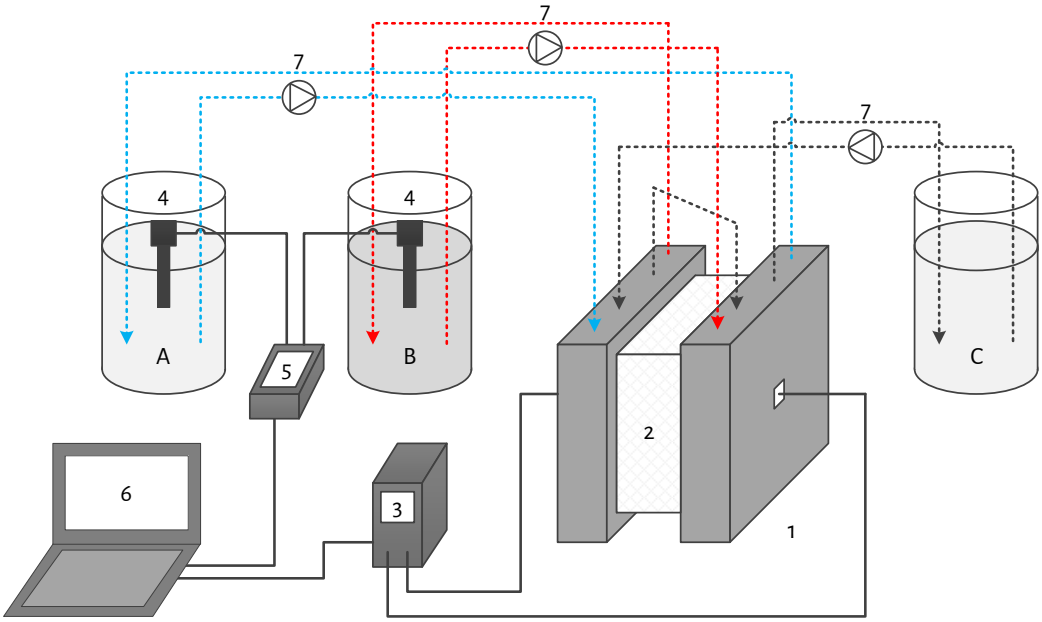

Figure 3-1 - A schematic representation of the used experimental set-up, including the ED cell (1), membrane stack (2), power supply (3), EC sensors (4), multimeter (5), laptop (6), peristaltic pumps (7) and the diluate (A), concentrate (B) and electrode rinse (C) solution.

The diluate and concentrate solutions were recirculated through the ED cell at a cross-flow velocity of 2 $cm \cdot s^{-1}$, following the recommendations of Strathmann (2010). The cross-flow velocity was controlled by using a calibrated peristaltic Watson-Marlow 520S pump at a flow rate of 19 $L \cdot h^{-1}$. The electrodes were rinsed with an electrode rinse solution at the same flow rate used for the diluate and concentrate. Separate Watson-Marlow 323 pump heads were used for each solution. For the application of electrical current, a Tenma 72-2535 power supply with an electrical current and electrical potential range of 0.001 – 3.000 A and 0.01 – 30.00 V, respectively, was used. The electrical conductivity (EC) and pH of the electrode rinse, diluate and concentrate were measured in the respective solution bottles, using two calibrated TetraCon 925 EC-sensors and a calibrated IDS SenTix 940 pH sensors, respectively, on a WTW Multi 3630 IDS multi-meter.

NH_4^+ concentrations were measured with Machery-Nagel NANOCOLOR Ammonium 200 (range: 0.04 – 0.2 $g \cdot L^{-1}$) and 2,000 (range: 0.4 – 2.0 $g \cdot L^{-1}$) test kits. Solution volumes were determined using calibrated volumetric cylinders.

Initial diluate and concentrate solutions consisting of 6.6 $g \cdot L^{-1}$ NH_4HCO_3 were used, equal to an NH_4^+ concentration of 1.5 $g \cdot L^{-1}$, simulating NH_4^+ concentrations commonly present in sludge reject waters. Synthetic solutions were used to be able to study the effect of back-diffusion and (electro-)osmosis as a function of the NH_4^+ concentration gradient on the concentration factor and energy consumption at different current density operations. The initial electrode rinse solutions consisted of 1 M $NaNO_3$. The salts were of analytical grade (Sigma Aldrich Reagent Plus, ≥ 99%) and were added to 1 L of demi-water. The experiments were conducted at room temperature (T = 22 ± 1 °C).

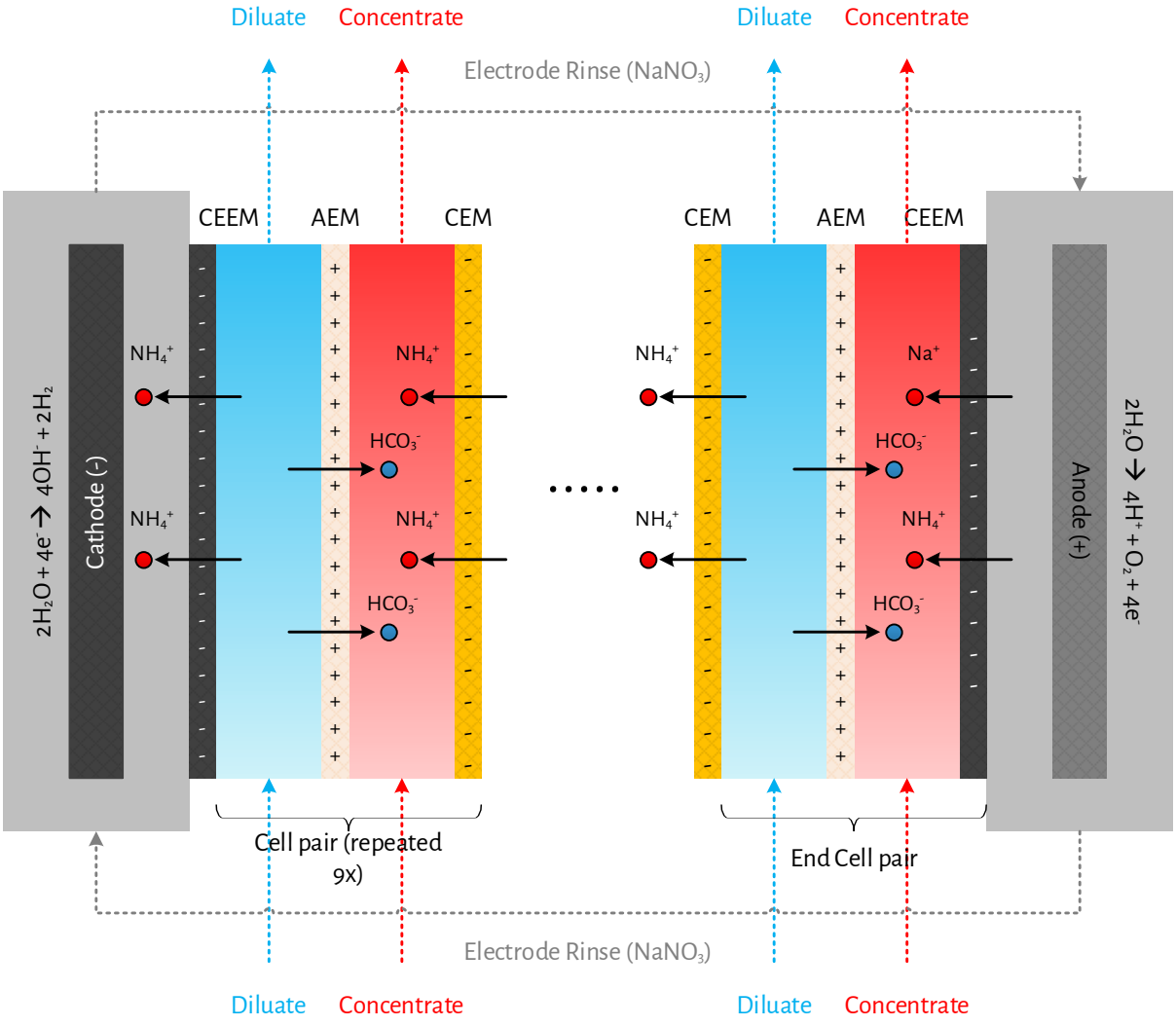

Figure 3-2 - A schematic representation of the membrane and flow channel sequence in the membrane stack, including ion transport due to the electrical current. The transport of cations at the electrodes through the CEEMs explains the accumulation of NH_4^+ in the electrode rinse: NH_4^+ is transported from the diluate to the electrode rinse at the cathode, while the same amount of charge transported through the CEEM at the anode is represented by both NH_4^+ and Na^+.

3.2.2. Performance indicators

To assess H_2O transfer, it was determined how much H_2O was transported from the diluate to the concentrate. By relating the H_2O transfer to the initial H_2O mass, the relative H_2O transfer was determined (Eq. 3-1). H_2O transfer to the electrode rinse was neglected, as only one diluate and concentrate channel were in contact with the electrode chambers. Besides, extra thick CEEMs were placed next to electrode compartments to minimise H_2O transfer.

$$\theta_{H_2O,t} = \frac{V_{d,i} \cdot \rho_{H_2O} - V_{d,f} \cdot \rho_{H_2O}}{V_{d,i} \cdot \rho_{H_2O}} \cdot 100\% \qquad \text{Eq. 3-1}$$

Where $\theta_{H_2O,t}$ = total H_2O transfer from the diluate (unitless), $V_{d,i}$ and $V_{d,f}$ = initial and final diluate volume, respectively (in L) and ρ_{H_2O} = density of H_2O (in $g \cdot L^{-1}$, ρ_{H_2O} = 995 $g \cdot L^{-1}$ at T = 22 °C).

Water transfer in ED is caused by an ion concentration gradient (osmosis), resulting in H_2O transfer from the diluate to the concentrate. In addition, H_2O transfer is caused by the application of electrical current, which causes H_2O transfer in the hydration shell of the transported ions from the diluate to the concentrate (electro-osmosis). The electro-osmotic H_2O transfer (Eq. 3-2) was determined based on the amount of transported ions and their respective H_2O transfer numbers (Strathmann, 2004a). It was assumed that for every transported mole of NH_4^+, one mole of HCO_3^- was transported to maintain charge balance in the diluate and concentrate flow channels. Based on the hydration numbers (amount of moles of H_2O in the first hydration shell per mole of ions) determined in the studies of Brugé et al. (1999) and Leung et al. (2007), H_2O transfer numbers of four and seven were used for NH_4^+ and HCO_3^-, respectively, agreeing with the range of four to eight of Strathmann (2004a). The osmotic H_2O transfer was determined based on the mass balance of H_2O transfer (Eq. 3-3).

$$\theta_{H_2O,e-o} = \frac{n_{NH_4^+,d} \cdot (T_w^{NH_4^+} + T_w^{HCO_3^-}) \cdot MW_{H_2O}}{V_{d,i} \cdot \rho_{H_2O}} \cdot 100\% \qquad \text{Eq. 3-2}$$

Where $\theta_{H_2O,e-o}$ = electro-osmotic H_2O transfer (unitless), $n_{NH_4^+,d}$ = amount of transported diluate NH_4^+ (mol), $T_w^{NH_4^+}$ and $T_w^{HCO_3^-}$ = NH_4^+ and HCO_3^- transfer number of H_2O, respectively (unitless) and MW_{H_2O} = molecular weight of H_2O (in $g \cdot mol^{-1}$, MW_{H_2O} = 18 $g \cdot mol^{-1}$).

$$\theta_{H_2O,o} = \theta_{H_2O,t} - \theta_{H_2O,e-o} \qquad \text{Eq. 3-3}$$

Where $\theta_{H2O,o}$ = osmotic H_2O transfer (unitless).

We determined the NH_4^+ current efficiency (Eq. 3-4) by the transported charge as NH_4^+, relative to the total supplied electrical charge. Finally, the electrical energy consumption to remove and concentrate NH_4^+ (Eq. 3-5) was determined based on the mass of transported NH_4^+ from the diluate and the total used electrical energy to transport NH_4^+.

$$\eta_{NH_4^+} = \frac{z \cdot F \cdot n_{NH_4^+,d}}{N \cdot \sum_{t=0}^{t} I_t \cdot \Delta t} \cdot 100\% \qquad \text{Eq. 3-4}$$

Where $\eta_{NH_4^+}$ = NH_4^+ current efficiency (unitless), z = ion valence (unitless, z = 1 for NH_4^+), F = Faraday constant (in $C \cdot mol^{-1}$, F = 96,485 $C \cdot mol^{-1}$), N = number of cell pairs (unitless), I_t = electrical current (in A) and Δt = time interval (in s).

$$E = \frac{\sum_{t=0}^{t} U_t \cdot I_t \cdot \Delta t}{m_{NH_4^+,d}} \qquad \text{Eq. 3-5}$$

Where E = electrical energy consumption (in $MJ \cdot kg\text{-}N^{-1}$), U_t = electrical potential (in V) and $m_{NH_4^+,d}$ = amount of transported NH_4^+ from the diluate (in kg-N).

3.2.3. Methods

To determine the current densities for the application of an FCD and DCD, the relationship between the diluate EC and the LCD was experimentally determined. To this end, various dilutions of the initial diluate (1, 0.9, 0.8, 0.75, 0.6, 0.5, 0.25, 0.05 and 0.01) were prepared. Subsequently, the current density was increased with steps of 1.5 $A \cdot m^{-2}$, while the electrical current and electrical potential were logged automatically, to subsequently determine the LCD for each dilution following the method of Cowan and Brown (1959).
To avoid H_2O dissociation in local ion depleted zones, Strathmann (2004d) recommends using a safety factor (SF < 1) for the application of LCD. A safety factor for the LCD to apply DCD was determined, representing an optimum between the operational run time and the energy consumption. To find an optimum for these quantities with different units, the operational run time (Eq. 3-6) and energy consumption (Eq. 3-7) were normalised for SF = 1. Equal weights were assigned to operational run time and energy consumption, while in practice different weights can be assigned, to determine an economical (cost-based) optimum safety factor (Strathmann, 2004d). Safety factors of 0.5, 0.75 and 1 were used to experimentally determine the safety factor that represents an optimum between the operational run time and energy consumption.
According to theory, the operational run time to transport a fixed amount of charge as ions is minimal for SF = 1 and increases reciprocally for lower safety factors (see the Supporting Information of the paper of van Linden et al. (2019a)). The normalised operational run time as a function of the safety factor is therefore described by $\alpha = SF^{-1} - 1$. Contrarily, the energy consumption to transport a certain amount of charge as ions has a maximum at s = 1 and decreases linearly for lower safety factors (see the Supporting Information of the paper of van Linden et al. (2019a)). Therefore, the normalised energy consumption as a function of the safety factor is described by β = SF.

$$\alpha = \frac{t_{SF} - t_{SF=1}}{t_{SF=1}} \quad \text{Eq. 3-6}$$

$$\beta = \frac{E_{SF}}{E_{SF=1}} \quad \text{Eq. 3-7}$$

Where α = normalised operational run time (unitless) and β = normalised energy consumption (unitless).

To dynamically set the electrical current, a Python script was developed, which calculated the electrical current based on the real-time diluate EC, the used safety factor and the determined relationship between the diluate EC and the LCD. The diluate EC measurements were logged on a laptop every five seconds and subsequently, the laptop controlled the power supply automatically to apply the electrical current. Electrical current and electrical potential data were logged every five seconds on the laptop. The data of the concentrate EC was stored on a multimeter and the pH of all solutions was manually measured before and after each run. For the three chosen safety factors, duplicate runs with fresh solutions were conducted, in which the diluate EC was always decreased to 1 $mS \cdot cm^{-1}$.

Finally, sequencing batch experiments (SBEs) were conducted in duplicate, to assess the H_2O transfer and NH_4^+ current efficiency and study the effect of the current density (an FCD and DCD) on the concentration factor and the energy consumption. For the first batch, fresh diluate, concentrate and electrode rinse solutions were used and the NH_4^+ concentrations and volumes of all solutions were measured. After that, the diluate EC was again decreased to 1 $mS \cdot cm^{-1}$ and the NH_4^+ concentration and volume of all solutions were measured to make H_2O and NH_4^+ balances. For the subsequent nine batches, the diluate was replaced for a fresh diluate solution, and the concentrate and electrode rinse solutions of the previous batch were reused. The electrical current during the DCD SBE was again applied using the automated control based on the Python script.

3.3. Results

3.3.1. Determination of current densities

We found a linear (R^2 = 0.92) relationship between the diluate EC and the LCD at a cross-flow velocity of 2 cm·s^{-1} (Figure 3-3A), which was used to determine the current densities for the application of an FCD and DCD in the SBEs. Subsequently, an optimum between the operational run time and the energy consumption was determined by using a safety factor of 0.5, 0.75 and 1 for the LCD. Figure 3-3B depicts the experimentally determined α and β as a function of the safety factor. The experimentally determined α had a minimum at SF = 1 and increased for lower safety factors. On the contrary, the experimentally determined β had a maximum at SF = 1 and decreased for lower safety factors. By means of fitting trend lines for the experimentally determined α and β, an optimum for the safety factor at 0.62 was found.

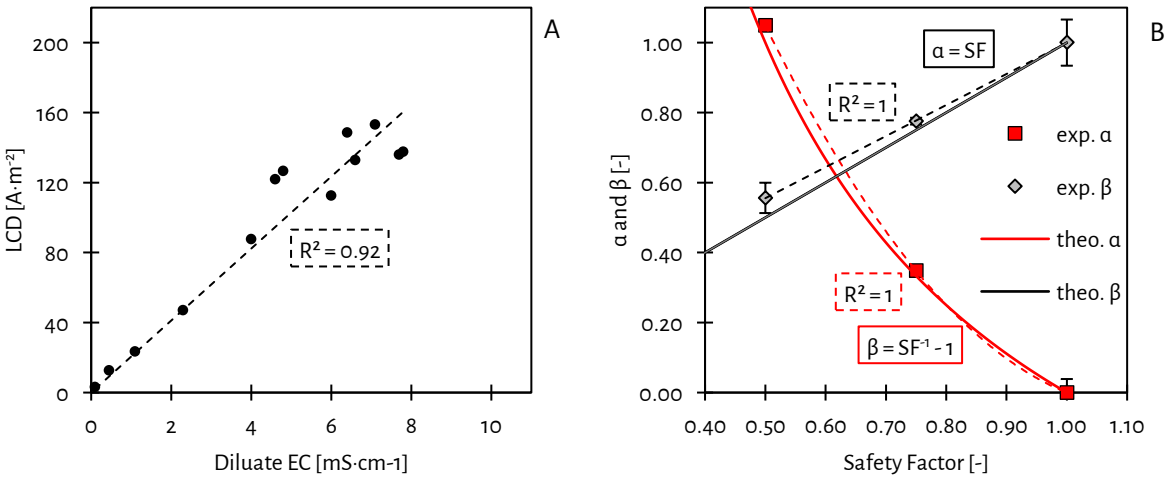

Figure 3-3 - The linear relationship between the diluate EC and the LCD (A). The theoretical (solid lines) and experimental (data points with error bars, representing the averages ± minimum and maximum values for duplicate experiments, dashed lines representing the trend lines) α and β as a function of the safety factor for the LCD (B). An optimum was found at a safety factor of 0.62, representing an optimum between the operational run time and energy consumption.

3.3.2. SBE at an FCD

For the FCD SBE, a current density of 16 A·m^{-2} was applied, based on the LCD of the final diluate EC (1 mS·cm^{-1}) and a safety factor of 0.62. Figure 3-4A presents the diluate and concentrate EC over the cumulative amount of consumed energy during the FCD SBE. The operational run time to decrease the diluate EC to 1 mS·cm^{-1} increased by 58% over the number of batches, from 158 minutes for the first batch to 250 minutes for the tenth batch. Because the concentrate was recirculated during the SBE, the concentrate EC increased but reached a plateau at 32 mS·cm^{-1}.

From the NH_4^+ concentrations during the FCD SBE experiment (Figure 3-4B), it follows that 91 ± 1% (AVG ± STD) of the NH_4^+ from the diluate was removed for all batches. The NH_4^+ concentration in the concentrate reached a plateau at 6.8 g·L^{-1}, corresponding to a concentration factor of 4.5. The difference in concentration

factor between the replicate FCD SBEs was < 5%. The increase in NH_4^+ concentration of the concentrate resulted in an increase in the NH_4^+ concentration gradient between the diluate and concentrate over the number of batches. The NH_4^+ concentration gradient was 2.4 g·L^{-1} for the first batch, and increased to 6.6 g·L^{-1} for the tenth batch. In addition to the diluate and concentrate NH_4^+ concentrations, Figure 3-4B also presents the NH_4^+ concentration in the electrode rinse, showing that 21 ± 3% of the NH_4^+ transported from each diluate batch was transported to and accumulated in the electrode rinse.

The electrical energy consumption increased for each sequencing batch, from 3.6 MJ·kg-N^{-1} for the first batch to 6.1 MJ·kg-N^{-1} for the tenth batch.

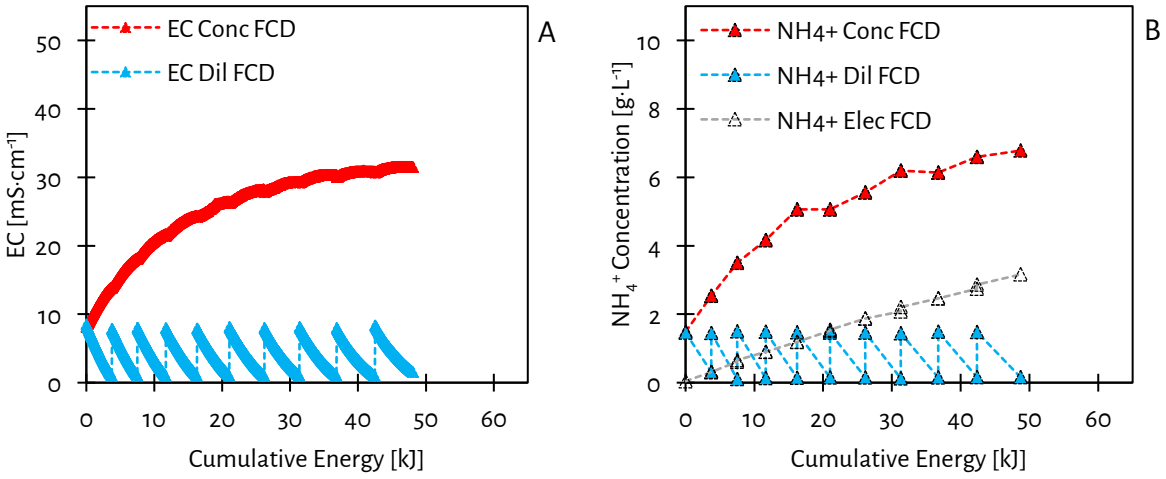

Figure 3-4 - The evolution of the EC (A) and NH_4^+ concentration (B) over the cumulative spent energy during the FCD SBE. The diluate EC was decreased to 1 mS·cm^{-1} for every sequencing batch, corresponding to 91% (on average) removal of NH_4^+ from the diluate. The concentrate reached a plateau at 32 mS·cm^{-1}, corresponding to an NH_4^+ concentration of 6.6 g·L^{-1} and a concentration factor of 4.5. Besides transport of NH_4^+ from the diluate to the concentrate, 21% (on average) of the NH_4^+ was transported to and accumulated in the electrode rinse.

3.3.3. SBE at DCD

For the DCD SBE, a safety factor of 0.62 was used for the LCD as current density. Figure 3-5A presents the diluate and concentrate EC over the cumulative amount of consumed energy during the DCD SBE. Similar to the FCD SBE, the operational run time increased over the number of batches. However, the operational run time increased only by 29%, from 49 min for the first batch to 63 min for the tenth batch. The application of DCD resulted in a reduction of 69 - 75% of the operational run time, with respect to the application of an FCD, which can be translated to a decrease in the required membrane area. In addition, the concentrate EC did not reach a plateau and reached 40 mS·cm^{-1} after ten batches.

During the DCD SBE, 90 ±1% of the NH_4^+ from the diluate was removed for each sequencing batch, as follows from Figure 3-5B. However, in contrast to the FCD SBE, the concentration of NH_4^+ in the concentrate did not reach a plateau, but increased linearly to 10 g·L^{-1} after ten batches, corresponding to a concentration factor of 6.7. The difference in concentration factor between the replicate DCD SBEs was negligible: <1%. The NH_4^+

concentration gradient increased from 2.4 g·L^{-1} for the first batch to 9.8 g·L^{-1} for the final batch. Similar to the FCD SBE, 24 ± 7% of NH_4^+ that was transported from the diluate accumulated in the electrode rinse during the DCD SBE.

In contrast to the increasing electrical energy consumption during the FCD SBE, the electrical energy consumption during the DCD SBE remained stable at 5.4 ± 0.4 MJ·kg-N^{-1}. The electrical energy consumption of the tenth batch was lower for the application of DCD (5.9 MJ·kg-N^{-1}) than for the application of an FCD (6.1 MJ·kg-N^{-1}), while the NH_4^+ concentration gradient was actually higher for the application of DCD (6.6 g·L^{-1}) than an FCD (9.8 g·L^{-1}).

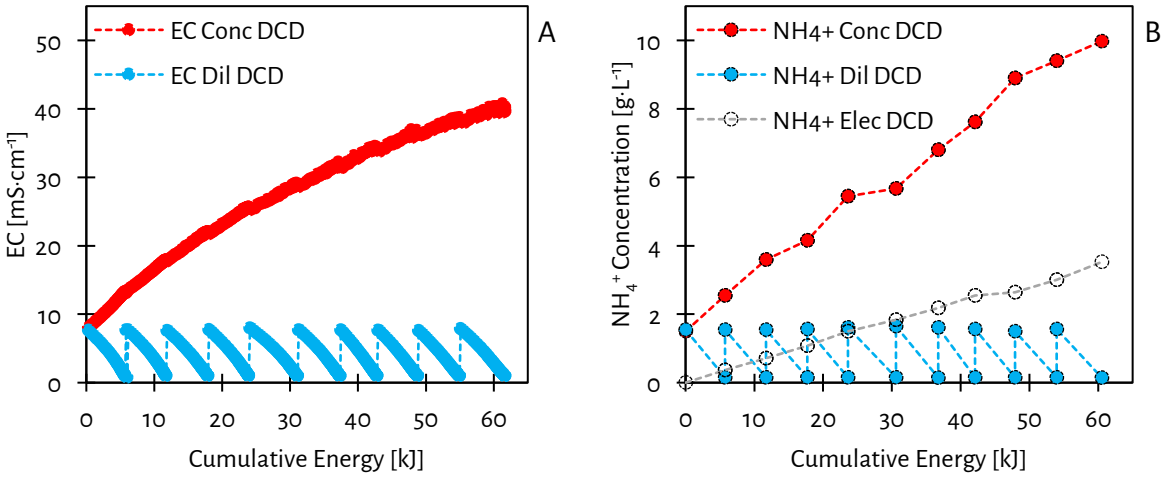

Figure 3-5 - The evolution of the EC (A) and NH_4^+ concentration (B) over the cumulative spent energy during the DCD SBE. The diluate EC was again decreased to 1 mS·cm^{-1} for every sequencing batch, corresponding to 90% (on average) removal of NH_4^+ from the diluate. The EC and NH_4^+ concentration in the concentrate did not reach a plateau, but increased to 40 mS·cm^{-1} and 10 g·L^{-1} (concentration factor = 6.7), respectively. For the DCD SBE, 24% (on average) of the NH_4^+ accumulated in the electrode rinse.

3.4. Discussion

3.4.1. Determination of current densities

The found linear relationship between the diluate EC and the LCD corresponds with Strathmann (2004c), who reported that the LCD is linearly related to the diluate ion concentration for a specific flow channel geometry and cross-flow velocity.

In addition, an optimum between the operational run time and the energy consumption was experimentally found at a safety factor of 0.62. Figure 3-5B also presents the theoretical α and β. Similar to the experimentally determined α and β, a theoretical optimum was found at a safety factor of 0.62, by equating the theoretical expressions for α and β.

3.4.2. SBE at an FCD

The plateau of the NH_4^+ concentration in the concentrate, and thus the limitation of the concentration factor, was caused by H_2O transfer from the diluate to the concentrate. Figure 3-6A shows how much H_2O was transported during each batch by electro-osmosis and osmosis, as a function of the NH_4^+ concentration gradient. For the FCD SBE, osmosis was the dominant mechanism of H_2O transfer. The electro-osmotic H_2O transfer remained constant at 1.5% of the diluate throughout the SBE, because always the same amount of NH_4^+ was removed from the diluate (1.34 ± 0.02 g). The removal of NH_4^+ was constant because the diluate EC of the fresh solutions was always decreased to 1 $mS \cdot cm^{-1}$. The osmotic H_2O transfer increased from 2.5% at an NH_4^+ concentration gradient of 2.4 $g \cdot L^{-1}$ to 10.5% at an NH_4^+ concentration gradient of 6.6 $g \cdot L^{-1}$. The increase in osmotic H_2O transfer was caused by two factors: as the NH_4^+ concentration gradient increased, the driving force for osmosis was higher and as the operational run time increased, more time was available to allow osmosis to take place.

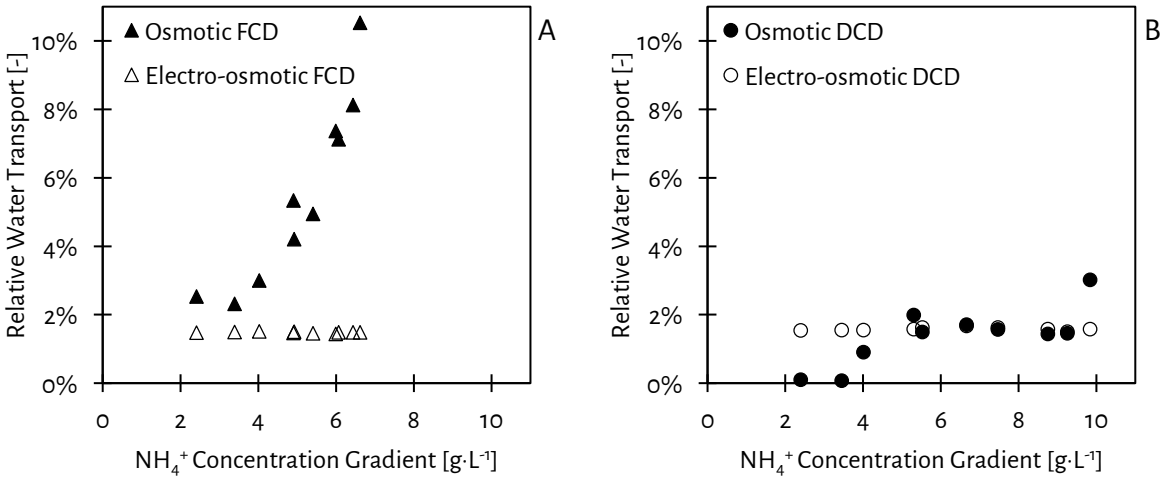

Figure 3-6 - The H_2O transfer during the FCD SBE (A) and the DCD SBE (B). During both SBEs, the electro-osmotic H_2O transfer was stable at 1.5 – 1.6% and the osmotic H_2O transfer for both SBEs increased over the NH_4^+ concentration gradient as both the driving force for osmosis and the operational run time increased.

NH_4^+ accumulation in the electrode rinse was caused by transport of NH_4^+ from the diluate through a cation exchange (end) membrane, ending up in the electrode rinse at the cathode side of the membrane stack. At the anode side of the membrane stack, an equivalent amount of charge migrated as cations from the electrode rinse to the concentrate. However, because the electrode rinse consisted of 1 M $NaNO_3$, the transported charge not only consisted of NH_4^+, but also of Na^+. This phenomenon is schematically presented in Figure 3-2. By taking into account the accumulated NH_4^+ in the electrode rinse solution, the NH_4^+ mass balances fitted within 5%, while previous researchers assigned a 17 - 28% NH_4^+ loss to volatilisation of ammonia (NH_3) from the diluate, concentrate and electrode rinse (Mondor et al., 2008b; Ward et al., 2018). Figure 3-7A presents the NH_4^+ current efficiency over the NH_4^+ concentration gradient during the FCD SBE. The NH_4^+ current efficiency was 76% at an NH_4^+ concentration gradient of 2.4 $g \cdot L^{-1}$ and decreased to 48% at an NH_4^+ concentration gradient of 6.6 $g \cdot L^{-1}$. In general, current efficiency in ED is mainly affected by H_2O dissociation at current densities higher than the LCD, the transport of other ions than the target ion and back-diffusion (Strathmann, 2004b; Pronk et al., 2006a). Because during the FCD SBE, the LCD was never exceeded due to the application of the safety factor, the effect of H_2O dissociation on the NH_4^+ current efficiency was negligible. Besides, the pH ranged between 7.8 – 8.8 throughout the entire SBE. At pH = 7.8, H^+ represented only $1.5 \cdot 10^{-3}$ C, while NH_4^+ in the initial diluate represented approximately 7,500 C. In addition, Na^+ is transported from the electrode rinse solution to the concentrate and is therefore assumed not to be relevant for the assessment of the NH_4^+ current efficiency. Therefore, also the effect of the transport of other cations such as H^+ and Na^+ on the NH_4^+ current efficiency was negligible. According to Rottiers et al. (2014), the ion concentration gradient and back-diffusion are linearly related. Because during the FCD SBE the NH_4^+ current efficiency decreased over the increasing NH_4^+ concentration gradient, the decrease in the NH_4^+ current efficiency is assigned to back-diffusion, also in line with Pronk et al. (2006a). During the FCD SBE, the NH_4^+ concentration gradient increased, resulting in a higher driving force for back-diffusion for each sequencing batch. Because back-diffusion took place from the concentrate to the diluate, NH_4^+ needed to be transported back and forth to decrease the diluate EC to 1 $mS \cdot cm^{-1}$, resulting in an increase in the operational run time. The transport of back-diffused NH_4^+ was at the expense of more supplied electrical charge, which led to a decrease in the NH_4^+ current efficiency. Because for each batch more back-diffusion took place over the number of batches, more electrical energy was required to transport NH_4^+ to decrease the diluate EC to 1 $mS \cdot cm^{-1}$. The electrical energy consumption increased from 3.6 $MJ \cdot kg\text{-}N^{-1}$ to 6.1 $MJ \cdot kg\text{-}N^{-1}$ when the NH_4^+ concentration gradient increased from 2.4 $g \cdot L^{-1}$ to 6.6 $g \cdot L^{-1}$, as presented in Figure 3-7B.

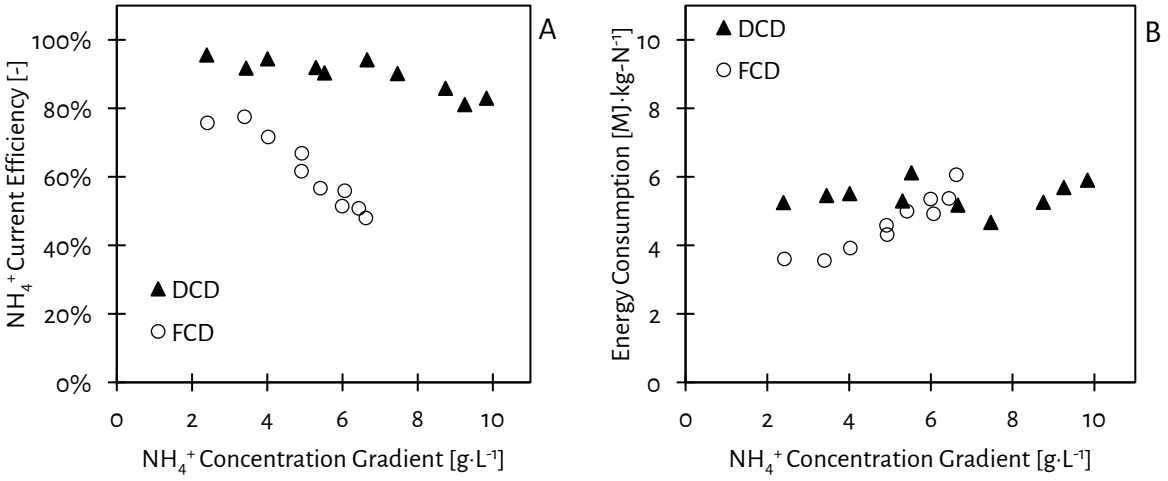

Figure 3-7 - The NH_4^+ current efficiency (A) and the electrical energy consumption (B) over the NH_4^+ concentration gradient during the SBEs. The NH_4^+ current efficiency decreased during both SBEs, but the NH_4^+ current efficiency during the DCD SBE was always higher than during the FCD SBE. The electrical energy consumption during the FCD SBE increased because the driving force for back-diffusion and the operational run time increased, while on the other, the electrical energy consumption during the DCD SBE remained stable at 5.4 MJ·kg-N^{-1}.

3.4.3. SBE at DCD

Figure 3-6B depicts the H_2O transfer during the DCD SBE. For the first nine batches, electro-osmosis was dominant and only for the last batch osmosis was the dominant H_2O transfer mechanism. The electro-osmotic H_2O transfer of 1.6% was constant during the DCD SBE and was similar to the electro-osmotic H_2O transfer during the FCD SBE (1.5%). The osmotic H_2O transfer was only 0.1% at an NH_4^+ concentration gradient of 2.4 g·L^{-1} and increased to 3% at an NH_4^+ concentration gradient of 9.8 g·L^{-1}. Since the osmotic driving force was higher during the DCD SBE than the during FCD SBE, the decrease in osmotic H_2O transfer is caused by the decreased operational run time, due to the application of DCD. Results indicate that due to the decrease in the operational run time by means of the application of DCD, less osmosis took place, resulting in a higher concentration factor, with respect to an FCD.

Figure 3-7A presents the NH_4^+ current efficiency over the NH_4^+ concentration gradient for the DCD SBE. If Na^+ from the electrolyte ended up in the diluate and was transported to the concentrate, it would account for a 24% loss in the NH_4^+ current efficiency. However, the NH_4^+ current efficiency for the first batch was 96% at an NH_4^+ concentration gradient of 2.4 g·L^{-1}. This high NH_4^+ current efficiency supports the claim that the NH_4^+ current efficiency was not affected by the transport of other ions than NH_4^+, such as H^+ and Na^+. Throughout the SBE, the NH_4^+ current efficiency decreased to 83% in the tenth batch at an NH_4^+ concentration gradient of 9.8 g·L^{-1}. Similar to the FCD SBE, more back-diffusion took place due to the increase in NH_4^+ concentration gradient and the increase in operational run time. However, the effect of back-diffusion on the NH_4^+ current efficiency only caused a decrease in NH_4^+ current efficiency of 13% during the DCD SBE, in comparison to a decrease in NH_4^+ current efficiency of 28% during the FCD SBE. Since the NH_4^+ concentration gradient was

even higher for the DCD SBE than for the FCD SBE, the higher current efficiencies and the lower decrease in NH_4^+ current efficiency are assigned to the decreased operational run times during the DCD SBE. Apparently, decreasing the operational run time by the application of DCD, results in less back-diffusion compared to an FCD, leading to a higher NH_4^+ current efficiency.

The increase in operational run time and NH_4^+ concentration gradient did not affect the electrical energy consumption for the application of DCD (5.4 ± 0.4 MJ·kg-N^{-1}), in contrast to an FCD. The increase in electrical energy consumption due to back-diffusion was countered by the decrease of the electrical resistance, because the EC of the concentrate increased.

3.5. Conclusions

The experimental work to optimise the operation of ED in terms of concentration factor and energy consumption while achieving 90% NH_4^+ removal resulted in the following conclusions:

- Concentrating NH_4^+ by ED resulted in an NH_4^+ concentration gradient between the diluate and the concentrate stream. The increasing gradient subsequently resulted in increased mass transfer by osmosis and back-diffusion;
- The increased back-diffusion of NH_4^+ decreased the NH_4^+ current efficiency from 76% to 48% when applying an FCD and the electrical energy consumption for the removal of 90% NH_4^+ increased from 3.6 MJ·kg-N^{-1} to 6.1 MJ·kg-N^{-1};
- When a DCD was applied, the operational run time for removing 90% NH_4^+ decreased by 75%, which can be translated to a decrease in the required membrane area;
- The application of DCD resulted in a decrease in osmotic H_2O transfer, compared to an FCD, leading to an increased concentration factor of 6.7;
- When applying a DCD, the NH_4^+ current efficiency decreased over the NH_4^+ concentration gradient from 96% to 83% and eventually 90% NH_4^+ was removed at the expense of a stable electrical energy consumption of 5.4 MJ·kg-N^{-1};
- The results show that the application of DCD allows for a lower operational run time, a higher concentration factor and a lower electrical energy consumption to concentrate NH_4^+ by ED, compared to an FCD.

3.6. References

Brugé, F., Bernasconi, M., & Parrinello, M. (1999). Ab Initio Simulation of Rotational Dynamics of Solvated Ammonium Ion in Water. *Journal of the American Chemical Society, 121*(47), 10883-10888. doi:10.1021/ja990520y

Cowan, D. A., & Brown, J. H. (1959). Effect of Turbulence on Limiting Current in Electrodialysis Cells. *Industrial & Engineering Chemistry, 51*(12), 1445-1448. doi:10.1021/ie50600a026

Ippersiel, D., Mondor, M., Lamarche, F., Tremblay, F., Dubreuil, J., & Masse, L. (2012). Nitrogen potential recovery and concentration of ammonia from swine manure using electrodialysis coupled with air stripping. *Journal of Environmental Management, 95*, S165-S169. doi:http://dx.doi.org/10.1016/j.jenvman.2011.05.026

Leung, K., Nielsen, I. M. B., & Kurtz, I. (2007). Ab Initio Molecular Dynamics Study of Carbon Dioxide and Bicarbonate Hydration and the Nucleophilic Attack of Hydroxide on CO2. *The Journal of Physical Chemistry B, 111*(17), 4453-4459. doi:10.1021/jp068475l

Mondor, M., Masse, L., Ippersiel, D., Lamarche, F., & Massé, D. I. (2008b). Use of electrodialysis and reverse osmosis for the recovery and concentration of ammonia from swine manure. *Bioresource Technology, 99*(15), 7363-7368. doi:http://dx.doi.org/10.1016/j.biortech.2006.12.039

PCA. (2016b). PCA Ion Exchange Membranes: Technical Data Sheet. Retrieved from https://www.pca-gmbh.com/publi/PCAMembranes.pdf

Pronk, W., Biebow, M., & Boller, M. (2006a). Electrodialysis for Recovering Salts from a Urine Solution Containing Micropollutants. *Environmental Science & Technology, 40*(7), 2414-2420. doi:10.1021/es051921i

Rottiers, T., Ghyselbrecht, K., Meesschaert, B., Van der Bruggen, B., & Pinoy, L. (2014). Influence of the type of anion membrane on solvent flux and back diffusion in electrodialysis of concentrated NaCl solutions. *Chemical Engineering Science, 113*, 95-100. doi:https://doi.org/10.1016/j.ces.2014.04.008

Strathmann, H. (2004a). Chapter 2 - Electrochemical and Thermodynamic Fundamentals. In *Ion-Exchange Membrane Separation Processes* (9 ed., pp. 23-88): Elsevier.

Strathmann, H. (2004b). Chapter 3 - Preparation and Characterization of Ion-Exchange Membranes. In *Ion-Exchange Membrane Separation Processes* (9 ed., pp. 89-146): Elsevier.

Strathmann, H. (2004c). Chapter 4 - Operating Principle of Electrodialysis and Related Processes. In *Ion-Exchange Membrane Separation Processes* (9 ed., pp. 147-225): Elsevier.

Strathmann, H. (2004d). Chapter 5 - Ion-Exchange Membrane Process and Equipment Design. In *Ion-Exchange Membrane Separation Processes* (9 ed., pp. 227-286): Elsevier.

Strathmann, H. (2010). Electrodialysis, a mature technology with a multitude of new applications. *Desalination, 264*(3), 268-288. doi:https://doi.org/10.1016/j.desal.2010.04.069

van Linden, N., Spanjers, H., & van Lier, J. B. (2019a). Application of dynamic current density for increased concentration factors and reduced energy consumption for concentrating ammonium by electrodialysis. *Water Research*, 114856. doi:https://doi.org/10.1016/j.watres.2019.114856

Wang, X., Zhang, X., Wang, Y., Du, Y., Feng, H., & Xu, T. (2015). Simultaneous recovery of ammonium and phosphorus via the integration of electrodialysis with struvite reactor. *Journal of Membrane Science, 490*, 65-71. doi:https://doi.org/10.1016/j.memsci.2015.04.034

Ward, A. J., Arola, K., Thompson Brewster, E., Mehta, C. M., & Batstone, D. J. (2018). Nutrient recovery from wastewater through pilot scale electrodialysis. *Water Research, 135*, 57-65. doi:https://doi.org/10.1016/j.watres.2018.02.021

Chapter 4.

Bipolar membrane electrodialysis for ammonium removal and producing concentrated dissolved ammonia solutions

Based on: Bipolar membrane electrodialysis for energetically competitive ammonium removal and dissolved ammonia production

Niels van Linden, Giacomo L. Bandinu, David A. Vermaas, Henri Spanjers, Jules B. van Lier

https://doi.org/10.1016/j.jclepro.2020.120788

Abstract

Bipolar membrane electrodialysis (BPMED) can be used to convert salt solutions to acid and base solutions without the use of chemicals. This chapter focuses on the application of BPMED to remove total ammoniacal nitrogen (TAN) from water and to simultaneously produce concentrated dissolved NH_3 solutions. The current efficiency and electrical energy consumption to transport ammonium (NH_4^+) from the diluate (the feed water) were assessed throughout sequencing batch experiments.

The NH_4^+ removal efficiency for BPMED ranged between 85 and 91% and the electrical energy consumption was stable at 19 MJ·kg-N^{-1}, taking both electrochemical and pumping energy into account. The base pH increased from 7.8 to 9.8 and the TAN concentration increased from 1.5 to 7.3 g·L^{-1}, corresponding to a final NH_3 concentration of 4.5 g·L^{-1} in the base. Only 48% of the TAN transported from the diluate ended up in the base as NH_3 due to accumulation of TAN in the electrode rinse and diffusion of NH_3 from the base to the acid and back to the dilute. Furthermore, leakage of hydroxide (OH^-) and diffusion of dissolved NH_3 and ions (such as NH_4^+ and bicarbonate (HCO_3^-)) from the base to the diluate all contributed to a loss in NH_4^+ current efficiency. Due to the increase in operational run time and concentration gradients throughout the sequencing batch experiments, the NH_4^+ current efficiency decreased from 69 to 54%.

BPMED proved to be able to simultaneously remove TAN from water and produce concentrated dissolved NH_3 while avoiding the use of chemicals. The energy consumption was competitive with that of the combination of electrodialysis and the addition of chemicals (22 MJ·kg-N^{-1}).

Keywords

water treatment; ammonia recovery; water dissociation; current efficiency; energy consumption;

4.1. Introduction

Chapter 1 of this thesis identifies bipolar membrane electrodialysis (BPMED) as a suitable technology to produce concentrated NH_3 solutions. Subsequently, a literature review presented in Chapter 2 of this thesis confirms that BPMED is a suitable technology for the production of NH_3 solutions, but that there is a lack of information on the fate of TAN during the operation and on the energy consumption to achieve NH_4^+ removal and produce NH_3 solutions.

4.1.1. Chemical addition to convert NH_4^+ to dissolved NH_3

The amount of added chemicals to increase the solution pH at standard temperature and pressure conditions (T = 25 °C and p = 101,325 Pa) to a certain value depends on the buffer capacity and the ionic strength of the solution. Various nitrogen-loaded (N-loaded) residual waters, such as urine, reject water and industrial condensates contain buffering anions, such as bicarbonate (HCO_3^-). Figure 4-1A depicts the effect of the buffer capacity on the required addition of sodium hydroxide (NaOH) to increase the solution pH from 7.8 to 10 for solutions with various TAN concentrations. Because HCO_3^- reacts with hydroxide (OH^-) to form carbonate (CO_3^{2-}), less OH^- is available to effectively increase the pH. Therefore, double the amount of NaOH is required to increase the pH in buffered solutions (NH_4HCO_3), compared to non-buffered solutions (NH_4Cl). Besides, the ammoniacal nitrogen equilibrium pH (pK_a) increases when the ionic strength of the solution increases. Figure 4-1B shows the distribution of NH_4^+ and NH_3 at standard conditions as a function of the pH for solutions with various TAN (as NH_4HCO_3) concentrations. The pK_a for a solution with a TAN concentration of 1.5 g·L^{-1} is 9.4, while for 10 g·L^{-1} the pK_a is 9.6, meaning that the pH must be further increased for solutions with TAN concentrations of 1.5 g·L^{-1} to have the same amount of NH_4^+ and NH_3, compared to solutions with TAN concentrations of 10 g·L^{-1}.

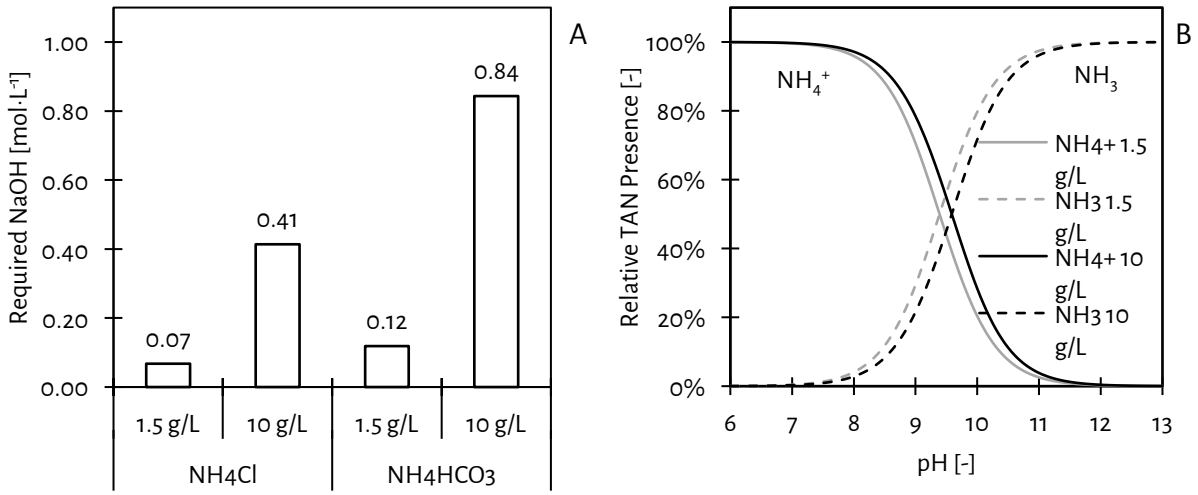

Figure 4-1 - The required NaOH addition to increase the pH from 7.8 to 10 for solutions containing NH_4Cl and NH_4HCO_3 (A). The ammoniacal nitrogen equilibrium pH shifts for TAN concentrations of 1.5 and 10 g·L^{-1} (as NH_4HCO_3) from 9.4 to 9.6, respectively, as a result of an increase in ionic strength (B). Both graphs are derived from PHREEQC software simulations using the phreeqc.dat database.

4.1.2. Bipolar membrane electrodialysis for NH_4^+ removal from N-loaded residual waters

To avoid the addition of chemicals, bipolar membrane electrodialysis (BPMED) can be used to change the solution pH in situ by only using electrical energy (Mani, 1991; Tongwen, 2002). BPMED can be used to remove ions from a feed stream (the diluate) and simultaneously concentrate cations in a base stream (the base) and anions in an acid stream (the acid). The cations in the base are combined with hydroxide ions (OH^-), while the anions are combined with protons (H^+), which are produced in the bipolar membranes by dissociating water when an electric current is applied.

Previous studies showed that BPMED can be applied for the treatment of N-loaded residual waters containing TAN mainly as NH_4^+. Various studies assessed the application of BPMED to produce dissolved NH_3 and acids such as HCl and HNO_3 from industrial N-loaded residual waters containing NH_4Cl and NH_4NO_3, respectively (Graillon et al., 1996; Ali et al., 2004; Li et al., 2016; Lv et al., 2018). In addition, Pronk et al. (2006d) and Shi et al. (2018) used BPMED for the recovery of nitrogen and phosphorus from source-separated urine and pig manure hydrolysate, respectively. Finally, Shuangchen et al. (2015) applied BPMED to recover CO_2 from spent NH_3-based carbon capture solutions (NH_4HCO_3).

4.1.3. Problem description

In previous research, the efficiency of BPMED to use supplied electric charge (current efficiency) to produce acid and base was mainly limited by leakage of H^+, while also diffusion of NH_3 and leakage of OH^- through the (imperfect) membranes comprised the current efficiency (Graillon et al., 1996; Ali et al., 2004). However, these studies were conducted with high concentrations of NH_4^+ in the diluate (ranging 2 - 4 mol·L^{-1} NH_4^+), at high current densities (ranging 480 – 900 A·m^{-2}) and in the absence of buffering anions, such as HCO_3^- (Ali et al., 2004; Li et al., 2016; Lv et al., 2018). These feed water compositions and operational conditions are not representative for the application of BPMED on N-loaded residual waters such as (sludge) reject water and industrial condensates, which have a typical NH_4^+ concentration ranging from 0.5 to 2.5 g·L^{-1} (Gonzalez-Martinez et al., 2018). Besides, the previously conducted studies merely focused on the current efficiency of acid and base production, rather than on the current efficiency to transport NH_4^+ (NH_4^+ current efficiency) from the diluate (Ali et al., 2004; Shuangchen et al., 2015; Li et al., 2016). Finally, there are no studies available that assess the energy consumption to remove NH_4^+ from water by BPMED.

4.1.4. Research objective

This chapter presents the assessment of the current efficiency and energy consumption to remove TAN from feed water by BPMED, while simultaneously producing concentrated dissolved NH_3. This chapter focuses on the fate and concentrations of TAN throughout BPMED operation and the processes affecting the NH_4^+ current efficiency and energy consumption. Furthermore, the energy consumption of BPMED and of ED in combination with the addition of chemicals to remove TAN from water and produce concentrated dissolved NH_3 were compared.

4.2. Materials and methods

4.2.1. Materials

We used a bench-scale PC-Cell 64004 ED cell, consisting of a Pt/Ir-MMO coated and Ti-stretched metal anode and a stainless-steel cathode, both with a surface area of 8 x 8 cm^2. The cell contained a BPMED membrane stack consisting of ten cell triplets. Each cell triplet consisted of a cation exchange membrane (CEM), an anion exchange membrane (AEM) and a bipolar membrane (BPM), as depicted in Figure 4-2. Two PCA SC cation exchange end membranes (CEEM) were placed next to the electrodes, similar to the studies conducted by Graillon et al. (1996) and Pronk et al. (2006d) on BPMED and similar to the study of Ward et al. (2018) and the study of van Linden et al. (2019a) on NH_4^+ removal by ED. The rest of the BPMED membrane stack consisted of ten PCA Acid-60 AEMs, nine PCA SK CEMs and ten PCA BPMs. Specific membrane characteristics can be found through the supplier (PCA, 2016a). The membranes and electrodes were separated by 0.5 mm thick wire mesh spacers made from silicon/polyethylene sulfone to form diluate, acid and base (flow) cells and electrode rinse compartments.

The electric current was applied by a Tenma 72-2535 power supply, having an electric current and potential range of 0.001 – 3.000 A and 0.01 – 30.00 V, respectively.

The diluate, acid, base and electrode rinse solutions were stored in 1 L borosilicate bottles and were continuously mixed by magnetic stirrers on a mixing plate. The solutions were recirculated through the BPMED membrane stack by a calibrated peristaltic Watson-Marlow 520S pump with separate Watson-Marlow 313 pump heads for each solution. The pump was set at a flow rate of 19 $L \cdot h^{-1}$, corresponding to a cross-flow velocity of 2 $cm \cdot s^{-1}$ in the diluate, acid and base cells. The diluate, acid and base pH were measured in the respective bottles, using three calibrated IDS SenTix 940 pH sensors and a WTW Multi 3630 IDS multimeter. The acid and base EC were also measured in the respective bottles, using two calibrated TetraCon 925 EC-sensors and a separate multimeter. The diluate EC was measured with a separate EC-sensor and multimeter. Figure 4-3 presents a schematic representation of the complete experimental BPMED set-up.

TAN concentrations were measured with Machery-Nagel NANOCOLOR Ammonium 200 (range: 0.04 – 0.2 $g \cdot L^{-1}$) and 2,000 (range: 0.4 – 2.0 $g \cdot L^{-1}$) test kits. Calibrated volumetric cylinders were used to determine the solution volumes. The initial diluate, acid and base solutions contained 6.6 $g \cdot L^{-1}$ NH_4HCO_3, corresponding to an NH_4^+ concentration of 1.5 $g \cdot L^{-1}$, which is a representative concentration of N-loaded residual waters such as (sludge) reject water and certain industrial condensates. The initial electrode rinse solutions consisted of 1 M $NaNO_3$. It must be noted that due to BPMED membrane stack configuration (equipped with CEEMs) and the use of $NaNO_3$ in the initial electrode rinse solution, NH_4^+ can be transported to the electrode rinse at the cathode, while sodium (Na^+) can be washed-out from the electrode rinse at the anode, as depicted in Figure 4-2. Furthermore, for the NH_3 diffusion experiment, Acros Organics 25% NH_4OH and NaCl were used. All salts were of analytical grade (Sigma Aldrich Reagent Plus, ≥ 99%) and were added to 1 L of demi-water. All experiments were conducted at a temperature of 24 ± 2 °C (AVG ± STD, n = 20).

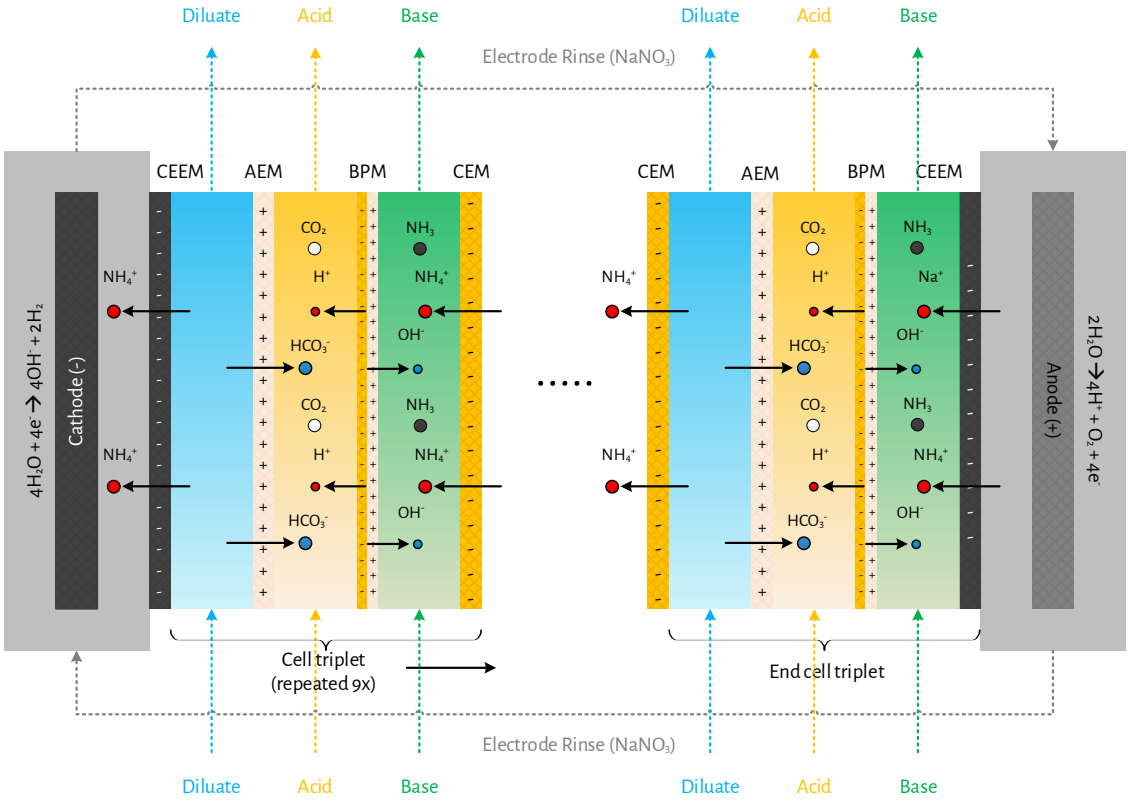

Figure 4-2 - The membrane and (flow) cell sequence in the BPMED membrane stack and the intended ion transport (electro-migration and water dissociation) as a result of the applied current. In the acid, H^+ and HCO_3^- are combined and react to CO_2, while in the base OH^- and NH_4^+ are combined and react to NH_3. At the cathode, NH_4^+ is transported to the electrode rinse, while at the anode, both Na^+ and NH_4^+ are transported to the base, resulting in the accumulation of NH_4^+ in the electrode rinse and the wash-out of Na^+ to the base.

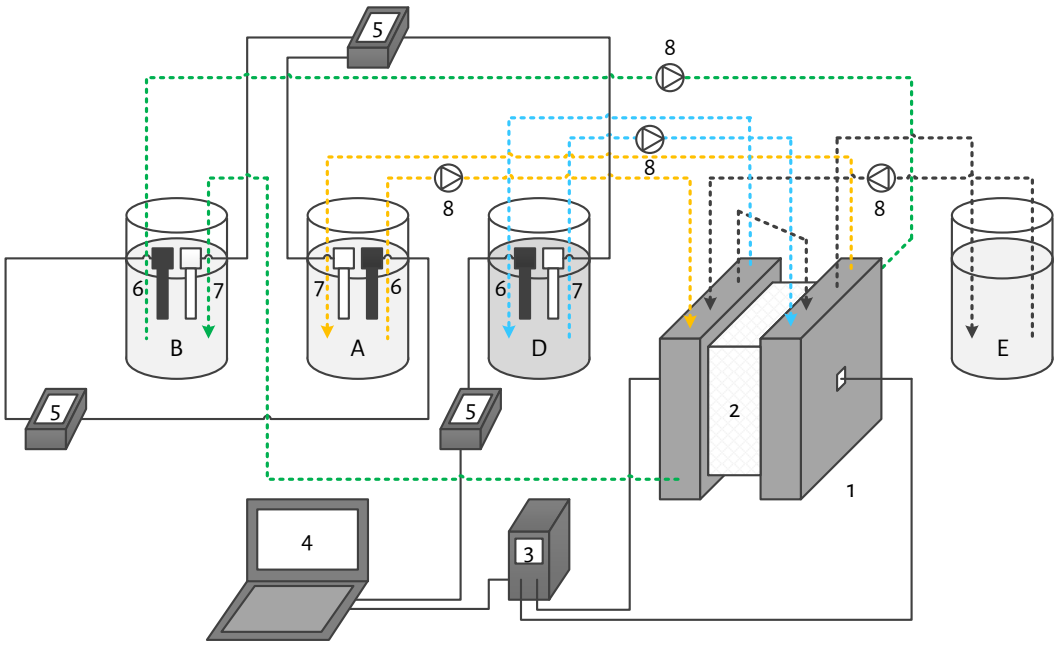

Figure 4-3 - The used experimental set-up, including the cell (1), the BPMED membrane stack (2), power supply (3), laptop (4), multimeters (5), EC-sensors (6), pH-sensors (7), peristaltic pumps (8) and the diluate (D), acid (A), base (B) and electrode rinse (E) bottles and solutions.

4.2.2. Methods

4.2.2.1. Removal of NH_4^+ and production of concentrated dissolved NH_3

To assess the current efficiency and electrical energy consumption to remove NH_4^+ from water by BPMED, while simultaneously producing concentrated dissolved NH_3, duplicate sequencing batch experiments (SBEs) were performed. For the first batch of the SBEs, new diluate, acid, base and electrode rinse solutions were used. The diluate EC of each consecutive batch was decreased to 1 mS·cm^{-1} by applying dynamic current density, as described in the study of van Linden et al. (2019a), which shows that the decrease of the diluate EC to 1 mS·cm^{-1} corresponds to 90% removal of NH_4^+ from the new diluate solutions. The removal of NH_4^+ by 90% is comparable to state-of-the-art NH_4^+ removal technologies such as anammox and air stripping. In both ED and BPMED, the diluate is determining for the limiting current density. Because the same diluate solution, spacer geometry and cross-flow velocity were used, the same procedure of dynamic current density application was followed, using a safety factor of 0.62 (van Linden et al. (2019a). When the diluate EC was decreased from 8 to 1 mS·cm^{-1}, the treated diluate batch was replaced by a new diluate batch, while the acid, base and electrode rinse batches were recycled. Solution volumes and TAN concentrations were measured at the beginning and end of each batch to assess the TAN mass balance. In addition, the electric current and electric potential were automatically logged every five seconds on a laptop. Finally, the EC and pH of the diluate, acid and base were also logged automatically every five seconds, while the EC and pH of the electrode rinse were manually measured at the beginning and end of each batch.

4.2.2.2. Diffusion of NH_3 through the BPMED membrane stack

Additionally, a diffusion experiment to study the diffusion of NH_3 was performed. During this experiment, a 1 L base solution containing NH_3 (as NH_4OH) in demi water was recirculated through the BPMED cell containing the same BPMED membrane stack as was used in the SBEs. In addition, 1 L diluate and acid solutions without NH_3 (demi water) were also recirculated through the ED cell. NaCl was added to the diluate, acid and base, to obtain equal ionic strengths (corresponding to an EC of 8 mS·cm^{-1}), to minimise osmotic water transport. A 1 L solution consisting of 1 M $NaNO_3$ was again used as electrode rinse. The same hydraulic conditions were used for the diffusion experiment as during the SBEs, but no electric current was applied. TAN concentrations were measured in all solutions every hour and the diluate, acid, base and electrode rinse pH and EC were measured and logged automatically every five minutes. Finally, initial and final solution volumes were determined to assess the TAN mass balance.

4.2.2.3. Avoiding accumulation of TAN in the electrode rinse

Additional experiments aimed to avoid any accumulation of TAN in the electrode rinse. To this end, a BPMED membrane stack equipped with AEEMs was constructed, by replacing the CEEMs of the original BPMED membrane stack by additional identical AEMs already used in the original BPMED membrane stack. The membrane sequence was adjusted in such a way that again ten cell triplets were formed. A schematisation with the membrane configuration of the BPMED membrane stacks equipped with CEEMs

and AEEMs can be found in the Supporting Information of the paper of van Linden et al. (2020). Only the first batch of the SBEs with the adjusted BPMED membranes stack was repeated in duplicate, at identical operational conditions and applied settings and used the same analytical procedures.

4.2.3. Performance indicators

As a measure for utilisation of electric current to remove NH_4^+ from the diluate, the NH_4^+ current efficiency was assessed. The NH_4^+ current efficiency represents the efficiency to transport NH_4^+ by electro-migration through the CEMs. Ideally, the charge transported as NH_4^+ is equal to the supplied electric charge, but diffusion and leakage processes, and the transport of other cations through the CEM all decrease the NH_4^+ current efficiency. The NH_4^+ current efficiency was determined by the ratio between the charge transported as NH_4^+ and the supplied electric charge (Eq. 4-1).

$$\eta_{NH_4^+} = \frac{z \cdot F \cdot n_{NH_4^+,d}}{N \cdot \sum_{t=0}^{t} I_t \cdot \Delta t} \cdot 100\% \qquad \text{Eq. 4-1}$$

Where $\eta_{NH_4^+}$ = NH_4^+ current efficiency (unitless), z = ion valence (unitless, z = 1 for NH_4^+), F = Faraday constant (in $C \cdot mol^{-1}$, F = 96,485 $C \cdot mol^{-1}$), $n_{NH_4^+,d}$ = amount of NH_4^+ transported from the diluate (in mol), N = number of cell triplets in the BPMED membrane stack (unitless, N = 10), I_t = average electric current during each time interval (in A = $C \cdot s^{-1}$) and Δt = time interval (in s).

Furthermore, the electrochemical energy consumption to transport NH_4^+ from the diluate by BPMED was determined based on the consumed electrical energy and the transported NH_4^+ mass (Eq. 4-2).

$$E_e = \frac{\sum_{t=0}^{t} U_t \cdot I_t \cdot \Delta t}{m_{NH_4^+,d}} \qquad \text{Eq. 4-2}$$

Where E_e = electrochemical energy consumption (in $MJ \cdot kg\text{-}N^{-1}$), U_t = average electric potential during each time interval (in V) and $m_{NH_4^+,d}$ = amount of transported NH_4^+ from the diluate (in g-N).

4.3. Results

4.3.1. Removal of NH_4^+ and production of concentrated dissolved NH_3

The presented values represent the average results of the duplicate SBEs unless indicated differently. The deviation (min-max) of the duplicate results was always below 10%. Figure 4-4A presents the diluate, acid and base EC over the cumulative electrochemical energy consumption throughout one SBE. In the Supporting Information of the paper of van Linden et al. (2020), the evolution of the EC and pH throughout the duplicate SBE is presented. The diluate EC for each new batch was decreased from 8 to 1 mS·cm^{-1}. For each consecutive diluate batch, more time was needed to decrease the diluate EC to 1 mS·cm^{-1}. The operational run time increased from 66 minutes for the first batch to 89 minutes for the tenth batch. However, the increase in operational run time did not result in an increase in electrochemical energy consumption per batch, as for the first batch 18.7 kJ was used and for the tenth batch 18.1 kJ was used. The base EC increased steadily throughout the SBEs and finally reached 18 mS·cm^{-1}. The acid EC only increased from 8 to 10 mS·cm^{-1} during the first three batches. Subsequently, the increase in acid EC accelerated and the acid EC exceeded the base EC after six batches. The acid EC reached a final value of 25 mS·cm^{-1}.

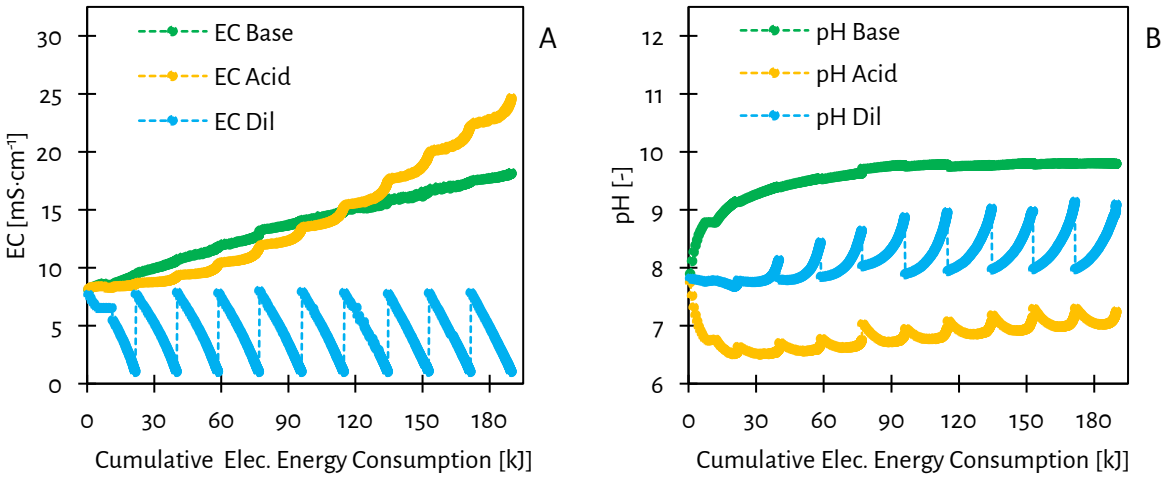

Figure 4-4 - The EC (A) and pH (B) throughout one of the SBE duplicates. The diluate EC decreased to 1 mS·cm^{-1} for each batch, while the acid and base EC increased to 25 and 19 mS·cm^{-1} throughout the SBE, respectively. The diluate pH increased during each batch and the final diluate pH increased over the consecutive batches from 7.8 to 9.1. The base pH increased throughout the SBEs and reached a plateau at 9.8, while the acid pH initially decreased to 6.5 and subsequently increased each consecutive batch to a final value of 7.3.

Figure 4-4B presents the pH of the diluate, acid and base. The base pH increased during the first five batches and subsequently reached a plateau at a pH of 9.8. The acid pH decreased from 7.8 to 6.5 after the first two batches and subsequently increased for each consecutive batch. The acid pH eventually reached a pH of 7.3 after the tenth batch. The new diluate batches had an average pH of 7.8 and for each batch after the first batch, the diluate pH increased and reached 9.1 for the tenth batch.

According to Figure 4-5A, the decrease in diluate EC to 1 $mS \cdot cm^{-1}$ corresponded to a TAN removal efficiency ranging 85 – 91%. The amount of transported NH_4^+ was 1.3 ± 0.1 g (AVG ± STD, n = 20) for consecutive batches in duplicate. For the first five batches, at least 90% of NH_4^+ was removed from the diluate, but the TAN removal efficiency decreased to 85% for the tenth batch. The TAN concentration in the base increased from 1.5 to 7.3 $g \cdot L^{-1}$, corresponding to a concentration factor of 5, but approached a plateau (decelerating increase). Based on the intended ion transport (Figure 4-2), no NH_4^+ transport should take place to the acid. However, the TAN concentration in the acid increased from 1.5 to 5.4 $g \cdot L^{-1}$ and showed a first-order kinetics trend (accelerating increase). Finally, the TAN concentration also increased in the electrode rinse, from 0 to 3.4 $g \cdot L^{-1}$. The acid EC reached a final value of 25 $mS \cdot cm^{-1}$. In the Supporting Information of the paper of van Linden et al. (2020), the evolution of the TAN and NH_3 concentrations throughout the duplicate SBE is presented. The TAN mass balance of all batches fitted with an average error of 3%.

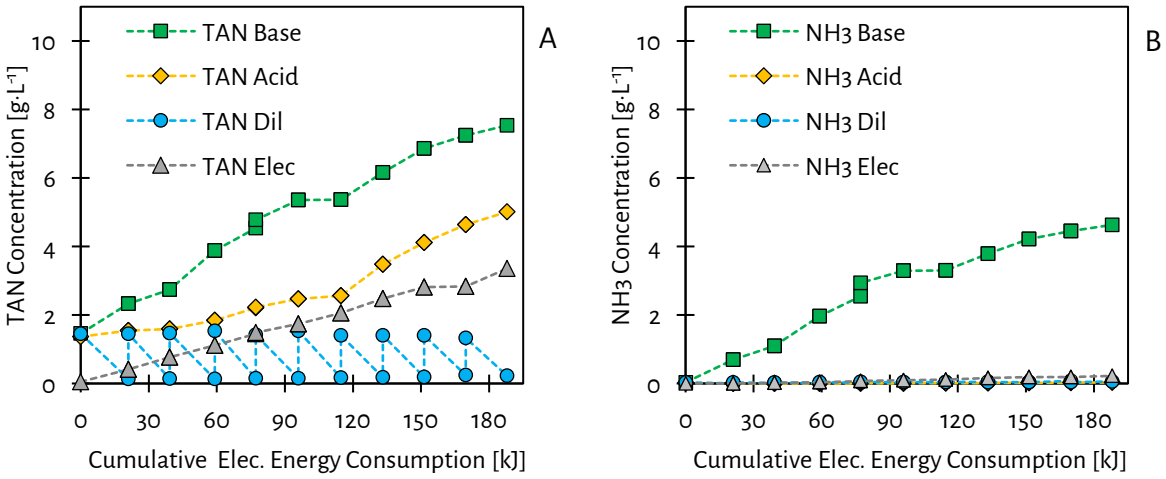

Figure 4-5 - The concentrations of TAN (A) and NH_3 (B) in the diluate, acid, base and electrode rinse throughout one of the SBE duplicates. The removal efficiency of TAN from the diluate decreased from 91% for the first batch to 85% for the tenth batch. The transported NH_4^+ partially ended to the base, which had a final pH of 9.8, resulting in a final NH_3 concentration in the base of 4.5 $g \cdot L^{-1}$. The residual fraction of the transported NH_4^+ ended up as NH_4^+ in the acid and the electrode rinse.

Figure 4-5B presents the actual NH_3 concentrations throughout the SBEs, as calculated based on the measured TAN concentrations, temperature, pH and ionic strength in the various solutions. The concentration of NH_3 in the base increased from 0 to 4.5 $g \cdot L^{-1}$ after the tenth batch and, similarly to the TAN concentration in the base, also approached a plateau, indicating a decelerating increase. On the other hand, the NH_3 concentration in the diluate, acid and electrode rinse throughout the SBE never exceeded 0.2 $g \cdot L^{-1}$. Due to the accumulation of NH_3 in the base, an NH_3 concentration gradient, ranging 0.7 – 4.5 $g \cdot L^{-1}$, established between the base and diluate and the base and acid.

Figure 4-6A shows that the NH_4^+ current efficiency decreased from 69% for the first batch to 54% for the tenth batch during the SBEs. Interestingly, according to Figure 4-6B, the electrochemical energy consumption to remove NH_4^+ by 85 – 91% was stable at 18 ± 1 $MJ \cdot kg\text{-}N^{-1}$ (AVG ± STD, n = 20).

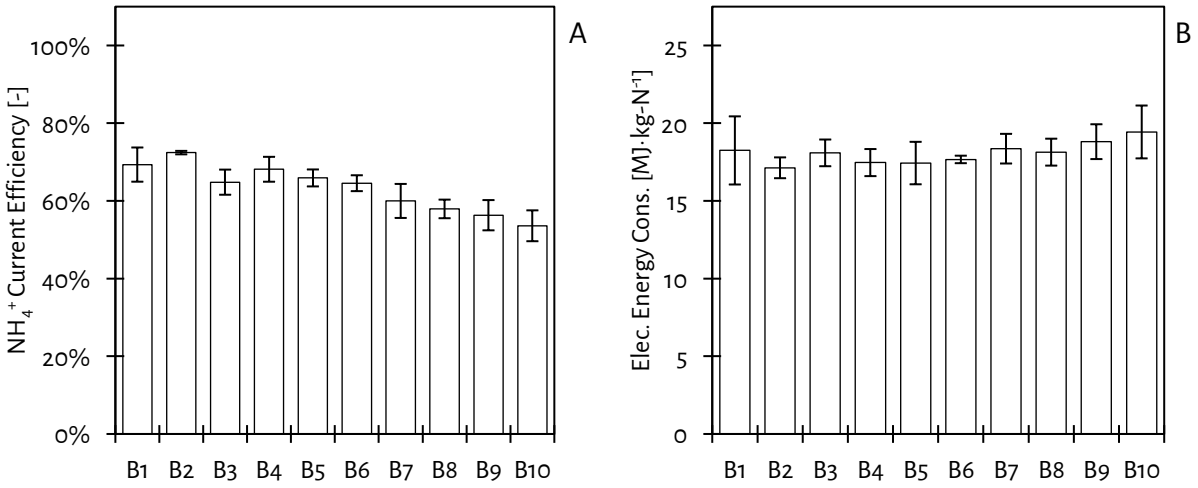

Figure 4-6 - The NH_4^+ current efficiency (A) decreased over the consecutive batches from 69% to 54%, while the electrochemical energy consumption (B) to remove NH_4^+ by 85 – 91% remained stable at 18 $MJ \cdot kg\text{-}N^{-1}$ over the consecutive batches. Average values of the duplicate SBEs are presented, along with the minimum and maximum values (outer values of error bars).

4.3.2. Diffusion of NH_3 through the BPMED membrane stack

Figure 4-7 shows the NH_3 concentrations throughout the additionally conducted diffusion experiment, during which no electric current was applied. The NH_3 concentrations are again calculated based on the measured TAN concentrations, temperature, pH and ionic strength of the solutions. The pH of the diluate, acid and base pH was always higher than 10.3 after the start of the experiment, indicating that TAN was present as NH_3 for at least 90%. The initial NH_3 concentration in the base was 12.5 $g \cdot L^{-1}$ and decreased to 6.4 $g \cdot L^{-1}$ after 480 minutes, showing a decelerating trend. The NH_3 concentration in the diluate and acid increased, also showing a decelerating trend. The NH_3 in the diluate and the acid increased from 0 to 2.4 and 3.1 $g \cdot L^{-1}$, respectively. The NH_3 concentration in the electrode rinse throughout the diffusion experiment did not exceed 0.1 $g \cdot L^{-1}$. The NH_3 mass balance of the diffusion experiment fitted with an error of 6%, which was probably caused by the volatilisation of NH_3.

Due to the decrease in NH_3 concentration in the base and increase in NH_3 in the diluate and acid, the NH_3 concentration gradient between the base and acid and the base and diluate, decreased over time, from 12.5 $g \cdot L^{-1}$ to 3.3 $g \cdot L^{-1}$ and 4.0 $g \cdot L^{-1}$, respectively. The NH_3 concentration gradient between the diluate and acid increased from 0 to only 0.8 $g \cdot L^{-1}$.

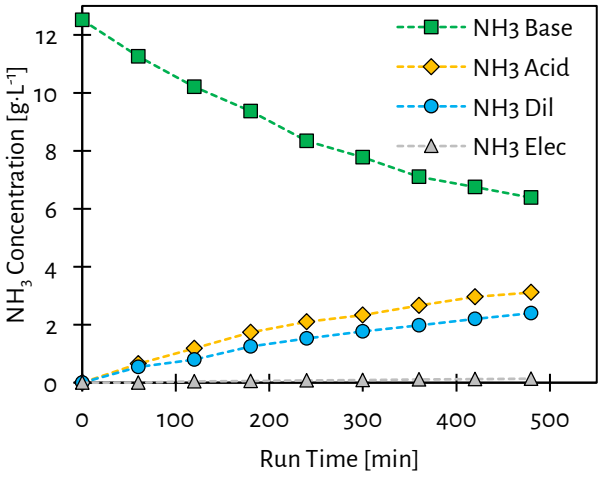

Figure 4-7 - The NH_3 concentration in the base decreased during the diffusion experiment due to NH_3 diffusion from the base to the diluate and the acid.

4.3.3. Avoiding accumulation of TAN in the electrode rinse

During the duplicate SBEs, 27 ± 11% (AVG ± STD, n = 20) of the TAN transported from new diluate batches ended up and accumulated as NH_4^+ in the electrode rinse, resulting in a final TAN concentration in the electrode rinse of 3.4 $g \cdot L^{-1}$. The observed accumulation of TAN in the electrode rinse was similar to the findings in the study of van Linden et al. (2019a), in which ED was to remove TAN as NH_4^+ from the same diluate. Figure 4-8 shows that during the first batch of the duplicate SBEs 26% of the TAN that was transported from the diluate accumulated in the electrode rinse when the BPMED membrane stack was

equipped with CEEMs. Concurrently, only 64% of the TAN transported from the diluate accumulated in the base for the first batches of the duplicate SBEs.

By using a BPMED membrane stack equipped with AEEMs, the accumulation of TAN in the electrode rinse was prevented. During the experiments with a BPMED membrane stack equipped with AEEMs, the fraction of TAN that accumulated in the electrode rinse was negligible, while the fraction of TAN that accumulated in the base increased to 94%.

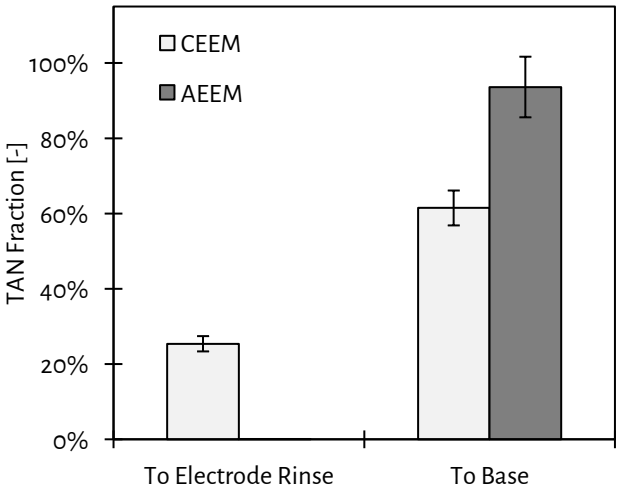

Figure 4-8 - The accumulation of TAN transported from the diluate in the electrode rinse decreased from 26% for the use of CEEMs to 0% for the use of AEEMs in the BPMED membrane stack. In addition, the accumulation of TAN transported from the diluate in the base increased from 64% for the use of CEEMs to 94% for the use of AEEMs. Average values of the duplicate experiments are shown, along with the minimum and maximum values (outer values of the error bars).

4.4. Discussion

4.4.1. Removal of NH_4^+ and production of concentrated dissolved NH_3

4.4.1.1. Evaluation of the diluate

The decrease in diluate EC from 8 to 1 mS·cm^{-1} (Figure 4-4A) was the result of the effective removal of NH_4^+ and HCO_3^- from the diluate. The diluate pH increased during the treatment of a new diluate batch (Figure 4-4B), in contrast to multiple previous studies (Li et al., 2016; Shi et al., 2018). Two phenomena probably caused the increase in diluate pH. Firstly, diffusion of NH_3 from the base, which was validated to take place in the diffusion experiment (section 3.3), resulted in the consumption of H^+ in the diluate to form NH_4^+, leading to the diluate pH increase. Secondly, the diluate pH increased due to leakage of OH^- from the base to the diluate. OH^- is prone to leak through CEMs due to, amongst others, its high diffusivity (Strathmann, 2010). The effect of NH_3 diffusion and OH^- leakage on the diluate pH became more apparent at the end of each batch (Figure 4-4B), when the concentration gradients were highest and the buffer capacity of the diluate was decreased, due to the removal of NH_4^+ and HCO_3^-. Apparently, NH_3 diffusion and OH^- leakage affected the diluate pH more than any diffusion of CO_2 or leakage of H^+ from the acid, which would cause a decrease in the diluate pH. Because the operational run time and the NH_3 and OH^- concentration gradients between the base and diluate increased throughout the SBEs, the final diluate pH increased from 7.7 for the first batch to 9.1 for the tenth batch. The decrease in NH_4^+ removal efficiency from 91 to 85% over the consecutive batches was also a result of the diluate pH increase throughout each batch. Due to the pH increase, a fraction of the NH_4^+ was converted to NH_3 and was therefore not transported by electro-migration.

4.4.1.2. Evaluation of the base

The base pH reached a plateau at pH = 9.8 (Figure 4-4B), whereas in previous studies pH values higher than 11 were achieved (Li et al., 2016; Shi et al., 2018). One of the causes of the plateauing of the base pH was the consumption of OH^- by NH_4^+, resulting in the formation of NH_3 and water. Therefore, a certain fraction of OH^- produced by the BPMs was not translated to an increase in base pH. Besides, in contrast to previous studies, the initial base contained HCO_3^-, which reacted with the produced OH^- to CO_3^{2-}. Therefore, not all generated OH^- was available to increase the pH effectively. Finally, any diffusion of CO_2 from the acid also contributed to the plateauing of the base pH. The OH^- concentration gradient between the base and diluate increased from 1.2·10^{-5} to 4.9·10^{-5} mol·L^{-1} throughout the SBEs. At a final base pH of 9.8, a temperature of 24 °C and an EC of 18 mS·cm^{-1}, 71% of the TAN was present as NH_3. Eventually, only 48 ± 21% (AVG ± STD, n = 20) of the NH_4^+ that was transported from the diluate accumulated in the base. The residual NH_4^+ that was transported from the diluate accumulated in the acid and the electrode rinse. The NH_3 concentration in the base increased from 0 to 4.5 g·L^{-1}, while the NH_4^+ concentration in the acid increased from 1.5 to 2.9 g·L^{-1}. As mentioned in section 2.1, the transport of NH_4^+ to the electrode rinse led to the wash-out of Na^+ from the electrode rinse, resulting in the accumulation of Na^+-species (such as NaOH, $NaHCO_3$ and Na_2CO_3) in the

base. NH_4^+ and Na^+ accumulated with the anions OH^-, HCO_3^- and CO_3^{2-} in the base, explaining the increase in base EC (Figure 4-4A). Of these anions, OH^- was produced by the BPMs, while HCO_3^- either diffused as CO_2 (as mentioned by Pronk et al. (2006d)) or as HCO_3^--species from the acid and CO_3^{2-} was formed by OH^- and HCO_3^-. The NH_3 and NH_4^+ concentration gradients between the base and diluate ranged 0.04 – 0.27 mol·L^{-1} and 0.08 – 0.15 mol·L^{-1}, respectively.

4.4.1.3. Evaluation of the acid

The limited increase in acid EC after the first three batches (Figure 4-4A) was a result of the formation of uncharged CO_2 from the generated H^+ and the HCO_3^- in the acid. Because CO_2 has a relatively low solubility (1.5 g·L^{-1} at T = 24 °C, based on the Henry's constant and thermodynamic data taken from Sander (2015)), it became supersaturated in the acid, indicated by the observation of obvious gas bubbles. The transport of gas bubbles to the headspace of the acid solution bottle indicated spontaneous stripping of CO_2 from the acid, which prevented the accumulation of H^+ in the acid. In previous studies H^+ accumulated in the acid with ions such as Cl^-, resulting in H^+ leakage from the acid to the diluate and ultimately a decrease in diluate pH (Li et al., 2016; Shi et al., 2018). Because in this study HCO_3^- was the main anion, accumulation and leakage of H^+ from the acid to the diluate was limited. After the sixth batch, the increase in acid EC and also TAN concentration accelerated (Figure 4-4A and Figure 4-5A). Because the operational run time and the NH_3 concentration gradient between the base and acid both increased throughout the SBEs, more NH_3 diffusion to the acid took place, causing the accelerated increase in acid EC and TAN concentration. Besides, the acid pH increased each consecutive batch (Figure 4-4B), due to NH_3 diffusion and OH^- leakage from the base.

4.4.1.4. Assessment of the NH_4^+ current efficiency

For the treatment of each consecutive diluate batch, a loss in NH_4^+ current efficiency was observed. The loss in NH_4^+ current efficiency was caused by the leakage of OH^-, the diffusion of dissolved NH_3 and the diffusion of ionic species. Because a concentration gradient was present, TAN species such as NH_4HCO_3 could diffuse from the base back to the diluate. Therefore, to decrease the diluate EC to 1 mS·cm^{-1}, NH_4^+ must be transported back and forth, at the expense of additional electric charge. Besides, the accumulated Na^+-species could also diffuse from the base to the diluate and therefore contributed to the loss in NH_4^+ current efficiency, because electric charge was also used to transport Na^+ from the diluate to decrease the diluate EC. The mentioned OH^- leakage, dissolved NH_3 diffusion and diffusion of TAN-species and Na^+-species (the ionic species) all took place from the base, through the CEMs, to the diluate. The contribution of H^+ leakage in the form of proton or hydronium (H_3O^+) ions was neglected, because the H^+ concentration gradient was at least two orders of magnitude lower than the NH_3, OH^- and ionic species concentration gradients between the base and the diluate. Also, electro-migration of H^+ was neglected because the amount of charge in the new diluate batches represented by H^+ was only 1·10^{-3} C, compared to approximately 8,000 C for NH_4^+ (corresponding to 1.5 g NH_4^+). However, based on the available data, no

conclusions can be drawn on what process (OH^- leakage, dissolved NH_3 diffusion or ionic species diffusion) had the largest contribution to the loss in NH_4^+ current efficiency.

Because more electric charge needed to be supplied used to transport NH_4^+, the operational run time to treat the new diluate batches increased. The NH_4^+ current efficiency decreased over consecutive batches, as is depicted in Figure 4-6A. Because a fixed amount of TAN mass was transported per batch of new diluate, a fixed amount of charge as NH_4^+ was transported. Therefore, according to Eq. 4-1, the loss in NH_4^+ current efficiency was a result of an additionally supplied electric charge. Ultimately, the decrease in NH_4^+ current efficiency throughout the SBEs was a result of both the increase in operational run time and concentration gradients, which led to more OH^- leakage and dissolved NH_3 diffusion and ionic species diffusion.

4.4.1.5. Assessment of the electrochemical energy consumption

Even though the NH_4^+ current efficiency decreased over the consecutive batches, the electrochemical energy consumption to remove NH_4^+ by 85 – 91% was stable at 18 MJ·kg-N^{-1} (Figure 4-6B). The decrease in NH_4^+ current efficiency was compensated by a decrease in electric potential throughout the SBEs. Figure 4-9 shows that the average electric potential throughout a batch decreased over the consecutive batches. The average electric potential was 15.5 V for the first batch and dropped to 12.6 V for the tenth batch. The decrease in electric potential was a result of the increase in acid and base EC throughout the SBEs (Figure 4-4A), which led to a decrease in electrical resistance of the BPMED membrane stack.

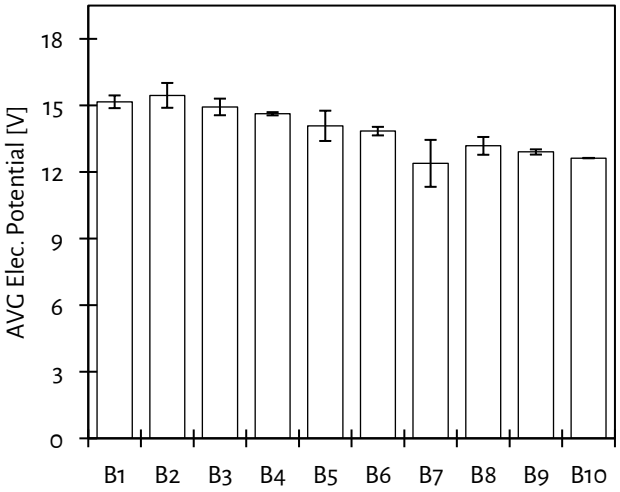

Figure 4-9 - The average electric potentials during each consecutive batch decreased throughout the SBEs due to a decrease in electrical resistance of the BPMED membrane stack as a result of the increase in acid and base EC. Average values of the duplicate experiments are shown, along with the minimum and maximum values (outer values error bars).

4.4.2. Diffusion of NH_3 through the BPMED membrane stack

During the diffusion experiment (Figure 4-7), diffusion of NH_3 took probably place from the base (through the BPMs) to the acid and (through the CEMs) to the diluate, because the NH_3 concentration gradients between the base and acid and the base and diluate (ranging 3.3 to 12.5 $g \cdot L^{-1}$) were at least four times higher than the NH_3 concentration gradient that between the diluate and acid (ranging 0.0 – 0.8 $g \cdot L^{-1}$). Furthermore, the decelerated changes (first-order kinetics) in NH_3 concentrations in the base, acid and diluate during the diffusion experiment were caused by the decrease in NH_3 concentration gradients, which is typical for diffusion experiments. The NH_3 concentration in the acid was always higher than in the diluate, suggesting that NH_3 diffused more easily from the base, through the BPMs, to the acid than from the base, through the CEMs, to the diluate. While the diffusion of NH_3 through CEMs and BPMs was also observed by (Ali et al., 2004), drawing firm conclusions on what membranes are more susceptible to NH_3 diffusion requires the determination of membrane permeability constants.

4.4.3. Avoiding accumulation of TAN in the electrode rinse

According to the results of the diffusion experiment in section 3.3, the transport of TAN to the electrode rinse by diffusion of NH_3 from the base was negligible. Therefore, the main mechanism responsible for the transport of TAN to the electrode rinse was electro-migration of NH_4^+, even though TAN-species can also diffuse from the electrode rinse to the adjacent diluate and base cells. During the SBEs, NH_4^+ was transported by electro-migration from the diluate, through the CEEM at the cathode, to the electrode rinse. Because the electrode rinse consisted of $NaNO_3$, both Na^+ and NH_4^+ were transported from the electrode rinse, through the CEEM at the anode, to the base (Figure 4-2), resulting in the accumulation of NH_4^+ in the electrode rinse and the wash-out of Na^+.

By replacing CEEMs by AEEMs in the BPMED membrane stack, electro-migration to the electrode rinse was prevented and the transport of TAN to the base increased (Figure 4-8), suggesting that higher TAN and NH_3 concentrations potentially can be achieved in the base when the same amount of diluate is treated. Furthermore, the use of AEEMs also resulted in an increase in NH_4^+ current efficiency from 69 to 78% and a decrease in electrochemical energy consumption from 18 to 16 $MJ \cdot kg\text{-}N^{-1}$. The observed increase in NH_4^+ current efficiency and decrease in energy consumption may be explained by the avoided diffusion of Na^+-species from the base to the diluate, as wash-out of Na^+ was avoided.

The results show that the use of AEEMs instead of CEEMs in the BPMED membrane stack effectively prevented the accumulation of NH_4^+ in the electrode rinse, without notable negative side-effects. However, it is expected that HCO_3^- accumulated in the electrode rinse, at the expense of the anion initially present in the electrode rinse (NO_3^-). To avoid the loss of NO_3^- from the electrode rinse, it could be considered to use HCO_3^- as an anion in the initial electrode rinse, to avoid any accumulation and wash-out of ions. Another option is to equip the BPMED membrane stack with CEEMs and use NH_4^+ as the cation for the initial electrode rinse. The latter would not require an adjustment in the initially used BPMED membrane stack configuration containing CEEMs.

4.4.4. Energetic evaluation of BPMED and ED in combination with the addition of chemicals

The electrochemical energy consumption to transport NH_4^+ by BPMED was three times as much compared to the 5.4 MJ·kg-N^{-1} reported for ED in the study of van Linden et al. (2019a). The difference in electrochemical energy consumption is partially explained by the lower NH_4^+ current efficiency of BPMED, compared to ED. The NH_4^+ current efficiency of BPMED ranged 54 – 69%, whereas the NH_4^+ current efficiency of ED ranged 83 – 96%. Thus, for BPMED more electric charge was required to transport the same amount of NH_4^+. In addition, the average electric potential during a batch for BPMED (ranging 12.6 – 15.2 V) was higher than for ED (ranging 5.7 – 7.0 V). The higher electric potential for BPMED was a result of the presence of additional cells and the presence of BPMs. While ED contains cell pairs (diluate and concentrate), BPMED contains cell triplets (diluate, acid and base). The addition of extra cells introduces additional electrical resistance of the liquids and the spacers. Besides, BPMED makes use of BPMs, which introduce an electrical resistance and an additional electric potential for the dissociation of water, depending on the pH gradient between the acid and base (Mani, 1991). For BPMED, 30% more electric charge was required, whereas the electric potential was 130% higher than for ED. Together, the extra electric charge and the higher electric potential explain the higher electrochemical energy consumption of BPMED to transport NH_4^+.

Besides the energy to drive the electrochemical processes, energy is required to pump the solutions through the ED cell. The pumping energy was determined based on additional hydraulic pressure measurements over the membrane stack and the respective hydraulic flow rates. The hydraulic pressure loss at a flow rate of 19 L·h^{-1} was 9.3 kPa for the diluate, acid and base, having ten cells each. In addition, the hydraulic pressure loss for the electrode rinse was 8.4 kPa. With a maximum operational run time of 89 minutes for BPMED and 66 minutes for ED, the pumping energy was 1.0 kJ and 0.5 kJ, respectively. More information on the determination of the pumping energy is presented in the Supporting Information of the paper of van Linden et al. (2020).

In the study van Linden et al. (2019a), a concentrate solution with a TAN concentration of 10 g·L^{-1} was produced, which was present as NH_4HCO_3. To compare the energy consumption of BPMED and ED for the removal of NH_4^+ and simultaneous production of NH_3, an equal NH_3 concentration should be taken as a reference point. In this chapter, after ten batches, a base solution with a TAN concentration of 7.3 g·L^{-1} at a pH of 9.8 was produced, corresponding to an NH_3 concentration of 4.5 g·L^{-1}. To achieve this, in total 13 grams of TAN was transported as NH_4^+ from the diluate by BPMED. For ED, seven identical diluate batches (1 L solutions containing 1.5 g·L^{-1} TAN as NH_4HCO_3) were treated the same way (reduction of EC to 1 mS·cm^{-1}) to produce a concentrate solution with a TAN concentration of 7.3 g·L^{-1}, corresponding to the transport of 10 grams of TAN as NH_4^+ from the diluate. However, the final pH of the ED concentrate only reached 8.8. The amount of NaOH addition to increase the pH to 9.8 was obtained from the results of PHREEQC software simulations, in order to subsequently calculate how much energy is associated with the industrial production of NaOH. According to the study of Hong et al. (2014) on the life cycle analysis of NaOH

production, 2,176 kWh of electricity is consumed to produce one ton of NaOH by electrolysis, which corresponds to 7.8 kJ·g-NaOH^{-1}.

Table 4-1 presents the amount of required NaOH to increase the pH from 8.8 to 9.8 of the ED concentrate. When the energy consumption for driving the electrochemical processes, pumping and chemical production is considered, BPMED appears to be energetically competitive to ED in combination with the addition of chemicals. The energy consumption to produce 4.5 g·L^{-1} NH_3 by BPMED and ED with the addition of chemicals was 19 and 22 MJ·kg-N^{-1}, respectively.

Table 4-1 - The energetic evaluation of the production of a solution with an NH_3 concentration of 4.5 g·L^{-1} by BPMED and ED, including on the energy input to drive the electrochemical processes, the pumping energy to recirculate the solutions and the energy to produce chemicals.

		Unit	BPMED Base	ED Concentrate
Solution Conditions	Final TAN	g·L^{-1}	7.3	7.3
	Final pH	-	9.8	8.8
Chemical Addition	NaOH	g	-	16.5
Energy Consumed	Electrochemical	kJ	18·10 = 180	5.4·7 = 38
	Pumping	kJ	1.0·10 = 10	0.5·7 = 3.5
	NaOH	kJ	-	129
Mass Transported	TAN	g	13	10
Energy Consumption		MJ·kg-N^{-1}	19	22

4.5. Conclusions

The experimental study to assess the feasibility and energy consumption of BPMED to produce concentrated NH_3 solutions resulted in the following conclusions:

- BPMED proved to be able to remove 85 – 91% of the NH_4^+ from feed water with an initial NH_4^+ concentration of 1.5 $g \cdot L^{-1}$ as NH_4HCO_3.
- The pH in the base was effectively increased from 7.8 to 9.8 and the NH_3 concentration was increased from 0 to 4.5 $g \cdot L^{-1}$.
- Only 48% of the NH_4^+ transported from the diluate ended up in the base as NH_3 due to accumulation of NH_4^+ in the electrode rinse and diffusion of NH_3 from the base to the acid and back to the dilute;
- Replacing the CEEMs by AEEMs in the BPMED membrane stack prevented the transport to the NH_4^+ to the electrode rinse and therewith the accumulation of NH_4^+ in the electrode rinse.
- The electrical energy consumption for BPMED remained stable at 19 $MJ \cdot kg\text{-}N^{-1}$, comprising the required energy for the transport of NH_4^+ from the diluate, the dissociation of water for the production of H^+ and OH^- and the pumping energy to recirculate the solutions.
- The losses in NH_4^+ current efficiency were caused by the leakage of OH^-, the diffusion of dissolved NH_3 and the diffusion of ionic species (such as NH_4HCO_3) from the base to the diluate.
- The electrochemical energy consumption eventually remained stable because the decrease in NH_4^+ current efficiency was compensated by a decrease in electric potential, caused by a decrease in the electrical resistance of the BPMED membrane stack as a result of an increase in the acid and base EC.
- An energetic evaluation showed that the energy consumption of BPMED to remove NH_4^+ and simultaneously produce concentrated dissolved NH_3 was competitive to the combination of ED and the addition of chemicals (22 $MJ \cdot kg\text{-}N^{-1}$).

4.6. References

Ali, M. A. B., Rakib, M., Laborie, S., Viers, P., & Durand, G. (2004). Coupling of bipolar membrane electrodialysis and ammonia stripping for direct treatment of wastewaters containing ammonium nitrate. *Journal of Membrane Science, 244*(1-2), 89-96. doi:10.1016/j.memsci.2004.07.007

Gonzalez-Martinez, A., Muñoz-Palazon, B., Rodriguez-Sanchez, A., & Gonzalez-Lopez, J. (2018). New concepts in anammox processes for wastewater nitrogen removal: recent advances and future prospects. *FEMS Microbiology Letters, 365*(6). doi:10.1093/femsle/fny031

Graillon, S., Persin, F., Pourcelly, G., & Gavach, C. (1996). Development of electrodialysis with bipolar membrane for the treatment of concentrated nitrate effluents. *Desalination, 107*(2), 159-169. doi:http://dx.doi.org/10.1016/S0011-9164(96)00155-5

Hong, J., Chen, W., Wang, Y., Xu, C., & Xu, X. (2014). Life cycle assessment of caustic soda production: a case study in China. *Journal of Cleaner Production, 66*, 113-120. doi:https://doi.org/10.1016/j.jclepro.2013.10.009

Li, Y., Shi, S., Cao, H., Wu, X., Zhao, Z., & Wang, L. (2016). Bipolar membrane electrodialysis for generation of hydrochloric acid and ammonia from simulated ammonium chloride wastewater. *Water Research, 89*(Supplement C), 201-209. doi:https://doi.org/10.1016/j.watres.2015.11.038

Lv, Y., Yan, H., Yang, B., Wu, C., Zhang, X., & Wang, X. (2018). Bipolar membrane electrodialysis for the recycling of ammonium chloride wastewater: Membrane selection and process optimization. *Chemical Engineering Research and Design, 138*, 105-115. doi:https://doi.org/10.1016/j.cherd.2018.08.014

Mani, K. N. (1991). Electrodialysis water splitting technology. *Journal of Membrane Science, 58*(2), 117-138. doi:https://doi.org/10.1016/S0376-7388(00)82450-3

PCA. (2016a). PCA Ion Exchange Membranes: Technical Data Sheet. In. Heusweiler: PCA GmbH.

Pronk, W., Biebow, M., & Boller, M. (2006d). Treatment of source-separated urine by a combination of bipolar electrodialysis and a gas transfer membrane. *Water Sci Technol, 53*(3), 139-146.

Sander, R. (2015). Compilation of Henry's law constants (version 4.0) for water as solvent. *Atmos. Chem. Phys., 15*(8), 4399-4981. doi:10.5194/acp-15-4399-2015

Shi, L., Hu, Y., Xie, S., Wu, G., Hu, Z., & Zhan, X. (2018). Recovery of nutrients and volatile fatty acids from pig manure hydrolysate using two-stage bipolar membrane electrodialysis. *Chemical Engineering Journal, 334*, 134-142. doi:https://doi.org/10.1016/j.cej.2017.10.010

Shuangchen, M., Tingting, H., Lan, M., Jingxiang, M., Gongda, C., & Jing, Y. (2015). Experimental study on desorption of simulated solution after ammonia carbon capture using bipolar membrane electrodialysis. *International Journal of Greenhouse Gas Control, 42*, 690-698. doi:https://doi.org/10.1016/j.ijggc.2015.09.020

Strathmann, H. (2010). Electrodialysis, a mature technology with a multitude of new applications. *Desalination, 264*(3), 268-288. doi:https://doi.org/10.1016/j.desal.2010.04.069

Tongwen, X. (2002). Electrodialysis processes with bipolar membranes (EDBM) in environmental protection—a review. *Resources, Conservation and Recycling, 37*(1), 1-22. doi:https://doi.org/10.1016/S0921-3449(02)00032-0

van Linden, N., Bandinu, G. L., Vermaas, D. A., Spanjers, H., & van Lier, J. B. (2020). Bipolar membrane electrodialysis for energetically competitive ammonium removal and dissolved ammonia production. *Journal of Cleaner Production*, 120788. doi:https://doi.org/10.1016/j.jclepro.2020.120788

van Linden, N., Spanjers, H., & van Lier, J. B. (2019a). Application of dynamic current density for increased concentration factors and reduced energy consumption for concentrating ammonium by electrodialysis. *Water Research*, 114856. doi:https://doi.org/10.1016/j.watres.2019.114856

Ward, A. J., Arola, K., Thompson Brewster, E., Mehta, C. M., & Batstone, D. J. (2018). Nutrient recovery from wastewater through pilot scale electrodialysis. *Water Research, 135*, 57-65. doi:https://doi.org/10.1016/j.watres.2018.02.021

Chapter 5.

Recovery of ammonia-water mixtures by vacuum membrane stripping

Based on: Selectivity of vacuum ammonia stripping using porous gas-permeable and dense pervaporation membranes under various hydraulic conditions and feed water compositions
Niels van Linden, Yundan Wang, Ernst Sudhölter, Henri Spanjers, Jules B. van Lier
https://doi.org/10.1016/j.memsci.2021.120005

Abstract

Simultaneous evaporation of water (H_2O) during ammonia (NH_3) stripping under vacuum dilutes the recovered NH_3 gas. Whereas porous gas-permeable membranes are already used for vacuum NH_3 stripping, the use of non-porous silica-based pervaporation (PV) membranes showed promising results in recent literature, with respect to more selective transfer of NH_3 compared to H_2O. This chapter presents the assessment of the selectivity of NH_3 over H_2O transfer (S_{NH_3/H_2O}) for different types of membranes under various hydraulic conditions and for feed water compositions. The three following membranes were tested: a porous gas-permeable polytetrafluoroethylene (PTFE) membrane, a hydrophilic (Hybrid Silica PV) membrane and a hydrophobic polydimethylsiloxane PV (PDMS PV) membrane.

For all tested membranes, S_{NH_3/H_2O} ranged between 0.1 and 0.4, indicating that the transfer of NH_3 was consistently less preferred over the transfer of H_2O. The preference for H_2O over NH_3 transfer through the membranes at various hydraulic conditions and feed water compositions can be assigned to the similarity in polarity and kinetic diameter of NH_3 and H_2O and the low relative concentration of NH_3 in the used feed waters (approximately 0.1 – 1.0 wt%). The PDMS PV membrane showed negligible NH_3 transfer and deteriorated rapidly during the NH_3 stripping experiments. The S_{NH_3/H_2O} of both gas-permeable and PV membranes was higher for unsteady than for steady hydraulic conditions. Furthermore, the S_{NH_3/H_2O} of the both PTFE and the Hybrid Silica decreased when the ionic strength of the feed water increased from 0.0 to 0.8 $mol \cdot L^{-1}$ and when the NH_3 feed water concentration increased from 1 to 10 $g \cdot L^{-1}$. According to the results, the used PV membranes did not show selectivity of NH_3 over H_2O transfer. In fact, the used PV membranes consistently had a lower S_{NH_3/H_2O} than the PTFE membrane. Hence, the dense silica-based PV membranes do not offer opportunities to recover gaseous NH_3 from water while decreasing the content of H_2O in the recovered gas, compared to porous PTFE membranes.

Keywords

ammonia; water vapour; stripping; selectivity; mass transfer coefficient; pervaporation;

5.1. Introduction

Chapter 1 of this thesis identifies vacuum membrane stripping (VMS) as a suitable technology to recover gaseous NH_3 solutions. Subsequently, a literature review presented in Chapter 2 of this thesis confirms that VMS is a suitable technology for the production of NH_3 solutions, but that water transfer due to evaporation leads to dilution of the recovered NH_3 gas.

5.1.1. Evaporation of H_2O during recovery of gaseous NH_3 from water

During NH_3 recovery by vacuum stripping processes, such as vacuum membrane stripping (VMS) using porous gas-permeable membranes, stripping of NH_3 is accompanied by the evaporation of H_2O, which dilutes the obtained gaseous NH_3 (Ding et al., 2006; El-Bourawi et al., 2007; van Linden et al., 2022a). To obtain more concentrated NH_3 gas, the concentration of NH_3 in the feed water can be increased (He et al., 2018; Scheepers et al., 2020; van Linden et al., 2022a). Moreover, according to the study of van Linden et al. (2022a), increasing the feed water temperature at an NH_3 feed concentration of 10 $g \cdot L^{-1}$ from 25 to 35 °C results in an increase in NH_3 concentration in the permeate from 8 to 11 wt%. However, a further increase in the feed water temperature to 45 and 55 °C leads to dilution of NH_3 in the gaseous permeate to 5 and 4 wt%, respectively. To obtain more concentrated NH_3 by VMS, the evaporation of H_2O must be minimised. To this end, a physical barrier for the transfer of H_2O that does not negatively affect the NH_3 transfer may be introduced. Porous gas-permeable membranes are not considered to be effective barriers, because the pore size of about 0.1 µm is at least two orders of magnitude larger than the kinetic diameter of transferred gases such as NH_3 (< 1 nm). To recover more concentrated NH_3 by vacuum stripping processes, the use of dense pervaporation (PV) membranes to more selectively transfer NH_3 through the membrane was initially proposed by Yang et al. (2014).

5.1.2. Selectivity of NH_3 transfer through PV membranes

For PV, selectivity (S) is defined as the ratio of the permeances of the respective gases permeating through the membrane, whereas the permeance describes the normalised transfer rate: the mass flux normalised for the driving force (Baker et al., 2010). Hence, selectivity ($S_{i/j}$) describes the normalised transfer rate of gas 'i' with respect to another gas 'j'. In this view, selective transfer of 'i' over 'j' is considered when $S_{i/j} > 1$. Selective permeation of NH_3 over hydrogen (H_2) and N_2 by using PV membranes proved to be feasible for gas separation, for the recovery of NH_3 from gas mixtures consisting of the respective gases (Camus et al., 2006; Kanezashi et al., 2010): S_{NH_3/H_2} and $S_{NH_3/N_2} > 1$. Camus et al. (2006) showed that silica-based PV membranes had a seven and fourteen times higher NH_3 permeance compared to the permeance of H_2 and N_2 when using mixtures of NH_3-H_2 and NH_3-N_2 gas as a feed at a temperature of 80 °C. Subsequently, Kanezashi et al. (2010) reported H_2 permeances up to twenty times higher than the NH_3 permeances for silica-based PV membranes when pure H_2 and NH_3 gas were used as the feed at a temperature of 50 °C. However, when mixtures of NH_3/H_2 gas were used as feed at the same temperature, selective transfer of NH_3 over H_2 took place (S_{NH_3/H_2} of 29), in agreement with Camus et al. (2006). Both Camus et al. (2006) and Kanezashi et al. (2010) attributed

the selective transfer of NH_3 over H_2 to the adsorption of NH_3 to the membrane material, which contained silica groups. According to Kanezashi et al. (2010), NH_3 and H_2 have a kinetic diameter of 0.33 and 0.26 nm, respectively. Hence, for pure gases, transfer of H_2 is faster than the transfer of NH_3 based on the higher reported permeances, but when gaseous NH_3-H_2 mixtures are present in the feed, NH_3 adsorbs on the membrane interface and hinders the adsorption and permeation of H_2, resulting in selective transfer of NH_3 over H_2 (Camus et al., 2006; Kanezashi et al., 2010).

5.1.3. Recovery of gaseous NH_3 from feed waters using PV membranes

In addition to the application to obtain more enriched permeate streams from gas mixtures by gas separation, PV membranes can also be used to remove and/or recover gases from a liquid feed such as water. According to the review of Jyoti et al. (2015), different types of PV membranes are used to allow for either selective transfer of water (H_2O) or volatile organics from liquid H_2O-organics mixtures. For the selective transfer of H_2O from liquid H_2O-organics mixtures, hydrophilic PV membranes are used, whereas hydrophobic PV membranes are used for selective transfer of volatile organics, such as alcohols or volatile fatty acids.

Research of Yang et al. (2014) focused on the recovery of gaseous NH_3 from liquid feed water, using silica-based PV membranes that were hydrothermally-treated by addition of iron and cobalt in the membrane material. Yang et al. (2014) did not report on the transfer selectivity of the PV membranes according to the proposed definition of Baker et al. (2010), but did report concentration factors up to 63 for a PV membrane for an NH_3 feed concentration of 0.8 $g \cdot L^{-1}$ at feed temperatures ranging between 45 and 50 °C. Because the concentration factor represents the ratio of the NH_3 concentration in the permeate and the feed, the relatively high concentration factors suggest high transfer rates of NH_3 compared to H_2O. In a follow-up study, Yang et al. (2016) stripped NH_3 from liquid water using a PV membrane that contained a combination of silica and organic groups for hydrothermal stability in the selective layer and was further referred to as hybrid-silica. For an NH_3 feed concentration of 50 $mg \cdot L^{-1}$ and at a feed temperature of 45 °C, the authors reported a concentration factor of 12 and an S_{NH_3/H_2O} of 0.5, indicating selective transfer of H_2O over NH_3 for the used PV membranes. Finally, Yang et al. (2018) assessed the effect of cobalt content in the selective layer of silica-based PV membranes on the transfer of H_2O and NH_3 and observed again selective transfer of H_2O over NH_3 ($S_{NH_3/H_2O} < 1$).

Hence, in currently available literature, there is no consensus on whether selective transfer of NH_3 over H_2O can be achieved by using silica-based PV membranes. The differences in transfer selectivity observed in previous studies may be explained by the differences in applied experimental conditions, as Yang et al. (2014) and Yang et al. (2018) used configurations in which the membranes were submerged in the feed water, whereas Yang et al. (2016) used a cross-flow configuration. The mentioned studies did not describe the location of the selective layer on the membranes. The location of the selective layer of the membrane and the used configuration are key to control the hydraulic conditions, which affect polarisation effects at the membrane interface, which in their turn affect the mass transfer rates through the membrane (Oliveira

et al., 2001). Furthermore, the contradicting results on the transfer selectivity of NH_3 over H_2O also may be explained by differences in tested feed characteristics, such as feed temperature and NH_3 feed concentration.

5.1.4. Research objective

Currently available literature showed that silica-based PV membranes allow for selective transfer of NH_3 over N_2 and H_2 when treating gas mixtures, but it remains unclear whether also selective transfer of NH_3 over H_2O can be achieved when stripping NH_3 from liquid water. Silica-based PV membranes are considered to be hydrophilic, indicating that these membranes allow for the transfer of H_2O. Currently, it is unknown whether hydrophobic silica-based PV membranes allow for selective transfer of NH_3 when stripping NH_3 from water. Furthermore, according to available literature, there is no clarity whether PV membranes have higher S_{NH_3/H_2O} compared to conventional porous gas-permeable membranes. Therefore, this chapter presents the assessment of the mass transfer rates and S_{NH_3/H_2O} of a porous gas-permeable membrane and dense hydrophilic and hydrophobic PV membranes while stripping NH_3 from water, using the hydraulic conditions and the feed composition, in terms of NH_3 feed concentration and ionic strength as variable operational conditions.

5.2. Materials and methods

5.2.1. Materials

For the porous gas-permeable membrane experiments, the same equipment and spacer-filled flat sheet membrane configuration as described in the study of van Linden et al. (2022a) was used. For the experiments with the PV membranes, again the same experimental set-up was used, except a stainless-steel membrane housing was used for the tubular PV membranes, including rubber rings at the ends of the PV membranes to ensure liquid and gas tightness. Figure 5-1 presents the experimental setup, including the membrane housings for the porous gas-permeable and PV membranes. The porous gas-permeable membrane was a Sterlitech polytetrafluoroethylene membrane (hereafter PTFE membrane) and the PV membranes were a hydrophilic Pervatech Hybrid Silica (hereafter Hybrid Silica PV membrane) and a hydrophobic Pervatech polydimethylsiloxane membrane (hereafter PDMS PV membrane). Table 5-1 presents an overview of the specific characteristics and measured dimensions of the used membranes.

The feed waters were prepared by the addition of Acros Organics 25 wt% ammonium hydroxide (NH_4OH) stock solution, or Sigma Aldrich ammonium bicarbonate (NH_4HCO_3) salt and Merck 1M sodium hydroxide (NaOH) solution to demineralised water. The used NH_4OH solution, NH_4HCO_3 salt and NaOH solution were all analytical grade. The prepared feed waters consisted of NH_4HCO_3 because bicarbonate (HCO_3^-) is often the main anion in nitrogen-loaded (N-loaded) residual streams, such as reject waters, urine and industrial condensates. All experimental runs were conducted in at least triplicate.

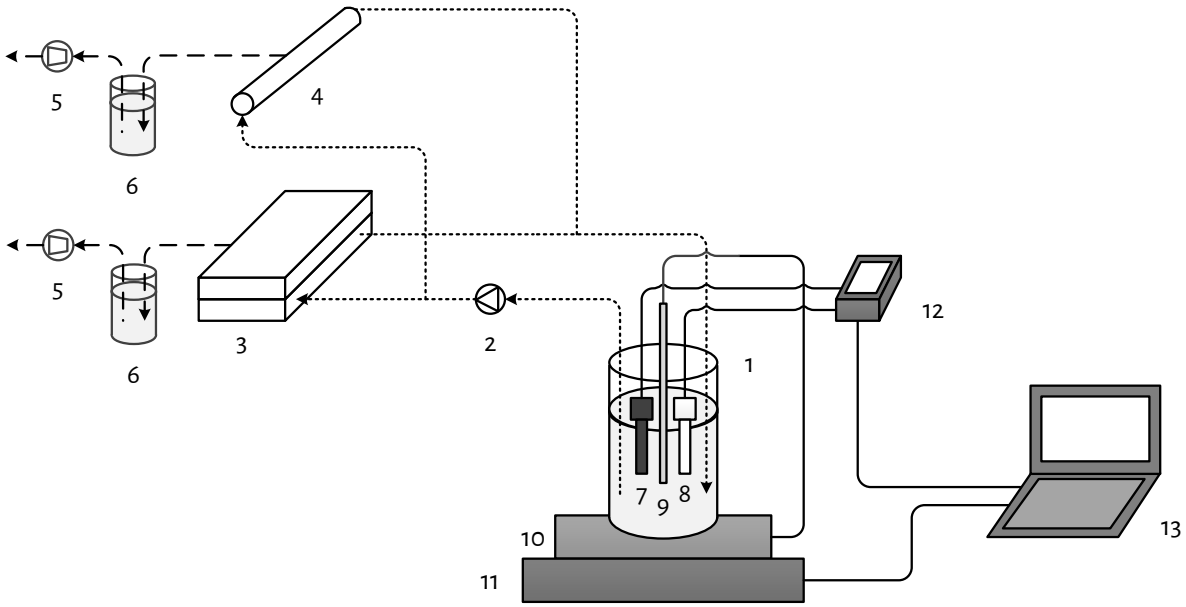

Figure 5-1 - Schematic representation of the used experimental set-up including feed water bottle (1), peristaltic pump (2), gas-permeable membrane housing including membrane (3), PV membrane housing including membrane (4), vacuum pump (5), pressure sensor (6), cooled permeate scrubber (7), EC-sensor (8), pH-sensor (9), temperature sensor (10), integrated heating and mixing plate (11), balance (12), multimeter (13) and laptop (14).

Table 5-1 - Key characteristics of the membranes used for the NH_3 stripping experiments.

	Unit	Porous gas-permeable (PTFE) membrane	Hydrophilic (Hybrid Silica) PV membrane	Hydrophobic (PDMS) PV membrane
Channel height	mm	2.3	-	-
Channel width	mm	39	-	-
Internal diameter	mm	-	7	7
Membrane thickness	mm	0.2	1.5	1.5
Membrane length	mm	87	250	250
Effective membrane area	m^2	0.0034	0.0055	0.0055
Pore size[5]	nm	100	0.5[6]	-
Selective membrane layer	-	PTFE[1]	Hybrid Silica – AR[3]	PDMS[4]
Membrane material	-	PTFE – PP[2]	α-Al_2O_3	α-Al_2O_3
Maximum temperature[5]	°C	82	150	70
pH range[5]		1 - 14	0.5 – 8.5	1 - 12

[1]PTFE = polytetrafluoroethylene, [2]PP = polypropylene, [3]Hybrid Silica – AR = organic (methyl and ethanol) groups and silica (Yang et al., 2016), [4]PDMS = polydimethylsiloxane, [5]according to the supplier, [6](van Veen et al., 2011)

5.2.2. Performance indicators

For the assessment of the S_{NH_3/H_2O}, the overall mass transfer coefficient (K_o) for NH_3 and H_2O was determined. The K_o normalises the mass flux with respect to the respective driving force for the transfer of gases, which for NH_3 and H_2O is the vapour pressure difference between the liquid feed water and the gaseous permeate. K_o is usually described by a series-resistance model, consisting of three separate components: the mass transfer coefficients for the liquid feed water (K_f), the membrane (K_m) and the gaseous permeate (K_p) as described in Eq. 5-1.

$$\frac{1}{K_o} = \frac{1}{K_f} + \frac{1}{K_m} + \frac{1}{K_p} \qquad \text{Eq. 5-1}$$

Where, K_o, K_f, K_m and K_p = the overall, the liquid feed water, the membrane, and the gaseous permeate mass transfer coefficient (in $s \cdot m^{-1}$), respectively.

K_p is negligible for vacuum stripping applications due to the low absolute pressure of the gaseous permeate, according to the studies of Bandini et al. (1992), Lawson and Lloyd (1997) and Jyoti et al. (2015).

K_f can be determined as a function of the hydraulic conditions and the diffusion characteristics of the dissolved gases in the feed water (Oliveira et al., 2001; Chiam & Sarbatly, 2013), but this is only applicable for uniform hydraulic conditions of the feed water. At the interface of the feed water and the membrane, the hydraulic conditions are different from those in the bulk phase, due to polarisation phenomena. For stripping of gases from water in vacuum configurations, three polarisation phenomena are relevant:

1. Temperature polarisation;
2. Ion accumulation concentration polarisation;
3. Gas depletion concentration polarisation;

Firstly, temperature polarisation, which is the decrease in temperature of the feed water at the membrane interface as a result of heat transport due to the evaporation of H_2O (Lawson & Lloyd, 1997; Martínez-Díez & Vázquez-González, 1999). Secondly, accumulation concentration polarisation, describing the increase in concentration of non-volatile solutes such as ions at the membrane interface as a result of the evaporation of H_2O (Lawson & Lloyd, 1997; Martínez-Díez & Vázquez-González, 1999). Thirdly, gas depletion concentration polarisation, which is the decrease in concentration of volatile solutes such as dissolved gases at the membrane interface, caused by a faster transfer rate of the respective gas through the membrane than the transfer rate from bulk-phase of the feed liquid to the membrane interface (Bandini et al., 1992; Wijmans et al., 1996).

Finally, K_m depends on the type of membrane. For porous gas-permeable membranes, the main mass transfer mechanism is Knudsen diffusion because the ratio of the kinetic diameter of the gas molecule and pore size is smaller than 0.05 (Lawson & Lloyd, 1997; Khayet & Matsuura, 2004; El-Bourawi et al., 2007), whereas PV membranes are dense membranes for which the main mass transfer mechanisms rely on sorption/dissolution and diffusion (Jyoti et al., 2015). In general, for both types of membranes, K_m is a function of the specific membrane characteristics, such as thickness, and the temperature of the membranes

(Lawson & Lloyd, 1997; Jyoti et al., 2015). However, due to temperature polarisation, the actual temperature of the membrane is different from the temperature of the bulk phase of the liquid feed.

The mentioned three polarisation phenomena occur simultaneously during vacuum stripping of gases such as NH_3 from water and do not only affect the mass transfer coefficients K_f and K_m. The polarisation phenomena also affect the driving force of NH_3 and H_2O transfer, because the local accumulation of ions, the local depletion of dissolved NH_3 and the lower temperature at the membrane interface compared to the bulk feed water temperature affect the vapour pressures of NH_3 and H_2O at the liquid side of the membrane. Understanding the mass transfer in vacuum membrane stripping processes, including all three polarisation phenomena and their interdependency is lacking in current literature. Therefore, this chapter does not present specific results on the investigation of the respective contribution of K_f and K_m separately, but only K_o.

To calculate the K_o of NH_3 (K_{o,NH_3}), various studies used the logarithmic decrease in NH_3 concentration over time, in combination with the initial feed volume (El-Bourawi et al., 2007; He et al., 2018). However, this method of determining the K_o only applies to the transfer of the solute (NH_3) and not to the solvent (H_2O). Moreover, this method assumes a fixed feed volume, whereas the feed water volumes decrease due to the evaporation of H_2O during the stripping process. Therefore, the K_o for NH_3 and H_2O were determined using the measured fluxes and the calculated vapour pressure difference, in line with the study of (Jyoti et al., 2015). The NH_3 (Eq. 5-2) and H_2O (Eq. 5-3) fluxes were determined using the mass changes in the feed water over time. The vapour pressures of NH_3 and H_2O in the liquid feed were obtained by simulations using chemical equilibrium simulation software named PHREEQC, whereas the vapour pressures of NH_3 (Eq. 5-4) and H_2O (Eq. 5-5) in the gaseous permeate were calculated using the ratio of the fluxes and the absolute pressure of the permeate. More details on the determination of the fluxes can be found in the study of van Linden et al. (2022a). Based on the NH_3 and H_2O fluxes and vapour pressures, the K_{o,NH_3} and K_{o,H_2O} were determined using Eq. 5-6 and Eq. 5-7, respectively. Finally, S_{NH_3/H_2O} was determined using Eq. 5-8, as the ratio of K_{o,NH_3} and K_{o,H_2O}, in line with Camus et al. (2006) and Baker et al. (2010).

$$J_{NH_3} = \frac{-(m_{NH_3,i+1} - m_{NH_3,i})}{A_m \cdot (t_{i+1} - t_i)} \quad \text{Eq. 5-2}$$

$$J_{H_2O} = \frac{-(m_{H_2O,i+1} - m_{H_2O,i})}{A_m \cdot (t_{i+1} - t_i)} \quad \text{Eq. 5-3}$$

Where, J_{NH_3} and J_{H_2O} = NH_3 and H_2O flux (in $kg \cdot m^{-2} \cdot s^{-1}$), $m_{NH_3,i}$ and $m_{H_2O,i}$ = NH_3 and H_2O mass at time instant 'i', respectively (in kg), A_m = membrane area (in m^2) and t_i = time instant 'i' (in s).

$$p_{p,NH_3} = \frac{J_{NH_3}}{J_{NH_3} + J_{H_2O}} \cdot p_p \quad \text{Eq. 5-4}$$

$$p_{p,H_2O} = \frac{J_{H_2O}}{J_{NH_3} + J_{H_2O}} \cdot p_p \quad \text{Eq. 5-5}$$

Where, p_{p,NH_3} and p_{p,H_2O} = vapour pressure of NH_3 and H_2O in the gaseous permeate, respectively (in Pa = $kg \cdot m^{-2} \cdot s^{-1}$) and p_p = permeate pressure (in Pa = $kg \cdot m^{-2} \cdot s^{-1}$, p_p = 1,500 Pa).

$$K_{o,NH_3} = \frac{J_{NH_3}}{p_{f,NH_3} - p_{p,NH_3}} \quad \text{Eq. 5-6}$$

$$K_{o,H_2O} = \frac{J_{H_2O}}{p_{f,H_2O} - p_{p,H_2O}} \quad \text{Eq. 5-7}$$

Where K_{o,NH_3} and K_{o,H_2O} = mass transfer coefficient of NH_3 and H_2O, respectively (in $s \cdot m^{-1}$) and p_{f,NH_3} and p_{f,H_2O} = vapour pressure of NH_3 and H_2O in the liquid feed water (in Pa = $kg \cdot m^{-2} \cdot s^{-1}$).

$$S_{NH_3/H_2O} = \frac{K_{NH_3}}{K_{H_2O}} \quad \text{Eq. 5-8}$$

Where S_{NH_3/H_2O} = selectivity of NH_3 over H_2O transfer (no unit).

5.2.3. Experimental conditions

For all conducted experiments in this chapter, the vacuum pressure at the permeate side was fixed at 1,500 Pa by a vacuum pump, while unsteady hydraulic flow conditions were maintained unless stated otherwise. Moreover, the temperature of the feed water was 35 °C, unless stated differently, as in the study of van Linden et al. (2022a), stripping NH_3 at 35 °C resulted in the most concentrated NH_3 in the vapour permeate. Initially, the transfer of H_2O through the various membranes was assessed at three different feed water temperatures: 25, 35 and 45 °C. Subsequently, unless stated differently, feed waters with a feed water concentration of 1 $g \cdot L^{-1}$ of NH_3 as NH_4OH were used to assess the S_{NH_3/H_2O} for the various membranes, similar to Yang et al. (2014) and Yang et al. (2016).

5.2.3.1. Hydraulic conditions

We assessed the effect of the hydraulic conditions on the S_{NH_3/H_2O}, by using various Reynolds numbers, corresponding to steady (poorly mixed, or laminar) or unsteady (well-mixed, or transition/turbulent) hydraulic conditions. Unsteady flow conditions refer to the hydraulic flow conditions with good mixing properties. The unsteady flow conditions cover the range between laminar and turbulent hydraulic conditions. The Reynolds number is a function of the feed water properties, the cross-flow velocity and the hydraulic diameter of the flow channel (Eq. 5-9). According to the study of Oliveira et al. (2001), the hydraulic flow conditions are unsteady at a Reynolds number of 2,300 in tubular channels, whereas according to Mojab et al. (2014) unsteady hydraulic conditions in spacer-filled channels correspond to a Reynolds number of 500. By taking the feed water properties into account, the Reynolds numbers were set by controlling the cross-flow velocity through the flow channels using the peristaltic pump.

$$Re = \frac{\rho_f \cdot u \cdot d_h}{\mu_f} \quad \text{Eq. 5-9}$$

Where ρ_f = feed water density (in $kg \cdot m^{-3}$), u = average cross-flow velocity (in $m \cdot s^{-1}$), d_h = hydraulic diameter (in m), μ_w = dynamic viscosity of feed water (in $kg \cdot m^{-1} \cdot s^{-1}$).

The hydraulic diameter relates the surface tension and the shear stress of a liquid flowing through a channel. For circular open channels (for the tubular PV membranes), the hydraulic diameter is equal to the diameter of the respective channel. For spacer-filled channels (for the flat-sheet PTFE membrane), the determination of the hydraulic diameter is more elaborate, as the liquid is in contact with both the spacer and the perimeter of the flow channel. To this end, Schock and Miquel (1987) proposed a general expression for the hydraulic diameter in spacer-filled channels (Eq. 5-10), as a function of the void volume and the wetted surface area of the flow channel.

$$d_h = \frac{4 \cdot V_v}{A_w} \qquad \text{Eq. 5-10}$$

Where, V_v = void volume (in m^3) and A_w = wetted surface area (in m^2).

The determination of the void volume and the wetted surface area of the flow channels as a function of the specific channel geometries are described in detail in the Supporting Information of the paper of van Linden et al. (2022b). The hydraulic diameters were 2.3 and 7.0 mm for the PTFE and PV membranes, respectively. For the PTFE membrane, the range of the cross-flow velocity was 8 – 20 $cm \cdot^{-1}$ and 14 – 36 $cm \cdot^{-1}$ for the PV membranes. The cross-flow velocities for the PTFE membrane to achieve unsteady hydraulic conditions are lower compared to the PV membranes, because the PTFE membrane is in contact with a spacer (to enhance mixing), while the PV membranes are open tubular channels.

5.2.3.2. NH_3 feed water concentration and ionic strength of the feed water

Current literature mainly reports on the transfer of NH_3 from feed water through membranes, in which the NH_3 is only present as NH_4OH. Only the study of He et al. (2018) and the study of van Linden et al. (2022a) did not use NH_4OH solutions as feed water, but used pre-treated biogas slurry and NH_4HCO_3 solutions at a pH of 10, respectively. Whereas 1 $g \cdot L^{-1}$ is a representative concentration of NH_3 in N-loaded residual waters, 10 $g \cdot L^{-1}$ represents the concentration of NH_3 in pre-concentrated streams (Deng et al., 2021). Obtaining NH_3 concentrations up to 10 $g \cdot L^{-1}$ can be achieved by using electrodialysis to concentrate NH_4^+ from 1.5 to 10 $g \cdot L^{-1}$ (van Linden et al., 2019a), followed by the addition of chemicals to increase the solution pH, or by using bipolar membrane electrodialysis to directly obtain concentrated NH_3 without chemical addition (van Linden et al., 2020). Because various N-loaded residual waters, typically contain NH_4^+ in combination with HCO_3^- as the main anion, the addition of NaOH to obtain concentrated NH_3 from feed water with high NH_4^+ concentrations results in a high ionic strength, as a result of the presence of Na^+, HCO_3^- and CO_3^{2-}. The presence of ions affects the vapour pressure of NH_3 in two ways. On the one hand, when the ionic strength increases, the equilibrium between NH_4^+ and NH_3 shifts towards NH_4^+, according to chemical equilibrium simulations performed with PHREEQC software. On the other hand, the solubility of gases decreases when the ionic strength increases, which is called the salting-out effect, increasing the vapour pressure. According to Figure 5-2, the vapour pressure of NH_3 increases linearly when the ionic strength of the feed water

increases, indicating that the salting-out effect is stronger than the effect of the ionic strength on the equilibrium between NH_3 and NH_4^+. Furthermore, an increase in ionic strength results in a linear decrease in H_2O vapour pressure according to Raoult's Law. Hence, by increasing the ionic strength of the feed water, the NH_3 vapour pressure increases, while the H_2O vapour pressure decreases. The effect of the ionic strength on the vapour pressure of NH_3 and H_2O is similar for feed waters with NH_3 concentrations of 1 and 10 $g \cdot L^{-1}$. However, in addition to the effect of the ionic strength on the vapour pressures, the ionic strength also affects the resistance to mass transfer of NH_3 and H_2O. Due to the evaporation of H_2O, ions accumulate at the membrane interface (ion accumulation concentration polarisation), which can hinder the transfer of NH_3 and H_2O, particularly under steady hydraulic conditions.

We assessed the effect of ionic strength on S_{NH_3/H_2O}, because the presence of ions affects both the vapour pressure of dissolved gases (salting-out effect) and the mass transfer coefficient (ion accumulation concentration polarisation). To assess the effect of the NH_3 feed concentration and ionic strength on S_{NH_3/H_2O}, various feed waters containing dissolved NH_3 were prepared, with initial concentrations of 1 and 10 $g \cdot L^{-1}$ as NH_4OH and NH_4HCO_3 (at a pH of 10 by addition of NaOH). According to chemical equilibrium simulations, the ionic strength of feed water consisting of NH_4OH is negligible, whereas feed waters consisting of NH_4HCO_3 at a pH of 10 have an ionic strength of 0.1 and 0.8 $mol \cdot L^{-1}$ at NH_3 feed water concentration of 1 and 10 $g \cdot L^{-1}$, respectively. For these calculations, the contribution of both NH_4HCO_3 and NaOH to the ionic strength were taken into account.

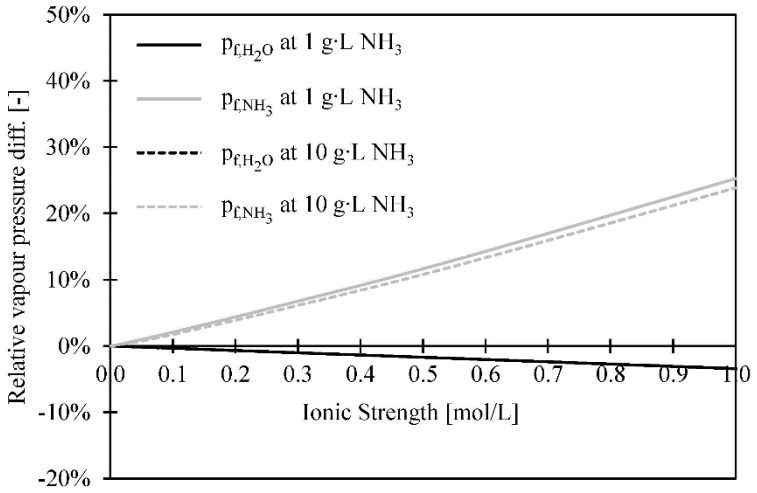

Figure 5-2 - The calculated vapour pressures of NH_3 and H_2O in water with an NH_3 feed water concentration of 1 and 10 $g \cdot L^{-1}$, as a function of the ionic strength of the feed water. The vapour pressures were calculated using PHREEQC simulation software, using the phreeqc.dat database.

5.3. Results and discussion

5.3.1. H_2O transfer through the various membranes as a function of the feed temperature

Initially, the transfer rate of H_2O as the H_2O flux and the K_{o,H_2O} through the membranes was assessed at various temperatures, using water as a feed without dissolved gaseous and ions, at unsteady hydraulic conditions. Figure 5-3A presents the H_2O fluxes as a function of the feed water temperature for the PTFE, Hybrid Silica PV and PDMS PV membrane. The reported values represent averages of at least triplicate experimental runs. At a feed water temperature of 25 °C, the H_2O flux for the PTFE membrane was 12.0 $kg \cdot m^{-2} \cdot h^{-1}$, compared to 2.3 and 0.4 $kg \cdot m^{-2} \cdot h^{-1}$ for the Hybrid Silica PV and PDMS PV membrane, respectively. By increasing the feed water temperature to 45 °C, the H_2O fluxes increased to 24.5, 6.3 and 0.7 $kg \cdot m^{-2} \cdot h^{-1}$ for the PTFE, Hybrid Silica PV and PDMS PV membranes, respectively, because the vapour pressure of H_2O and thus the driving force increased as a function of temperature. The H_2O flux for the PTFE membrane was at least four times higher than the H_2O flux for the Hybrid Silica PV membrane, which in its turn was at least five times higher than the H_2O flux of the PDMS PV membrane.

Because the same feed water temperature range and same vacuum pressure were applied for the experiments, the higher H_2O fluxes of the PTFE membrane compared to the PV membranes are explained by the higher K_{o,H_2O} of the PTFE membrane (ranging between $1 \cdot 10^{-6}$ and $2 \cdot 10^{-6}$ $s \cdot m^{-1}$) compared to the K_{o,H_2O} of the Hybrid Silica PV (ranging between $2 \cdot 10^{-7}$ and $4 \cdot 10^{-7}$ $s \cdot m^{-1}$) and the PDMS PV membrane (ranging between $7 \cdot 10^{-8}$ and $2 \cdot 10^{-7}$ $s \cdot m^{-1}$), as presented in Figure 5-3B. The difference in K_{o,H_2O} between the PTFE membrane and the PV membranes can be assigned to the differences in selective layers of the membranes. The PTFE membrane had pores of 0.1 µm, whereas the Hybrid Silica PV and PDMS PV membranes were dense membranes, resulting in lower transfer rates of H_2O than compared to the porous PTFE membrane. The difference in K_{o,H_2O} between the Hybrid Silica PV and the PDMS PV membrane can be explained by the functional groups present in the selective layers of the respective membranes. The selective layer of the Hybrid Silica PV membrane was hydrophilic and contained polar organosilica groups, allowing for the permeation of polar H_2O molecules. On the contrary, the selective layer of the PDMS PV membrane was hydrophobic, which hindered the dissolution of H_2O in the membrane and the subsequent diffusion of H_2O through the membrane.

According to Figure 5-3B, the K_{o,H_2O} of all three membranes decreased when the feed water temperature increased. The decrease of K_{o,H_2O} as a function of the increasing feed water temperature can be assigned to a stronger effect of temperature polarisation (Martínez-Díez & Vázquez-González, 1999), as no ions or dissolved gases were present in the feed water. For the PTFE membrane, the decrease in K_{o,H_2O} as a function of the feed water temperature can be assigned to the decrease in K_m, which decreases as a function of the temperature according to Knudsen diffusion. In addition, for the PV membranes, the mass transfer through the membranes can be described by sorption-diffusion models. When the temperature increases, diffusion increases, while sorption decreases. Therefore, the decrease in K_{o,H_2O} of the PV membranes as a function of

the increasing feed water temperature may, besides temperature polarisation, also be caused by the effect of the feed water temperature on the sorption and diffusion mechanisms taking place during the transfer of H_2O. However, because the temperature at the interface of the liquid feed water and the membranes was not determined, it remains unclear which component of the series resistance model for mass transfer (Eq. 5-1) caused the decrease of the K_{o,H_2O} as a function of the increasing feed water temperature.

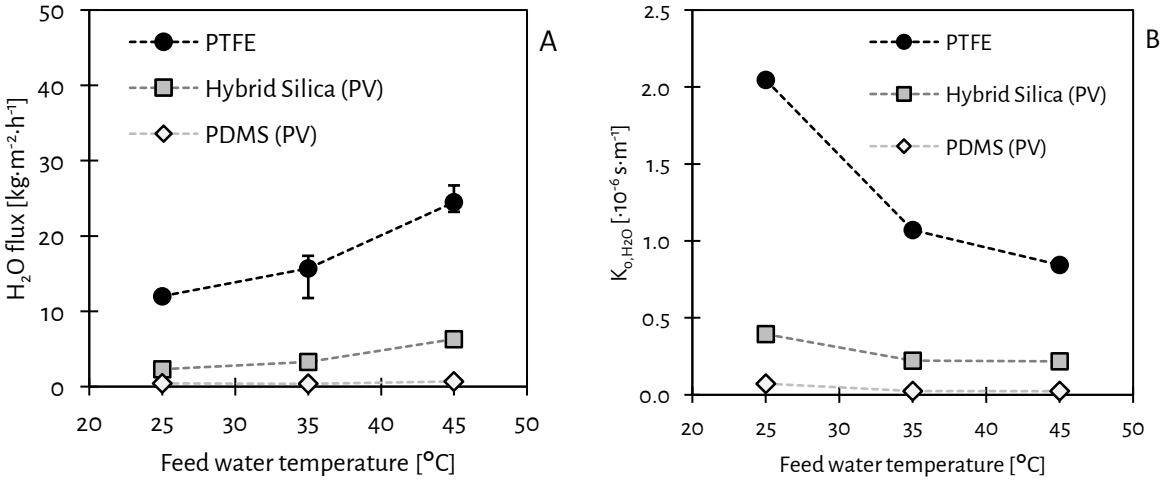

Figure 5-3 - The H_2O fluxes (A) and the K_{o,H_2O} (B) of the gas permeable PTFE membrane and the hydrophilic Hybrid Silica PV and hydrophobic PV membrane as a function of the feed water temperature. The reported values and error bars represent the average and the minimum and maximum measurements of at least three replicate experiments.

5.3.2. Selectivity of NH_3 over H_2O transfer for various membranes

Figure 5-4A presents the fluxes of both NH_3 and H_2O for the various membranes. The H_2O and NH_3 fluxes of the PTFE membrane were 11 and 0.11 $kg \cdot m^{-2} \cdot h^{-1}$, respectively. For the Hybrid Silica PV membrane, the H_2O flux was 4 $kg \cdot m^{-2} \cdot h^{-1}$ and the NH_3 flux was 0.02 $kg \cdot m^{-2} \cdot h^{-1}$. Furthermore, the H_2O flux for the PDMS PV membrane was 1 $kg \cdot m^{-2} \cdot h^{-1}$, but the NH_3 flux was negligible. Moreover, the selective layer of the PDMS PV membrane deteriorated rapidly during the experiments (see Figure 5-5), indicating that treating alkaline feed waters with an NH_3 concentration of 1 $g \cdot L^{-1}$ was not possible for periods exceeding three hours. Therefore, this chapter does not further report on the applicability of the PDMS PV membrane.

The K_{o,H_2O} of the Hybrid Silica PV ($3 \cdot 10^{-8}$ $s \cdot m^{-1}$) and PDMS PV ($7 \cdot 10^{-8}$ $s \cdot m^{-1}$) membranes were again (also in 5.3.1.) lower compared to the PTFE membrane K_{o,H_2O} ($8 \cdot 10^{-7}$ $s \cdot m^{-1}$), caused by the lower resistance of H_2O transfer through the PTFE membrane. The lower resistance of H_2O transfer for the PTFE membrane compared to the Hybrid Silica PV membrane, which is expressed as higher H_2O flux and higher K_{o,H_2O}, can mainly be assigned to the membrane characteristics. According to Table 5-1, the pore size of the PTFE membrane was orders of magnitude higher compared to the PV membranes, while also the membrane thickness of the PTFE membrane was lower compared to the PV membranes. Hence, both the higher pore size and the lower membrane thickness contributed to the higher H_2O transfer rates through the PTFE membrane compared

to the PV membranes. Furthermore, the K_{o,NH_3} of the PTFE membrane ($3 \cdot 10^{-7}$ s·m^{-1}) was more than seven times higher than the Hybrid Silica PV ($4 \cdot 10^{-7}$ s·m^{-1}). The differences in NH_3 flux and K_{o,NH_3} between the PTFE membrane and Hybrid Silica PV membrane can again be assigned to the pore size and the thickness of the respective membranes. Due to the negligible NH_3 flux, the K_{o,NH_3} of the PDMS PV membrane was not determined.

The PTFE membrane showed a preference to permeate H_2O over NH_3 indicated by the S_{NH_3/H_2O} of 0.3. The S_{NH_3/H_2O} of the PTFE membrane was higher than the S_{NH_3/H_2O} of the Hybrid Silica PV membrane (0.2). Hence, the Hybrid Silica PV did not show an increased preference to permeate NH_3 compared to H_2O, in contrast to the findings of Yang et al. (2014), but in line with the findings of Yang et al. (2016). The adsorption of NH_3 on the silica groups of the PV membranes, leading to blocking of the H_2O transfer, as described by Yang et al. (2014), was not present or not strong enough to promote selective NH_3 permeation. This blocking mechanism was responsible for the selective transfer of NH_3 over H_2 in studies conducted by Camus et al. (2006) and Kanezashi et al. (2010). However, in contrast to the non-polar H_2, NH_3 (dipole moment of 1.47 D) and H_2O (dipole moment of 1.85 D) are both polar molecules (Lide & Haynes, 2011) and both bind with the polar silica groups at the selective layer of the Hybrid Silica PV membrane. In fact, H_2O is more polar than NH_3 and probably bonded stronger with the selective layer of the Hybrid Silica PV membrane, contributing to the lower S_{NH_3/H_2O}. Furthermore, H_2O was more abundantly present in the bulk phase of the feed water than NH_3 (> 99 wt%), as the feed water NH_3 concentration was 1 g·L^{-1}, corresponding to 0.1 wt%. Therefore, also gas depletion concentration polarisation affected the transfer of NH_3, possibly explaining the preference of H_2O over NH_3 transfer.

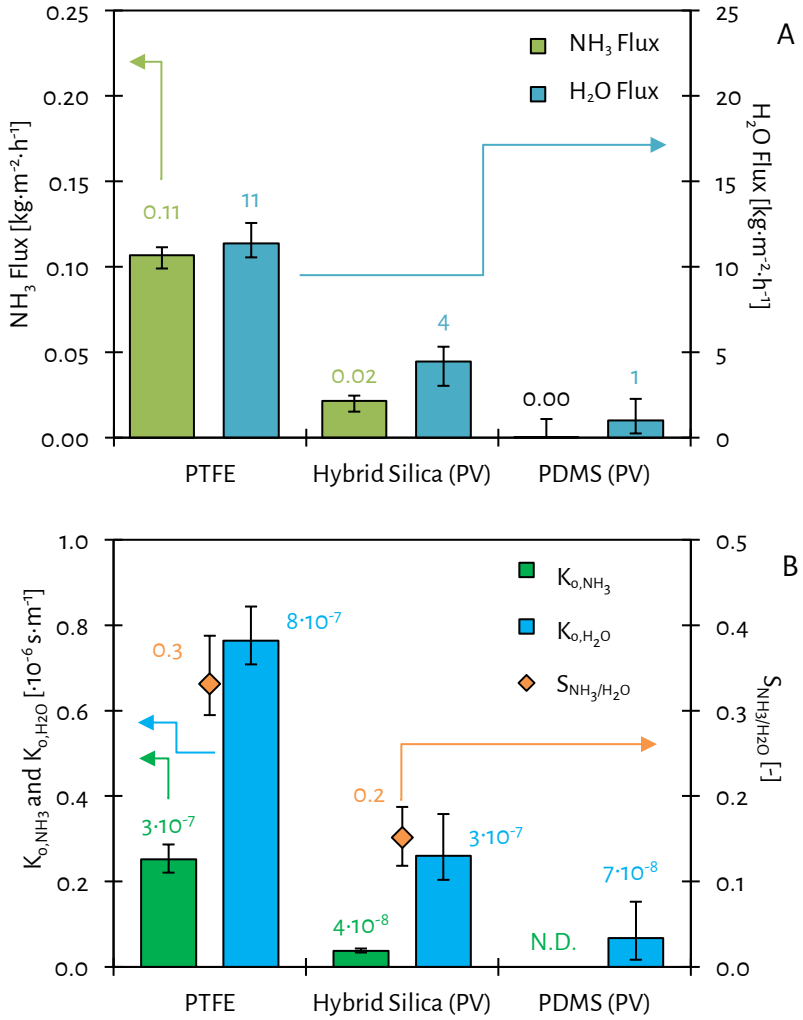

Figure 5-4 - The NH_3 (A) and H_2O fluxes and the K_{o,NH_3}, K_{o,H_2O} and S_{NH_3/H_2O} (B) of the various membranes for stripping NH_3 from feed waters with an NH_3 feed concentration of 1 $g \cdot L^{-1}$ (as NH_4OH) at a feed water temperature of 35 °C at unsteady hydraulic conditions. The reported values and error bars represent the average and the minimum and maximum measurements of at least three replicate experiments. N.D. = not determined (too low flux).

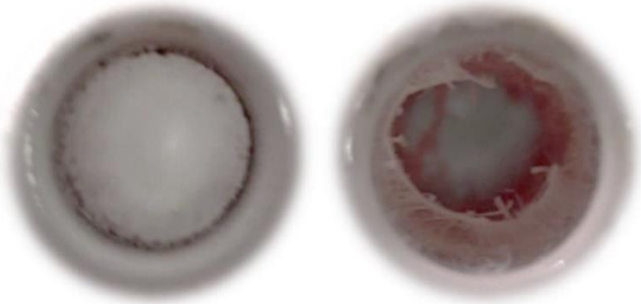

Figure 5-5 - A new PDMS PV membrane (left) and a deteriorated PDMS PV membrane (right) after exposure to feed water of 35 °C with an NH_3 concentration of 1 $g \cdot L^{-1}$ for less than six hours.

5.3.3. Selectivity of NH_3 over H_2O under various hydraulic conditions

5.3.3.1. Identification of hydraulic condition ranges

According to the studies of Oliveira et al. (2001) and Mojab et al. (2014), unsteady flow regions for tubular and spacer-filled channels start at a Reynolds number of 2,300 and 500, respectively. Figure 5-6A and Figure 5-6B present the H_2O flux as a function of the Reynolds number for the PTFE and the Hybrid Silica PV membrane, respectively, when using demineralised water as feed water. For the PTFE membrane, the H_2O flux was 11 $kg \cdot m^{-2} \cdot h^{-1}$ up to a Reynolds number of 300. The H_2O flux increased to 15 $kg \cdot m^{-2} \cdot h^{-1}$ when the Reynolds number increased to 400 and remained stable when the Reynolds number further increased to 500 and 600. For the Hybrid Silica PV membrane, the H_2O flux increased from 3 to 4 $kg \cdot m^{-2} \cdot h^{-1}$ when the Reynolds number increased from 1,000 to 2,400 and remained 4 $kg \cdot m^{-2} \cdot h^{-1}$ when the Reynolds number further increased to 3,000, 4,000 and 5,000. Hence, the indicated Reynolds numbers for steady and unsteady hydraulic conditions were in line with the changes in H_2O flux for both spacer-filled rectangular and open tubular channels (Oliveira et al., 2001; Mojab et al., 2014).

Because during the H_2O permeation experiments at various Reynolds numbers the driving force for H_2O transfer was equal, as the same feed water temperature and vacuum pressure were used, the increase in H_2O flux due to the shift from steady to unsteady hydraulic conditions was caused by an increase in K_{o,H_2O}. By shifting from steady to unsteady hydraulic conditions, the effect of temperature polarisation was less apparent, resulting in a higher feed vapour pressure at the membrane interface and thus the actual driving force for H_2O transfer. Moreover, as the membrane temperature was probably higher at higher Reynolds numbers due to the weaker effect of temperature polarisation, the K_m for the PTFE decreased, according to mass transfer described Knudsen diffusion. Apparently, the increase in actual H_2O driving force had a greater impact than the decrease in K_m on the H_2O flux. For the Hybrid Silica PV membrane, the increase in Reynolds number probably resulted in an increased actual H_2O driving force, as well as an increased K_m, due to the reduced effect of temperature polarisation, ultimately leading to an increase in H_2O flux.

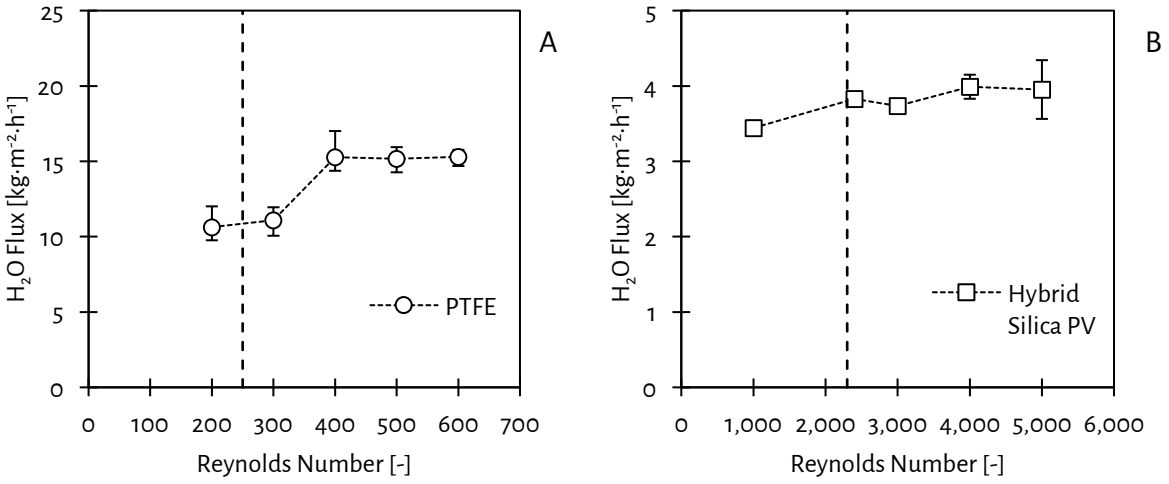

Figure 5-6 - The H_2O flux of the PTFE (A) and the Hybrid Silica PV (B) membrane at a feed water temperature of 35 °C as a function of the Reynolds numbers. The dotted vertical lines represent the Reynolds numbers at which theoretically the hydraulic conditions become unsteady: 250 for spacer-filled rectangular flow channels and 2,300 for tubular flow channels. The reported values and error bars represent the average and the minimum and maximum measurements of at least three replicate experiments.

5.3.3.2. Selectivity of NH_3 over H_2O transfer under steady and unsteady hydraulic conditions

Subsequently, NH_3 transfer was assessed under both steady and unsteady hydraulic conditions for the PTFE and the Hybrid Silica PV membranes. Based on results of H_2O transfer as a function of the Reynolds number experiments (see 5.3.3.1.), Reynolds numbers of 200 and 500 for the PTFE membrane and 1,000 and 2,400 for the Hybrid Silica PV membrane were used as representative values of steady and unsteady hydraulic conditions, respectively. In line with the findings in 5.3.2., the transfer rates of NH_3 and H_2O, expressed as flux and K_o were consistently lower for the Hybrid Silica PV membrane, compared to the PTFE membrane, which can be explained by the membrane thickness and pore size of the respective membranes.

Figure 5-7A shows that the NH_3 flux for the PTFE membrane increased from 0.08 to 0.11 $kg \cdot m^{-2} \cdot h^{-1}$ when the hydraulic conditions shifted from steady to unsteady, whereas for the Hybrid Silica PV the NH_3 flux increased from 0.01 to 0.02 $kg \cdot m^{-2} \cdot h^{-1}$. The H_2O fluxes for the PTFE and Hybrid Silica PV membrane remained stable at 11 and 3 $kg \cdot m^{-2} \cdot h^{-1}$, respectively, when the hydraulic conditions shifted from steady to unsteady. The rate of H_2O transfer during the experiments with demineralised water in 5.3.1. and 5.3.3.1. was consistently higher compared to the experiments using feed waters containing NH_4OH, indicating that the transfer of NH_3 affected the transfer of H_2O. Furthermore, the shift from steady to unsteady hydraulic conditions had a greater impact on the K_{o,NH_3} than on the K_{o,H_2O}. The K_{o,NH_3} increased from $1 \cdot 10^{-7}$ to $3 \cdot 10^{-7}$ $s \cdot m^{-1}$ and from $2 \cdot 10^{-8}$ to $3 \cdot 10^{-8}$ $s \cdot m^{-1}$ for the PTFE and the Hybrid Silica PV membrane, respectively, whereas the K_{o,H_2O} remained at $7 \cdot 10^{-7}$ - $8 \cdot 10^{-7}$ $s \cdot m^{-1}$ and $2 \cdot 10^{-7}$ $s \cdot m^{-1}$, respectively. The increase in NH_3 fluxes and K_{o,NH_3} by shifting from steady

to unsteady hydraulic conditions can be explained by a decrease in the effect of gas depletion concentration polarisation.

The S_{NH_3/H_2O} increased when the hydraulic conditions shifted from steady to unsteady conditions, in line with the findings of Ding et al. (2006) and El-Bourawi et al. (2007). For the PTFE membrane, S_{NH_3/H_2O} increased from 0.2 to 0.3, while S_{NH_3/H_2O} for the Hybrid Silica PV membrane increased from 0.1 to 0.2, indicating that the PTFE membrane again had a higher selectivity for NH_3 over H_2O transfer than the Hybrid Silica PV membrane, in line with the findings described in 5.3.2. The observed increase in S_{NH_3/H_2O} for the PTFE membrane contradicted the observations of He et al. (2018), who found that K_{o,H_2O} increased more than K_{o,NH_3} for higher cross-flow velocities. However, it was unclear whether these experiments were conducted in either steady or unsteady hydraulic conditions as the hydraulic diameter and geometry of the feed channel were not reported. Hence, the results show that stripping NH_3 at unsteady hydraulic conditions were preferred over operating at steady hydraulic conditions to maximise S_{NH_3/H_2O}, irrespective of the used type of membrane, also in line with the findings of Scheepers et al. (2020).

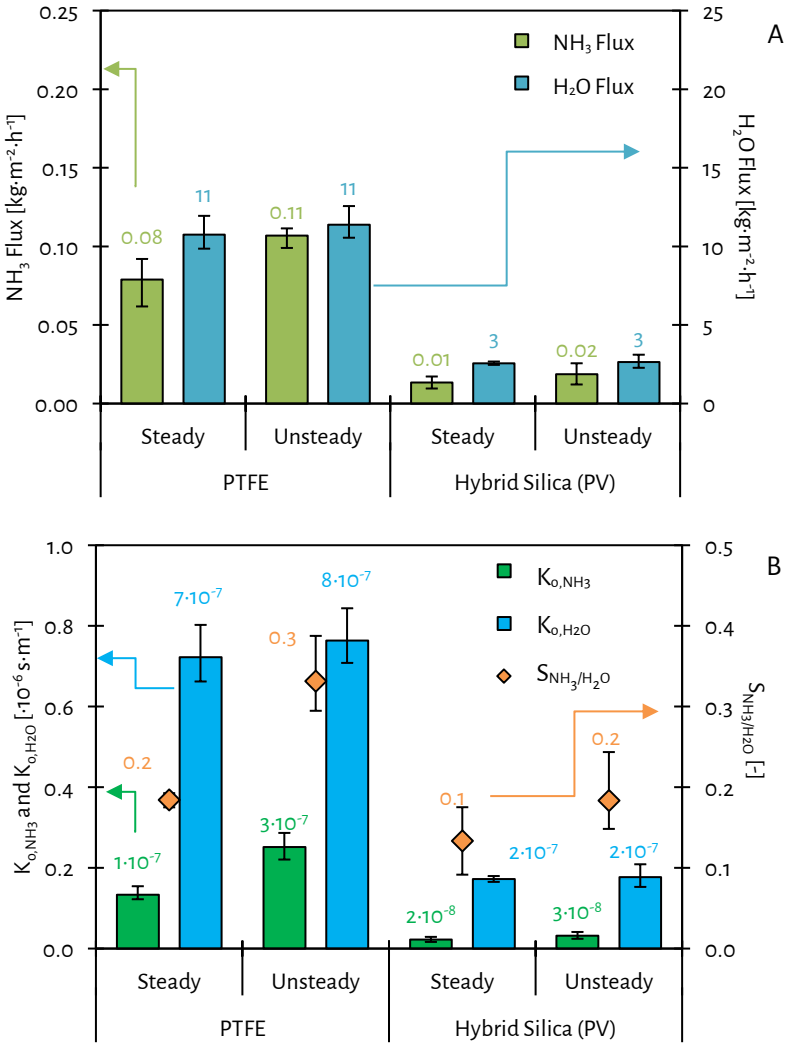

Figure 5-7 - The NH_3 and H_2O fluxes (A) and the K_{o,NH_3}, K_{o,H_2O} and S_{NH_3/H_2O} (B) of the PTFE and the hydrophilic Hybrid Silica PV membrane for stripping NH_3 for steady and unsteady hydraulic conditions, from feed waters with an NH_3 feed concentration of 1 $g \cdot L^{-1}$ (as NH_4OH) at a feed water temperature of 35 °C at both steady and unsteady hydraulic conditions. The reported values and error bars represent the average and the minimum and maximum measurements of at least three replicate experiments.

5.3.4. Selectivity of NH_3 over H_2O transfer for various membranes and feed water compositions

5.3.4.1. NH_3 feed water concentration of 1 $g \cdot L^{-1}$ at various ionic strengths

Figure 5-8A shows that the fluxes of NH_3 for the PTFE membrane were 0.11 and 0.14 $kg \cdot m^{-2} \cdot h^{-1}$ when feed waters had a negligible ionic strength (NH_4OH) and an ionic strength of 0.1 $mol \cdot L^{-1}$ (NH_4HCO_3 at a pH of 10), respectively. The H_2O flux of the PTFE membrane ranged between 11 and 12 $kg \cdot m^{-2} \cdot h^{-1}$ for the feed waters with negligible and 0.1 $mol \cdot L^{-1}$ ionic strengths, respectively, while the K_{o,H_2O} was $8 \cdot 10^{-7}$ $s \cdot m^{-1}$ (see Figure 5-8B). Based on the ratio of the NH_3 and H_2O fluxes (0.01), the electrical energy consumption can be derived, based on the study of van Linden et al. (2022a). The electrical energy consumption for stripping NH_3 at an NH_3 feed water concentration of 1 $g \cdot L^{-1}$ was approximately 100 $MJ \cdot kg\text{-}N^{-1}$. According to Figure 5-8B, the K_{o,NH_3} was $3 \cdot 10^{-7}$ $s \cdot m^{-1}$ for both feed waters, indicating that the effect of the difference in ionic strength of 0.1 $mol \cdot L^{-1}$ was negligible on the NH_3 transfer. The S_{NH_3/H_2O} for the PTFE membrane for these experiments ranged between 0.3 and 0.4, which indicates the transfer of H_2O was again preferential over NH_3 (similar as in 5.3.2. and 5.3.3.), independent of the difference in ionic strength. In addition, in line with the findings in 5.3.2. and 5.3.3., the transfer rates of NH_3 and H_2O, expressed as flux and K_o were consistently lower for the Hybrid Silica PV membrane, compared to the PTFE membrane, which can be explained by the membrane thickness and pore size of the respective membranes.

For the Hybrid Silica PV membrane, the NH_3 and H_2O fluxes were 0.02 and 3 $kg \cdot m^{-2} \cdot h^{-1}$, respectively, when using feed water with a negligible and 0.1 $mol \cdot L^{-1}$ ionic strength at an NH_3 feed concentration of 1 $g \cdot L^{-1}$. The K_{o,H_2O} of the Hybrid Silica PV membrane for the feed water with different ionic strengths was $2 \cdot 10^{-7}$ $s \cdot m^{-1}$ and the K_{o,NH_3} was $3 \cdot 10^{-8}$ $s \cdot m^{-1}$. The S_{NH_3/H_2O} of the Hybrid Silica PV membrane for both feed waters was 0.2, suggesting that the increase in ionic strength of 0.1 $mol \cdot L^{-1}$ did not affect the selectivity of NH_3 over H_2O transfer, which is in agreement with the findings for the PTFE membrane.

5.3.4.2. NH_3 feed water concentration of 10 $g \cdot L^{-1}$ at various ionic strengths

At last, the S_{NH_3/H_2O} was assessed for the PTFE and Hybrid Silica PV membrane using feed waters with an NH_3 feed concentration of 10 $g \cdot L^{-1}$ with a negligible ionic strength (NH_4OH) and an ionic strength of 0.8 $mol \cdot L^{-1}$ (NH_4HCO_3 at a pH of 10). The NH_3 fluxes for the PTFE membrane were 1.00 and 0.74 $kg \cdot m^{-2} \cdot h^{-1}$ for the feed waters with a negligible and 0.8 $mol \cdot L^{-1}$ ionic strength, respectively, whereas the H_2O fluxes were 14 and 11 $kg \cdot m^{-2} \cdot h^{-1}$, respectively (see Figure 5-9A). Hence, the fluxes of both NH_3 and H_2O decreased when the ionic strength of the feed water increased from 0.0 to 0.8 $mol \cdot L^{-1}$. With a ratio of the NH_3 flux and the total flux of 0.06, the electrical energy consumption for stripping NH_3 at an NH_3 feed water concentration of 10 $g \cdot L^{-1}$ was approximately 10 $MJ \cdot kg\text{-}N^{-1}$, based on (van Linden et al., 2022a). For the Hybrid Silica PV membrane, the NH_3 flux was 0.12 and 0.05 $kg \cdot m^{-2} \cdot h^{-1}$ for feed waters with a negligible and 0.8 $mol \cdot L^{-1}$ ionic strength, respectively, while the H_2O flux was stable for both feed waters at 3 $kg \cdot m^{-2} \cdot h^{-1}$. In line with the findings on the PTFE membrane, the NH_3 flux also decreased for the Hybrid Silica PV membrane when the ionic strength increased from 0.0 to 0.8 $mol \cdot L^{-1}$ for feed water with an NH_3 feed concentration of 10 $g \cdot L^{-1}$.

According to Figure 5-9B, the K_{o,NH_3} ($2 \cdot 10^{-7}$ $s \cdot m^{-1}$) for the PTFE membrane did not change when the ionic strength increased from 0.0 to 0.8 $mol \cdot L^{-1}$, suggesting that the additional presence of ions did not affect the NH_3 transfer. In addition, the increase in ionic strength also did not affect the transfer of H_2O for the PTFE membrane, as the K_{o,H_2O} ($8 \cdot 10^{-7}$ - $9 \cdot 10^{-7}$ $s \cdot m^{-1}$) was similar for a negligible and 0.8 $mol \cdot L^{-1}$ ionic strength. Eventually, the S_{NH_3/H_2O} was 0.2 for feed water with an NH_3 feed water concentration of 10 $g \cdot L^{-1}$ with both a negligible and 0.8 $mol \cdot L^{-1}$ ionic strength, indicating that the selectivity of NH_3 transfer was not affected by the increase in ionic strength for the PTFE membrane. For the Hybrid Silica PV membrane, the K_{o,NH_3} decreased from $2 \cdot 10^{-8}$ to $1 \cdot 10^{-8}$ $s \cdot m^{-1}$ when the ionic strength increased from 0.0 to 0.8 $mol \cdot L^{-1}$, while K_{o,H_2O} for the Hybrid Silica PV membrane was stable at $2 \cdot 10^{-7}$ $s \cdot m^{-1}$. Hence, the increase in ionic strength of 0.8 $mol \cdot L^{-1}$ affected only the transfer of NH_3, which can be assigned to the increased effect of gas depletion concentration polarisation. Eventually, the S_{NH_3/H_2O} for the Hybrid Silica was 0.1 for an NH_3 feed water concentration of 10 $g \cdot L^{-1}$ with both a negligible and 0.8 $g \cdot L^{-1}$ ionic strength.

By increasing the NH_3 feed concentration from 1 to 10 $g \cdot L^{-1}$, the NH_3 flux increased for the PTFE membrane from 0.08 – 0.11 to 0.74 – 1.00 $kg \cdot m^{-2} \cdot h^{-1}$, in line with the study of Scheepers et al. (2020) However, the K_{o,NH_3} of the PTFE membrane decreased when increasing the NH_3 feed water concentration, while the K_{o,H_2O} remained equal, resulting in a decrease in S_{NH_3/H_2O} from 0.3 – 0.4 to 0.2. In line with the findings for the PTFE membrane, also the S_{NH_3/H_2O} for the Hybrid Silica decreased when the NH_3 feed water concentration increased from 1 to 10 $g \cdot L^{-1}$, from 0.2 to 0.1, respectively. Hence, the increases in NH_3 flux for both the PTFE and Hybrid Silica PV membrane when the NH_3 feed water concentration increased from 1 to 10 $g \cdot L^{-1}$ was caused by the higher driving force as a result of the higher NH_3 vapour pressure in the feed water. Moreover, the selectivity of NH_3 transfer over H_2O decreased further for both membranes when the NH_3 feed water concentration increased. Apparently, even at a ten-fold higher NH_3 feed concentration, the relative presence of NH_3 was low (approximately 1 wt%) compared to H_2O, explaining partially the preferential transfer of H_2O over NH_3 for both membranes, under all various feed water compositions.

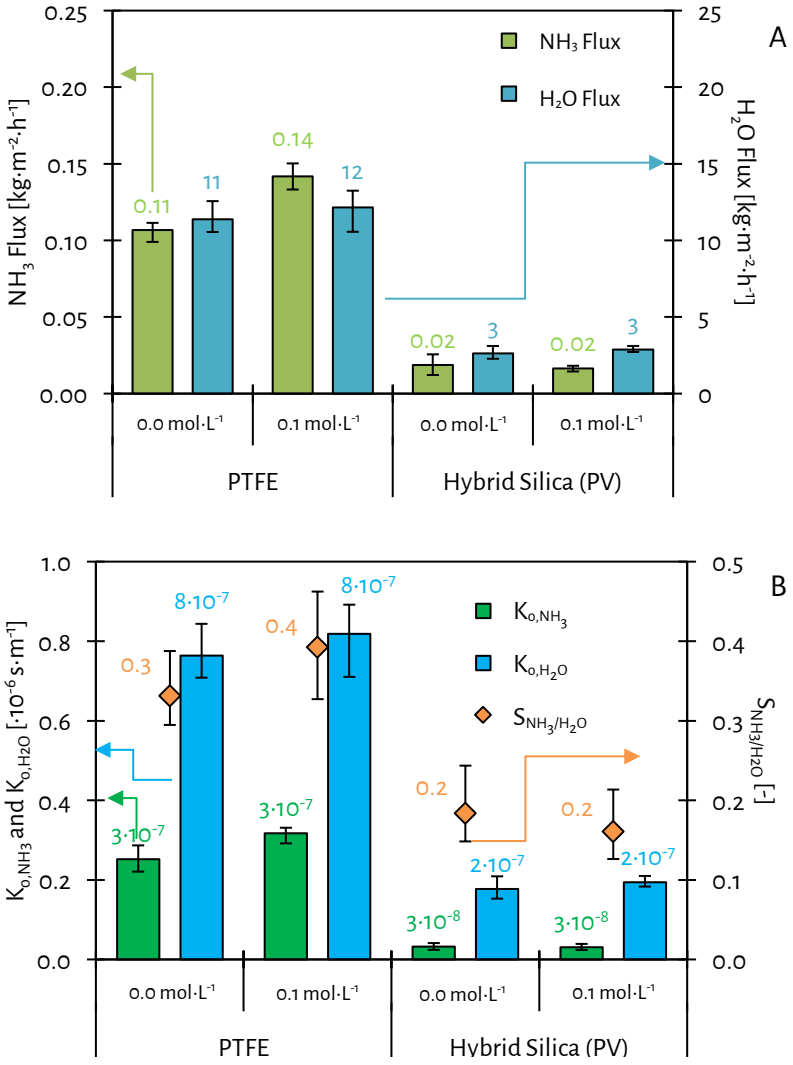

Figure 5-8 - The NH_3 and H_2O fluxes (A) and the K_{o,NH_3}, K_{o,H_2O} and S_{NH_3/H_2O} (B) of the PTFE and the Hybrid Silica PV membrane for stripping NH_3 from feed waters with an NH_3 feed concentration of 1 $g \cdot L^{-1}$ having a negligible (as NH_4OH) and 0.1 $mol \cdot L^{-1}$ (as NH_4HCO_3 at a pH of 10) ionic strength at a feed water temperature of 35 °C at unsteady hydraulic conditions. The reported values and error bars represent the average and the minimum and maximum measurements of at least three replicate experiments.

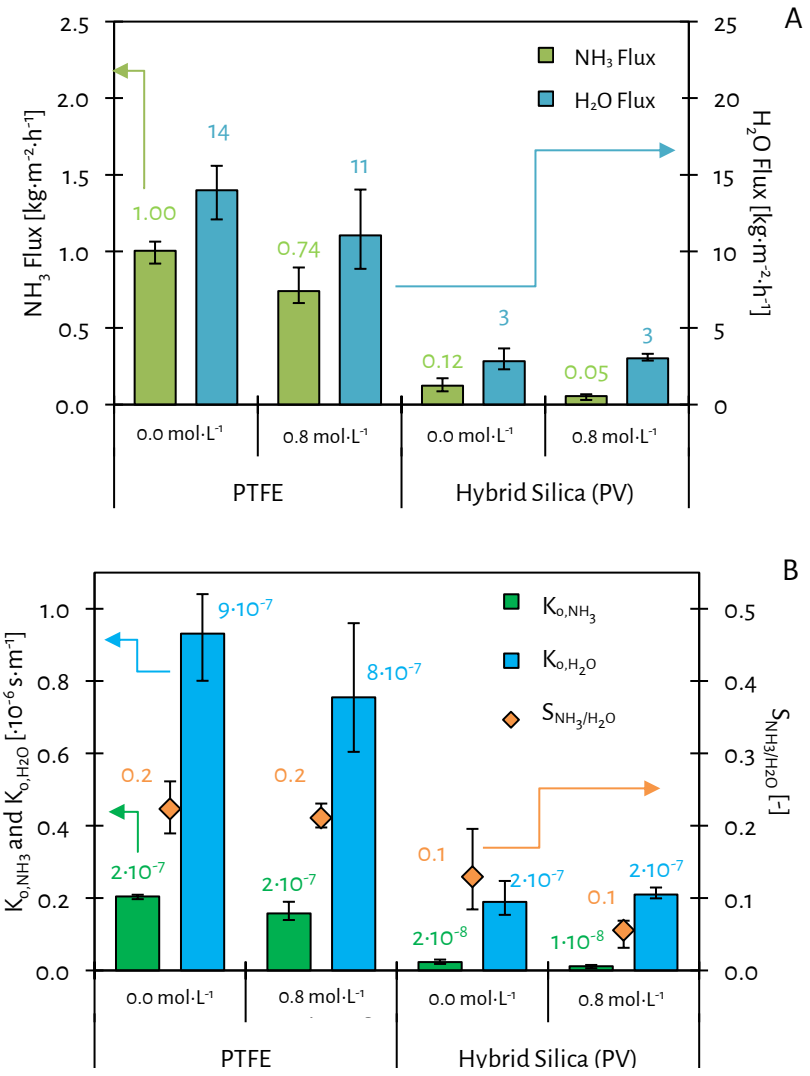

Figure 5-9 - The NH_3 and H_2O fluxes (A) and the K_{o,NH_3}, K_{o,H_2O} and S_{NH_3/H_2O} (B) of the PTFE and the Hybrid Silica PV membrane for stripping NH_3 from feed waters with an NH_3 feed concentration of 10 g·L^{-1} having a negligible (as NH_4OH) and 0.8 mol·L^{-1} (as NH_4HCO_3 at a pH of 10) ionic strength at a feed water temperature of 35 °C at unsteady hydraulic conditions. The reported values and error bars represent the average and the minimum and maximum measurements of at least three replicate experiments.

5.4. Conclusions

The experimental study to assess the selectivity of NH_3 and water transfer during the stripping of NH_3 under vacuum using various membranes resulted in the following conclusions:

- The transfer rate of H_2O (as H_2O flux and K_{o,H_2O}) through the used dense hydrophilic Hybrid Silica PV membrane is lower than the transfer rate of H_2O of the used porous gas-permeable PTFE membrane;
- The transfer rate of H_2O through the used dense hydrophobic PDMS PV membrane is lower than the transfer rate of H_2O of the Hybrid Silica PV and the PTFE membrane;
- The transfer of NH_3 through the PMDS PV membrane is negligible and the membrane deteriorates rapidly when using feed waters containing NH_3;
- The used PTFE membrane and Hybrid Silica PV membranes show selectivity for transfer of H_2O over NH_3 for all tested hydraulic conditions and feed water compositions;
- The S_{NH_3/H_2O} of the Hybrid Silica PV membrane (0.1 – 0.2) is consistently lower than the S_{NH_3/H_2O} of the used PTFE membrane (0.2 – 0.4);
- Unsteady hydraulic conditions result in a higher S_{NH_3/H_2O} compared to steady hydraulic conditions for both the PTFE and the Hybrid Silica PV membrane;
- An increase in ionic strength of the feed water from 0.0 to 0.8 $mol \cdot L^{-1}$ decreases the S_{NH_3/H_2O} of both the PTFE and the Hybrid Silica PV membranes;
- An increase in NH_3 feed concentration from 1 to 10 $g \cdot L^{-1}$ leads to a decrease in S_{NH_3/H_2O} for both the PTFE and the Hybrid Silica PV membrane;

5.5. References

Baker, R. W., Wijmans, J. G., & Huang, Y. (2010). Permeability, permeance and selectivity: A preferred way of reporting pervaporation performance data. *Journal of Membrane Science, 348*(1), 346-352. doi:https://doi.org/10.1016/j.memsci.2009.11.022

Bandini, S., Gostoli, C., & Sarti, G. C. (1992). Separation efficiency in vacuum membrane distillation. *Journal of Membrane Science, 73*(2), 217-229. doi:https://doi.org/10.1016/0376-7388(92)80131-3

Camus, O., Perera, S., Crittenden, B., van Delft, Y. C., Meyer, D. F., P. A. C. Pex, P., Kumakiri, I., Miachon, S., Dalmon, J.-A., Tennison, S., Chanaud, P., Groensmit, E., & Nobel, W. (2006). Ceramic membranes for ammonia recovery. *AIChE Journal, 52*(6), 2055-2065. doi:10.1002/aic.10800

Chiam, C.-K., & Sarbatly, R. (2013). Vacuum membrane distillation processes for aqueous solution treatment—A review. *Chemical Engineering and Processing: Process Intensification, 74*, 27-54. doi:https://doi.org/10.1016/j.cep.2013.10.002

Deng, Z., van Linden, N., Guillen, E., Spanjers, H., & van Lier, J. B. (2021). Recovery and applications of ammoniacal nitrogen from nitrogen-loaded residual streams: A review. *Journal of Environmental Management, 295*, 113096. doi:https://doi.org/10.1016/j.jenvman.2021.113096

Ding, Z., Liu, L., Li, Z., Ma, R., & Yang, Z. (2006). Experimental study of ammonia removal from water by membrane distillation (MD): The comparison of three configurations. *Journal of Membrane Science, 286*(1-2), 93-103. doi:10.1016/j.memsci.2006.09.015

El-Bourawi, M. S., Khayet, M., Ma, R., Ding, Z., Li, Z., & Zhang, X. (2007). Application of vacuum membrane distillation for ammonia removal. *Journal of Membrane Science, 301*(1-2), 200-209. doi:10.1016/j.memsci.2007.06.021

He, Q., Tu, T., Yan, S., Yang, X., Duke, M., Zhang, Y., & Zhao, S. (2018). Relating water vapor transfer to ammonia recovery from biogas slurry by vacuum membrane distillation. *Separation and Purification Technology, 191*(Supplement C), 182-191. doi:https://doi.org/10.1016/j.seppur.2017.09.030

Jyoti, G., Keshav, A., & Anandkumar, J. (2015). Review on Pervaporation: Theory, Membrane Performance, and Application to Intensification of Esterification Reaction. *Journal of Engineering, 2015*, 24. doi:10.1155/2015/927068

Kanezashi, M., Yamamoto, A., Yoshioka, T., & Tsuru, T. (2010). Characteristics of ammonia permeation through porous silica membranes. *AIChE Journal, 56*(5), 1204-1212. doi:10.1002/aic.12059

Khayet, M., & Matsuura, T. (2004). Pervaporation and vacuum membrane distillation processes: Modeling and experiments. *AIChE Journal, 50*(8), 1697-1712. doi:10.1002/aic.10161

Lawson, K. W., & Lloyd, D. R. (1997). Membrane distillation. *Journal of Membrane Science, 124*(1), 1-25. doi:https://doi.org/10.1016/S0376-7388(96)00236-0

Lide, D. R., & Haynes, W. M. (2011). *CRC handbook of chemistry and physics : a ready-reference book of chemical and physical data*. Boca Raton, Fla.: CRC Press.

Martínez-Díez, L., & Vázquez-González, M. I. (1999). Temperature and concentration polarization in membrane distillation of aqueous salt solutions. *Journal of Membrane Science, 156*(2), 265-273. doi:https://doi.org/10.1016/S0376-7388(98)00349-4

Mojab, S. M., Pollard, A., Pharoah, J. G., Beale, S. B., & Hanff, E. S. (2014). Unsteady Laminar to Turbulent Flow in a Spacer-Filled Channel. *Flow, Turbulence and Combustion, 92*(1), 563-577. doi:10.1007/s10494-013-9514-4

Oliveira, T. A. C., Cocchini, U., Scarpello, J. T., & Livingston, A. G. (2001). Pervaporation mass transfer with liquid flow in the transition regime. *Journal of Membrane Science, 183*(1), 119-133. doi:https://doi.org/10.1016/S0376-7388(00)00576-7

Scheepers, D. M., Tahir, A. J., Brunner, C., & Guillen-Burrieza, E. (2020). Vacuum membrane distillation multi-component numerical model for ammonia recovery from liquid streams. *Journal of Membrane Science, 614*, 118399. doi:https://doi.org/10.1016/j.memsci.2020.118399

Schock, G., & Miquel, A. (1987). Mass transfer and pressure loss in spiral wound modules. *Desalination, 64*, 339-352. doi:http://dx.doi.org/10.1016/0011-9164(87)90107-X

van Linden, N., Bandinu, G. L., Vermaas, D. A., Spanjers, H., & van Lier, J. B. (2020). Bipolar membrane electrodialysis for energetically competitive ammonium removal and dissolved ammonia production. *Journal of Cleaner Production*, 120788. doi:https://doi.org/10.1016/j.jclepro.2020.120788

van Linden, N., Spanjers, H., & van Lier, J. B. (2019a). Application of dynamic current density for increased concentration factors and reduced energy consumption for concentrating ammonium by electrodialysis. *Water Research*, 114856. doi:https://doi.org/10.1016/j.watres.2019.114856

van Linden, N., Spanjers, H., & van Lier, J. B. (2022a). Fuelling a solid oxide fuel cell with ammonia recovered from water by vacuum membrane stripping. *Chemical Engineering Journal, 428*, 131081. doi:https://doi.org/10.1016/j.cej.2021.131081

van Linden, N., Wang, Y., Sudhölter, E., Spanjers, H., & van Lier, J. B. (2022b). Selectivity of vacuum ammonia stripping using porous gas-permeable and dense pervaporation membranes under various hydraulic conditions and feed water compositions. *Journal of Membrane Science, 642*, 120005. doi:https://doi.org/10.1016/j.memsci.2021.120005

van Veen, H. M., Rietkerk, M. D. A., Shanahan, D. P., van Tuel, M. M. A., Kreiter, R., Castricum, H. L., ten Elshof, J. E., & Vente, J. F. (2011). Pushing membrane stability boundaries with HybSi® pervaporation membranes. *Journal of Membrane Science, 380*(1), 124-131. doi:https://doi.org/10.1016/j.memsci.2011.06.040

Wijmans, J. G., Athayde, A. L., Daniels, R., Ly, J. H., Kamaruddin, H. D., & Pinnau, I. (1996). The role of boundary layers in the removal of volatile organic compounds from water by pervaporation. *Journal of Membrane Science, 109*(1), 135-146. doi:https://doi.org/10.1016/0376-7388(95)00194-8

Yang, X., Ding, L., Wolf, M., Velterop, F., Bouwmeester, H. J. M., Smart, S., Diniz da Costa, J. C., Liubinas, A., Li, J.-D., Zhang, J., & Duke, M. (2016). Pervaporation of ammonia solution with γ-alumina

supported organosilica membranes. *Separation and Purification Technology, 168*, 141-151. doi:http://dx.doi.org/10.1016/j.seppur.2016.05.017

Yang, X., Fraser, T., Myat, D., Smart, S., Zhang, J., Diniz da Costa, J. C., Liubinas, A., & Duke, M. (2014). A Pervaporation Study of Ammonia Solutions Using Molecular Sieve Silica Membranes. *Membranes, 4*(1), 40-54. doi:10.3390/membranes4010040

Yang, X., Sheridan, S., Ding, L., Wang, D. K., Smart, S., Diniz da Costa, J. C., Liubinas, A., & Duke, M. (2018). Inter-layer free cobalt-doped silica membranes for pervaporation of ammonia solutions. *Journal of Membrane Science, 553*, 111-116. doi:https://doi.org/10.1016/j.memsci.2018.02.049

Chapter 6.

Solid oxide fuel cell to generate electricity using ammonia-water mixtures recovered by vacuum membrane stripping

Based on: Fuelling a solid oxide fuel cell with ammonia recovered from water by vacuum membrane stripping

Niels van Linden, Henri Spanjers and Jules B. van Lier

https://doi.org/10.1016/j.cej.2021.131081

Abstract

Gaseous ammonia (NH_3) recovered from nitrogen-loaded (N-loaded) residual waters may be used as a fuel in solid oxide fuel cells (SOFCs) to generate energy without the emission of undesirable oxidised nitrogen species. NH_3 can be directly recovered as a gas by vacuum membrane stripping (VMS), which also results in the evaporation of water (H_2O), resulting in the recovery of NH_3-H_2O mixtures. However, in currently available literature, information is lacking on the attainable NH_3 concentrations in these NH_3-H_2O mixtures that will be used as a fuel for an oxygen-conducting SOFC (SOFC-O). This chapter presents the assessment of the effect of feed water temperature and the NH_3 feed water concentration on the attainable NH_3 concentrations in NH_3-H_2O mixtures obtained in the gaseous VMS permeate. Besides, this chapter presents the assessment of the feasibility to use dilute NH_3-H_2O mixtures in the concentration range between 5 and 25 wt%, for the generation of electricity in an SOFC-O. The results showed that increasing the NH_3 feed water concentration from 1 to 10 $g{\cdot}L^{-1}$ increased the NH_3 concentration in NH_3-H_2O mixtures obtained in the gaseous VMS permeate from 1 wt% to up to 11 wt%. Increasing the feed water temperature from 25 to 35 °C also results in an increase in the NH_3 concentration in the gaseous permeate, whereas increasing the feed water temperature from 35 °C to 55 °C leads to dilution of the NH_3-H_2O mixtures obtained in VMS permeate. Furthermore, energy was generated in an SOFC-O when the NH_3 concentration in the NH_3-H_2O fuel was only 5 wt%. Hence, the obtained NH_3 concentrations in the NH_3-H_2O mixtures obtained in gaseous VMS permeate show that VMS and SOFC-O can be combined for the generation of electricity from NH_3 recovered from water (aqueous solution). Moreover, the electrical energy generation of the SOFC-O, which reached values of 9 $MJ{\cdot}kg\text{-}N^{-1}$, was higher than the electrical energy consumption for VMS, for which values of 7 $MJ{\cdot}kg\text{-}N^{-1}$ were calculated.

Keywords

ammonia recovery; ammonia stripping; ammonia-water mixture; energy generation; vacuum membrane stripping; solid oxide fuel cell;

6.1. Introduction

Based on Chapter 1 of this thesis, vacuum membrane stripping (VMS) using porous gas-permeable membranes allow for higher ammonia (NH_3) transfer rates and higher selectivity of NH_3 over H_2O transfer, compared to dense pervaporation membranes. In addition, the literature review presented in Chapter 2 of this thesis shows that a solid oxide fuel cell (SOFC) is a suitable energy-conversion technology to generate energy from NH_3. However, information on the feasibility of combining VMS and SOFC for NH_3 recovery and subsequent electricity generation is missing.

6.1.1. Use of gaseous NH_3 for electricity generation by SOFCs

The chemically stored energy in NH_3, which equals 21 MJ·kg-N^{-1}, referring to the lower heating value at 750 °C, can be converted to electricity and heat by various energy-conversion technologies (Valera-Medina et al., 2018). NH_3 as an energy source opens new opportunities for the application of recovered NH_3 from nitrogen-loaded (N-loaded) residual waters. Whereas conventional combustion-based technologies initially convert the chemical energy to heat and subsequently generate electricity at efficiencies ranging between 30 - 40%, fuel cells allow for direct generation of electricity at up to 60% efficiency (Stambouli & Traversa, 2002).

Amongst the various fuel cell types, three types are so-called direct NH_3 fuel cells: 1) alkaline fuel cells (AFCs), 2) alkaline membrane fuel cells (AMFCs) and 3) solid oxide fuel cells (SOFCs). According to review studies of Cheddie (2012) and Lan and Tao (2014b), the reported maximum (peak) power density of AFCs (16 mW·cm^{-2}) and AMFCs (40 mW·cm^{-2}) are an order of magnitude lower than the reported peak power density of SOFCs (ranging between 580 and 1,190 mW·cm^{-2}), using gaseous NH_3 directly as a fuel. Moreover, the use of AMFCs is challenged by catalyst poisoning by adsorbed N species at the anode, diffusion of NH_3 through the membrane electrolyte, and slow kinetics due to the low operating temperature (between 25 and 80 °C) (Suzuki et al., 2012). Furthermore, the use of AFCs is challenged by carbonate formation in the liquid hydroxide electrolyte (Lan & Tao, 2010, 2014b).

The high peak power densities of SOFCs are explained by the fast kinetics and the low resistances, as SOFCs operate at temperatures ranging between 600 and 1,000 °C, allowing for electrical efficiencies up to 60% and total energy efficiencies up to 90% when the high-grade generated heat is used (Stambouli & Traversa, 2002). The operational temperature combined with the presence of nickel catalysts allows for spontaneous cracking of NH_3 to hydrogen (H_2) and N_2 (Eq. 6-1) (Staniforth & Ormerod, 2003), without the need to change the materials or design of H_2-fuelled SOFCs to use NH_3 as a fuel (Wojcik et al., 2003). SOFC types are distinguished based on their electrolyte properties (Stambouli & Traversa, 2002; Ni et al., 2009). SOFC-Os have an oxygen-conducting electrolyte, while SOFC-Hs have a proton-conducting solid electrolyte. In both types of SOFCs, cracking of NH_3 takes place at the anode. However, in SOFC-Os, oxygen (O_2) reduction to oxygen ions (O^{2-}) takes place at the cathode (Eq. 6-2). Subsequently, O^{2-} transfer from the cathode to the anode allows for the reaction of O^{2-} with H_2 (Eq. 6-3), resulting in the release of electrons. The electrons go through an electrical circuit to the cathode, allowing again for O_2 reduction. In contrast, in SOFC-Hs, protons (H^+) are formed at the anode and subsequent H^+ transfer takes place from the anode to the cathode. At the

cathode, H^+ reacts with O_2, resulting in the release of electrons, which are again used at the anode to form H^+ from H_2. Currently, the reported peak power densities of SOFC-Os exceed the reported peak power densities of SOFC-Hs, due to optimal material selection and design of SOFC-Os as a result of extensive research (Ni et al., 2009; Afif et al., 2016). Moreover, the conversion of NH_3 in SOFC-Os leads to very low emission of N-species. Dekker and Rietveld (2006) reported near-complete (> 99.9%) cracking of NH_3 at the anode and only traces of NO_x (ranging between 0.5 and 4 ppm) in the anode off-gas of their SOFC-O. Research conducted by Staniforth and Ormerod (2003), Ma et al. (2006) and Okanishi et al. (2017) confirmed these findings and detected no NH_3, NO, NO_2 nor N_2O in the anode off-gas of their SOFC-O. Hence, SOFC-Os are potentially suitable to efficiently convert the chemically stored energy from recovered NH_3 to energy, without the emission of undesirable oxidised N-species.

$$^2/_3\, NH_3 + x\, H_2O \rightarrow {}^1/_3\, N_2 + H_2 + x\, H_2O \qquad \text{Eq. 6-1}$$

$$0.5\, O_2 + 2\, e^- \rightarrow O^{2-} \qquad \text{Eq. 6-2}$$

$$H_2 + O^{2-} \rightarrow (x+1)\, H_2O + 2e^- \qquad \text{Eq. 6-3}$$

6.1.2. Direct gaseous NH_3 recovery from water by VMS

To allow for using the recovered NH_3 as a fuel for SOFC-Os, NH_3 must be extracted from the water phase as a gas. Hereto, vacuum stripping of NH_3 can be used, which avoids the presence of O_2 in the recovered gas. In contrast, applying air stripping will lead to the deactivation of the nickel anode catalyst of SOFC-Os by oxidation of nickel to nickel oxide (NiO). The use of membranes in vacuum membrane stripping (VMS) configurations, results in large gas-liquid exchange areas in a small volume, allowing for compact systems. However, stripping of NH_3 from water (aqueous solution) is accompanied by the evaporation of H_2O, resulting in gaseous NH_3-H_2O mixtures in the VMS permeate. El-Bourawi et al. (2006) and Ding et al. (2006) studied the effects of the solution pH, feed water temperature, vacuum pressure, feed flow velocity, and feed water concentration NH_3 concentration on the NH_3 mass transfer coefficient, which relates the mass flux and the corresponding driving force. However, both studies did not report the effects on the individual transfer of NH_3 and H_2O, nor on the obtained NH_3 concentration in the recovered NH_3 stream. On the other hand, the studies of He et al. (2017) and He et al. (2018) reported concentrations of NH_3 in a range between 4 and 18 g-N·L^{-1} in the gaseous NH_3-H_2O mixtures recovered from biogas slurry by VMS, corresponding to a range between 0.5 and 2.2 wt% (weight %) of NH_3.

6.1.3. Direct use of recovered NH_3 from water as a fuel for SOFCs

Only recent studies of Stoeckl et al. (2019a) and Stoeckl et al. (2020) mentioned the use of recovered NH_3 as fuel for an SOFC-O. However, the authors used fuel with an NH_3 concentration of 70 wt%, as an NH_3-H_2O mixture, and did not mention for what kind of feed water and operating conditions this NH_3 concentration can be obtained. Hence, currently reported NH_3 concentrations, which are obtained by VMS (up to 2 wt%) and those that are used in NH_3-H_2O mixtures as fuel for SOFC-Os (70 wt%), do not match. This discrepancy

makes it unclear whether VMS and SOFC-Os can be combined for the recovery of NH_3 from water (aqueous solution) and the subsequent direct use of the recovered NH_3 as a fuel. Therefore, more information is needed to bridge the gap in applicable NH_3 concentrations in NH_3-H_2O mixtures that can be obtained by VMS and directly be used by SOFC-O.

To obtain more concentrated NH_3-H_2O mixtures during the recovery of NH_3 by VMS, the amount of H_2O evaporated relative to the amount of NH_3 stripped must be minimised. In currently available literature on NH_3 recovery by VMS, feed water temperatures ranging between 40 and 75 °C are used (Ding et al., 2006; El-Bourawi et al., 2007; He et al., 2017; He et al., 2018; Scheepers et al., 2020). All mentioned studies showed that when the feed water temperature increased, the NH_3 in the gaseous permeate was diluted. Therefore, VMS seems to be a suitable technology only for feed water temperatures below 40 °C. In addition, when increased NH_3 concentrations are present in the feed water, also the NH_3 flux increases (Ding et al., 2006; El-Bourawi et al., 2007; He et al., 2017; Scheepers et al., 2020). Based on the study of van Linden et al. (2019a), NH_3 concentrations of 10 $g \cdot L^{-1}$ can be obtained, using electrodialysis to concentrate NH_4^+, followed by chemical addition for pH increase. As an alternative for adding chemicals to obtain dissolved NH_3, bipolar membrane electrodialysis can be applied, which allows for the direct production of concentrated dissolved NH_3 without the addition of chemicals (van Linden et al., 2020).

6.1.4. Research objectives

This chapter aimed to link VMS and SOFC-O for NH_3 recovery from water (aqueous solution) and to directly use the recovered NH_3 for energy generation. The first goal of this chapter was to determine what NH_3 concentrations in the recovered NH_3-H_2O mixtures obtained in the gaseous VMS permeate can be obtained for various feed water temperatures ranging between 25 and 55 °C and NH_3 feed water concentrations ranging between 1 and 10 $g \cdot L^{-1}$, which is considered a relevant range for NH_3 recovery from N-loaded residual waters. The second goal of this chapter was to determine the required NH_3 concentrations for electricity generation in an SOFC-O, using NH_3-H_2O mixtures with NH_3 concentrations ranging between 5 and 25 wt%. As the third goal of this chapter, the electrical energy consumption to recover NH_3 by VMS, as well as the electricity generation of the SOFC-O using NH_3-H_2O mixtures as a fuel were calculated.

6.2. Materials and methods

6.2.1. Materials

6.2.1.1. Experimental VMS set-up

For the VMS experiments, an acrylic Sterlitech flow-cell was used, containing a flat-sheet polytetrafluoroethylene (PTFE) hydrophobic membrane with polypropylene (PP) backing, with a pore size of 0.1 µm and a membrane area of 34 cm^2. A wire mesh spacer with a filament thickness of 0.8 mm and a void fraction of 91% was placed at the feed side to create the desired turbulence, while another wire mesh spacer was placed at the permeate side to avoid the membrane from sticking to the flow-cell.

The feed waters were stored in a 1 L borosilicate bottle and were recirculated through the flow-cell by a calibrated peristaltic Watson Marlow 520S pump equipped with Watson-Marlow 313 pump heads (0.3 – 46 $L \cdot h^{-1}$). A calibrated digital Festo IP40 pressure sensor (100 – 200,000 Pa) was used to measure the hydraulic pressure drop over the VMS flow cell. The pH and electrical conductivity (EC) of the feed waters were continuously measured in the bottle, using a calibrated IDS SenTix 940 pH sensor and a calibrated TetraCon 925 EC-sensor, respectively. The data was automatically logged on a WTW Multi 3630 IDS multimeter and stored on a laptop. The feed water bottle was sealed during operation to avoid the loss of water and NH_3 from the feed water to the atmosphere. The feed water bottle was placed on an IKA RH Digital KT/C heating plate and magnetic stirrer combination, while an IKA Ikatron ETC 1 temperature sensor measured the temperature of the feed water and controlled the heating plate to maintain a stable feed water temperature. The heating-mixing combination and feed water bottle were placed on a Kern PCB 6000-1 mass balance (0.1 – 6,000 g) to continuously measure the total mass of the feed water. The data was automatically logged and stored on a laptop.

A calibrated KNF N816.3KT.45.18 vacuum pump was used to create a partial vacuum of 1,500 Pa at the permeate side of the membrane. The gaseous VMS permeate was scrubbed in a cooled acid trap containing 200 mL 1 M hydrochloric acid (HCl) solution (Merck), to protect the vacuum pump. Ammonium bicarbonate (NH_4HCO_3) (Sigma Aldrich Reagent Plus) and 1 M sodium hydroxide (NaOH) (Merck) was used to prepare the feed waters. Finally, the NH_3 concentrations in the feed waters were measured with Machery-Nagel NANOCOLOR 2,000 test kits (concentration range 0.4 – 2.0 $g \cdot L^{-1}$). Figure 6-1 shows a schematic representation of the experimental VMS setup.

6.2.1.2. Experimental SOFC set-up

For the SOFC-O experiments, a Fiaxell Open Flanges Set-up was used, which contained a 10 cm^2 planar anode-supported membrane electrode assembly (MEA). The MEA consisted of a NiO-8YSZ (nickel oxide coated zirconia stabilised by 8% yttria) anode, an O^{2-}-conducting 8YSZ electrolyte and a 20GDC-LSCF (lanthanum strontium cobalt ferrite stabilised by 20% gallium doped ceria) cathode. The MEA was sealed by a 0.5 mm thick mica sheet to limit the leakage of fuel from the anode to the cathode. At the anode, nickel foam with a thickness of 0.6 mm and a diameter of 40 mm was placed to provide extra surface area to crack

NH_3. A golden mesh grid current collector was placed on top of the cathode to measure the electric potential and to draw electric current. Alumina sheets were placed at the cathode side of the MEA to avoid contact between the anode and cathode. The MEA and associating accessories were placed between a fuel and an air diffuser, both made of Inconel 601 (nickel-chromium alloy), which were put together by wired rods and wing nuts. The anode and cathode temperature during the operation were measured by two K-type thermocouples, which were connected to a TM-947SD thermometer (max. 1,700 °C, accuracy of 0.1 °C) to read and log the temperature. An electrical circuit including the SOFC-O anode and cathode and a Rigol DL3021 electronic load (0.001 – 40 A) was made to draw and measure the electric current. By connecting cables with alligator clips to the fuel diffuser and the current collector at the top of the Open Flanges Set-up, the electric potential was measured on a UNI-T UT58E multimeter (0.001 – 1,000 V). Finally, a Manson HCS-3202 power supply (1 – 36 V) was used as a booster to compensate for the electric potential loss caused by the electrical resistance of the electrical circuit when drawing an electric current.

The Open Flanges Set-up was placed in a Kittec Squadro SQ11 oven (max. 1,320 °C, accuracy of 1 °C) to control the operating temperature. Calibrated rotameters were used to control the supply of industrial grade pressurised air to the cathode (40 – 800 mL·min^{-1}) and forming gas, consisting of 5 v% (volume %) H_2 and 95 v% N_2, to the anode (20 – 400 mL·min^{-1}). The connections of the gas cylinders and connections to the Open Flange Set-up were Swagelok fittings to limit any gas leakages. For the fuel, Acros Organics 25% NH_4OH solution and demineralised water were used to obtain various NH_3-H_2O mixtures. A calibrated Lead Fluid BT101L peristaltic pump (0.001 – 575 mL·min^{-1}) was used to supply liquid NH_3-H_2O mixtures to the anode. Finally, 1 M HCl solution was used to capture any remaining NH_3 in the anode off-gas. The complete SOFC-O set-up is schematically presented in Figure 6-2.

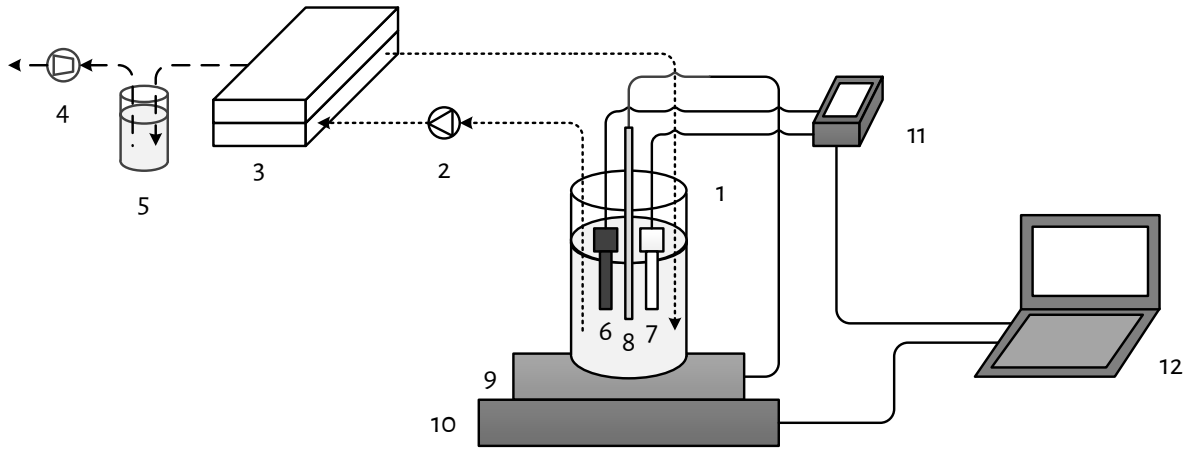

Figure 6-1 - A schematic representation of the used experimental VMS setup including a feed water bottle (1), peristaltic pump (2), flow-cell including membrane (3), vacuum pump (4), permeate scrubber (5), EC-sensor (6), pH-sensor (7), temperature sensor (8), pressure sensor (9), integrated heating and mixing plate (10), balance (11), multimeter (12) and laptop (13).

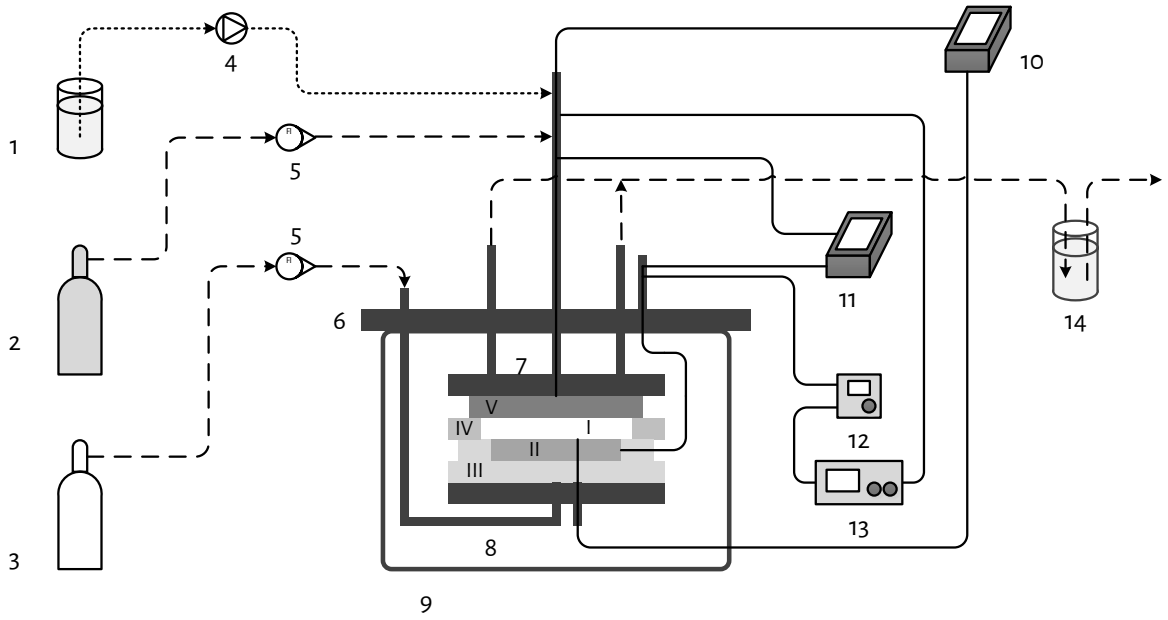

Figure 6-2 - A schematic representation of the used experimental SOFC setup including a fuel storage bottle (1), forming gas cylinder (2), air cylinder (3), peristaltic pump (4), fuel diffuser (5), Open Flange set-up (6), fuel diffuser (7), air diffuser (8), oven (9), thermometer (10), multimeter for electric potential (11), electric potential booster (12), electronic load (13) and off-gas scrubbing bottle (14). The MEA (I), electric current collector (II), alumina isolation sheets (III), mica sealing sheet (IV) and nickel foam (V) are all placed between the fuel and air diffuser.

6.2.2. Methods

6.2.2.1. VMS experiments

For the VMS experiments, feed waters with various initial NH_3 concentrations were prepared by adding NH_4HCO_3 to demi water. NH_4HCO_3 was used as representative salt for N-loaded residual waters with high TAN concentrations, because bicarbonate (HCO_3^-) is typically the main counter ion of NH_4^+ in N-loaded residual waters as industrial condensates, sludge reject waters and hydrolysed urine. To obtain NH_3 in the feed water, the solution pH was increased to 10 by adding NaOH to the NH_4HCO_3 solutions.

During the stripping of NH_3 from the feed waters, the NH_3 feed water concentration decreased. By taking samples of the feed water to measure the NH_3 concentration, the NH_3 flux at various NH_3 feed water concentrations was determined. Besides, the H_2O fluxes were determined to assess how much water evaporated along with the stripped NH_3. Based on both the NH_3 and H_2O fluxes, the concentrations of NH_3 in NH_3-H_2O mixtures obtained in the gaseous VMS permeate as a function of the NH_3 feed water concentration were determined. Next, the effect of the feed water temperature on both the NH_3 and H_2O flux was assessed for feed water temperatures of 25, 35, 45 and 55 °C. For the two mentioned variables, a full factorial design of experiments was set up, and each combination of feed water temperature and NH_3 feed water concentration was assessed in duplicate.

The feed waters were recirculated over the hydrophobic membrane under so-called unsteady hydraulic conditions, corresponding to a Reynolds number of 500 in spacer-filled channels (Mojab et al., 2014). The pump speed was adjusted accordingly to maintain unsteady conditions for the various feed waters and the cross-flow velocity for the various feed waters ranged between 10 and 20 $cm \cdot s^{-1}$. A detailed description of the determination of the cross-flow velocity to obtain unsteady hydraulic conditions based on the feed water characteristics and the dimensions of the flow channel can be found in the Supporting Information of the paper of van Linden et al. (2022a). At the permeate side of the membrane, an absolute pressure of 1.5 kPa was maintained by the vacuum pump. Throughout each run, the total mass, temperature, EC and pH of the feed water were continuously logged and samples were taken every 15 minutes to measure the NH_3 concentration in the feed water.

6.2.2.2. SOFC experiments

When the MEA was installed and the Open Flange Set-up was placed in the oven, the oven temperature was increased at a ramping speed of 120 °C per hour to 400 °C, followed by 200 °C per hour to 750 °C. During the heating of the oven, air was supplied to the cathode at a flow rate of 400 $mL \cdot min^{-1}$, while forming gas was supplied to the anode at a flow rate of 200 $mL \cdot min^{-1}$ to supply H_2 to gradually reduce NiO to nickel, which catalyses the cracking of NH_3 and the oxidation of H_2. When the oven temperature reached 750 °C, various NH_3-H_2O mixtures were supplied to the anode. NH_3-H_2O mixtures with NH_3 concentrations of 5, 7.5, 10, 12.5 and 25% were prepared by mixing 25 wt% NH_4OH stock solution with demi water. Throughout all

experiments, the airflow rate remained 400 mL·min^{-1}, corresponding to 0.1 mol-O_2·cm^{-2}·h^{-1}, based on an O_2 concentration of 21% in air and an air pressure of 101,325 Pa.

After a stabilisation period of 15 minutes, the open circuit potential (OCP) was measured for each fuel. Subsequently, the electrical circuit was closed and an electric current was drawn in steps of 10 mA·cm^{-2}. By logging the electric potential measured between the anode and cathode for each electric current step, the peak power density achieved by the SOFC-O for the various fuels was determined. A fuel flow rate of 200 µL·min^{-1} was used, based on the recommendations of the MEA supplier, which corresponded to an NH_3 flux of 12 kg·m^{-2}·h^{-1}, considering a fuel density ranging from 950 to 986 g·L^{-1}. Each NH_3 concentration in the fuel was tested in duplicate experiments.

6.2.3. Performance indicators

6.2.3.1. VMS

The NH_3 and H_2O fluxes were determined using the respective mass differences per unit of membrane area and time (Eq. 6-4 and Eq. 6-5, respectively), which were based on the measured feed water masses, NH_3 concentrations, salt concentrations and solution densities at each time instant. A more detailed description of the NH_3 and H_2O mass determination is presented in the Supporting Information of the paper of van Linden et al. (2022a).

$$J_{NH_3} = \frac{-(m_{NH_3,i+1} - m_{NH_3,i})}{A_m \cdot (t_{i+1} - t_i)} \quad \text{Eq. 6-4}$$

$$J_{H_2O} = \frac{-(m_{H_2O,i+1} - m_{H_2O,i})}{A_m \cdot (t_{i+1} - t_i)} \quad \text{Eq. 6-5}$$

Where J_{NH_3} and J_{H_2O} = ammonia and water mass flux (in kg·m^{-2}·h^{-1}), $m_{NH_3,i}$ and $m_{H_2O,i}$ = ammonia and water mass at time t_i (in kg), A_m = membrane area (in m^2, A_m = 0.034 m^2) and t_i = time instant 'i' (in h).

Subsequently, the concentration of NH_3 obtained by VMS in the permeate followed from the ratio of the NH_3 flux and the total flux (Eq. 6-6).

$$c_{NH_3} = \frac{J_{NH_3}}{J_{NH_3} + J_{H_2O}} \quad \text{Eq. 6-6}$$

Where c_{NH_3} = NH_3 concentration in NH_3-H_2O mixtures obtained in the gaseous VMS permeate (unitless).

The total molar flow rate through the VMS membrane was determined based on the mass flow rates of NH_3 and H_2O (Eq. 6-7). Subsequently, the volumetric flow rate was determined by using the ideal gas law (Eq. 6-8).

$$n_t = \frac{J_{NH_3} \cdot A_m}{MW_{NH_3}} + \frac{J_{H_2O} \cdot A_m}{MW_{H_2O}} \quad \text{Eq. 6-7}$$

$$Q_{t,in} = \frac{n_t \cdot R \cdot T_f}{p_v} \quad \text{Eq. 6-8}$$

Where, n_t = total molar flow rate (mol·s^{-1}), MW_{NH_3} and MW_{H_2O} = molecular weight of NH_3 and H_2O, respectively (in g·mol^{-1}, MW_{NH_3} = 17 g·mol^{-1} and MW_{H_2O} = 18 g·mol^{-1}), $Q_{t,in}$ = volumetric gas flow rate (m^3·s^{-1}), R = universal gas constant (in J·mol^{-1}·K^{-1}, R = 8.31 J·mol^{-1}·K^{-1}), T_f = feed water temperature (in K) and p_v = vacuum pressure (in Pa, p_v = 1,500 Pa).

The required electrical power for the vacuum pump was determined based on the study of Huttunen et al. (2017) (Eq. 6-9):

$$P_{v.p.} = \frac{Q_{t,in} \cdot p_v \cdot \ln\left(\frac{p_{atm}}{p_v}\right)}{\eta_{v.p.}} \quad \text{Eq. 6-9}$$

Where $P_{v.p}$ = electrical power vacuum pump (in W = J·s^{-1}), p_{atm} = atmospheric pressure (in Pa, p_{atm} = 101,325 Pa = 101,325 kg·m^{-1}·s^{-2}), $\eta_{v.p.}$ = vacuum pump efficiency (unitless, $\eta_{v.p.}$ = 60%).

In addition, the required power of the feed pump to recirculate the feed waters was determined based on the feed flow rate and the measured hydraulic pressure loss over the VMS flow-cell (Eq. 6-10).

$$P_{f.p.} = \frac{Q_f \cdot \Delta p_h}{\eta_{f.p.}} \quad \text{Eq. 6-10}$$

Where $P_{f.p}$ = electrical power feed pump (in J·s^{-1}), Q_f = flow rate feed pump (in m^3·s^{-1}), Δh = hydraulic pressure loss (in Pa, Δp_h = 15,490 Pa), $\eta_{f.p.}$ = feed pump efficiency (unitless, $\eta_{f.p.}$= 60%).

At last, the electrical energy consumption for NH_3 stripping from the various feed water at various feed water temperatures and various NH_3 feed water concentrations was determined using Eq. 6-11.

$$E_{VMS} = \frac{P_{v.p.} + P_{r.p.}}{J_N \cdot A_m} \quad \text{Eq. 6-11}$$

Where E_{VMS} = electrical energy consumption of VMS to strip NH_3 (in MJ·kg-N^{-1}), J_N = nitrogen mass flux (in kg·m^{-2}·h^{-1}).

6.2.3.2. SOFC

For each of the tested fuels, the theoretical Nernst potential was calculated using Eq. 6-12. The Nernst potential represents the theoretical potential of the oxidation of H_2 (Eq. 6-3) after NH_3 cracking in the presence of excess H_2O in the fuel (Eq. 6-1). The effect of the excess of H_2O is incorporated in the molar fraction of H_2 and H_2O in Eq. 6-12.

$$U_{Nernst} = \frac{-\Delta_r G(T)}{N_{e^-,H_2} \cdot F} + \frac{R \cdot T}{N_{e^-,H_2} \cdot F} \cdot ln\left(\frac{[\gamma_{H_2}] \cdot [\gamma_{O_2}]^{0.5}}{[\gamma_{H_2O}]}\right) \quad \text{Eq. 6-12}$$

Where U_{Nernst} = Nernst potential (in V), $\Delta_r G(T)$ = Gibbs Free Energy of reaction at a certain temperature (in kJ·mol^{-1}, $\Delta_r G$(750 °C) = -196 kJ·mol^{-1}, lower heating value), T = operating temperature (in K, T = 750 °C = 1023 K), N_{e^-,H_2} = number of electrons per mole of hydrogen during oxidation (unitless, n = 2), F = Faraday constant

($C \cdot mol^{-1}$, F = 96,485 $C \cdot mol^{-1}$), R = universal gas constant ($J \cdot mol^{-1} \cdot K^{-1}$, R = 8.31 $J \cdot mol^{-1} \cdot K^{-1}$), γ_{H_2}, γ_{O_2} and γ_{H_2O} = molar fraction of hydrogen, oxygen and water, respectively (unitless).

Subsequently, the power density, representing the generated electrical power per unit of MEA area, followed from the measured electric potential at a certain electric current (Eq. 6-13).

$$p_{SOFC} = \frac{U \cdot I}{A_{MEA}} \quad \text{Eq. 6-13}$$

Where p_{SOFC} (in $mW \cdot cm^{-2}$), U = electric potential (in mV), I = electric current (in mA) and A_{MEA} = membrane electrode assemble area (in cm^2, A_{MEA} = 10 cm^2)

Furthermore, the fuel (Eq. 6-14) and oxygen utilisation (Eq. 6-15) were determined to assess how efficient NH_3 in the fuel and O_2 in the air were used to generate electricity, based on the measured amount of charge (electric current) and the supplied amounts of reactants (H_2 and O_2) for the oxidation of H_2. In addition, the electrical efficiency of the SOFC-O was determined based on the generated power and supplied amount of chemical energy per unit of time (Eq. 6-16).

$$\mu_f = \frac{I}{n_{H_2} \cdot N_{e^-,H_2} \cdot F} \quad \text{Eq. 6-14}$$

$$\mu_{O_2} = \frac{I}{n_{O_2} \cdot N_{e^-,O_2} \cdot F} \quad \text{Eq. 6-15}$$

Where μ_f and μ_{O2} = fuel and oxygen utilisation (unitless), respectively, n_{H_2} and n_{O_2} = molar flow rate of H_2 and O_2, respectively ($mol \cdot s^{-1}$) and N_{e^-,O_2} = the number of electrons per mole of oxygen in the hydrogen oxidation reaction (unitless, n = 4).

$$\eta_{elec} = \frac{p_{SOFC} \cdot A_{MEA}}{n_{H_2} \cdot -\Delta_r H(T)} \quad \text{Eq. 6-16}$$

Where, η_{elec} = electrical efficiency (unitless), p_{SOFC} = electric power generated by the SOFC (in W = $J \cdot s^{-1}$) and $\Delta_r H(T)$ = enthalpy of reaction at a certain temperature (in $kJ \cdot mol^{-1}$, $\Delta_r H(750\ °C)$ = -237 $kJ \cdot mol^{-1}$, lower heating value).

Finally, the electrical energy generation of the SOFC-O was calculated using Eq. 6-17.

$$E_{SOFC-O} = \frac{p_{SOFC} \cdot A_{MEA}}{m_N} \quad \text{Eq. 6-17}$$

Where, E_{SOFC-O} = electrical energy generation of the SOFC-O ($MJ \cdot kg\text{-}N^{-1}$).

6.3. Results and discussion

6.3.1. Recovery of NH_3-H_2O mixtures by VMS

6.3.1.1. NH_3 flux for various feed water temperatures and NH_3 feed water concentrations

For the VMS experiments, various feed waters consisting of NH_4HCO_3 at a pH of 10.0 ± 0.1 (average ± standard deviations, n = 17) were prepared. Subsequently, NH_3 was stripped at feed water temperatures of 25, 35, 45 and 55 °C. The deviation in feed water temperature during the experiments was less than 1% of the respective feed water temperature. Due to the addition of NaOH to form dissolved NH_3 in the feed waters, sodium (Na^+), HCO_3^- and carbonate (CO_3^{2-}) ions were also present in the feed waters. The transfer of CO_2 was neglected, because the CO_2 vapour pressure of the feed water was ten times lower than the NH_3 and H_2O vapour pressure of the feed water; at a pH of 10, inorganic carbon is only present as HCO_3^- and CO_3^{2-}.

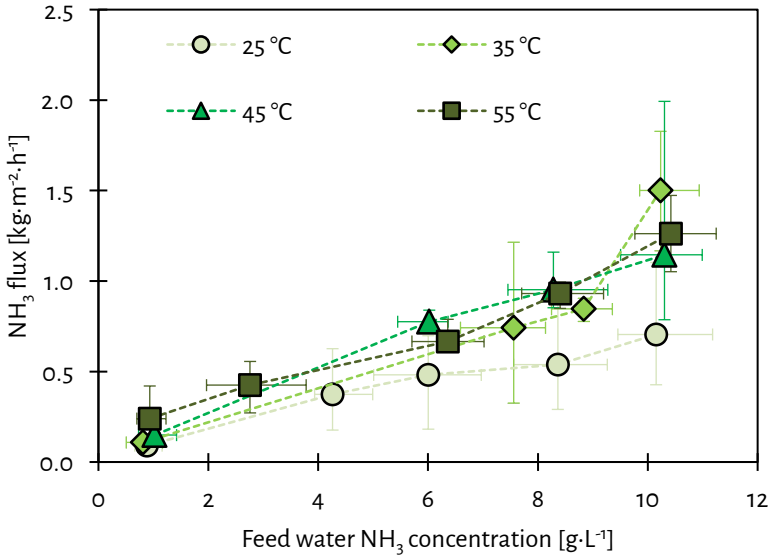

Figure 6-3 - The NH_3 flux as a function of NH_3 feed water concentration for various feed water temperatures. The vertical error bars represent the minimum and maximum deviations of the measured NH_3 flux of at least triplicate measurements, whereas the horizontal error bars represent the minimum and maximum deviations in the measured feed water NH_3 concentration.

The reported values of the NH_3 flux in Figure 6-3 and the NH_3 feed water concentration for the various feed water temperatures were calculated based on the measured TAN concentration, temperature, pH and ionic strength, and feed water temperature. At a feed water temperature of 25 °C, the NH_3 flux increased from 0.1 to 0.7 $kg \cdot m^{-2} \cdot h^{-1}$ for an increase in NH_3 feed water concentration from 1 to 10 $g \cdot L^{-1}$. For the same NH_3 feed water concentration range, the NH_3 flux increased from 0.1 to 1.5 $kg \cdot m^{-2} \cdot h^{-1}$ at a feed water temperature of 35 °C, from 0.1 to 1.1 $kg \cdot m^{-2} \cdot h^{-1}$ at 45 °C and from 0.2 to 1.2 $kg \cdot m^{-2} \cdot h^{-1}$ for 55 °C.

For all measured temperatures, the NH_3 flux increased linearly (R^2 = 0.86 – 0.99) as a function of the increasing NH_3 feed water concentration, in line with the studies of El-Bourawi et al. (2007) and Scheepers et al. (2020). The linear increase in NH_3 flux as a function of the NH_3 feed water concentration was in contrast to findings of He et al. (2017), who found a logarithmic relationship for an NH_3 concentration ranging between 1 and 4 $g \cdot L^{-1}$, which was probably a result of a high mass transfer resistance, as biogas slurry was used as feed. Henry's Law states that the vapour pressure of dissolved gases in water at a certain temperature is a linear function of the concentration of the respective dissolved gas. Figure 6-4 presents the vapour pressures of NH_3 in water as a function of both the feed water temperature and the NH_3 feed water concentration. The vapour pressures of the feed water are obtained by PHREEQC simulation software, taking the NH_3 concentrations, pH, ionic strength and temperature into account to determine chemical equilibria and vapour pressures of solutes (NH_3) and solvent (H_2O). Furthermore, the Dusty Gas Model and Fick's Law, which are applicable for vapour transfer through porous hydrophobic membranes (Lawson & Lloyd, 1997), describe that the diffusion flux is linearly proportional to the driving force of gas transfer. Hence, the observed linear increase in NH_3 flux as a function of the NH_3 feed water concentration at each tested feed water temperature was caused by the increase in NH_3 vapour pressure of the feed water. The observed linear increase in NH_3 flux as a function of the NH_3 feed water concentration indicated that the NH_3 mass transfer coefficient remained unaffected, suggesting that no concentration polarisation phenomena affected the NH_3 transfer at increased NH_3 feed water concentrations.

According to Figure 6-4, the NH_3 vapour pressure of the feed water increased exponentially with increasing feed water temperatures for a certain NH_3 feed water concentration, which is explained by the temperature dependency of Henry's constant, determined using the van 't Hoff equation, and the decreased solubility of gases for higher feed water temperatures. However, according to Figure 6-3, the NH_3 fluxes did not increase consistently as a function of the feed water temperature. The NH_3 fluxes increased when the feed water temperature increased from 25 to 35 °C. However, a further increase in temperature from 35 to 45 and 55 °C, did not result in an increased NH_3 flux. Apparently, when the feed water temperature increased to 45 and 55 °C, the NH_3 mass transfer coefficient decreased, counteracting the increase in NH_3 vapour pressure of the feed water. The decrease in NH_3 mass transfer coefficient over the increasing feed water temperature can be assigned to NH_3 depletion, concentration polarisation, and temperature polarisation, of which the effects become more severe at increased feed water temperatures (He et al., 2017; He et al., 2018). However, to draw firm conclusions on which polarisation phenomenon affected the NH_3 mass transfer most, more research is required.

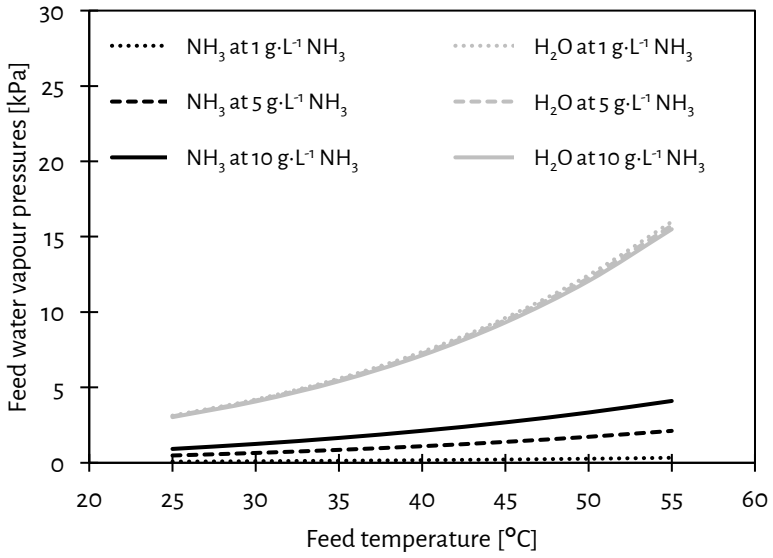

Figure 6-4 - The NH_3 and H_2O vapour pressure of the feed water as a function of the feed water temperature for various NH_3 feed water concentrations. The vapour pressures were obtained by simulations with PHREEQC software, using the phreeqc.dat database.

6.3.1.2. H_2O flux for various feed water temperatures and NH_3 feed water concentrations

Besides the stripping of NH_3, also evaporation of H_2O through the hydrophobic membrane took place during the VMS experiments. Figure 6-5 presents the H_2O flux as a function of the concentration of NH_3 in the feed and the feed water temperature. At a feed water temperature of 25 °C, the H_2O flux decreased from 10 to 7 $kg \cdot m^{-2} \cdot h^{-1}$ for an increase in NH_3 feed water concentration from 1 to 10 $g \cdot L^{-1}$. When the NH_3 feed water concentration increased from 1 to 10 $g \cdot L^{-1}$ at a feed water temperature of 35 and 45 °C, the H_2O flux decreased from 16 to 12 $kg \cdot m^{-2} \cdot h^{-1}$ and from 24 to 22 $kg \cdot m^{-2} \cdot h^{-1}$, respectively. The H_2O flux at a feed water temperature of 55 °C remained stable at 30 $kg \cdot m^{-2} \cdot h^{-1}$ as the NH_3 feed water concentration increased from 1 to 10 $g \cdot L^{-1}$.

According to Figure 6-4, the H_2O vapour pressure of the feed water increased exponentially with the feed water temperature, following the Clausius–Clapeyron relation. However, according to the data, the H_2O flux increased linearly ($R^2 = 0.96 – 1.00$) as a function of the increase in feed water temperature. The observation that the H_2O flux increased linearly while the driving force increases exponentially indicates that the H_2O mass transfer coefficient decreased over the increasing feed water temperature, which might be attributed to temperature polarisation (Martínez-Díez & Vázquez-González, 1999; Ding et al., 2006; El-Bourawi et al., 2007).

According to Figure 6-5, the H_2O flux decreased as a function of the increasing NH_3 feed water concentration. For increasing NH_3 in the feed water, increased amounts of NH_4HCO_3 and NaOH were added, resulting in higher ion concentrations during NH_3 stripping. Raoult's Law describes that the vapour pressure of a solvent decreases when the molar fraction of the solutes increases. Based on the data presented in Figure 6-4, the H_2O vapour decreased by 3% when the NH_3 concentration increased from 1 to 10 $g \cdot L^{-1}$. The decrease in H_2O flux as a function of the increasing NH_3 concentration might also be explained by temperature polarisation,

which decreases the H_2O mass transfer coefficient, as described by Martínez-Díez and Vázquez-González (1999).

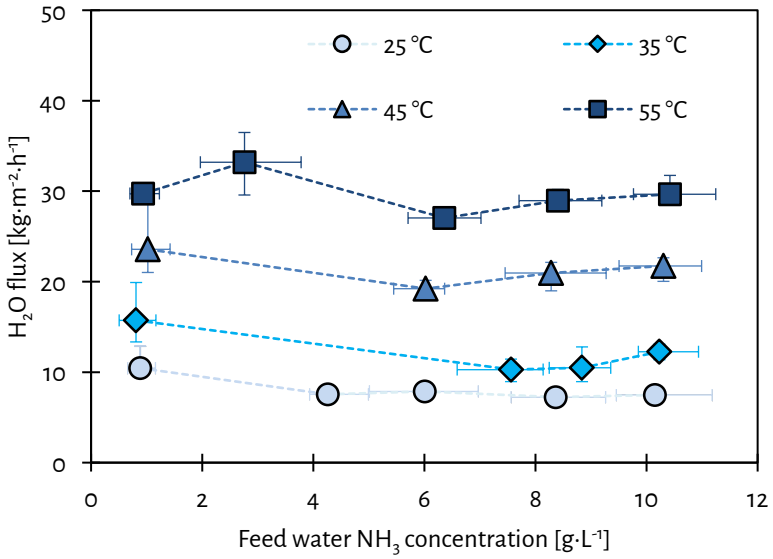

Figure 6-5 - The H_2O flux as a function of the increasing NH_3 feed water concentration for various feed water temperatures. The vertical error bars represent the minimum and maximum deviations of the measured H_2O flux of at least triplicate measurements, whereas the horizontal error bars represent the minimum and maximum deviations in the measured feed water NH_3 concentration.

6.3.1.3. NH_3 concentration in gaseous VMS permeate for various feed water temperatures and NH_3 feed water concentrations

One of the objectives of this chapter was to determine the attainable NH_3 concentration in NH_3-H_2O mixtures obtained in the gaseous VMS permeate for NH_3 reuse purposes. Figure 6-6 presents the concentration of NH_3 in NH_3-H_2O mixtures obtained in the gaseous VMS permeate for the various tested feed water temperatures as a function of the NH_3 feed water concentration. For an increase in the NH_3 feed water concentration from 1 to 10 $g \cdot L^{-1}$, the NH_3 concentration in NH_3-H_2O mixtures obtained in the VMS permeate increased from 1 to 8 wt% at a feed water temperature of 25 °C. For the same increase in NH_3 feed water concentration, the NH_3 concentration in NH_3-H_2O mixtures obtained in the gaseous VMS permeate increased from 1 to 11 wt% for a feed water temperature of 35 °C, from 1 to 5 wt% for 45 °C and from 1 to 4 wt% for 55 °C. Hence, increasing the NH_3 feed water concentration resulted in a more NH_3 concentrated gaseous NH_3-H_2O mixture obtained in VMS permeate, for all tested feed water temperatures, which can also be derived from the experimental results obtained by Ding et al. (2006) and El-Bourawi et al. (2007) and the modelling study conducted by Scheepers et al. (2020). The increasing NH_3 concentrations in NH_3-H_2O mixtures obtained in the gaseous VMS permeate as a function of the increasing NH_3 feed water concentration can be attributed to the increased NH_3 fluxes, while the H_2O flux did not increase.

By increasing the feed water temperature from 25 to 45 and 55 °C, the H_2O flux increased more than the NH_3 flux, leading to more diluted NH_3 in NH_3-H_2O mixtures obtained in the gaseous VMS permeate, in line with

Scheepers et al. (2020). According to Figure 6-4, the H_2O vapour pressure of the feed water increases faster than the NH_3 vapour pressure of the feed water as a function of the feed water temperature, which explains the observed higher increase in H_2O flux compared to NH_3 flux as a function of the feed water temperature. Interestingly, by increasing the feed water temperature from 25 to 35 °C, more concentrated NH_3 in NH_3-H_2O mixtures obtained in the gaseous VMS permeate was obtained, while further increasing the feed water temperature diluted the NH_3-H_2O mixtures obtained in the gaseous VMS permeate. The feed water temperature increase from 25 to 35 °C resulted in a higher increase in NH_3 flux than the increase in H_2O flux. The initial increase in gaseous NH_3 concentration for the feed water temperature increase from 25 to 35 °C can be explained by the combined effect of the various polarisation phenomena: temperature polarisation, accumulated ion concentration polarisation and NH_3 depletion concentration polarisation.

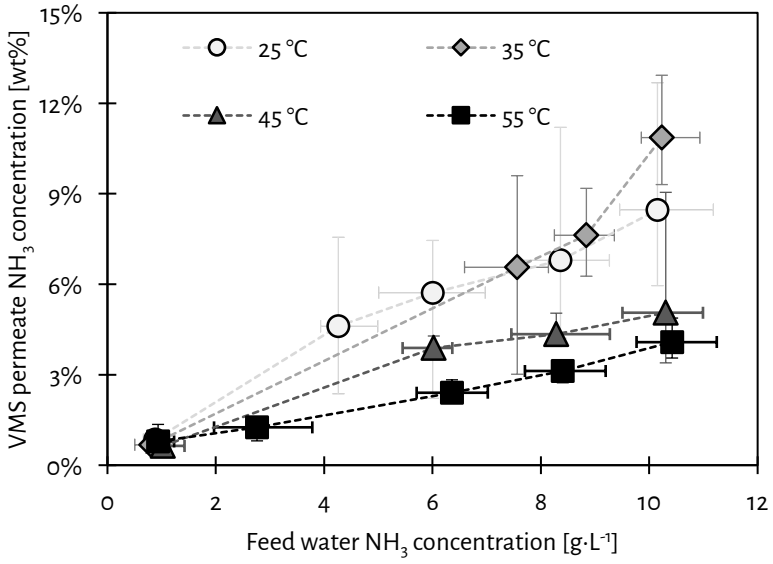

Figure 6-6 - The concentration of NH_3 in NH_3-H_2O mixtures obtained in the gaseous VMS permeate as a function of the increasing NH_3 feed water concentration for various feed water temperatures. The vertical error bars represent the minimum and maximum deviations of the measured NH_3 concentrations of at least triplicate measurements, whereas the horizontal error bars represent the minimum and maximum deviations in the measured feed water NH_3 concentration.

6.3.2. Use of NH_3-H_2O mixtures as fuel for an SOFC

6.3.2.1. Open circuit potential for various NH_3-H_2O mixtures used as a fuel

For the SOFC-O experiments, NH_3-H_2O mixtures with various NH_3 concentrations were prepared. During all experiments, the anode and cathode temperatures were stable at 755 and 761 °C, respectively.

Figure 6-7A shows the calculated Nernst potential as a function of the NH_3 concentration in the fuel, based on the respective Nernst potential calculation for H_2 oxidation (Eq. 6-12), the relevant reactions of NH_3 cracking, and subsequent H_2 oxidation in the presence of H_2O in the fuel (Eq. 6-1, 6-2 and 6-3). When more NH_3 is present in the fuel, the molar fraction of H_2 at the anode increases, while the molar fraction of H_2O decreases, leading to a higher Nernst potential at a certain temperature.

Figure 6-7B shows that by increasing the NH_3 concentration in the fuel from 5 to 25 wt%, the open circuit electric potential increased from 0.82 to 0.93 V. The differences between the measured open circuit electric potential and the calculated Nernst potentials (Figure 6-7B) were always below 2% for fuels with 7.5, 10, 12.5 and 25 wt% NH_3, suggesting that even in the presence of excess H_2O, almost complete cracking of NH_3 took place. However, the open circuit electric potential of fuel with 5 wt% NH_3 was unstable throughout the measurements, suggesting that the cracking of NH_3 was affected by the high content of H_2O in this fuel.

According to mass balance calculations based on the amount of supplied NH_3 in the fuel and absorbed in the off-gas scrubber, 95% of the supplied NH_3 in the various fuels was cracked during open-circuit conditions, which is lower than the at least 99.9 % reported by Dekker and Rietveld (2006) and Ma et al. (2006) in absence of H_2O in the fuel. According to Ni et al. (2009), the NH_3 cracking efficiency decreases when the partial pressure of NH_3 decreases, explaining the obtained results in this chapter.

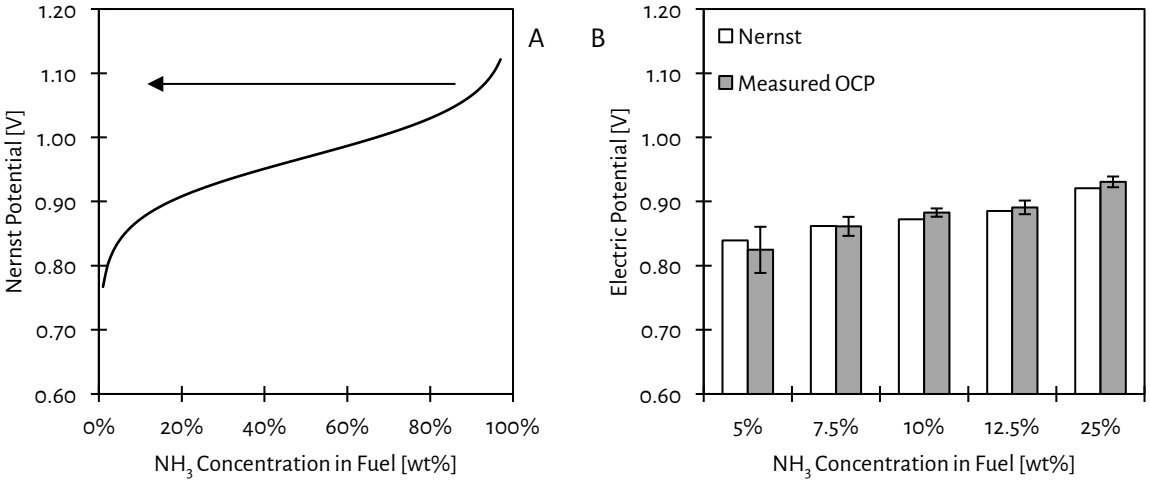

Figure 6-7 - The Nernst potential as a function of NH_3 concentration in the fuel (A). The arrow indicates the direction of interpreting the Nernst potential when the fuel becomes diluted with increasing amounts of water. The measured open circuit electric potentials and calculated Nernst potentials for the various NH_3 concentrations in the fuel (B). The vertical error bars represent the minimum and maximum deviations of at least triplicate measurements.

6.3.2.2. Generation of energy using various NH_3-H_2O mixtures as a fuel for an SOFC

Figure 6-8 presents the measured closed circuit electric potentials and power densities as a function of the current densities for the various fuels in a representative duplicate experiment. In addition, Table 6-1 presents the average and the minimum and maximum deviations of the peak power density, fuel utilisation, O_2 utilisation and electrical efficiency for the NH_3-H_2O fuels with various NH_3 concentrations in the fuel. The peak power densities, ranging between 114 and 347 $mW \cdot cm^{-1}$ were in line with studies in which pure NH_3 was used as a fuel (Ni et al., 2009; Lan & Tao, 2014b; Afif et al., 2016). According to the results, the peak power density increased as a function of the increasing NH_3 concentrations in the fuel. However, the fuel utilisation decreased when the NH_3 concentration in the fuel increased. Interestingly, the fuel utilisation was 68% when the fuel only contained 5 wt% NH_3, indicating that besides the cracking of NH_3 also subsequent oxidation of H_2 still effectively took place in the presence of high concentrations of H_2O. Hence, although the peak power density of the SOFC-O increased with increasing NH_3 concentrations in the fuel, not all additionally supplied NH_3 resulted in the generation of electricity. To maximise fuel utilisation, all produced H_2 after NH_3 cracking must come in contact with transferred O^{2-} at the triple-phase boundary, which is the interface of the electrolyte, the anode and the electric current collector. However, the O_2 utilisation was at most 31%, suggesting that there was no lack of O_2 supply to the cathode. Therefore, the decrease in fuel utilisation at higher NH_3 concentrations in the fuel was probably caused by less efficient NH_3 cracking, which agrees with the results of Stoeckl et al. (2020), who found a similar decrease when more NH_3 was fed to the anode. The electrical efficiency using NH_3-H_2O mixtures with concentrations between 5 and 25 wt% NH_3 as fuel for the SOFC-O ranged between 22 and 36%. According to these results, a SOFC-O can be used to generate energy, applying NH_3-H_2O mixtures with NH_3 concentrations as low as 5 wt%.

Table 6-1 - The obtained peak power density, fuel and oxygen utilisation, and the electrical efficiency of the SOFC-O for various concentrations of NH_3 in the fuel. The presented values represent the averages and the minimum and maximum deviations of duplicate measurements.

NH_3 in the fuel	Peak Power Density	Fuel Utilisation	Oxygen Utilisation	Electric Efficiency
-	$mW \cdot cm^{-2}$	-	-	-
25%	347 ± 11	42 ± 1%	31 ± 1%	22 ± 1%
12.5%	212 ± 14	51 ± 3%	19 ± 1%	26 ± 2%
10%	157 ± 1	52 ± 7%	16 ± 2%	25%
7.5%	138 ± 6	54 ± 1%	12%	29 ± 2%
5%	114	68%	10%	36%

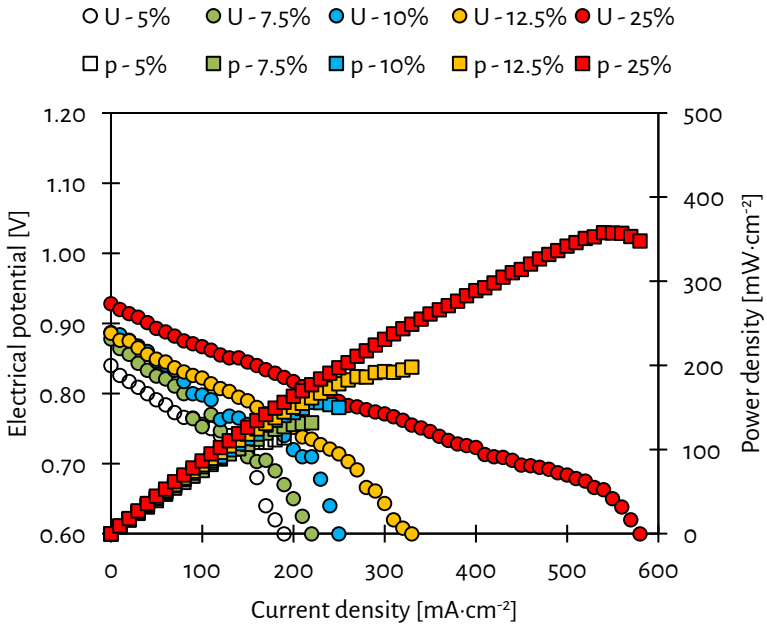

Figure 6-8 - The measured electric potentials (in circles) and the power densities (in squares) as a function of the generated current density for the tested NH_3-H_2O mixtures with various NH_3 concentrations.

6.3.3. Energetic evaluation of VMS and SOFC for the recovery and the use of NH_3

No previous studies quantified the electrical energy consumption to drive the pumps during the stripping of NH_3 in a VMS configuration, although Scheepers et al. (2020) assessed the thermal energy consumption to strip NH_3 by VMS. Notably, N-loaded residual waters with high TAN concentrations, such as sludge reject water, often already have temperatures in the range of 30 - 40 °C, because they originate from anaerobic digesters. Therefore, heat addition for VMS may not be needed. Figure 6-9 shows the electrical energy consumption for stripping NH_3 from water (aqueous solution) by VMS as a function of the feed water temperature and the NH_3 feed water concentration. The electrical energy consumption ranged between 84 and 113 MJ·kg-N^{-1} at an NH_3 feed water concentration of 1 g·L^{-1} and decreased to between 7 and 17 MJ·kg-N^{-1} when the NH_3 feed water concentration increased to 10 g·L^{-1}. The electrical energy consumption was mainly used for the transfer of H_2O water by the vacuum pump. The electrical energy consumption to strip NH_3 decreased with increasing NH_3 feed water concentration. The recirculation of the feed water accounted at most for 2% of the electrical energy consumption and can therefore be neglected.

The SOFC-O reached electrical efficiencies ranging between 22% and 36% using NH_3-H_2O mixtures with NH_3 concentrations ranging between 5 and 25 wt%. Based on the determined electrical efficiencies and additional calculations using Eq. 6-17, the electrical energy generation of the SOFC-O ranged between 6 and 9 MJ·kg-N^{-1}.

Hence, the NH_3 concentrations obtained in the gaseous permeate of VMS reaching up to 11 wt% agreed with the NH_3 concentrations in NH_3-H_2O mixtures that were used for the generation of electricity in an SOFC-O, which were as low as 5 wt%. Moreover, also the electrical energy consumption of VMS of 7 MJ·kg-N^{-1} and the electrical energy electricity of the SOFC-O of 9 MJ·kg-N^{-1} aligned, suggesting that the consumed energy of recovering NH_3 from water (aqueous solution) can be provided by converting the NH_3 to energy in an SOFC-O.

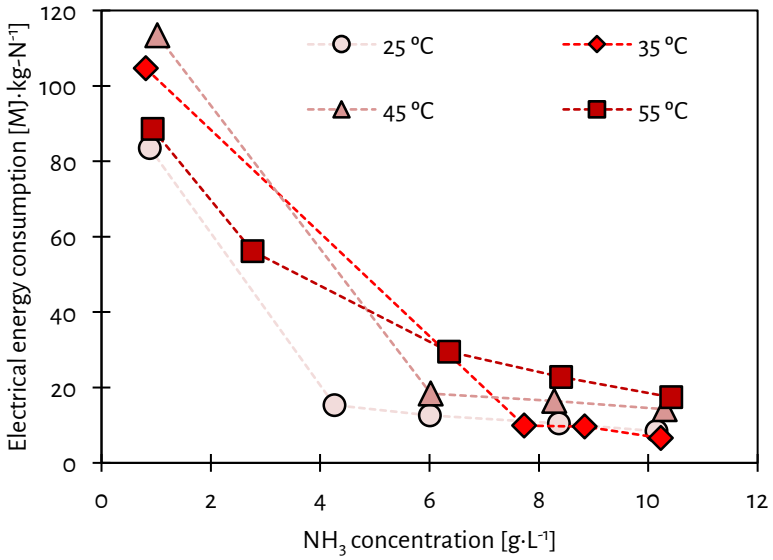

Figure 6-9 - The calculated average electrical energy consumption to strip NH_3 from water (aqueous solution) by VMS as a function of the NH_3 concentration for the various feed temperatures.

6.4. Conclusions

The experimental study to assess the feasibility of combining VMS and SOFC to recover NH_3 from water (aqueous solution) and subsequently generate energy from the recovered NH_3 resulted in the following conclusions:

- VMS allowed for the recovery of NH_3 as gaseous NH_3-H_2O mixtures with NH_3 concentrations ranging between 1 and 11 wt% at NH_3 feed water concentrations ranging between 1 and 10 $g \cdot L^{-1}$;
- The NH_3 concentration in NH_3-H_2O mixtures obtained in the gaseous VMS permeate increased when the feed water temperature increased from 25 to 35 °C. However, the NH_3 concentration in NH_3-H_2O mixtures obtained in the gaseous VMS permeate decreased when the feed water temperature increased to 45 and 55 °C;
- The NH_3 concentration in NH_3-H_2O mixtures obtained in the gaseous VMS permeate increased as a function of the increasing NH_3 feed water concentration;
- The electrical energy consumption for NH_3 stripping by VMS decreased from 113 to 7 $MJ \cdot kg\text{-}N^{-1}$ when the NH_3 feed water concentrations increased from 1 to 10 $g \cdot L^{-1}$, respectively;
- The SOFC-O generated energy from NH_3-H_2O mixtures with NH_3 concentrations ranging between 5 and 25 wt%, indicating that NH_3 cracking and subsequent H_2 oxidation still took place in the presence of excess H_2O at the anode;
- The efficiency of cracking NH_3 at the anode was lower than reported in studies that used dry NH_3 as a fuel, suggesting that NH_3 cracking is affected by excess H_2O at the anode;
- The electrical efficiency of the SOFC-O ranged between 22 and 36% and decreased as a function of the increasing NH_3 concentration in the fuel;
- The electrical energy consumption of VMS of 7 $MJ \cdot kg\text{-}N^{-1}$ for stripping NH_3 from water (aqueous solution) was lower than the electrical energy generation of the SOFC-O of 9 $MJ \cdot kg\text{-}N^{-1}$.

6.5. References

Afif, A., Radenahmad, N., Cheok, Q., Shams, S., Kim, J. H., & Azad, A. K. (2016). Ammonia-fed fuel cells: a comprehensive review. *Renewable and Sustainable Energy Reviews, 60*, 822-835. doi:http://dx.doi.org/10.1016/j.rser.2016.01.120

Cheddie, D. (2012). Ammonia as a Hydrogen Source for Fuel Cells: A Review. In D. Minic (Ed.), *Hydrogen Energy - Challenges and Perspectives* (pp. Ch. 13). Rijeka: InTech.

Dekker, N. J. J., & Rietveld, G. (2006). Highly efficient conversion of ammonia in electricity by solid oxide fuel cells. *Journal of Fuel Cell Science and Technology, 3*(4), 499-502. doi:10.1115/1.2349536

Ding, Z., Liu, L., Li, Z., Ma, R., & Yang, Z. (2006). Experimental study of ammonia removal from water by membrane distillation (MD): The comparison of three configurations. *Journal of Membrane Science, 286*(1-2), 93-103. doi:10.1016/j.memsci.2006.09.015

El-Bourawi, M. S., Ding, Z., Ma, R., & Khayet, M. (2006). A framework for better understanding membrane distillation separation process. *Journal of Membrane Science, 285*(1), 4-29. doi:https://doi.org/10.1016/j.memsci.2006.08.002

El-Bourawi, M. S., Khayet, M., Ma, R., Ding, Z., Li, Z., & Zhang, X. (2007). Application of vacuum membrane distillation for ammonia removal. *Journal of Membrane Science, 301*(1-2), 200-209. doi:10.1016/j.memsci.2007.06.021

He, Q., Tu, T., Yan, S., Yang, X., Duke, M., Zhang, Y., & Zhao, S. (2018). Relating water vapor transfer to ammonia recovery from biogas slurry by vacuum membrane distillation. *Separation and Purification Technology, 191*(Supplement C), 182-191. doi:https://doi.org/10.1016/j.seppur.2017.09.030

He, Q., Yu, G., Tu, T., Yan, S., Zhang, Y., & Zhao, S. (2017). Closing CO2 Loop in Biogas Production: Recycling Ammonia As Fertilizer. *Environmental Science & Technology, 51*(15), 8841-8850. doi:10.1021/acs.est.7b00751

Huttunen, M., Nygren, L., Kinnarinen, T., Häkkinen, A., Lindh, T., Ahola, J., & Karvonen, V. (2017). Specific energy consumption of cake dewatering with vacuum filters. *Minerals Engineering, 100*, 144-154. doi:https://doi.org/10.1016/j.mineng.2016.10.025

Lan, R., & Tao, S. (2010). Direct Ammonia Alkaline Anion-Exchange Membrane Fuel Cells. *Electrochemical and Solid-State Letters, 13*(8), B83-B86. doi:https://doi.org/10.1149/1.3428469

Lan, R., & Tao, S. (2014b). Ammonia as a Suitable Fuel for Fuel Cells. *Frontiers in Energy Research, 2*(35). doi:10.3389/fenrg.2014.00035

Lawson, K. W., & Lloyd, D. R. (1997). Membrane distillation. *Journal of Membrane Science, 124*(1), 1-25. doi:https://doi.org/10.1016/S0376-7388(96)00236-0

Ma, Q., Peng, R., Tian, L., & Meng, G. (2006). Direct utilization of ammonia in intermediate-temperature solid oxide fuel cells. *Electrochemistry Communications, 8*(11), 1791-1795. doi:http://dx.doi.org/10.1016/j.elecom.2006.08.012

Martínez-Díez, L., & Vázquez-González, M. I. (1999). Temperature and concentration polarization in membrane distillation of aqueous salt solutions. *Journal of Membrane Science, 156*(2), 265-273. doi:https://doi.org/10.1016/S0376-7388(98)00349-4

Mojab, S. M., Pollard, A., Pharoah, J. G., Beale, S. B., & Hanff, E. S. (2014). Unsteady Laminar to Turbulent Flow in a Spacer-Filled Channel. *Flow, Turbulence and Combustion, 92*(1), 563-577. doi:10.1007/s10494-013-9514-4

Ni, M., Leung, M. K. H., & Leung, D. Y. C. (2009). Ammonia-fed solid oxide fuel cells for power generation—A review. *International Journal of Energy Research, 33*(11), 943-959. doi:10.1002/er.1588

Okanishi, T., Okura, K., Srifa, A., Muroyama, H., Matsui, T., Kishimoto, M., Saito, M., Iwai, H., Yoshida, H., Saito, M., Koide, T., Iwai, H., Suzuki, S., Takahashi, Y., Horiuchi, T., Yamasaki, H., Matsumoto, S., Yumoto, S., Kubo, H., Kawahara, J., Okabe, A., Kikkawa, Y., Isomura, T., & Eguchi, K. (2017). Comparative Study of Ammonia-fueled Solid Oxide Fuel Cell Systems. *Fuel Cells, 17*(3), 383-390. doi:10.1002/fuce.201600165

Scheepers, D. M., Tahir, A. J., Brunner, C., & Guillen-Burrieza, E. (2020). Vacuum membrane distillation multi-component numerical model for ammonia recovery from liquid streams. *Journal of Membrane Science, 614*, 118399. doi:https://doi.org/10.1016/j.memsci.2020.118399

Stambouli, A. B., & Traversa, E. (2002). Solid oxide fuel cells (SOFCs): a review of an environmentally clean and efficient source of energy. *Renewable and Sustainable Energy Reviews, 6*(5), 433-455. doi:https://doi.org/10.1016/S1364-0321(02)00014-X

Staniforth, J., & Ormerod, R. M. (2003). Clean destruction of waste ammonia with consummate production of electrical power within a solid oxide fuel cell system. *Green Chemistry, 5*(5), 606-609. doi:10.1039/B307396N

Stoeckl, B., Preininger, M., Subotić, V., Gaber, C., Seidl, M., Sommersacher, P., Schroettner, H., & Hochenauer, C. (2019a). High Utilization of Humidified Ammonia and Methane in Solid Oxide Fuel Cells: An Experimental Study of Performance and Stability. *Journal of The Electrochemical Society, 166*(12), F774-F783. doi:10.1149/2.0781912jes

Stoeckl, B., Preininger, M., Subotić, V., Megel, S., Folgner, C., & Hochenauer, C. (2020). Towards a wastewater energy recovery system: The utilization of humidified ammonia by a solid oxide fuel cell stack. *Journal of Power Sources, 450*, 227608. doi:https://doi.org/10.1016/j.jpowsour.2019.227608

Suzuki, S., Muroyama, H., Matsui, T., & Eguchi, K. (2012). Fundamental studies on direct ammonia fuel cell employing anion exchange membrane. *Journal of Power Sources, 208*(Supplement C), 257-262. doi:https://doi.org/10.1016/j.jpowsour.2012.02.043

Valera-Medina, A., Xiao, H., Owen-Jones, M., David, W. I. F., & Bowen, P. J. (2018). Ammonia for power. *Progress in Energy and Combustion Science, 69*, 63-102. doi:https://doi.org/10.1016/j.pecs.2018.07.001

van Linden, N., Bandinu, G. L., Vermaas, D. A., Spanjers, H., & van Lier, J. B. (2020). Bipolar membrane electrodialysis for energetically competitive ammonium removal and dissolved ammonia production. *Journal of Cleaner Production*, 120788. doi:https://doi.org/10.1016/j.jclepro.2020.120788

van Linden, N., Spanjers, H., & van Lier, J. B. (2019a). Application of dynamic current density for increased concentration factors and reduced energy consumption for concentrating ammonium by electrodialysis. *Water Research*, 114856. doi:https://doi.org/10.1016/j.watres.2019.114856

van Linden, N., Spanjers, H., & van Lier, J. B. (2022a). Fuelling a solid oxide fuel cell with ammonia recovered from water by vacuum membrane stripping. *Chemical Engineering Journal, 428*, 131081. doi:https://doi.org/10.1016/j.cej.2021.131081

Wojcik, A., Middleton, H., Damopoulos, I., & Van herle, J. (2003). Ammonia as a fuel in solid oxide fuel cells. *Journal of Power Sources, 118*(1–2), 342-348. doi:http://dx.doi.org/10.1016/S0378-7753(03)00083-1

Chapter 7.

Removal and recovery of ammoniacal nitrogen from real residual streams

Abstract

This chapter assesses the feasibility of total ammoniacal nitrogen (TAN) removal and recovery from various real nitrogen-loaded (N-loaded) residual waters. The N-loaded residual waters were algae digestion reject water (ADRW), sludge digestion reject water (SDRW) and fertiliser industry condensate (FIC).

At least 85% TAN removal proved to be feasible by electrodialysis (ED) for all three N-loaded residual waters, with an electrical energy consumption ranging between 5 and 15 MJ·kg-N^{-1}. The electrical energy consumption was consistently higher for the real residual waters compared to the synthetic ADRW and SDRW, due to lower current efficiencies to transport TAN as ammonium (NH_4^+), as a result of the transport of other cations than NH_4^+. The use of ED allowed for the simultaneous removal of TAN (as NH_4^+) and volatile fatty acids from ADRW. Furthermore, during the production of a concentrated NH_4^+ solution by ED from SDRW, accumulation of multivalent ions took place in the concentrate, resulting in scaling and subsequent clogging of the spacers. For FIC, no interfering processes were encountered for the removal of TAN by ED.

For the treatment of FIC, a sequencing batch experiment (SBE) was performed, in which multiple batches of FIC were treated by ED. The TAN that was removed by ED was converted to dissolved NH_3 by bipolar membrane electrodialysis (BPMED) and vacuum membrane stripping (VMS) allowed for the recovery of an ammonia-water (NH_3-H_2O) mixture from the produced dissolved NH_3 solution. The combination of ED, BPMED and VMS allowed for 93% TAN removal from real FIC, at the expense of 37 – 39 MJ·kg-N^{-1} of electrical energy. Finally, the recovered NH_3-H_2O with an ammonia (NH_3) concentration of 4 wt% was used as the fuel for a solid oxide fuel cell (SOFC). The SOFC generated 11 MJ·kg-N^{-1} of electrical energy. Hence, the combination of ED, BPMED, VMS and SOFC allowed for the removal of TAN (as NH_4^+) from real FIC and the subsequent generation of electricity from the recovered NH_3, but still had a net electrical energy consumption of 26 – 28 MJ·kg-N^{-1}.

Keywords

nitrogen-loaded residual water; total ammoniacal nitrogen; energy generation; electrodialysis; bipolar membrane electrodialysis; vacuum membrane stripping; solid oxide fuel cell;

7.1. Introduction

In the previous chapters, only synthetic feed waters were used to demonstrate the removal of total ammoniacal nitrogen (TAN) and subsequent recovery of ammonia (NH_3), using electrodialysis (ED), bipolar membrane electrodialysis (BPMED) and vacuum membrane stripping (VMS). Furthermore, only synthetic fuels were used to generate energy from NH_3 using a solid oxide fuel cell (SOFC). This chapter assesses the feasibility of TAN removal from three different nitrogen-loaded (N-loaded) residual waters by ED. In addition, this chapter assesses the feasibility to remove TAN and subsequently recover NH_3 from one of the N-loaded residual waters by ED, BPMED and VMS for the generation of electricity in an SOFC. The three N-loaded residual waters were: algae digestion reject water (ADRW), sludge digestion reject water (SDRW) and fertiliser industry condensate (FIC).

7.1.1. Nitrogen-loaded residual waters

The research of Magdalena Cadelo (2020) focused on the production of VFAs during anaerobic digestion (AD) of algae biomass by steering the AD process towards the maximisation of VFA production. However, algae typically have a high nitrogen content. According to the review of Deng et al. (2021), during AD, practically all organic nitrogen will eventually become present in the form of TAN following hydrolysis of the biopolymers. Hence, AD of algae results in the presence of high TAN concentrations, in addition to the high VFA concentrations, in the obtained liquid fraction after solid-liquid separation of the digestate: the ADRW. According to the review of Atasoy et al. (2018), ED can be used for the removal and recovery of VFA from the digestate of algae digestion. However, limited experimental information is available on the simultaneous recovery of VFAs and TAN after algae digestion, especially on the achievable TAN removal efficiency and the energy consumption. Therefore, ADRW was selected as the first N-loaded residual stream to assess the feasible TAN removal and the associating electrical energy consumption.

More common than the digestion of algae is the AD of waste activated sludge from sewage treatment plants, as described in Chapter 2. Ward et al. (2018) and Kedwell et al. (2021) assessed the feasibility to remove TAN from the liquid fraction obtained after solid-liquid separation of the digestate from sludge digestion: SDRW. However, the respective studies showed TAN removal efficiencies that were yet not competitive to current state-of-the-art TAN removal processes. Whereas Ward et al. (2018) and Kedwell et al. (2021) reached TAN removal efficiencies ranging between 23% and 70%, competitive state-of-the-art TAN removal processes, such as the biochemical partial nitritation + anammox process reach TAN removal efficiencies up to 90% (Lackner et al., 2014). Hence, it remains unclear whether ED can be used to achieve competitive TAN removal after sludge digestion. Moreover, previous research showed that SDRW also contains various other cations, which may affect the TAN removal and the associating energy consumption from SDRW. To this end, SDRW was selected as the second N-loaded residual stream to assess the feasible TAN removal and the associating electrical energy consumption.

The third selected N-loaded residual water is condensate generated in the fertiliser industry (see also Chapter 2), more specifically, during the production of urea. In such condensates, TAN is present along with

bicarbonate (HCO_3^-) as the main anion, while also several alcohols and other organics are present in the FIC. However, in literature, no studies report on the removal of TAN from FIC by ED. Therefore, the feasibility of using ED for TAN removal remains unclear, as well as the possible interference of organics present in FIC during ED.

7.1.2. Objectives

The first objective of this chapter was to determine the feasibility of TAN removal by ED from three N-loaded real residual streams. To assess the feasibility of treating N-loaded residual waters, ED is characterised in terms of the TAN removal efficiency and the associating electrical energy consumption. The second objective of this chapter was to assess the feasibility of TAN removal and subsequent NH_3 recovery by BPMED and VMS for one of the real N-loaded residual streams. Finally, the recovered NH_3 from one of the real N-loaded residual streams was used as a fuel of an SOFC, to determine the feasibility of electrical energy generation from the recovered NH_3. To this end, experiments with a combination of ED, BPMED, VMS and SOFC focused on the achievable TAN concentrations and the energy balance.

7.2. Materials and methods

7.2.1. Algae digestion reject water

For the ADRW experiments, the same experimental setup as described in Chapter 3.2 was used, including the corresponding analytical methods and associated materials. Additionally, the concentrations of eight (8) major VFAs were measured by high-performance liquid chromatography (HPLC). The real ADRW (see Figure 7-1) was produced within the research of Magdalena Cadelo (2020) and was provided for the assessment of TAN removal by ED. Before using the real ADRW for the ED experiments, the ADRW was filtered through a 20-micron filter to minimise the presence of particulate and suspended solids that could clog the spacers in the membrane stack.

The treatment of real ADRW was compared to the treatment of synthetic ADRW, which consisted of an ammonium bicarbonate (NH_4HCO_3) solution with an EC equal to that of the real ADRW sample: 26 $mS \cdot cm^{-1}$. During treatment of both synthetic and real ADRW, the EC was decreased to 3 $mS \cdot cm^{-1}$, corresponding to a decrease of 90%. A dynamic current density (DCD) with a safety factor of 0.62 was used, based on the results presented in Chapter 3.3. The treatment of ADRW comprised the treatment of only one single batch, due to the limited availability of ADRW. The initial concentrate consisted of a sodium chloride (NaCl) solution with an EC equal to the synthetic and real ADRW.

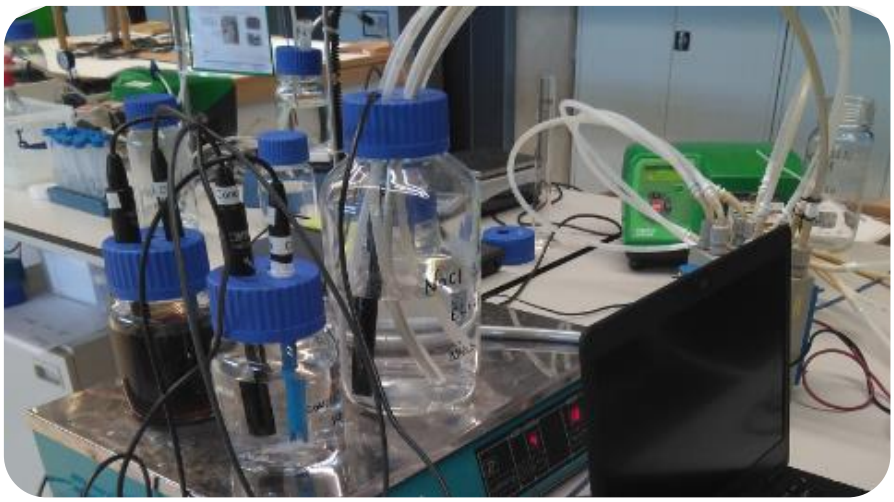

Figure 7-1 - The experimental setup for the removal of TAN from ADRW, with on the left the dark-brown ADRW.

7.2.2. Sludge digestion reject water

The real SDRW (see Figure 7-2) originated from the sludge processing line in a biological phosphorous removal removing sewage treatment plant. The real SDRW sample was obtained after the centrifuges that are used for solid-liquid separation of the digestate produced by AD of waste (activated) sludge. In addition to TAN, the real SDRW also contained metal cations sodium (Na^+), potassium (K^+), magnesium (Mg^{2+}) and calcium (Ca^{2+}), in concentrations of 312, 234, 219 and 130 $mg \cdot L^{-1}$, respectively. The analyses of the metal cations present in the real SDRW were conducted by ion chromatography (IC) and inductively coupled plasma mass spectrometry (ICP-MS). The relatively high concentrations of Mg^{2+} may be explained by the

over-dosing of magnesium chloride ($MgCl_2$) to the digestate, to allow for controlled struvite precipitation. To avoid clogging of the spacers in the membrane stack, the SDRW was filtered using 20-micron filters. In line with the ADRW experiments, unless stated differently, the used experimental and analytical materials, conditions and methods for the SDRW experiments can be found in Chapter 3.2. Based on the outcomes of Chapter 3, DCD was used during the SDRW experiments, using a safety factor of 0.62.

In addition to the treatment of the real SDRW, a synthetic SDRW consisting of NH_4HCO_3 at a similar EC as the real SDRW was treated. The synthetic and real SDRW had a pH of 7.6 and an EC of approximately 7 $mS \cdot cm^{-1}$, whereas the initial TAN concentrations were 1,410 and 777 $mg \cdot L^{-1}$, respectively. The initial concentrate consisted of the same synthetic and real SDRW as the initial diluate. The treatment of the synthetic and real SDRW was stopped when the diluate EC decreased to 1 $mS \cdot cm^{-1}$, aiming for a TAN removal efficiency of approximately 90%.

After the initial experiment with synthetic and real SDRW, multiple batches of real SDRW were processed, in a so-called sequencing batch experiment (SBE). During the SBE, the treated real SDRW (diluate) was replaced with a new batch of 1 L real SDRW, while the produced concentrate solution was used as the concentrate for the subsequent batch treatment. For the SBE, the initial concentrate solution consisted of an NH_4HCO_3 solution with an initial EC of 7 $mS \cdot cm^{-1}$ and an initial volume of 0.5 L. Throughout the SBE, the cation concentrations in the diluate and concentrate were measured to determine the ion removal efficiency, the cation current efficiency and the electrical energy consumption for TAN removal. To calculate the current efficiency for each cation, Eq. 7-1 was used. The calculation of the electrical energy consumption for TAN removal can be found in Chapter 3.2.2 of this thesis.

$$\eta_i = \frac{z \cdot F \cdot n_{i,d}}{N \cdot \sum_{t=0}^{t} I_t \cdot \Delta t} \cdot 100\% \qquad \text{Eq. 7-1}$$

where η_i = current efficiency of cation 'i' (unitless), z_i = valence of cation 'i' (unitless, z = 1 for NH_4^+, Na^+ and K^+ and z = 2 for Mg^{2+} and Ca^{2+}), F = Faraday constant (in $C \cdot mol^{-1}$, F = 96,485 $C \cdot mol^{-1}$), $n_{i,d}$ = amount of transported cation 'i' from diluate (mol), N = number of cell pairs (unitless), I_t = electrical current (in A) and Δt = time interval (in s).

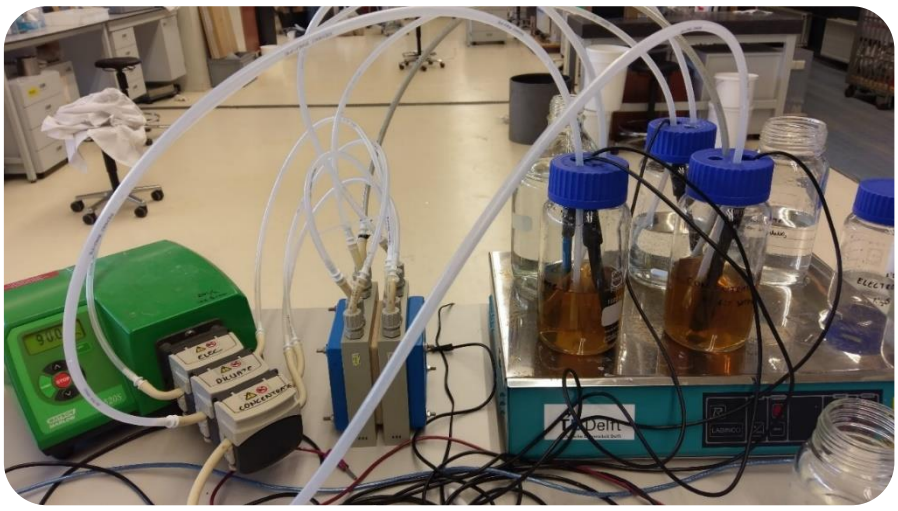

Figure 7-2 - The used experimental setup for the experiments on TAN removal by ED from real SDRW.

7.2.3. Fertiliser industry condensate

7.2.3.1. Removal of TAN by ED

The FIC originated from an industrial process involving the condensation of water during the production of urea. Because carbon dioxide and ammonia are also present in the vapours to be condensed, an aqueous solution containing mainly NH_4HCO_3 is formed. The FIC also contained organic solutes, such as methanol, ethanol and methyl diethanolamine (MDEA). Additional gas chromatography (GC) measurements were conducted to determine the concentrations of methanol, ethanol, whereas MDEA concentrations were determined by IC. The concentration of TAN in the real FIC was 781 $mg \cdot L^{-1}$. In line with the experiments with ADRW and SDRW, a synthetic feed solution comprising a similar concentration of TAN in the form of NH_4HCO_3 was prepared as a reference. During the initial experiments with synthetic and real FIC, the EC was decreased from approximately 5 to 0.5 $mS \cdot cm^{-1}$, corresponding to a 90% decrease. The initial concentrate consisted of a 0.5 L synthetic NH_4HCO_3 solution with an EC of 5 $mS \cdot cm^{-1}$. In contrast to the previous experiments, the safety factor for DCD was set to 0.8, to limit the back-diffusion of NH_4^+ to the diluate. A higher back diffusion was expected during the FIC experiments due to high NH_4^+ concentrations in the concentrate and low NH_4^+ concentrations in the final diluate, agreeing with 0.5 $mS \cdot cm^{-1}$.

7.2.3.2. TAN removal and NH_3 recovery for energy generation

After the initial experiment focusing on TAN removal from real FIC, the actual recovery of NH_3 for the generation of electricity was tested. To this end, ED was combined with BPMED and VMS during three different phases. During Phase 1, three consecutive batches (B1 – B3) of 1.6 L real FIC were treated by ED to produce a concentrated NH_4^+ solution. The initial concentrate consisted again of 0.5 L synthetic NH_4HCO_3 solution.

Subsequently, in Phase 2, the produced concentrate was kept used as the concentrate solution for subsequent batches in ED, but it was also used as the feed solution for BPMED. In the combination of ED and BPMED, ions were simultaneously transported from the FIC to the concentrate in ED and from the feed to

the acid and base in BPMED. To balance the amount of TAN transported from the FIC to the concentrate by ED and from the concentrate to the base, a BPMED membrane stack with four cell triplets was used at a fixed current density of 100 $A \cdot m^{-2}$. The details of the used materials for BPMED can be found in Chapter 4.2.1. Four additional batches of 1.6 L FIC were processed during the combination of ED and BPMED (B4 – B7), to produce a concentrated NH_3 solution.

In Phase 3, the combination of ED and BPMED was extended by including VMS, to recover gaseous NH_3 from the produced concentrated NH_3 solution. To this end, based on the findings of Chapter 1, a porous gas-permeable polytetrafluoroethylene (PTFE) membrane was used. Unless stated otherwise, the same materials and methods for VMS were used as described in Chapters 5.2.1 and 6.2.1. In contrast to Chapter 1 and Chapter 6, the recovered NH_3 gas was not scrubbed in an acid solution, but condensed, resulting in the recovery of a liquid NH_3-H_2O mixture. During Phase 3, four additional batches (B8 – B11) of 1.6 L FIC were treated in the combination of ED, BPMED and VMS. Figure 7-3 shows a schematic representation of the experimental setup combining ED, BPMED and VMS and Figure 7-4 shows the actual experimental setup. As a final step, the recovered NH_3-H_2O mixture was used as a fuel for an SOFC. The same materials and methods for the SOFC were used as described in Chapter 6.

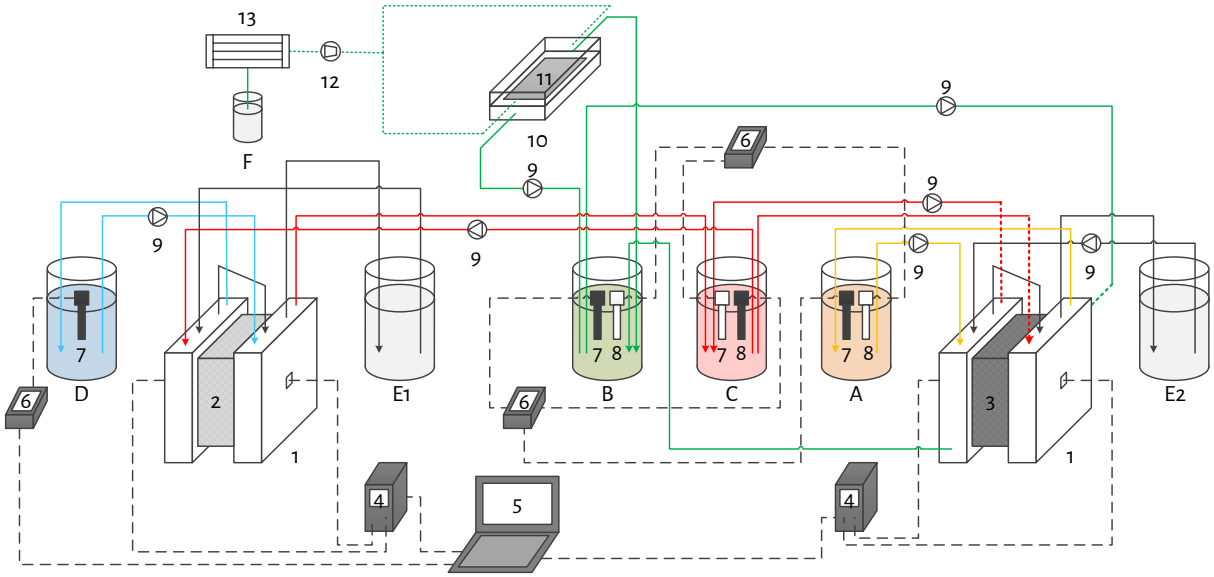

Figure 7-3 - A schematic representation of the used experimental setup of the combination of ED, BPMED and VMS: ED cell (1), ED membrane stack (2), BPMED membrane stack (3), direct current supply (4), laptop (5), multimeter (6), electrical conductivity (7), pH sensor (8), peristaltic pump (9), vacuum membrane stripping cell (10), porous gas-permeable membrane (11), vacuum pump (12) and condenser (13). With the following solutions: diluate, consisting of FIC (D), concentrate, also serving as BPMED feed (C), acid (A), base (B), electrode rinse for ED and BPMED (E1 and E2, respectively) and the condensed NH_3-H_2O mixture (F). The condensed NH_3-H_2O mixture served as the fuel for the SOFC, which is schematically presented in Chapter 6.2.1.

Figure 7-4 - The used experimental setup of the combination of ED, BPMED and VMS (left) and the SOFC (right).

7.3. Results

7.3.1. Removal of TAN from residual waters

7.3.1.1. Algae digestion reject water

Table 7-1 shows that the decrease in EC by 90% resulted in similar TAN removal efficiencies for the synthetic and real ADRW: 94% and 96%, respectively. Hence, for the removal of TAN from real ADRW, the EC was a suitable indicator of the TAN removal efficiency. In line with the findings in Chapter 3 and Chapter 4, accumulation of TAN (10 – 28% of the TAN that was transported from the diluate) in the electrode rinse solution (ERS) took place, as a result of the used combination of end membranes (cation exchange end membranes) and the composition of the ERS. The NH_4^+ current efficiency for the synthetic ADRW was 86%, which is lower than the values presented in Chapter 3, in which NH_4HCO_3 solutions with a TAN concentration of 1.5 $g \cdot L^{-1}$ were used as the feed water (96% for the first treated batch at DCD). The difference in NH_4^+ current efficiency can be explained by the higher NH_4^+ concentration gradient that was present during the synthetic ADRW experiment, compared to the experiments described in Chapter 3. In both experiments, the removal efficiencies and operational run times were similar, whereas the initial TAN concentration was approximately 6 $g \cdot L^{-1}$ for the synthetic ADRW compared to 1.5 $g \cdot L^{-1}$ as reported in Chapter 3. Therefore, during the synthetic ADRW experiment, a higher NH_4^+ concentration gradient was present between the diluate and concentrate. Results in Chapter 3 showed that an increase in NH_4^+ concentration gradient for similar operational run times resulted in more back-diffusion, leading to a lower NH_4^+ current efficiency. The electrical energy consumption for the synthetic ADRW (9 $MJ \cdot kg\text{-}N^{-1}$) was higher than that reported in Chapter 3 (5 $MJ \cdot kg\text{-}N^{-1}$), which was in the first place caused by the lower NH_4^+ current efficiency. Because the EC throughout the experiment was higher during the synthetic ADRW experiment than during the SBE experiments with the application of DCD presented in Chapter 3, a higher current density was applied: 148 versus 42 $A \cdot m^{-2}$. Hence, the second contributor to the higher electrical energy consumption for the synthetic ADRW compared to Chapter 3 was the higher applied current density, because as explained in Chapter 3, higher applied current densities result in higher electrical energy consumption.

According to Table 7-1, the NH_4^+ current efficiency of the real ADRW was lower than that of the synthetic ADRW: 63% and 86%, respectively. The difference in NH_4^+ current efficiency may be caused by the transport of other cations than NH_4^+. However, there is no information on the presence and fate of other cations during the real ADRW experiment, as these were not measured. Furthermore, the average electrical resistance during the experiment with real ADRW was 17 Ω, which was higher compared to the experiment with synthetic ADRW, when it was 12 Ω. This difference might be explained by increased mass transfer resistance due to the presence of organics, instead of solely bicarbonate (HCO_3^-), which was the case for synthetic ADRW. Hence, the lower NH_4^+ current efficiency and higher average electrical resistance contributed to the higher electrical energy consumption during the real ADRW treatment of 15 $MJ \cdot kg\text{-}N^{-1}$, compared to the electrical energy consumption for the synthetic ADRW treatment of 9 $MJ \cdot kg\text{-}N^{-1}$).

In addition to the removal of TAN from the ADRW, also VFAs were removed and recovered in the concentrate. Table 7-2 provides an overview of the VFA concentrations in the real initial and final ADRW, as well as the concentrations obtained in the ED concentrate. Because the pH of all solutions was consistently above 6, the VFAs were predominantly present as anions. The mass balance for VFAs fitted within a 5% error, while a negligible amount (< 1%) of VFAs accumulated in the electrode rinse solution. The latter can be explained by the used end-membranes, which do not allow for the transport of anions to the ERS. 87% of the volume of the real ADRW was recovered as treated water and the removal efficiency of VFAs ranged between 72 and 96%. Table 7-2 shows that the removal efficiency differed amongst the various VFAs, which were present in different initial concentrations. The current efficiency of the VFAs was 72% and the highest current efficiency was represented by acetic acid (29%), followed by butyric acid (19%). The loss in current efficiency may be attributed to the transport of other anions, such as bicarbonate and chloride, and back-diffusion of anions from the concentrate to the diluate.

Table 7-1 - Process performance indicators for the removal of TAN from ADRW by ED.

	unit	Synthetic	Real
Initial diluate NH_4^+ concentration	$mg \cdot L^{-1}$	6,036	5,253
TAN removal efficiency	-	94%	96%
Water recovery		90%	87%
NH_4^+ current efficiency	-	86%	63%
Average electrical resistance	Ω	12	17
Energy consumption	$MJ \cdot kg\text{-}N^{-1}$	9	15

Table 7-2 - The initial diluate and final concentrate concentrations, and the removal and current efficiency of VFAs during the treatment of real ADRW.

Name of acids and corresponding anions	Diluate Initial	Removal Efficiency	Current Efficiency	Concentrate Final
	$mg \cdot L^{-1}$	-	-	$mg \cdot L^{-1}$
Acetic acid / acetate	7,996	96%	29%	11,867
Propionic acid / propionate	3,106	93%	9%	4,187
Isobutyric acid / isobutyrate	1,417	82%	3%	1,687
Butyric acid / butyrate	7,057	87%	19%	8,777
Isovaleric acid / isovalerate	1,853	72%	3%	1,932
Valeric acid / valerate	2,343	84%	4%	2,801
Isocaproic acid / isocaproate	1,306	77%	2%	1,406
Caproic acid / caproate	1,652	83%	3%	1,911

7.3.1.2. Sludge digestion reject water

Table 7-3 shows that experiments with synthetic and real SDRW resulted in a similar TAN removal efficiency while decreasing the EC from 7 to 1 $mS \cdot cm^{-1}$ (88% decrease): 89 and 86%, respectively. Hence, in line with the treatment of ADRW, the decrease in EC agreed well with the TAN removal efficiencies. The TAN removal efficiencies were associated with water recoveries of 96 – 97%. The NH_4^+ current efficiency for the real SDRW (58%) was lower than that for the synthetic solutions (97%), for the treatment of a single batch. Also, the electrical energy consumption to remove NH_4^+ from the real SDRW (8 $MJ \cdot kg\text{-}N^{-1}$) was higher than that for the synthetic SDRW (4 $MJ \cdot kg\text{-}N^{-1}$). In addition to NH_4^+, also other cations (Na^+, K^+, Ca^{2+} and Mg^{2+}) were transported from the diluate to the concentrate, with a removal efficiency ranging between 39 and 95% (Figure 7-5A), affecting the transport of NH_4^+. Figure 7-6A presents the current efficiency per transferred ion and shows that the sum of the current efficiencies of the other cations is almost similar to the NH_4^+ current efficiency: 50 and 58%, respectively. In addition to the additional electric charge supply, also the electrical resistance of the membrane stack was higher for the real (36 Ω) than for the synthetic SDRW (31 Ω), which can be attributed to the presence of organic solutes and the transport of ions with lower diffusion coefficients. The lower NH_4^+ current efficiency and the higher electrical resistance throughout the experiments contributed to a higher electrical energy consumption for the real SDRW, compared to the synthetic SDRW. Hence, the differences in NH_4^+ current efficiency and electrical energy consumption can be attributed to the presence and transport of other solutes than NH_4^+ in the real SDRW.

Table 7-3 - Process performance indicators for the removal of TAN from SDRW by ED.

	unit	Synthetic	Real
Initial diluate NH_4^+ concentration	$mg \cdot L^{-1}$	1,410	777
TAN removal efficiency	-	89%	85%
Water recovery	-	96%	97%
NH_4^+ current efficiency	-	97%	58%
Average electrical resistance	Ω	31	36
Energy consumption	$MJ \cdot kg\text{-}N^{-1}$	4	8

For real SDRW, four additional sequencing batches were treated. During this SBE, the diluate was replaced with a new batch of real SDRW, while the concentrate was again used to allow for the production of a concentrated TAN (as NH_4^+ solution). The removal efficiency of the various cations and water recovery remained stable throughout the SBE. On the contrary, the NH_4^+ current efficiency decreased from 58 to 50%, which can be attributed to back-diffusion (see Chapter 3.4) as the NH_4^+ concentration difference between the diluate and concentrate increased due to the accumulation of NH_4^+ in the concentrate, as shown in Figure 7-5B. Furthermore, the sum of the current efficiencies of the various ions also decreased from 104 to 85% throughout the SBE, suggesting that back-diffusion also affected the current efficiency of the transport

of the other cations. The decrease in current efficiency resulted in an increase in electrical energy consumption from 8 to 9 MJ·kg-N^{-1} throughout the SBE, as presented in Figure 7-6B.

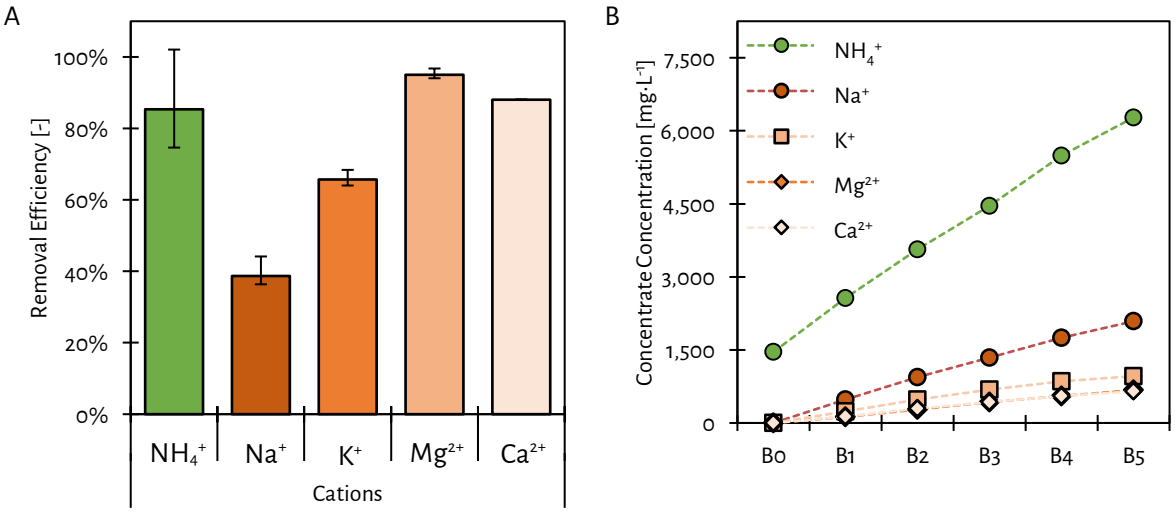

Figure 7-5 - The average ion removal efficiency (A) and the ion concentration in the concentrate during the SBE (B) during the removal of TAN from real SDRW by ED. The markers for Ca^{2+} and Mg^{2+} overlapped.

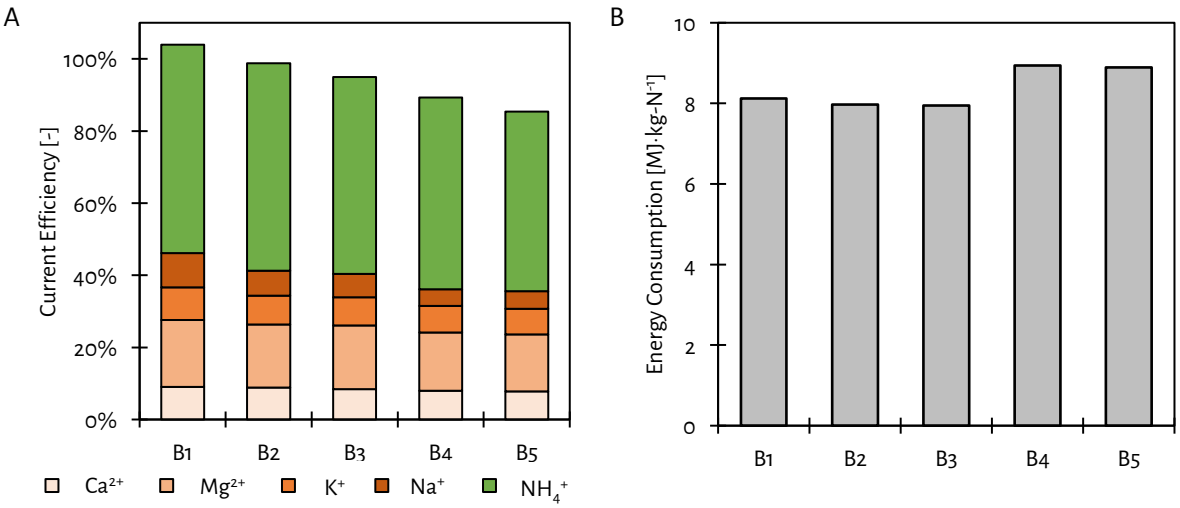

Figure 7-6 - The ion current efficiency (A) and the electrical energy consumption (B) throughout the SBE during the removal of TAN from real SDRW by ED.

At the end of the fifth batch during the SBE, the recirculation of concentrate through the ED membrane stack stagnated and eventually even stopped. Opening the membrane stack and a visual inspection resulted in the observation of white crystalline solids in the concentrate spacers (see Figure 7-7A). Especially at the locations where the concentrate entered the spacers that form the flow channels for the various solutions, these white precipitates accumulated, as shown in Figure 7-7B. The pH of the concentrate solution throughout the SBE ranged between 7.9 and 8.1. After taking a sample of the precipitate and dissolution in water, ion analysis was performed, showing that the dominant ions in the scale were Ca^{2+}, Mg^{2+} and HCO_3^-. In addition, simulations with PHREEQC chemical equilibrium software, using the water composition of the concentrate at a pH of 8, showed theoretical supersaturation (saturation index > 0) of mineral species such

as dolomite ($CaMg(CO_3)_2$). Hence, the accumulating precipitates probably consisted of carbonate species. This result aligns with the mass imbalance of Ca^{2+} and Mg^{2+}, which were off by more than 50%.

Figure 7-7 - The accumulation of, mostly Mg-based, precipitated minerals in the concentrate spacers in the ED membrane stack (A) after the treatment of multiple batches of real SDRW. The white precipitates especially accumulated at the entrance (at the right) of the spacer (B).

7.3.1.3. Fertiliser industry condensate

The third tested N-loaded residual water was FIC. Table 7-4 shows the decrease of 90% in EC for the synthetic and real FIC corresponding to a TAN removal efficiency of 93%, indicating that in line with the ADRW and SDRW experiments, the decrease in EC was a suitable indicator for TAN removal from FIC. The water recovery for both synthetic and real FIC was 98 – 99%. The NH_4^+ current efficiency was similar for the synthetic (90%) and real FIC (88%), indicating that there were limited losses in current efficiency due to the transport of other ions. Based on GC measurements of initial and final FIC solutions, no methanol and ethanol transfer from the diluate to the concentrate took place. These solutes were not transported because they are not charged when dissolved in water. However, the methanol and ethanol concentrations in both the diluate and concentrate decreased during the experiment. Because the ERS also did not have increased methanol and ethanol concentrations, the loss (21% in mass) of these alcohols may be attributed to volatilisation during the experiment. Furthermore, when dissolved in water, MDEA is positively charged and, therefore, can be transported as a cation. Because the MDEA mass balance fitted within 5%, the decrease in MDEA from the real FIC can be explained by electro-migration of cationic MDEA. However, due to the relatively high molecular weight (119 $g \cdot mol^{-1}$) and relatively low concentration (9 – 11 $mg \cdot L^{-1}$) compared to NH_4^+ (18 $g \cdot mol^{-1}$ and 993 $mg \cdot L^{-1}$, respectively), only 64% of MDEA was transported from the FIC to the concentrate. The transport of MDEA contributed with less than 1% to the loss in NH_4^+ current efficiency. Hence, the loss in NH_4^+ current efficiency was predominantly caused by the back-diffusion of NH_4^+. Furthermore, the average electrical resistance during the experiments with synthetic and real FIC was similar: 48 and 47 Ω, respectively. Due to the similar NH_4^+ current efficiency and the similar average electrical

resistance, the same electrical energy consumption of 5 MJ·kg-N^{-1} to remove 93% of TAN from synthetic and real FIC was observed.

Table 7-4 - Process performance indicators for the removal of TAN from synthetic and real FIC by ED.

	unit	Synthetic	Real
Initial diluate NH_4^+ concentration	mg·L^{-1}	1,050	781
TAN removal efficiency	-	93%	93%
Water recovery		99%	98%
NH_4^+ current efficiency	-	90%	88%
Average electrical resistance	Ω	48	47
Energy consumption	MJ·kg-N^{-1}	5	5

7.3.2. Ammonia recovery for electricity generation from FIC

Based on the results described in 7.3.1., FIC proved to be a readily suitable N-loaded residual for the removal of TAN and the subsequent recovery of NH_3 for the generation of electricity. To assess the combination between ED, BPMED and VMS, the same FIC was used, but from a different batch. Hence, the composition of the FIC differed from the experiments conducted in 7.2.3. The results are presented per phase, considering:

- Phase 1: ED (B1 – B3);
- Phase 2: ED + BPMED (B4 – B7);
- Phase 3: ED + BPMED + VMS (B8 – B11).

7.3.2.1. Phase 1: ED

For the first three batches (B1 – B3), ED produced a concentrated NH_4^+ solution, while achieving 93% TAN removal, on average. After the treatment of three batches of 1.6 L FIC, in which the TAN was transported as NH_4^+ to the 0.5 L of concentrate solution, the NH_4^+ concentration in the concentrate increased to 6.1 g·L^{-1}. The NH_4^+ current efficiency ranged between 77 and 81% and was lower than in the experiments described in Section 7.2.3 (88%). The difference in NH_4^+ current efficiency was caused by the longer run time and larger volumes treated per batch, resulting in an NH_4^+ concentration gradient ranging between 2.5 and 6.0 g·L^{-1}, compared to 1.5 g·L^{-1} for the previous experiments. The additional loss in NH_4^+ current efficiency can be attributed to the transport of MDEA. The FIC used for the SBE contained seventy times more MDEA (798 mg·L^{-1}) than the real FIC described in 7.2.3., while 63% of the MDEA was removed, representing 8% of the current efficiency. After the first three batches, the MDEA concentration in the concentrate reached 5.4 g·L^{-1}. Furthermore, the methanol concentration (161 mg·L^{-1}) was more than one order of magnitude lower than in the real FIC described in 7.2.3. Both methanol and ethanol remained in the diluate, suggesting that volatilisation was negligible, which can be due to the lower concentration present in the FIC (lower driving force for volatilisation) and improved solution preservation (closed bottles), compared to the experiment

described in 7.2.3. Eventually, the higher applied current density (dynamic current density with a safety factor of 0.8, instead of 0.62 as used in 7.2.3.) and the lower NH_4^+ current efficiency resulted in an increase in electrical energy consumption to 8 – 10 MJ·kg-N^{-1}, compared to 5 MJ·kg-N^{-1} for the previous FIC experiments.

7.3.2.2. Phase 2: ED + BPMED

Subsequently, the concentrated NH_4^+ solution produced by ED served as feed solution for BPMED to produce dissolved NH_3. Throughout this phase, four batches of FIC (B4 – B7) were treated by ED, while the concentrate served as the feed for BPMED. The NH_4^+ current efficiency and electrical energy consumption for ED were similar (75 – 82% and 8 - 9 MJ·kg-N^{-1}, respectively) to Phase 1, with a TAN removal of 94%. After B7, the TAN concentration stabilised at 4 g·L^{-1} in the concentrate, while the TAN concentration in the base reached 8.5 g·L^{-1}, as shown in Figure 7-8. Because the base pH was 10.2 after B7, the NH_3 concentration in the base was 7 g·L^{-1}. The concentrate pH increased steadily throughout the SBE, from 7.9 to 8.7, due to the leakage of OH^- and the diffusion of NH_3 from the base (see Chapter 4.3). Furthermore, also the TAN concentration in the acid increased from 0.8 to 1.9 g·L^{-1} between B4 and B7, in line with the results presented in Chapter 4.3. The accumulation of TAN can be attributed to the diffusion of NH_3 from the base to the acid, as described in Chapter 4.3. Because the acid pH ranged between 6.4 and 6.7, the predominant form of TAN was NH_4^+.

The NH_4^+ current efficiency for BPMED decreased from 88% for B4 to 63% for B7. The loss in NH_4^+ current efficiency for B4 partly (10%) can be attributed to the transport of MDEA from the base to the concentrate. Furthermore, the loss in NH_4^+ current efficiency can be attributed to OH^- leakage and NH_3 diffusion, as described in Chapter 4.3. Because the concentration gradients of OH^- and NH_3 between the BPMED feed and base increased and therefore more OH^- leakage and NH_3 diffusion took place, the NH_4^+ current efficiency for BPMED decreased between B4 and B7. However, despite the decrease in NH_4^+ current efficiency for BPMED, the electrical energy consumption to produce dissolved NH_3 in the base by BPMED decreased from 31 to 27 MJ·kg-N^{-1} between B4 and B7 (see Figure 7-9). In line with the results presented in Chapter 4.3, the average electrical resistance for each consecutive batch decreased, due to the accumulation of ionic species (such as NH_4^+ and HCO_3^-) in the acid and base. Hence, the decrease in electrical resistance resulted in a lower applied electric potential per consecutive batch, leading to a lower electrical energy consumption.

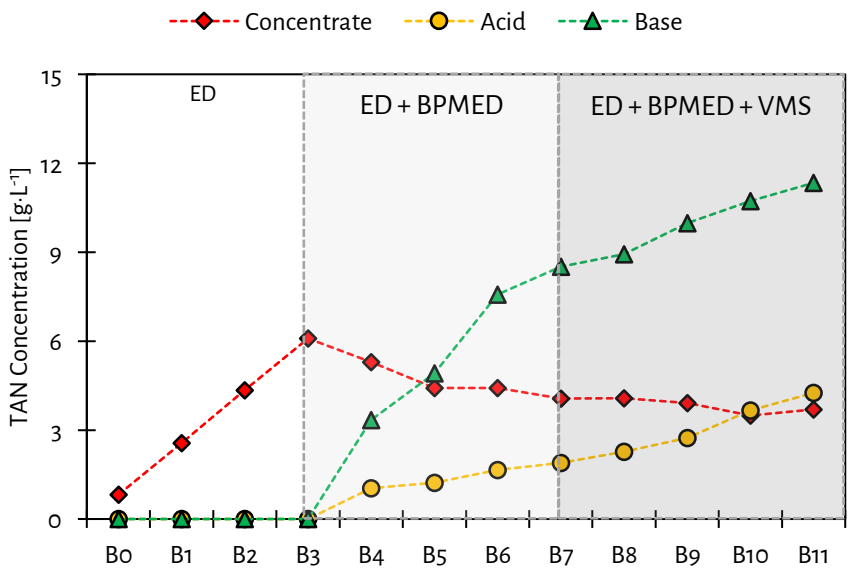

Figure 7-8 - TAN concentrations during the SBE for the treatment of FIC in the various phases using a combination of ED, BPMED and VMS.

7.3.2.3. Phase 3: ED + BPMED + VMS + SOFC

During B8 through B11, VMS was included in the system to strip dissolved NH_3 from the base, while the ED continued to remove TAN from the FIC and BPMED continued to produce dissolved NH_3. The addition of VMS did not affect the operation of ED in terms of TAN removal efficiency (93%) and NH_4^+ current efficiency (78%) between B8 and B11. Also, the NH_4^+ current efficiency for BPMED again averaged 78%. Figure 7-8 shows that the TAN concentration in the acid increased further throughout Phase 3, due to NH_3 diffusion from the base. To avoid excessive accumulation of TAN in the acid in the long term, periodic purging of the acid may be considered. Interestingly, as shown in Figure 7-9, the electrical energy consumption for ED and BPMED decreased to 7 – 8 MJ·kg-N^{-1} and 24 – 26 MJ·kg-N^{-1}, respectively, after the inclusion of VMS. The decrease in electrical energy consumption for the BPMED can be attributed to the further decrease in electrical resistance as a result of ion accumulation in the acid and base.

The stripped NH_3 was condensed along with H_2O that evaporated and was transported through the hydrophobic membrane, in line with the results presented in Chapter 5 and Chapter 6. The concentration of NH_3 in the recovered NH_3-H_2O mixture was 4 wt%. Figure 7-8 shows that the TAN concentration in the base continued to increase, reaching 11 g·L^{-1}, at a pH of 10.1 and an NH_3 concentration of 9 g·L^{-1}. To achieve steady-state operation, the mass transport and transfer should be improved, for example by higher NH_3 recovery by VMS, using a larger membrane area. The electrical energy consumption of VMS to recover NH_3 ranged between 6 and 7 MJ·kg-N^{-1}.

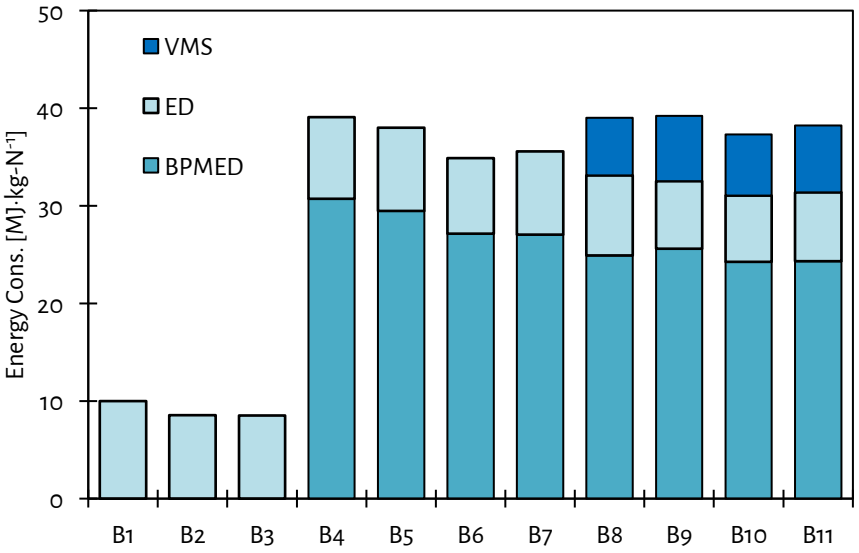

Figure 7-9 - Electrical energy consumption of ED, BPMED and VMS during 93% removal of TAN by ED from FIC, and recovery of NH_3 as 4 wt% NH_3-H_2O mixture for the generation of electricity.

7.3.3. Energy balance for the treatment of real FIC by ED, BPMED, VMS and SOFC

Figure 7-10 presents a flow scheme of the combination of technologies, along with the TAN concentrations, pH of the various streams and the electrical energy consumption for each technology. The total electrical energy consumption to remove TAN and recover NH_3 from FIC by ED, BPMED and VMS ranged between 37 and 39 MJ·kg-N^{-1}. Feeding the 4 wt% NH_3 fuel to a SOFC resulted in a peak power density of 114 mW·cm^2, corresponding to an electrical efficiency of 42% and an electrical energy generation of 11 MJ·kg-N^{-1}. Hence, the net energy consumption of the combined ED + BPMED + VMS + SOFC system was 27 – 28 MJ·kg-N^{-1}.

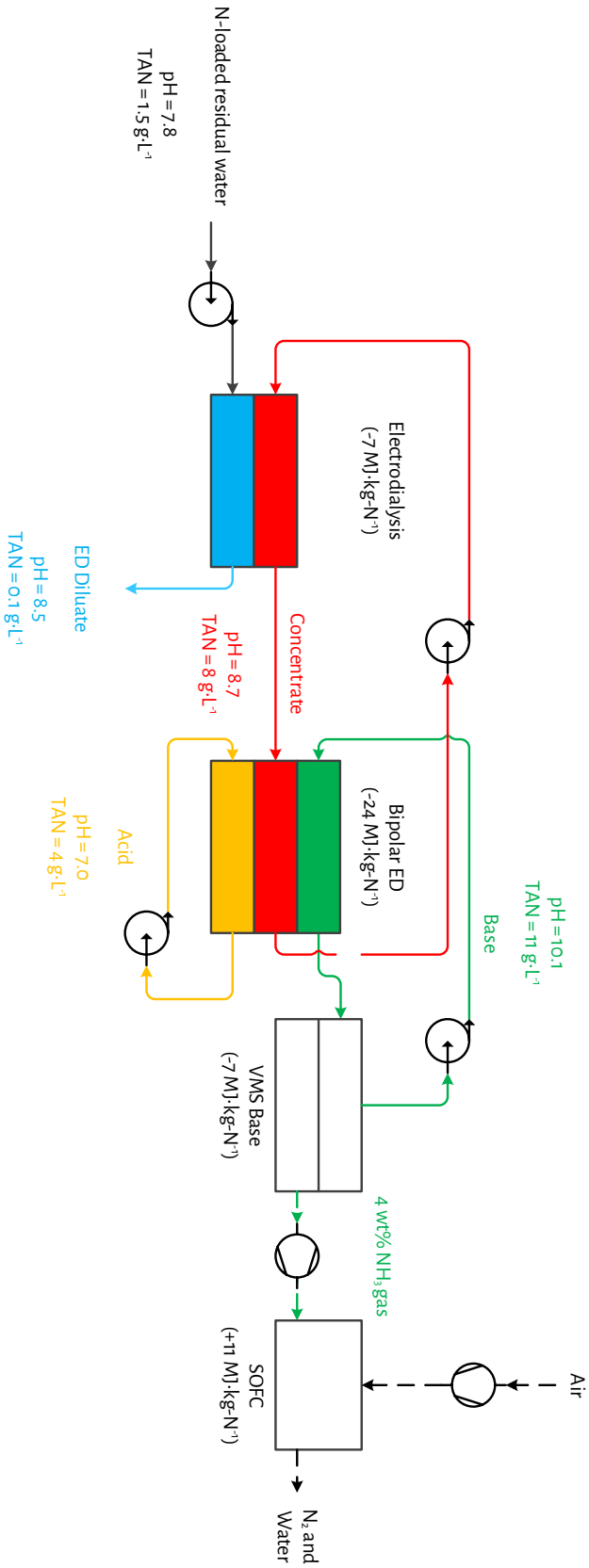

Figure 7-10 - A scheme of the combination of ED, BPMED and VMS for 93% removal of TAN by ED from FIC, and recovery of NH_3 as 4 wt% NH_3-H_2O mixture for the generation of electricity in an SOFC.

7.4. Conclusions

The objective of this chapter was to assess the feasibility of removing TAN from real N-loaded residual streams. Based on the experimental results, the following conclusions can be derived:

- ED allows for competitive (approximately 90%) TAN removal at a water recovery of at least 87% from the N-loaded residual waters ADRW, SDRW and FIC;
- The electrical energy consumption for NH_4^+ removal was consistently higher for real residual streams, compared to the synthetic residual waters;
- The NH_4^+ current efficiency for ED to remove TAN from SDRW was affected by the competitive transport of other cations including Na^+, K^+, Mg^{2+} and Ca^{2+};
- Accumulation of multivalent cations Mg^{2+} and Ca^{2+} in the concentrate during the treatment of SDRW by ED resulted in scaling that caused blockage of the flow channels;
- The presence of the organics methanol, ethanol and MDEA in FIC did not affect the electrical energy consumption to remove TAN by ED;

Furthermore, FIC served as the N-loaded residual water to assess the feasibility of removing TAN and recovering NH_3 for electricity generation in a combination of ED, BPMED, VMS and SOFC. Based on the experimental results, the following conclusions can be derived:

- The removal efficiency of TAN from FIC by ED was not affected by the inclusion of BPMED and VMS and remained 93%;
- BPMED allowed for the production of a concentrated NH_3 solution of 9 $g \cdot L^{-1}$ in the base, using the concentrate of the ED as the feed;
- VMS allowed for the recovery of an NH_3-H_2O mixture with an NH_3 concentration of 4 wt% by stripping the base produced by BPMED;
- The recovered NH_3-H_2O mixtures successfully served as a fuel for an SOFC, resulting in the generation of 11 $MJ \cdot kg\text{-}N^{-1}$ of electrical energy;
- The combination of ED, BPMED, VMS and SOFC successfully allowed for TAN removal from FIC and subsequent electricity generation from the recovered NH_3;
- The combination of ED, BPMED and VMS used more electrical energy (37 – 39 $MJ \cdot kg\text{-}N^{-1}$) than the SOFC generated, resulting in a net electrical energy consumption of 26 – 28 $MJ \cdot kg\text{-}N^{-1}$.

7.5. References

Atasoy, M., Owusu-Agyeman, I., Plaza, E., & Cetecioglu, Z. (2018). Bio-based volatile fatty acid production and recovery from waste streams: Current status and future challenges. *Bioresource Technology, 268*, 773-786. doi:https://doi.org/10.1016/j.biortech.2018.07.042

Deng, Z., van Linden, N., Guillen, E., Spanjers, H., & van Lier, J. B. (2021). Recovery and applications of ammoniacal nitrogen from nitrogen-loaded residual streams: A review. *Journal of Environmental Management, 295*, 113096. doi:https://doi.org/10.1016/j.jenvman.2021.113096

Kedwell, K. C., Jørgensen, M. K., Quist-Jensen, C. A., Pham, T. D., Van der Bruggen, B., & Christensen, M. L. (2021). Selective electrodialysis for simultaneous but separate phosphate and ammonium recovery. *Environmental Technology, 42*(14), 2177-2186. doi:10.1080/09593330.2019.1696410

Lackner, S., Gilbert, E. M., Vlaeminck, S. E., Joss, A., Horn, H., & van Loosdrecht, M. C. M. (2014). Full-scale partial nitritation/anammox experiences - An application survey. *Water Research, 55*, 292-303. doi:10.1016/j.watres.2014.02.032

Magdalena Cadelo, J. A. (2020). *Anaerobic digestion of microalgae biomass for volatile fatty acids production.* (PhD). Universidad Complutense de Madrid, Madrid. Retrieved from https://eprints.ucm.es/id/eprint/63697/

Ward, A. J., Arola, K., Thompson Brewster, E., Mehta, C. M., & Batstone, D. J. (2018). Nutrient recovery from wastewater through pilot scale electrodialysis. *Water Research, 135*, 57-65. doi:https://doi.org/10.1016/j.watres.2018.02.021

Chapter 8.

Conclusions and recommendations

8.1. Residual N-loaded streams and technologies (Chapter 2)

8.1.1. Conclusions

Chapter 2 assesses the feasibility of various technologies for the removal of total ammoniacal nitrogen (TAN) from so-called nitrogen-loaded (N-loaded) residual streams with subsequent electricity generation from the recovered ammonia (NH_3).

The results presented in Chapter 2.2 lead to the first conclusion that there is a large potential for TAN recovery from N-loaded residual streams, based on the thirteen (13) identified N-loaded residual streams with total Kjeldahl nitrogen concentrations > 0.5 $g \cdot L^{-1}$. After the removal of suspended solids from the N-loaded residual streams, TAN can be recovered by various technologies from the obtained N-loaded residual waters. The various technologies available for the removal of TAN and the recovery of TAN from N-loaded residual waters are based on different driving forces, for example, electricity, heat or chemicals. The evaluated technologies cover a wide range of achievable TAN concentrations in the various recovered products, such as concentrated ammonium (NH_4^+) solutions, solid NH_4^+-salt and NH_3 gas. The second conclusion derived from the results presented in Chapter 2.3 is that there is a lack of information on the (normalised) energy consumption that is associated with each technology. In addition, Chapter 2.4 reports on various technologies to generate energy from recovered NH_3. Thirdly, it was concluded that the reviewed literature in Chapter 2.4 lacks information on the feasible fuel composition and tolerance of contaminants in the fuel, when using NH_3 recovered from N-loaded residual waters as a fuel.

8.1.2. Recommendations

To address the lack of information on energy consumption regarding technologies to remove and recover TAN from water, Chapter 3, Chapter 4, Chapter 5 and Chapter 6 of this thesis consistently reported the normalised energy consumption as $MJ \cdot kg\text{-}N^{-1}$. For electrodialysis (ED), bipolar membrane electrodialysis (BPMED) and vacuum membrane stripping (VMS), the $kg\text{-}N^{-1}$ refers to kg of nitrogen transferred, whereas for the solid oxide fuel cells (SOFC), $kg\text{-}N^{-1}$ refers to one kg of nitrogen fed as fuel. Furthermore, Chapter 6 provides information on the minimum NH_3 concentration that still allows for electricity generation when using NH_3 recovered from water (aqueous solution) as a fuel in an SOFC.

The application potentials of recovered TAN from N-loaded residual streams depend on specific local conditions. For example, if there is a need for TAN as fertiliser near the location where TAN is present in residual streams, recovery of TAN as fertiliser may be proposed. However, in absence of such a need, perhaps the generation of electricity from NH_3 is a better option. Based on the categorisation of the N-loaded residual streams, strategies for TAN recovery can be defined and technologies can be selected: Category 1 requires conversion of organic-N to TAN, Category 2 requires solids removal and Category 3 is suitable for TAN recovery.

8.2. Electrodialysis (Chapter 3)

8.2.1. Conclusions

Chapter 3 optimises the ED operation in terms of maximising the concentration factor and minimising energy consumption for achieving NH_4^+ removal that is competitive to currently applied alternative methods, as described in Chapter 2.2, such as partial nitritation in combination with anammox (approximately 90% removal, hereafter representing competitive NH_4^+ removal), while producing concentrated NH_4^+ solutions. The experimental work focused on the application of dynamic current density during the ED operation, aiming to maximise the concentration factor and to minimise the energy consumption.

The results presented in Chapter 3 lead to the conclusion that ED allows for competitive (approximately 90%) NH_4^+ removal from synthetic feed water with a TAN (as NH_4^+) concentration of 1.5 $g \cdot L^{-1}$, while producing 6.7 times concentrated NH_4^+ solutions (10 $g \cdot L^{-1}$) at an electrical energy consumption of 5 $MJ \cdot kg\text{-}N^{-1}$.

8.2.2. Recommendations

The operation of ED to remove NH_4^+ and concentrate NH_4^+ inevitably results in ion concentration gradients and thus osmotic pressure gradients between the diluate and the concentrate; therefore, driving forces for back-diffusion and osmosis cannot be avoided. The results in Chapter 3 show that the application of dynamic current density resulted in less back-diffusion and osmotic water transfer, compared to the application of a fixed current density, resulting in a higher concentration factor and lower energy consumption.

The following recommendations may allow for further improved operation of ED for the removal of TAN from N-loaded residual waters, while producing concentrated NH_4^+ solutions:

1. The use of membranes with lower water (H_2O) permeabilities, for example with higher crosslinking densities, to achieve higher concentration factors, while having minimal impact on the resistances for NH_4^+ transport;
2. The use of improved spacer material and design to make more efficient use of the membrane area and to lower the electrical resistance and ultimately the energy consumption, for example with spacers that have higher void fractions than those used in this thesis (59% void fraction) and are made of conductive materials.

Furthermore, because Chapter 3 only reports on tests using synthetic feed waters, additional research should focus on the use of real N-loaded residual streams, as identified in Chapter 2, leading to the following recommendation:

3. More extensive assessment of the effect of the transfer of other cations on the NH_4^+ current efficiency and electrical energy consumption of ED;

8.3. Bipolar membrane electrodialysis (Chapter 4)

8.3.1. Conclusions

Chapter1 assessed whether bipolar membrane electrodialysis (BPMED) can be used to achieve NH_4^+ removal that is competitive to partial nitritation in combination with anammox while producing concentrated NH_3 solutions. The experimental work focused on the fate of TAN and corresponding TAN concentrations and the energy consumption during the BPMED operation.

The results presented in Chapter 4 lead to the conclusion that BPMED allows for competitive (85 - 91%) NH_4^+ removal from synthetic feed water with a TAN concentration of 1.5 $g \cdot L^{-1}$ (as NH_4^+), while producing concentrated NH_3 solutions (4.5 $g \cdot L^{-1}$) that can be used for TAN recovery. In addition, using BPMED to produce concentrated NH_3 solutions proved to be energetically competitive to the use of ED in combination with the addition of chemicals. For the latter, the energetic equivalence of the addition of chemicals was calculated and added to the electrical energy consumption of ED. To produce solutions with 4.5 $g \cdot L^{-1}$ of NH_3, BPMED required 19 $MJ \cdot kg\text{-}N^{-1}$ of electrical energy, while ED in combination with chemical addition required 22 $MJ \cdot kg\text{-}N^{-1}$.

8.3.2. Recommendations

Similar to ED, concentration gradients cannot be avoided in BPMED during the production of concentrated NH_3 in the base. Chapter 4 shows that hydroxide (OH^-) leakage, dissolved NH_3 diffusion and ionic species diffusion (such as NH_4^+), resulted in a loss in NH_4^+ current efficiency and ultimately in an increase in energy consumption. In addition, due to NH_3 diffusion from the base and the accumulation of TAN in the electrode rinse, only approximately half of the transported TAN (as NH_4^+) from the feed water ended up as NH_3 in the base. To improve the operation of BPMED, the following recommendations are suggested:

1. The use of membranes with lower OH^- and NH_3 permeabilities to achieve higher NH_4^+ current efficiencies and ultimately a lower energy consumption, while having minimal impact on the resistances for NH_4^+ transport;
2. The use of improved spacer material and design to make more efficient use of the membrane area and to lower the electrical resistance and ultimately the energy consumption, as described in Chapter 8.2.2.

Since Chapter 4 again only reports on tests using synthetic feed waters, additional research should focus on the use of real N-loaded residual streams, as identified in Chapter 2. For the treatment of real N-loaded residual waters, the following recommendations are suggested:

3. An assessment of the effect of the transfer of other cations on the NH_4^+ current efficiency and energy consumption of BPMED;
4. The use of (pre-)concentrated NH_4^+ solutions as feed water, for example by using ED, to allow for operating at higher current densities and to minimise the NH_4^+ current efficiency and potentially the energy consumption.

8.4. Vacuum membrane stripping (Chapter 5 and 6)

8.4.1. Conclusions

Chapter 5 and Chapter 6 assessed the selectivity of NH_3 over H_2O transfer, as well as to assess the achievable NH_3 concentrations and energy consumption when recovering gaseous NH_3 by vacuum membrane stripping (VMS). The experimental work in Chapter 5 focused on the transfer rates and selectivity of NH_3 over H_2O transfer for various types of membranes and various feed water compositions (NH_3 feed water concentration and ionic strength), feed water temperature and hydraulic conditions. The experimental work in Chapter 6 focused on the achievable concentrations and energy consumption of VMS for various feed water temperatures and NH_3 feed water concentrations.

The results from Chapter 5 and 6 lead to multiple conclusions on the recovery of NH_3 by VMS. Firstly, H_2O transfer during the recovery of NH_3 by VMS proved to be inevitable, resulting in the recovery of NH_3-H_2O mixtures. Secondly, the use of dense pervaporation membranes does not allow for more selective transfer of NH_3 over H_2O, compared to porous gas-permeable membranes and results in consistently lower NH_3 transfer rates. In fact, the transfer of H_2O was consistently preferred over NH_3 transfer, throughout all conducted experiments. Thirdly, adjusting the feed water composition (NH_3 concentration and ionic strength) and the operating conditions (temperature and hydraulic conditions) allowed for optimisation of the VMS process to achieve recovery of more concentrated NH_3-H_2O mixtures. Eventually, VMS allowed for the recovery of NH_3-H_2O mixtures with NH_3 concentrations up to 11 wt%, when recovering NH_3 at a temperature of 35 °C, at unsteady hydraulic conditions, at an NH_3 feed water concentration of 10 $g \cdot L^{-1}$. To achieve such high NH_3 concentrations in the recovered NH_3-H_2O mixtures, most N-loaded residual waters must be firstly concentrated by (BPM)ED, because most N-loaded residual waters are characterised by much lower N concentrations, as described in Chapter 2.

8.4.2. Recommendations

Based on the conclusions on the recovery of NH_3 by VMS, various attempts failed to selectively transfer NH_3 over H_2O. The use of various feed water compositions, operation conditions and membranes all resulted in the selective transfer of H_2O compared to NH_3. However, by optimising the operation of VMS in terms of NH_3 feed water concentration, feed water temperature and hydraulic conditions, the concentration of NH_3 in the recovered NH_3-H_2O mixtures increased from 1 to 11 wt%. To recover more concentrated NH_3-H_2O mixtures, the following recommendations are suggested:

1. To strip NH_3 from feed waters with NH_3 feed water concentrations higher than 10 $g \cdot L^{-1}$, by producing concentrated NH_3 solutions from N-loaded residual streams using ED and BPMED.
2. The use of membranes that allow for selective transfer of NH_3 over H_2O, for example, making use of a selective layer of dense membranes. The materials of the selective layer of the membrane should then avoid the dissolution of H_2O and allow for solution and diffusion of NH_3. Alternatively, the selective layer should strongly bind H_2O, while allowing for solution and diffusion of NH_3, for

example by taking advantage of the difference in acidity coefficients (pK_a) between NH_3 and H_2O. By allowing for less strong bonding of NH_3 than H_2O to the membrane material after sorption due to the differences in pK_a, potentially higher transfer rates of NH_3 compared to H_2O can be established.

3. To condense the recovered NH_3-H_2O mixtures, allowing for H_2O condensation while avoiding the dissolution of NH_3 in the condensed H_2O (flash condensation), to obtain more concentrated NH_3-H_2O mixtures.

Because also Chapter 5 and Chapter 6 only report on the use of synthetic feed waters and fuels, additional research should focus on the use of NH_3 recovered from real N-loaded residual streams or waters, as identified in Chapter 2. It must be realised that (BPM)ED is firstly required to produce concentrated TAN solutions, meaning that NH_3 recovery by VMS will not directly be applied to the N-loaded residual streams. Nonetheless, when VMS will be used to recover NH_3 from real N-loaded residual waters, the following recommendation is suggested:

4. An assessment of the presence of possible contaminants in the recovered NH_3-H_2O mixtures. Even though inorganic metal-based salts are not volatile and solutes such as volatile fatty acids, sulphide and (bi)carbonate are ionised at high pH, contaminants may be present in the recovered NH_3-H_2O mixtures when recovering NH_3 from real N-loaded residual streams or waters (aqueous solutions) that contain NH_3 originating from real N-loaded residual waters.

8.5. Solid oxide fuel cell (Chapter 6)

8.5.1. Conclusions

Chapter 6 determined the minimum NH_3 concentration in NH_3-H_2O mixtures when such mixture will be used as fuel for electricity generation in an SOFC. The results from Chapter 6 lead to the conclusion that an SOFC allowed for electrical energy generation of 9 $MJ \cdot kg\text{-}N^{-1}$ when using NH_3-H_2O mixtures with NH_3 concentrations of 5 wt%.

8.5.2. Recommendations

The results in Chapter 6 show that the concentrations of NH_3 in NH_3-H_2O mixtures recovery by VMS from water (aqueous solution) are high enough to allow for electricity generation in an SOFC. However, the following aspects were not studied yet and are recommended to serve as research topics for future work:

1. To validate whether and how much oxidised N-species are emitted by SOFC using NH_3-H_2O mixtures as a fuel, as current literature only reports on using pure NH_3 as a fuel;
2. An assessment of mass, electricity and heat balance of an SOFC using NH_3-H_2O mixtures as a fuel;
3. An assessment of the long-term effect of H_2O presence in the fuel on the SOFC;
4. An assessment and optimisation of the operating conditions, such as fuel flow rate, air flow rate and operating temperature, to allow for high power densities, electrical efficiencies, while emitting no oxidised-N species;

Again, because Chapter 6 only report on the use of synthetic solutions that served as fuel, additional research may focus on the use of real N-loaded residual streams, as identified in Chapter 2. To this end, the following recommendation can be taken into account:

5. An assessment of the presence and effect of contaminants present in the recovered NH_3 fuel.

8.6. Removal and recovery of TAN from real N-loaded residual waters (Chapter 7)

8.6.1. Conclusions

The objective of Chapter 7 was to assess the feasibility of TAN removal and subsequent NH_3 recovery from real N-loaded residual streams. Based on the experimental results, ED allowed for the removal of approximately 90% of TAN from algae digestion reject water (ADRW), sludge digestion reject water (SDRW) and fertiliser industry condensate (FIC), while reaching a recovery of the treated water of at least 87%. During the production of concentrated NH_4^+ solution by ED from SDRW, scaling took place in the concentrate flow channels, hampering the further treatment of SDRW. The treatment of FIC allowed for the production of a concentrated NH_4^+ solution (ranging between 4 and 6 $g \cdot L^{-1}$) by ED, while consistently achieving 93% TAN removal. The concentrated NH_4^+ solution was subsequently used for the production of a concentrated solution with 9 $g \cdot L^{-1}$ of NH_3 by BPMED, which in its turn was used at the feed water for VMS for the recovery of NH_3. The obtained NH_3-H_2O mixture had an NH_3 concentration of 4 wt%. Finally, the NH_3-H_2O mixture was used as the fuel of an SOFC, which generated 11 $MJ \cdot kg\text{-}N^{-1}$ of electrical energy. Hence, the combination of ED, BPMED, VMS and SOFC successfully allowed for competitive TAN removal from N-loaded residual water and subsequent electricity generation from the recovered NH_3. However, the combination of ED, BPMED and VMS used more electrical energy (37 – 39 $MJ \cdot kg\text{-}N^{-1}$) than the SOFC generated, resulting in a net electrical energy consumption of 26 – 28 $MJ \cdot kg\text{-}N^{-1}$.

8.6.2. Recommendations

The results in Chapter 7 show that the production of concentrated NH_4^+ solutions by ED from SDRW was hampered by scaling. To this end, the following recommendation is suggested:

1. The use of monovalent selective membranes to minimise the transport of multivalent ions to the concentrate, as the transfer of multivalent ions causes scaling when accumulated in the concentrate;

Furthermore, the results in Chapter 7 show that it is possible to achieve competitive TAN removal from FIC while NH_3 is recovered for the generation of electricity in an SOFC. However, the combination of ED, BPMED and VMS consumed more energy than the SOFC generated. In the previous paragraphs, various recommendations were given to decrease the energy consumption of ED, BPMED and VMS and increase the electricity generation by an SOFC, which potentially may lead to an energy-positive system for TAN removal from N-loaded residual waters.

Acknowledgements

After six years, I finally wrapped up my PhD research. Ten years I spent in Delft to obtain my bachelor's, master's and now also my PhD degree. What started with calculating structures and flood protection, ended with a book combining water treatment and energy generation. The big transition from the hardcore civil engineering disciplines started at the end of my bachelor's, when I chose to do a project mainly because it was abroad: the design of a water treatment plant in Portugal. After this experience, I was more intrigued about water treatment and continued with the MSc Watermanagement with a specialisation in Sanitary Engineering. After two three month trips to Indonesia and Spain, I was certain that I wanted to continue working in the field of water treatment.

I start by thanking Henri Spanjers, who first allowed me to conduct my MSc thesis on zero liquid discharge. I want to thank you for offering me the opportunity to do my PhD research, and for your trust in allowing me to conduct the research how I had in mind. I always enjoyed our late-night communications about the research, the Zero Brine project and the Industry Water course. Especially the latter two where for me a great nice introduction to the world of industrial water treatment. I also want to thank Jules van Lier for giving me the freedom and trust during my research. Furthermore, I want to thank Henri and Jules for the smooth collaboration and constructive feedback during the whole period of research.

To the students I supervised during my research, being Willy, Rob, Christiaan, Lasse, Sam, Matthijs, Evelien, Jan-Max, Lotte, Giacomo and Yundan: thanks a lot for all your efforts, critical thinking and discussions! Without all your input, I would not have been able to finish my research. I want to thank Mohammed, Armand, Patricia and all other Waterlab staff members for all their help and input. I claimed quite some space, but I hope I kept it all organised and tidy. To Mariska, Tamara and all other secretaries: thank you for all the support with scheduling and arranging meetings for having the door always open to help out. To Zhe and Elena: thank you for the great collaboration on the research paper. It took a long time, but we put together a nice piece of work! I also want to thank Ali Saadabadi for his patience and time to explain me the ins and outs of solid oxide fuel cells. I want to thank David Vermaas and Ernst Sudhölter for their input and the discussion we had on mass transport phenomena: I truly learned a lot from you! Subsequently, I would like to thank all the involved parties (KU Leuven, Fiaxell, Yara International, Waternet, Inopsys, Royal Haskoning DHV, Bioelectric and HoSt) from the N2kWh project for their contributions and feedback during the half-yearly meetings. I want to thank all my fellow PhD colleagues for all the serious notes, such as the First Year PhD Meetings, but especially for all the fun times we had in PSOR. A special thanks to those who had to share an office with me for three years. Magela, Pamela and Victor: it was a pleasure to spend my days with you. It was always interesting to see daily who showed up, at what time, what language we would speak that day, what to have for lunch and at what time, but especially to see who was in charge of the temperature control. Thank you for all the research-related and non-research-related discussions, which could become

quite intense. I still stand with the modest oneliners on the whiteboard, which are probably still there: I was the sunshine of the office and I am like a milky way (brown on the outside, white on the inside). I also want to thank another Latin representation, being Javier, Sara and David for involving me in your version of your Spanish language, your cultures and habits and I always enjoyed the Sinterklaas celebrations. To Victor and Steef: if only we spent the time we spent on Pokemon GO on our research, we would have finished incredibly much earlier. Either way, I really needed this distraction to motivate me to continue the actual work, so thanks for joining me on this journey. Another big thank you to all my colleagues at Lenntech, for your patience to listen to me when I was ventilating my thoughts and experiences while finishing the thesis in combination with working at Lenntech. A special thanks to David, Tobias, Eddy and Adriaan, for your trust and efforts to bring the technology to practice.

To my friends: jaaahaaa, mijn werkstuk is eindelijk af en ik hoop dat jullie mijn spreekbeurt leuk vonden. Mark en Bob, heel erg voor jullie geduld om naar dat eindeloze gepraat over ammoniak en water te luisteren. Ik ben alleen bang dat dat nog niet helemaal over is. Ik ben erg blij dat jullie mij wilden bijstaan als paranimf.

Voor pap en mam: zoals jullie weten, zei ik altijd dat ik nooit zou gaan promoveren. Maar goed, dat zei ik ook over het behalen van een bachelor en een master. Misschien moet ik maar niets meer zeggen.. Bedankt voor jullie eindeloze steun gedurende mijn studie en mijn onderzoek, maar ook vooral voor alles daarnaast. Tot slot, Loran: zonder jou had ik dit nooit kunnen doen. Jij bent er altijd voor mij geweest. Bedankt voor alle ruimte en tijd die je mij al die jaren gegeven hebt. Vaak was ik nog tot laat bezig of zat ik vast in mijn gedachten. Dankzij jou bleef ik daar nooit te lang in hangen. Jij hebt me zoveel andere dingen geleerd in het leven die nog veel belangrijker zijn dan onderzoek en werk. Nu is het tijd om te genieten van het belangrijkste in ons leven: Sen.

Curriculum vitae

Summary

I am passionate researcher and engineer and I am highly motivated to work on water treatment related challenges. With my creativity, systematic and pragmatic thinking and ability to set priorities, I aim to solve the problem. I like to work in a team and I am not afraid to take risks, take the lead and carry the associating responsibilities. With my wide variety of working experience, I think I am able to communicate well with people from different educational and geographical backgrounds.

Competences

Communicating, conceptual thinking, delegating, innovative, pragmatic, planning and organising, responsibility, teamwork, vision

Personal

Name: N van Linden (Niels)
Address: Spechtlaan 353
Zip code/Place: 3136 HG Vlaardingen
Date of birth: 03-10-1990
Place of Birth: Vlaardingen
Nationality: Dutch
Phone number: +31651260780
Email address: nielsvanlinden@gmail.com
Driver license: Driver license B

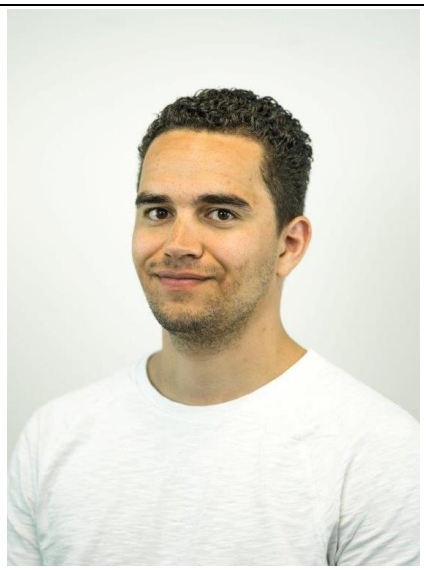

Personal interests

Crossfit, mountainbiking, snowboarding, spending time with friends and family

Curriculum vitae

Education/studies

2013 - 2016: Civil Engineering MSc, Watermanagement, Sanitary Engineering, Delft University of Technology

- Diploma: Master of Science (2016)
  - Master Thesis: Sodium chloride recovery from brines for reuse purposes in zero liquid discharge (http://resolver.tudelft.nl/uuid:ae640132-fbe7-45d3-a62a-479599f308ed)
  - Multidisciplinary project (3 months): Optimisation study for drinking water treatment in Jakarta, Indonesia
  - Internship (4 months): Experimental assessment of ultrafiltration and reverse osmosis for water recovery from sewage effluent in Barcelona, Spain

2009 - 2013: Civil Engineering BSc, Delft University of Technology

- Diploma: Bachelor of Science (2013)
  - Bachelor Thesis: “Mag het wat zachter”, design of water treatment system in Portugal.

2002 - 2008: Pre University Secondary Education, Lentiz College dep. Groen van Prinsterer, Vlaardingen

- Diploma: VWO (2008)
  - Subjects: Dutch, English, Physics 1, Mathematics B2, Chemistry 1, Informatics, Biology 2

Languages

Dutch: Excellent, mother tongue

English: Good, reading, writing, speaking

French: Reasonable, reading

German: Reasonable, reading, speaking

Working experience

April 2020 – present; Lenntech B.V. (40 hours per week)

Branch: Water treatment technology, *Position*: R&D Coordinator

Proceedings: Coordination of water treatment related R&D activities, comprising various different technologies at different scales: pilot and demonstration projects with research consortia and commercial proof-of-concept and pilot projects with industrial end-users

April 2016 – April 2020; TU Delft (40 hours per week)

Branch: Research, *Position*: PhD researcher

Proceedings: Scientific research on the recovery of ammonia from residual waters for the generation of electricity. https://www.tudelft.nl/citg/onderzoek/stories-of-science/energie-krijgen-van-urine

February 2015 – May 2015; CETAQUA Barcelona (40 hours per week)

Branch: Research, *Position*: Intern

Proceedings: Execution of experiments and data analysis on water treatment technologies

August 2013 – March 2016; TU Delft (12 hours per week)

Branch: Academic education, *Position*: Student assistant Water Management

Proceedings: Supporting BSc- and MSc-courses Water Treatment

January 2013 – September 2013: KneeClinic (12 hours per week)

Branch: Medical, *Position*: Project Manager

Proceedings: Administration, marketing and IT

June 2010 – November 2014: Argos Zorggroep (16 hours per week)

Branch: Healthcare, *Position*: Logistics, restaurant and front-desk employee

Proceedings: Logistic and technical proceedings, serving meals and administrative proceedings

October 2009 - March 2010: PWS Rotterdam (8 hours per week)

Branch: Engineering, *Position*: Draftsman

Proceedings: Digitalizing hardcopy technical drawings

November 2006 – May 2008: Lentiz College Dep. Groen van Prinsterer (5 hours per week)

Branch: Secondary education, *Position*: Student tutor

Proceedings: Tutoring student, providing study guidance

November 2005 – April 2011: PLUS Woudhoek supermarket (15 hours per week)

Branch: Retail, *Position*: Sales employee

Proceedings: Leadership of stocking employees, managing daily orders, managing schedules

Scientific publications

- (2022) Niels van Linden, Henri Spanjers and Jules B. van Lier, Fuelling a solid oxide fuel cell with ammonia recovered from water by vacuum membrane stripping, https://doi.org/10.1016/j.cej.2021.131081
- (2022) Niels van Linden, Yundan Wang, Ernst Sudhölter, Henri Spanjers, Jules B. van Lier, Selectivity of vacuum ammonia stripping using porous gas-permeable and dense pervaporation membranes under various hydraulic conditions and feed water compositions, https://doi.org/10.1016/j.memsci.2021.120005
- (2021) Zhe Deng, Niels van Linden, Elena Guillen, Henri Spanjers, Jules B. van Lier, Recovery and applications of ammoniacal nitrogen from nitrogen-loaded residual streams: A Review, https://doi.org/10.1016/j.jenvman.2021.113096
- (2021) S. Ali Saadabadi, Niels van Linden, Abel Heinsbroek, P.V. Aravind: A solid oxide fuel cell fuelled by methane recovered from groundwater, https://doi.org/10.1016/j.jclepro.2021.125877
- (2020) Niels van Linden, Ran Shang, Georg Stockinger, Bas Heijman, Henri Spanjers: Separation of natural organic matter and sodium chloride for salt recovery purposes in zero liquid discharge, https://doi.org/10.1016/j.wri.2019.100117
- (2020) Niels van Linden, Giacomo L. Bandinu, David A. Vermaas, Henri Spanjers, Jules B. van Lier: Bipolar membrane electrodialysis for energetically competitive ammonium removal and dissolved ammonia production, https://doi.org/10.1016/j.jclepro.2020.120788
- (2019) Niels van Linden, Henri Spanjers, Jules B. van Lier: Application of dynamic current density for increased concentration factors and reduced energy consumption for concentrating ammonium by electrodialysis, https://doi.org/10.1016/j.watres.2019.114856

Patent

- (2019) Niels van Linden, Henri Spanjers, Jules B. van Lier, Gas recovery from wastewater, Priority No. WO 2019/151855, https://worldwide.espacenet.com/patent/search/family/065995823/publication/CA3090320A1?q=pn%3DCA3090320A1

Appendix – Patent WO2019151855

(19) Europäisches Patentamt
European Patent Office
Office européen des brevets

(11) **EP 3 746 407 B1**

(12) **EUROPEAN PATENT SPECIFICATION**

(45) Date of publication and mention of the grant of the patent:
15.12.2021 Bulletin 2021/50

(21) Application number: **19714855.4**

(22) Date of filing: **31.01.2019**

(51) Int Cl.:
C02F 1/20 *(2006.01)* ***C02F 1/469*** *(2006.01)*
B01D 19/00 *(2006.01)* ***B01D 61/44*** *(2006.01)*
B01D 61/58 *(2006.01)* ***C02F 101/16*** *(2006.01)*

(86) International application number:
PCT/NL2019/050058

(87) International publication number:
WO 2019/151855 (08.08.2019 Gazette 2019/32)

(54) GAS RECOVERY FROM WASTEWATER

GASRÜCKGEWINNUNG AUS ABWASSER

RÉCUPÉRATION DE GAZ PROVENANT D'EAUX USÉES

(84) Designated Contracting States:
AL AT BE BG CH CY CZ DE DK EE ES FI FR GB GR HR HU IE IS IT LI LT LU LV MC MK MT NL NO PL PT RO RS SE SI SK SM TR

(30) Priority: **01.02.2018 NL 2020369**
05.03.2018 NL 2020528

(43) Date of publication of application:
09.12.2020 Bulletin 2020/50

(73) Proprietor: **Technische Universiteit Delft**
2628 CN Delft (NL)

(72) Inventors:
- **VAN LINDEN, Niels**
  2600 AA Delft (NL)
- **SPANJERS, Henricus Lambertus Franciscus**
  2600 AA Delft (NL)
- **VAN LIER, Julius Bernardus**
  2600 AA Delft (NL)

(74) Representative: **Cramwinckel, Michiel**
Cramwinckel Consultancy
Kallenkoterallee 82 A
8331 AJ Steenwijk (NL)

(56) References cited:
US-A- 4 969 983 US-A1- 2016 271 562

- **W. PRONK ET AL: "Treatment of source-separated urine by a combination of bipolar electrodialysis and a gas transfer membrane", WATER SCIENCE AND TECHNOLOGY, vol. 53, no. 3, 1 February 2006 (2006-02-01), pages 139-146, XP055449550, ISSN: 0273-1223, DOI: 10.2166/wst.2006.086 cited in the application**
- **SHUANGCHEN MA ET AL: "Experimental study on desorption of simulated solution after ammonia carbon capture using bipolar membrane electrodialysis", INTERNATIONAL JOURNAL OF GREENHOUSE GAS CONTROL, ELSEVIER, AMSTERDAM, NL, vol. 42, 3 November 2015 (2015-11-03), pages 690-698, XP029325593, ISSN: 1750-5836, DOI: 10.1016/J.IJGGC.2015.09.020 cited in the application**
- **ALI M A B ET AL: "Coupling of bipolar membrane electrodialysis and ammonia stripping for direct treatment of wastewaters containing ammonium nitrate", JOURNAL OF MEMBRANE SCI, ELSEVIER BV, NL, vol. 244, no. 1-2, 15 November 2004 (2004-11-15), pages 89-96, XP004619447, ISSN: 0376-7388, DOI: 10.1016/J.MEMSCI.2004.07.007 cited in the application**

EP 3 746 407 B1

Description

FIELD OF THE INVENTION

[0001] The present invention is in the field of a system for gas recovery from wastewater, a method for treating wastewater, and a method wherein ammonia and carbon dioxide are recovered. Typically a wastewater stream is fed into the system, treated and stripped from ammonia and carbon dioxide, and a cleaner water stream is released.

BACKGROUND OF THE INVENTION

[0002] Typically wastewater originates from households and industry. It may be collected and transferred to a treatment facility.

[0003] Wastewater treatment is aimed at converting wastewater into an aqueous effluent that can be returned to the nature water cycle, or aimed at (direct) reuse of water. The latter is also referred to as water reclamation. A minimal impact on the environment is aimed at. The treatment process typically takes place in a wastewater treatment plant or sewage treatment plant. Typically pollutants are removed or broken down. Various processes may be involved, such as phase separation, sedimentation, filtration, oxidation, polishing, tertiary treatment, and biochemical treatment, such as by using microorganisms. By-products from wastewater treatment plants may also be treated in a wastewater treatment plant.

[0004] A contaminant typically found in wastewater is nitrogen, such as in the form of urea, nitrate and nitrite. Excessive discharge of nitrogen (N) leads to eutrophication of receiving surface waters and subsequent deterioration of the aquatic environment. To prevent this, nitrogen compounds in wastewaters are preferably removed before discharge of the water. In various types of wastewater, N is present as ammonium ion ($NH4^+$) in combination with an ion such as bicarbonate (HCO_3^-). In many industrialized areas in the world, NH_4^+ is converted to nitrates and eventually to dinitrogen gas, at the expense of considerable capital costs and energy.

[0005] The majority of the produced NH_3 is used as fertilizer. As a consequence of use thereof, ultimately NH_3 becomes available in waste streams: for example, in manure, urine, and sewage. The total amount of NH_3 discharged to domestic sewage treatment plants in 2016 in the Netherlands was about 32 million kilogram, while the amount of NH_3 in manure in 2013 was about 471 million kilograms. Current state-of-the-art technologies require at least 11 MJ/kg-NH_3 to remove NH_3 from wastewater.

[0006] A treatment technology used is Anammox. In wastewater containing NH_4HCO_3, NH_4^+ is biochemically oxidized, forming N_2 and H_2O. This process requires energy. The application of Anammox finally does not lead to the possibility of resource or energy recovery. Also CO_2 may remain in treated water, leading to amongst others acidification.

[0007] Ammonium nitrate may be removed from wastewater. However, in such as treatment of wastewater containing NH_4NO_3 species, the NH_4NO_3 can unfortunately not be reused in certain cases because it contains traces of radioactive compounds.

[0008] For $(NH_4)_2SO_4$ fertilizer production initially CO_2 may be stripped and released into the air to increase the pH and lower the buffer capacity. Subsequently, NH_3 gas is stripped, requiring significant amounts of energy and the addition of chemicals. The NH_3 is then scrubbed in acid, to produce $(NH_4)_2SO_4$, which can be used as (resource for) fertilizer. However, the demand and economic yield of $(NH_4)_2SO_4$ are low: the required acid is more valuable per kg than the produced $(NH_4)_2SO_4$. Additionally, there are extra costs for the required chemicals and energy. Because this fertilizer has a high sulphur content, the applicability is limited to specific situations.

[0009] Some prior art documents relate to gas recovery from aqueous systems.

[0010] US 2016/271562 A1 recite a process and system for removing ammonia from an aqueous ammonia solution. A first aqueous solution and the ammonia solution are flowed respectively through a first and a second separation chamber of a bipolar membrane electrodialysis stack. The first separation chamber is bounded on an anodic side by a cation exchange membrane and the second separation chamber is bounded on a cathodic side by the cation exchange membrane and on an anodic side by a bipolar membrane. The bipolar membrane has an anion-permeable layer and a cation-permeable layer respectively oriented to face the stack's anode and cathode. While the solutions are flowing through the stack a voltage is applied across the stack that causes the bipolar membrane to dissociate water into protons and hydroxide ions. The protons migrate into the second separation chamber and react there with ammonia to form ammonium ions that migrate to the first separation chamber.

[0011] US 4,969,983 A recites an apparatus containing a multiplicity of three chamber units comprising a combination of ion exchange membranes and bipolar membranes with certain of said chambers containing a fluid permeable filler of ion-exchange material. The apparatus can be used in a process to remove weakly ionized gases from fluid mixtures.

[0012] An article by Pronk et al. "Treatment of source-separated urine by a combination of bipolar electrodialysis and a gas transfer membrane" in Water Science Technology, 53, 3, p. 139-146, 2006, recites that urine contains nutrients which can be applied usefully as a fertiliser in agriculture, but the relatively high pH can lead to ammonia evaporation. Electrodialysis with bipolar membranes was combined with an additional mass transfer unit in order to render a product containing ammonium and phosphate at a low pH. In one case, the additional mass transfer unit consisted of bubble columns placed in acid and basic concentrate streams, connected with a circulating gas phase. In the other case, the unit

consisted of a gas-filled (hydrophobic) membrane placed in between the circulating acid and basic concentrate streams. The results showed that ammonia was transferred through the gas phase, but also carbonate, which is present in stored urine originating from the hydrolysis of urea. Although the pH in the product stream decreases initially, it rises above pH 7 at longer operation times. This pH increase can be attributed to a combination of proton compensating effects. The use of ammonia-selective membranes for the transfer into the acid concentrate could provide a solution to generate an ammonium phosphate product at low pH and high recoveries.

[0013] An article by Shuangchen et al. "Experimental study on desorption of simulated solution after ammonia carbon capture using bipolar membrane electrodialysis", Int. J. Greenhouse Gas Control, Elsevier, Vol. 42, November 3, 2015, p. 690-698, recites ammonia capture in solutions.

[0014] An article by Ali et al. in J. Membrane Science, Elsevier, Vol. 244, Nr. 1-2, November 15, 2004, p. 89-96 recites that splitting of ammonium nitrate to nitric acid and ammonia was achieved by a coupled process including bipolar membrane electrodialysis and in situ ammonia stripping. The effect of homopolar ion-exchange membranes on current efficiency led to the selection of specific membranes. The main parameters influencing the current efficiency were acid and ammonia concentrations. Proton leakage through the anion-exchange membrane is proportional to acid concentration. Ammonia diffuses through the membranes independently of the current. Higher current efficiency was obtained at higher current density. Batch and continuous processing were compared.

[0015] A further issue with prior art systems may be potential fouling of the membranes used. Therefore one has to cope with the various contaminants present in wastewater. As mentioned the required energy, the process control strategy, and the economic feasibility, is suboptimal.

[0016] The present invention therefore relates to a system for gas recovery from wastewater, and a method of operating such a system, which solve one or more of the above problems and drawbacks of the prior art, providing reliable results, without jeopardizing functionality and advantages.

SUMMARY OF THE INVENTION

[0017] The present invention relates to a system for gas recovery from wastewater, a method for treating wastewater, and a method wherein ammonia and carbon dioxide are recovered. The present invention relates to an innovative process in which wastewater with dissolved NH_4HCO_3 is treated with a combination of two technologies: electrodialysis with bipolar membranes and stripping of gases, such as with a vacuum membrane. By applying an electrical potential difference in electrodialysis with bipolar membranes it has been found that NH_4^+ transfers from the wastewater to an alkaline recirculation solution. Simultaneously HCO_3^- is found to transfer from the wastewater to an acidic recirculation solution, leading to the depletion of NH_4HCO_3 in the wastewater. In addition to ion transfer through ion exchange membranes, bipolar membranes dissociate water into ions under the influence of an electrical potential difference. This results in the generation of H^+ ions in the acidic recirculation solution, leading to the formation of dissolved carbon dioxide gas (CO_2). In the alkaline solution, OH^- is generated, leading to the formation of dissolved ammonia gas (NH_3). The two gases (CO_2 and NH_3) are subsequently stripped, such as by separate vacuum membrane removal. A hydrophobic membrane (impermeable for liquids, but permeable for gases) may separate the liquid phase from the gaseous phase (CO_2 and NH_3, respectively). On the gaseous side of the membrane an under-pressure (vacuum) may be applied. Because of a vapour pressure difference, the gases are stripped from the liquid, resulting in recovery of CO_2 and NH_3 gas. These gases may be used to produce fertilizer, to produce energy (from NH_3), or to be applied directly as a resource in industry. The alkaline and acidic recirculation solutions are recycled in the electrodialysis with bipolar membranes. The present process is found to be very efficient in terms of energy used and in terms of product obtained.

[0018] The present combination of technologies enables separate recovery of resources (CO_2 gas and NH_3 gas) in treatment of wastewater comprising NH_4^+ and HCO_3^-. Additionally, the invention provides resource recovery in wastewater treatment without addition of chemicals in a continuously operated process. Only electrical energy is required, while additional low-grade energy (waste heat) can be used to improve the efficiency of the invention. Finally, the invention does not continuously generate a residual solution which needs to be treated further; CO_2 and NH_3 gas are potential end-products, whereas the treated water can be discharged or reused (optionally after post-treatment). The gases may be obtained in high purity, e.g. >90% pure. For both gaseous species, CO_2 and NH_3, the other species is virtually absent; in both cases water vapour may be present. The present invention is sustainable, as it contributes to a circular economy, where water, NH_3 and CO_2 may be reused. It is also very scalable. Both electrodialysis and membrane stripping can be applied in a very wide range of wastewater quantities, e.g. because these technologies can be implemented in a modular way.

[0019] The present invention provides economical and material savings for e.g. domestic wastewater treatment and manure. It has been found that 10 MJ/kg-NH_3 can be recovered as electrical energy when using NH_3 as fuel for a solid oxide fuel cell. This amount of recovered energy can be partly used to remove NH_3 from wastewater. In this situation, the removal of NH_3 does not cost energy anymore, resulting in a saving of 0.25 euro/kg-NH_3, assuming that electricity costs 0.08 euro/kWh. This is a total potential saving of 126 million euro per year in

the Netherlands only.

[0020] The production of NH_3 from N_2 and H_2 by the Haber-Bosch process requires 25 MJ/kg-NH_3 (theoretical minimum is 20 MJ/kg-NH_3). When NH_3 is recovered as a resource from wastewater and it can be reused 0.31 euro/kg-NH_3 can be saved, as the NH_3 does not have to be produced anymore. This is a total potential saving of 156 million euro per year in the Netherlands. For this situation, it is assumed that the amount of energy to recover NH_3 is equal to the current amount of energy for NH_3 removal from wastewater.

[0021] Some drawbacks exist however. At present there are relatively high costs for the membranes, some cleaning is still involved, and it is preferred, in view of transport, to have an application for the generated CO_2 close to the present system.

[0022] The system of the present invention is defined in claim 1 and comprises at least one ion exchange unit 30. Into the at least one exchange unit wastewater is provided through input 70, which is treated by the present system, and released from the system through output 71. In fluid connection with the at least one exchange unit are at least three recirculation units 51,52,74a,b, a first alkaline recirculation unit comprising a gaseous ammonia stripper, a second acidic recirculation unit comprising a gaseous CO_2 stripper, and a third electrode rinse recirculation unit 74a,b adapted to receive input from a first electrode rinse compartment (21,22), and for providing output to a second electrode rinse compartment, and vice versa. At least one of the gaseous ammonia stripper and of the gaseous CO_2 stripper comprises a hydrophobic membrane (61a, 62a), a molecular sieve for ammonia or for CO_2, respectively, a pervaporation membrane, or a combination thereof, and the system comprises a tube (72) for removing gaseous ammonia, and a tube (73) for removing gaseous CO_2. For providing flow of fluids a pump, 81 respectively, is provided. Clearly these alkaline and acidic recirculation units are separate from one and another. In the alkaline recirculation unit NH_3 (ammonia) is stripped, whereas in de acidic recirculation unit CO_2 is stripped, both as gaseous species. The stripped gases exit the present system over tubes 72,73, respectively. For stripping and flowing gases pumps 82 may be provided, which typically provide an under-pressure. The stripped gases may be combined to form NH_4HCO_3. Each ion exchange unit comprises at least three compartments separated by membranes. The membranes provide exchange of NH_4^+ (ammonium) from the second to the first compartment over the cation exchange membrane 12, and of HCO_3^- from the second to the third compartment over the anion exchange membrane 13; hence the membranes may be referred to as ion exchange membranes, such as cation and anion exchange membranes. The present also comprises at least two electrode rinse compartment 21,22, and typically two electrode rinse compartments; the at least two electrode rinse compartment have an adjacent membrane, selected from bipolar membranes, cation exchange membranes, and anion exchange membranes, respectively, which may provide exchange of NH_4^+, H^+, OH^-, or HCO_3^-, to or from the electrode rinse compartment 21,22, respectively. The third recirculation unit replenishes the at least electrode rinse compartment. The first electrode rinse compartment 21 is in electrical contact with an anode 41 and the second electrode rinse compartment 22 may be in electrical contact with an cathode 42. To the anode/cathode an electrical current is provided. Water and electrons form H^+ and OH^-. Typically the following redox reactions occur: Anode: $2H_2O$ --> $4H^+ + O_2 + 4e^-$; Cathode: $2H_2O + 2e^-$ --> $2OH^- + H_2$. If the electrode drain recirculates from compartment 21 to compartment 22, and vice versa, water is formed again. The bipolar membrane (11a,b) is typically facing the alkaline compartment 31 or electrode rinse compartment 22 with a positive side and mutatis mutandis is typically facing the acidic compartment 33 or electrode rinse compartment 21 with a negative side. The bipolar membranes can generate H^+, at a negative side thereof, and OH^-, at a positive side thereof.

[0023] In a second aspect the present invention relates to a method of treating wastewater, comprising NH_4^+, and HCO_3^-, using the present system.

[0024] Thereby the present invention provides a solution to one or more of the above mentioned problems and drawbacks.

[0025] Advantages of the present description are detailed throughout the description.

DETAILED DESCRIPTION OF THE INVENTION

[0026] The present invention relates in a first aspect to a system according to claim 1.

[0027] In the present system the third recirculation unit 74a,b is adapted to receive input from the first electrode rinse compartment 21, and for providing output to the second electrode rinse compartment 22, and vice versa. Therewith the liquids in the compartments may be replenished. A salt level in the compartments 21,22 may be 0.1-2 mole/l, such as by providing Na_2SO_4, $NaNO_3$, NH_4NO_3, or NH_4HCO_3.

[0028] In an exemplary embodiment of the present system the first electrode rinse compartment 21 may comprise NH_4^+ or H^+, or wherein the second electrode rinse compartment 22 comprises OH^- or HCO_3^-, or a combination thereof.

[0029] In an exemplary embodiment of the present system the at least one recirculation unit may comprise a membrane 61a, 62a, which typically is hydrophobic, such as a macroporous hydrophobic membrane, a molecular sieve for ammonia or for CO_2, respectively, a pervaporation membrane, a pump 82, or a combination thereof.

[0030] In an exemplary embodiment of the present system at least one membrane 61a,62a in the stripper may be impermeable to liquids, such as water, and permeable to gases, such as CO_2 and NH_3, respectively. The stripper 61,62 typically comprises a strip chamber 61b,62b,

respectively.

[0031] In an exemplary embodiment of the present system the (hydrophobic) membrane 61a, 62a may be macroporous, with an average pore size of 50-500 nm, or microporous, with an average pore size of 0.4-10 nm, preferably 0.5-1 nm (as determined by electron microscopy).

[0032] In an exemplary embodiment of the present system the membrane 11a,11b,12,13,61,62 may have a size from 50 cm^2 to 10^4 cm^2, such as 10^2-10^3 cm^2, and a thickness of 100-7000 μm, such as 200-900 μm, a compartment 31,32,33,21,22 may have a width of 0.1-50 mm, such as 1-30 mm, and a flow may be parallel to the membrane. A membrane may comprise a support. Membranes 12 may be polyvinyl chloride based, with sulphonic acid in Na+ ionic form, membranes 13 may be polyester based, with ammonium in Cl^- ionic form.

[0033] In an exemplary embodiment of the present system the membrane 61a,62a, may be selected from polymeric material, preferably thermoplastic polymers, such as poly propylene and poly vinylidene fluoride, inorganic material, such as silica, and reinforced silica, and combinations thereof.

[0034] In an exemplary embodiment of the present system the exchange unit 30 may comprise a stack of a cation exchange membrane 12, an alkaline compartment 31, a bipolar membrane 11a, an acidic compartment 33, an anion exchange membrane 13, and a wastewater compartment 32, and wherein the second electrode rinse compartment 22 is in fluidic contact with a further cation exchange membrane 12, and wherein the third recirculation unit 74a,b is adapted to receive input from a first electrode rinse compartment 21 to compartment 22, and adapted to provide output to compartment 22 (see fig. 1,2). Therein a cathode 42 may be provided in contact with a compartment 22 and an anode 41 may be provided in contact with compartment 21.

[0035] In an exemplary embodiment of the present system the exchange unit 30 may comprise a stack of an anion exchange membrane 13, an acidic compartment 33, a bipolar membrane 11a, an alkaline compartment 31, a cation exchange membrane 12, and a wastewater compartment 32, and wherein the second electrode rinse compartment 22 is in fluidic contact with a further anion exchange membrane 13, and wherein the third recirculation unit 74a,b is adapted to receive input from a first electrode rinse compartment 21 to compartment 22, and adapted to provide output to compartment 21. Therein a cathode 42 may be provided in contact with a compartment 22 and an anode 41 may be provided in contact with compartment 21.

[0036] In an exemplary embodiment of the present system the exchange unit 30 may comprise a stack of an bipolar membrane 11a, an alkaline compartment 31, a cation exchange membrane 12, a wastewater compartment 32, an anion exchange membrane 13, and an acidic compartment 33, and wherein the first electrode rinse compartment 21 is in fluidic contact with a further bipolar membrane 11b, and wherein the third recirculation unit 74a,b is adapted to receive input from a first electrode rinse compartment 21 to compartment 22, and adapted to provide output to compartment 21, and vice versa to compartment 22 (see fig. 3). Therein a cathode 42 may be provided in contact with a compartment 22 and an anode 41 may be provided in contact with compartment 21.

[0037] In an exemplary embodiment the present system may comprise 2-2^{10} ion exchange units 30 in parallel, preferably 4-2^9 ion exchange units, such as 200-400 ion exchange units.

[0038] The system of the invention comprises a tube 72 for removing gaseous ammonia, and a tube 73 for removing gaseous CO_2.

[0039] In an exemplary embodiment of the present system in operation at least one of a voltage of 0.1-5 V per ion exchange unit 30 may be applied, preferably 0.3- 3V, more preferably 0.5- 2V, such as 0.7-1.5V.

[0040] In an exemplary embodiment of the present system in operation a pH in the first alkaline compartment 31 may be from 7-14, preferably from 8-13, such as 9-12.

[0041] In an exemplary embodiment of the present system in operation a pH in the third acidic compartment 33 may be from 1-7, preferably 2-6.5, such as 2-6.

[0042] In an exemplary embodiment of the present system in operation a current density may be from 15-500 A/m^2, such as 50-100 A/m^2.

[0043] In an exemplary embodiment of the present system in operation a flow parallel to a membrane may each individually be from 0.01-0.20 m/s, such as 0.05-0.10 m/s.

[0044] In an exemplary embodiment of the present system in operation a NH_4^+ flux over a membrane may each individually be 0.2-20 mole/m^2/h, preferably 0.5-5 mole/m^2/h, such as 1-2 mole/m^2/h.

[0045] In an exemplary embodiment of the present system in operation a HCO_3^- flux over a membrane may each individually be 0.2-20 mole/m^2/h, preferably 0.5-5 mole/m^2/h, such as 1-2 mole/m^2/h.

[0046] In an exemplary embodiment of the present system in operation an operating temperature may be from 10-80 °C.

[0047] In an exemplary embodiment of the present system in operation the [NH_4^+] and [HCO_3^-] in the second compartment 32 may each individually be 10^{-3}-2 mole/l, preferably 10^{-2}-1 mole/l, such as 10^{-1}-0.5 mole/l.

[0048] In an exemplary embodiment of the present system in operation an NH_3 flux and a CO_2 flux in recirculation units 51,52 may each individually be 50-5000 g/m^2/h, preferably 70-2500 g/m^2/h, such as 100-1000 g/m^2/h.

[0049] In an exemplary embodiment of the present system membranes 11a,b,12 and 13 are separated by spacers 2 and the membranes 11a,b,12 and electrodes are also separated by spacers.

[0050] In an exemplary embodiment of the present method transferring NH_4^+ from the wastewater 70 to an alkaline recirculation solution 51 may be through a first

compartment 31.

[0051] In an exemplary embodiment of the present method transferring HCO_3^- from the wastewater to an acidic recirculation solution 52 may be through a third compartment 33.

[0052] In an exemplary embodiment of the present method NH_4^+ may be converted into NH_3 in the presence of OH^- in the first compartment 31, and wherein HCO_3^- may be converted into CO_2 in the presence of H^+ in the third compartment 33.

[0053] In an exemplary embodiment of the present method NH_3 may be stripped in ammonia stripper 61, and wherein CO_2 may be stripped in CO_2 stripper 62.

[0054] In an exemplary embodiment of the present method at a gaseous side of stripper 61,62 an under pressure may be applied, such as of 0.1-90 kPa, preferably 1.5-75 kPa, such as 5-50 kPa.

[0055] In an exemplary embodiment the present method may comprise forming NH_4HCO_3.

[0056] In an exemplary embodiment of the present method wastewater may be provided by at least one of a domestic sewage treatment plant, a manure treatment facility, a fertilizer production plant, food and beverage industry, and an industry producing nitrogen loaded wastewater.

[0057] In the present method an electrical potential difference over the cathode 42/anode 41 in electrodialysis with bipolar membranes 11a,11b is applied. Therewith decomposition of water is established. The wastewater fed into the second compartment of the at least one exchange unit. NH_4^+ is transferred from the wastewater 70 to an alkaline recirculation solution 51, and simultaneously, HCO_3^- is transferred from the wastewater to an acidic recirculation solution 52, over the respective membranes. NH_4HCO_3 is depleted in the wastewater, typically in a continuous or semi-continuous mode. However the present system may also be operated batch wise. Water is split over bipolar membranes 11a,11b thereby providing H^+ to the third compartment 33 and alkaline recycling compartment 21, respectively, and thereby providing OH^- to the first compartment 31 and acidic recycling compartment 22, respectively.

[0058] The one or more of the above examples and embodiments may be combined, falling within the scope of the invention.

EXAMPLES

[0059] The below relates to examples, which are not limiting in nature.

[0060] In experiments, $1.6 \cdot 10^{-5}$ kg of NH_4HCO_3 was removed from 1 litre synthetic wastewater, equalling 87% of the total NH_4HCO_3 initially present. In total, $3.6 \cdot 10^{-5}$ MJ of electrical energy was used to transfer the ions and generate OH^- and H^+. This required 2.3 MJ/kg-NH_3 for NH_3 production in the alkaline solution and 5.9 MJ/kg-CO_2 production in the acidic solution. This includes the pumping energy consumption, accounting for 10% of the total energy consumption. Also, NH_3 was stripped from alkaline synthetic solution with various initial NH_3 concentrations (1.2, 8.5 and 13 g-NH_3/L, respectively) at room temperature by vacuum membrane stripping. This resulted in fluxes of 0.10, 0.59 and 0.73 kg/m^2/h, respectively. The permeate content of NH_3 was 1.2%, 7.9% and 11.5%, respectively. The rest of the permeate was water vapour, making it possible to reuse the NH_3.

[0061] The invention is further detailed by the accompanying figures, which are exemplary and explanatory of nature and are not limiting the scope of the invention, which is defined by the claims.

FIGURES

[0062] The invention although described in detailed explanatory context may be best understood in conjunction with the accompanying figures.

[0063] Fig. 1-5 show schematics of the present system.

DETAILED DESCRIPTION OF THE FIGURES

[0064] In the figures:

100	present system
2	spacer
11	bipolar membrane
11a	first bipolar membrane
11b	second bipolar membrane
12	cation exchange membrane
13	anion exchange membrane
21	electrode rinse compartment (anodic)
22	electrode rinse compartment (cathodic)
30	ion exchange unit
31	first alkaline compartment
32	second salt compartment
33	third acidic compartment
41	anode
42	cathode
51	alkaline recirculation unit
52	acidic recirculation unit
61	ammonia stripper
61a	(hydrophobic) membrane
61b	strip chamber
62	gaseous CO_2 stripper
62a	(hydrophobic) membrane
62b	strip chamber
70	wastewater input
71	treated water output
72	tube for removing gaseous ammonia
73	tube for removing gaseous CO_2
74a	electrode rinse recirculation unit
74b	electrode rinse recirculation unit
81	liquid pump
82	vacuum pump

Fig. 1-3 show an exemplary set-ups of the present system.

Fig. 4 shows a stacked variant of the present system.
Fig. 5 shows optional spacers.

[0065] The figures have been detailed throughout the description.

[0066] Fig. 1 shows a cell triplet provided with cation exchange membranes at the electrodes.

[0067] Fig. 2 shows a cell triplet provided with anion exchange membranes at the electrodes.

[0068] Fig. 3 shows a cell triplet provided with bipolar membranes at the electrodes.

[0069] Fig. 4 represents a plural version of fig. 1.

[0070] Fig. 5 shows that all membranes (11,12 and 13) are separated by spacers 2. The spacers are made of polyethylene/silicone material and woven into a mesh. The liquids flow through the void fraction of the spacers, forming the salt, acid and alkaline chambers. The spacers are sealed on the top and bottom, making sure that the liquids are not leaking out of the membrane stack. The electrodes (anode and cathode) and the membranes next to the electrodes are also separated by spacers, forming the electrode rinse chambers.

Claims

1. Wastewater gas recovery system (100) for recovering NH_3 and CO_2 comprising

at least one ion exchange unit (30), each exchange unit comprising at least three ion exchange compartments (31,32,33), each ion exchange compartment being in contact over a membrane with at least one adjacent compartment,

a first alkaline ion exchange compartment (31) being in fluidic contact with a positive side of first bipolar membrane (11a) and with a cation exchange membrane (12) and comprising aqueous NH_4^+ and OH-,
a second ion exchange compartment (32) being in fluidic contact with an anion exchange membrane (13) and with a cation exchange membrane (12) and comprising water, NH_4^+, and HCO_3^-, and
a third acidic ion exchange compartment (33) being in fluidic contact with a negative side of a bipolar membrane (11a) and with an anion exchange membrane (13) and comprising aqueous H+ and HCO_3^-,

a wastewater input (70) for providing wastewater to the second compartment,
a treated water output (71) adapted to receive output from the second compartment,
a cathode (42) and an anode (41) for providing a voltage, at least two electrode rinse compartments (21,22) being in electrical contact with the cathode (42) or with the anode (41) and with a membrane (11a,11b,12,13), and comprising salt,
at least three recirculation units (51,52,74a,74b), including a first alkaline recirculation unit (51) adapted to receive input from the first alkaline compartment (31), comprising a pump (81), a gaseous ammonia stripper (61), and for providing stripped output to the first alkaline compartment (31), a second acidic recirculation unit (52) adapted to receive input from the third acidic compartment (33), comprising a pump (81), a gaseous CO_2 stripper (62),
and for providing stripped output to the third acidic compartment (33), and a third recirculation unit (74a,74b) adapted to receive input from a first electrode rinse compartment (21), in electrical contact with the anode (41),
and for providing output to a second electrode rinse compartment (22), in electrical contact with the cathode (42),
and vice versa, wherein at least one of the gaseous

ammonia stripper (61) and of the gaseous CO_2 stripper comprises a hydrophobic membrane (61a,62a), a molecular sieve for ammonia or for CO_2, respectively a pervaporation membrane, or a combination thereof, and
a tube (72) for removing gaseous ammonia, and a tube (73) for removing gaseous CO_2.

2. System according to claim 1, wherein at least one membrane (61a,62a) in the stripper is impermeable to liquids, and permeable to gases.

3. System according to any of claims 1-2, wherein the hydrophobic membrane (61a,62a) is macroporous, with an average pore size of 50-500 nm, or microporous, with an average pore size of 0.4-10 nm (as determined by electron microscopy) .

4. System according to any of claims 1-3, wherein the membrane (61a,62a) is selected from polymeric material, inorganic material, and combinations thereof.

5. System according to any of claims 1-4,
wherein the exchange unit (30) comprises a stack of a cation exchange membrane (12), an alkaline ion exchange compartment (31), a bipolar membrane (11a), an acidic ion exchange compartment (33), an anion exchange membrane (13), and a wastewater ion exchange compartment (32), and wherein the second electrode rinse compartment (22) is in fluidic contact with a further cation exchange membrane (12), or wherein the exchange unit (30) comprises a

stack of an anion exchange membrane (13), an acidic ion exchange compartment (33), a bipolar membrane (11a), an alkaline ion exchange compartment (31), a cation exchange membrane (12), and a wastewater ion exchange compartment (32), and wherein the first electrode rinse compartment (21) is in fluidic contact with a further anion exchange membrane (13), or wherein the exchange unit (30) comprises a stack of an bipolar membrane (11a), an alkaline ion exchange compartment (31), a cation exchange membrane (12), a wastewater ion exchange compartment (32), an anion exchange membrane (13), and an acidic ion exchange compartment (33), and wherein the first electrode rinse compartment (21) is in fluidic contact with a further bipolar membrane (11b).

6. System according to any of claims 1-5, comprising 2 - 1024 ion exchange units (30) in parallel.

7. System according to any of claims 1-6,wherein membranes (11a,11b,12 and 13) are separated by spacers (2) and the membranes *(*11a,11b,12*)* and electrodes are separated by spacers (2).

8. System according to any of claims 1-7, wherein in operation at least one of a voltage of 0.1-5 V per ion exchange unit (30) is applied,

a pH in the first alkaline ion exchange compartment (31) is from 7-14,
a pH in the third acidic ion exchange compartment (33) is from 1-7,
a current density is from 5-500 A/m^2,
a flow parallel to a membrane is each individually from 0.01-0.20 m/s,
a NH_4^+ flux over a membrane is each individually 0.2-20 $mole/m^2/h$,
a HCO_3^- flux over a membrane is each individually 0.2-20 $mole/m^2/h$,
an operating temperature is from 10-80 °C,
the $[NH_4+]$ and $[HCO_3-]$ in the second ion exchange compartment (32) is each individually 10^{-3} - 2 mole/l,
a vacuum of 0.1-90 kPa is each individually applied over membranes (61,62),
a flux of wastewater and recirculation is each individually 0.01-10 $kg/m^2/h$, and
an NH_3 flux and a CO_2 flux in recirculation units (51,52) is each individually 50-5000 $g/m^2/h$.

9. Method for treating wastewater comprising

providing a system (100) according to any of claims 1-8, applying an electrical potential difference over the anode (41)/cathode (42),
providing wastewater in second ion exchange compartment (32) comprising NH_4+, and HCO_3-,
transferring NH_4+ from the wastewater (70) to an alkaline recirculation solution (51),
simultaneously, transferring HCO_3- from the wastewater to an acidic recirculation solution (52),
depleting NH_4HCO_3 in the wastewater, and
splitting water over bipolar membranes (11a,11b) thereby providing H+ to the third acidic ion exchange compartment (33) and thereby providing OH- to the first alkaline ion exchange compartment (31),
wherein transferring NH_4+ from the wastewater (70) to an alkaline recirculation solution (51) is through a first alkaline ion exchange compartment (31),
wherein transferring HCO_3- from the wastewater to an acidic recirculation solution (52) is through a third acidic ion exchange compartment (33),
wherein NH_4+ is converted into NH_3 in the presence of OH-in the first alkaline compartment (31), and wherein $HCO_3-$is converted into CO_2 in the presence of H+ in the third acidic ion exchange compartment (33),
wherein NH_3 is stripped in ammonia stripper (61), and wherein CO_2 is stripped in CO_2 stripper (62).

10. Method according to any of claims 9, wherein at a gaseous side of stripper (61,62) an under pressure is applied.

11. Method according to any of claims 9-10, further comprising forming NH_4HCO_3.

12. Method according to any of claims 9-11, wherein wastewater is provided by at least one of a domestic sewage treatment plant, a manure treatment facility, a fertilizer production plant, food and beverage industry, and an industry producing nitrogen loaded wastewater.

13. Method according to claim 12, wherein wastewater is provided by a manure treatment facility.

14. Method according to any one of claims 9-13, wherein the NH_3 as stripped in ammonia stripper (61) is used as fuel for a solid oxide fuel cell to recover electrical energy.

15. Method according to claim 14, wherein the recovered electricity is used in the method for treating wastewater.

Fig. 1

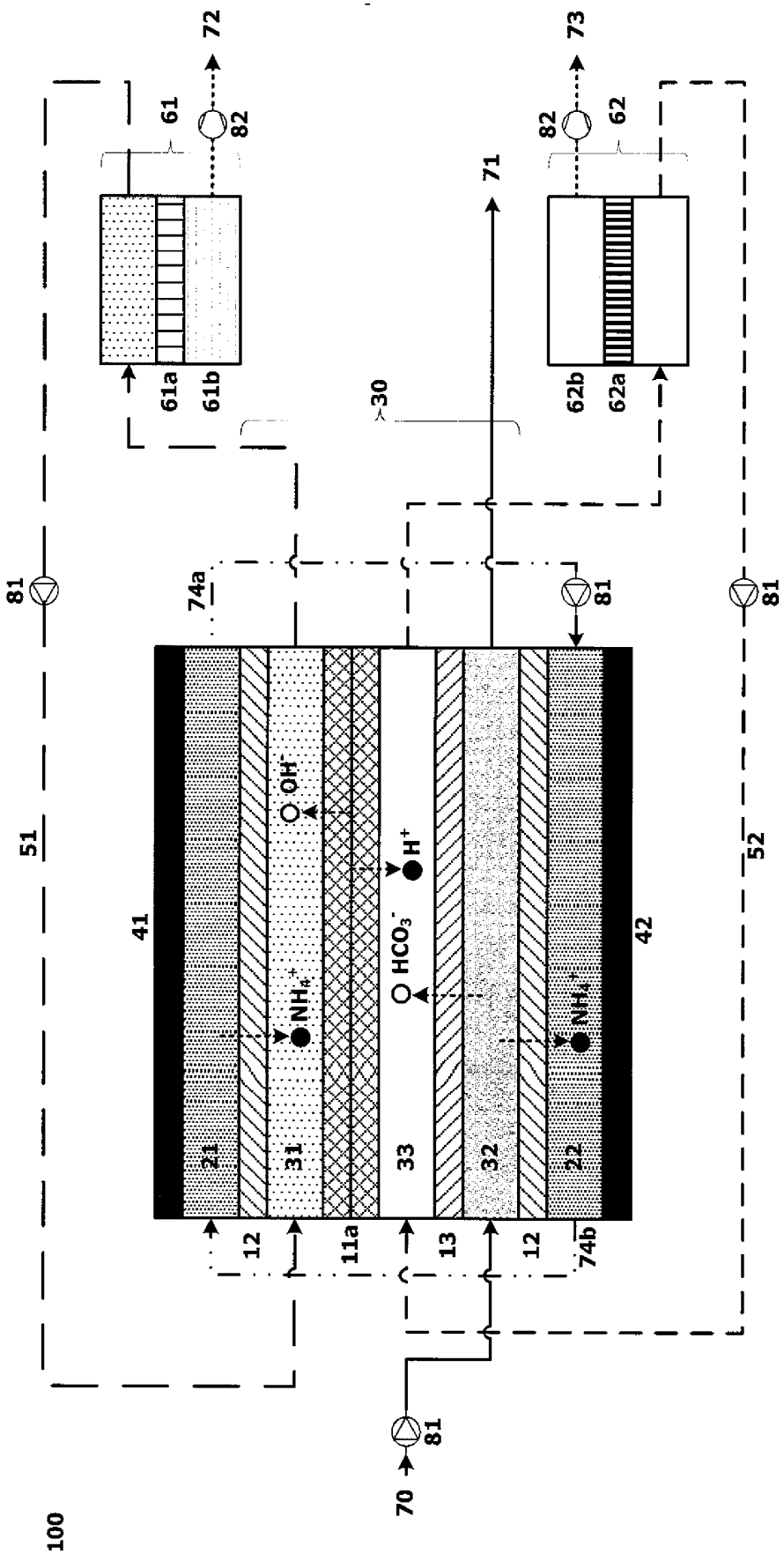
100
70
71
72
73
81
82
30
41
42
51
52
61
61a
61b
62
62a
62b
74a
74b
11a
12
13
21
22
31
32
33
OH⁻
H⁺
HCO₃⁻
NH₄⁺

Fig. 2

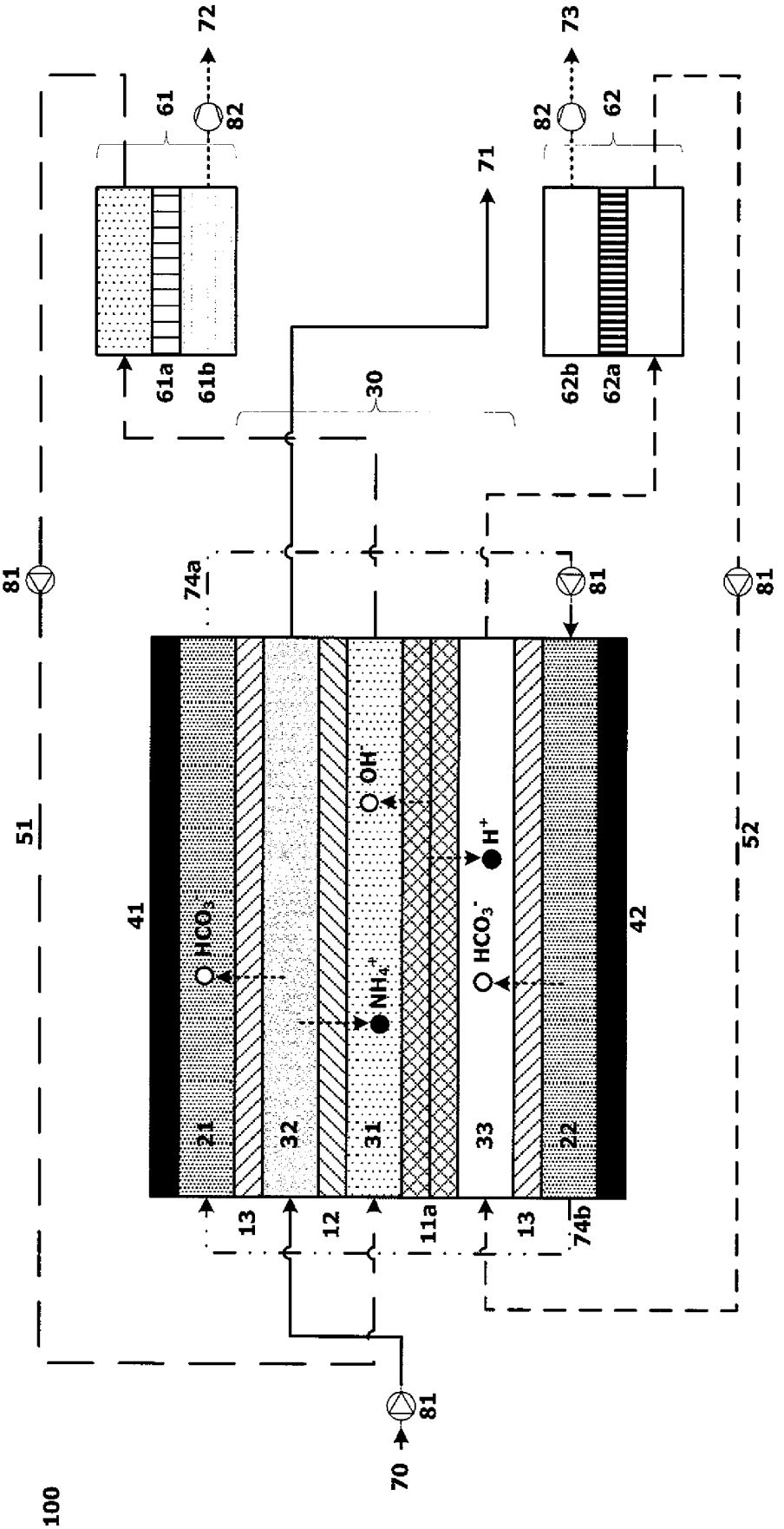
100
70
81
72
73
61
82
62
71
61a
61b
62b
62a
30
74a
74b
51
52
41
42
21
32
31
33
22
13
12
11a
HCO_3^-
NH_4^+
OH^-
H^+
HCO_3^-

Fig. 3

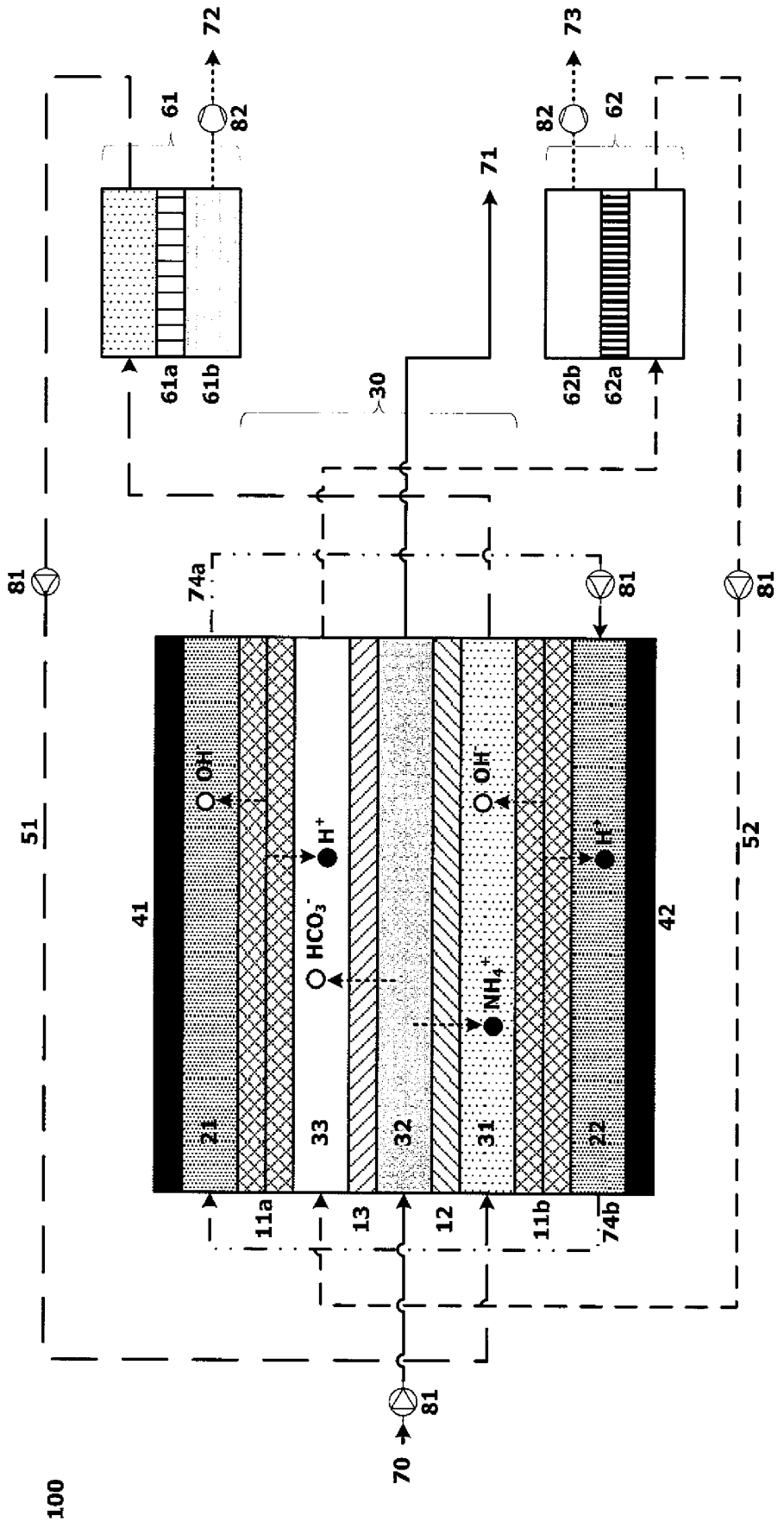
100
70
81
72
73
61
82
62
71
30
61a
61b
62b
62a
74a
74b
51
52
41
42
21
33
32
31
22
11a
13
12
11b
OH⁻
H⁺
HCO3⁻
NH4⁺

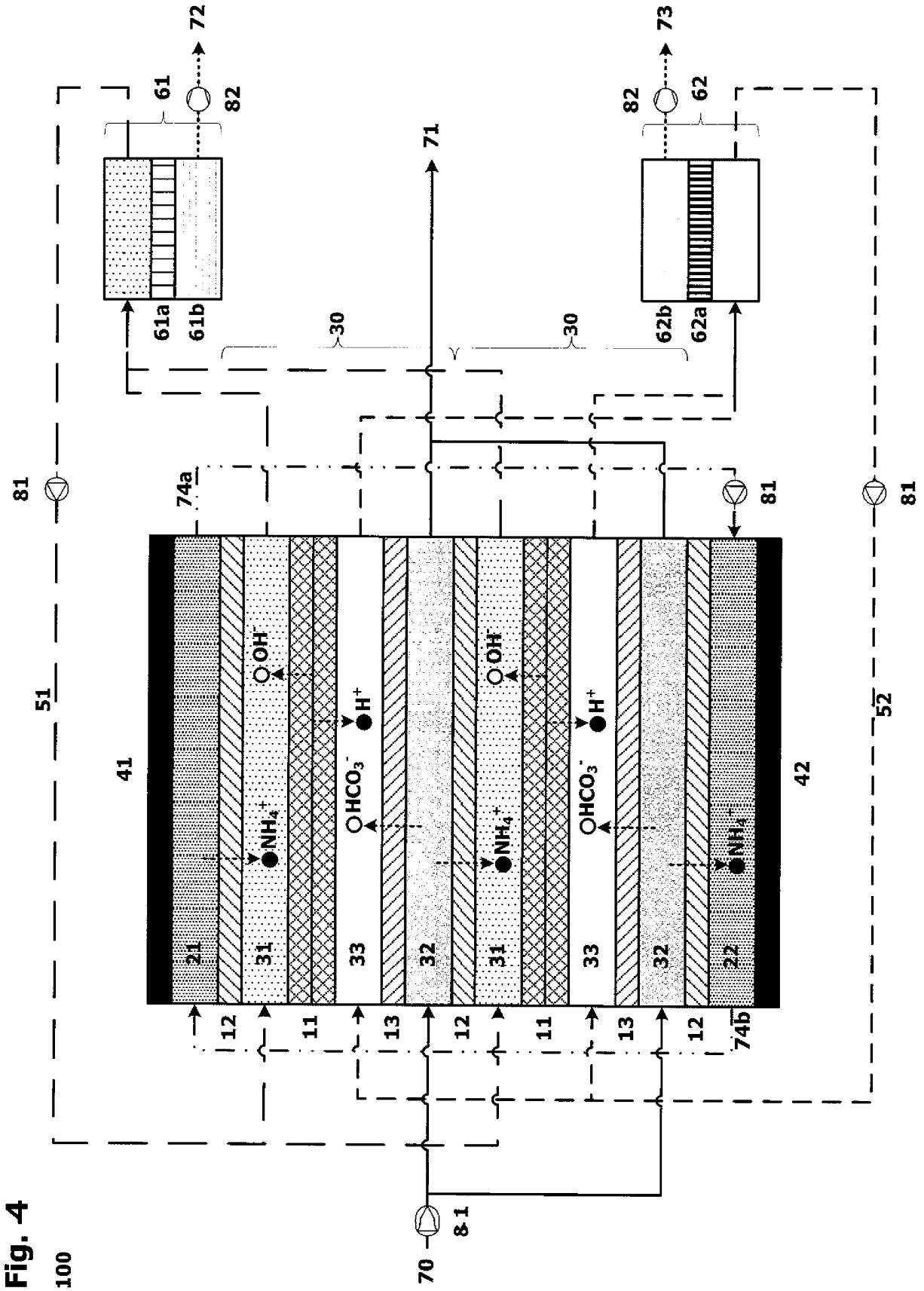
100
70
81
72
73
71
61
62
82
61a
61b
62a
62b
30
74a
74b
41
42
51
52
21
22
31
32
33
11
12
13
OH⁻
H⁺
HCO3⁻
NH4⁺

Fig. 4

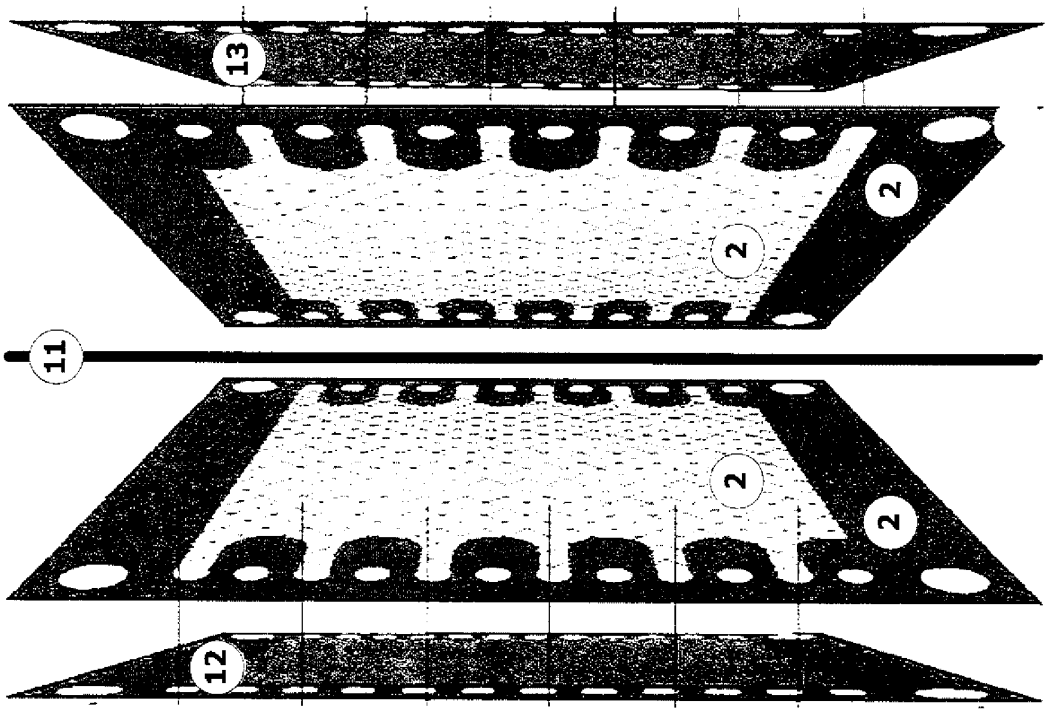

Fig. 5

REFERENCES CITED IN THE DESCRIPTION

This list of references cited by the applicant is for the reader's convenience only. It does not form part of the European patent document. Even though great care has been taken in compiling the references, errors or omissions cannot be excluded and the EPO disclaims all liability in this regard.

Patent documents cited in the description

- US 2016271562 A1 **[0010]**
- US 4969983 A **[0011]**

Non-patent literature cited in the description

- **PRONK et al.** Treatment of source-separated urine by a combination of bipolar electrodialysis and a gas transfer membrane. *Water Science Technology,* 2006, vol. 53 (3), 139-146 **[0012]**
- Experimental study on desorption of simulated solution after ammonia carbon capture using bipolar membrane electrodialysis. **SHUANGCHEN et al.** Int. J. Greenhouse Gas Control. Elsevier, 03 November 2015, vol. 42, 690-698 **[0013]**
- **ALI et al.** J. Membrane Science. Elsevier, 15 November 2004, vol. 244, 89-96 **[0014]**